Centre for Health Technologies
School of Biomedical Engineering
University of Technology Sydney

An Energy Harvesting System Using Biological Fuel Cells for Powering Medical Devices

Daniel N. Roxby

A thesis submitted in partial fulfilment of the requirements for the degree of Doctor of Philosophy

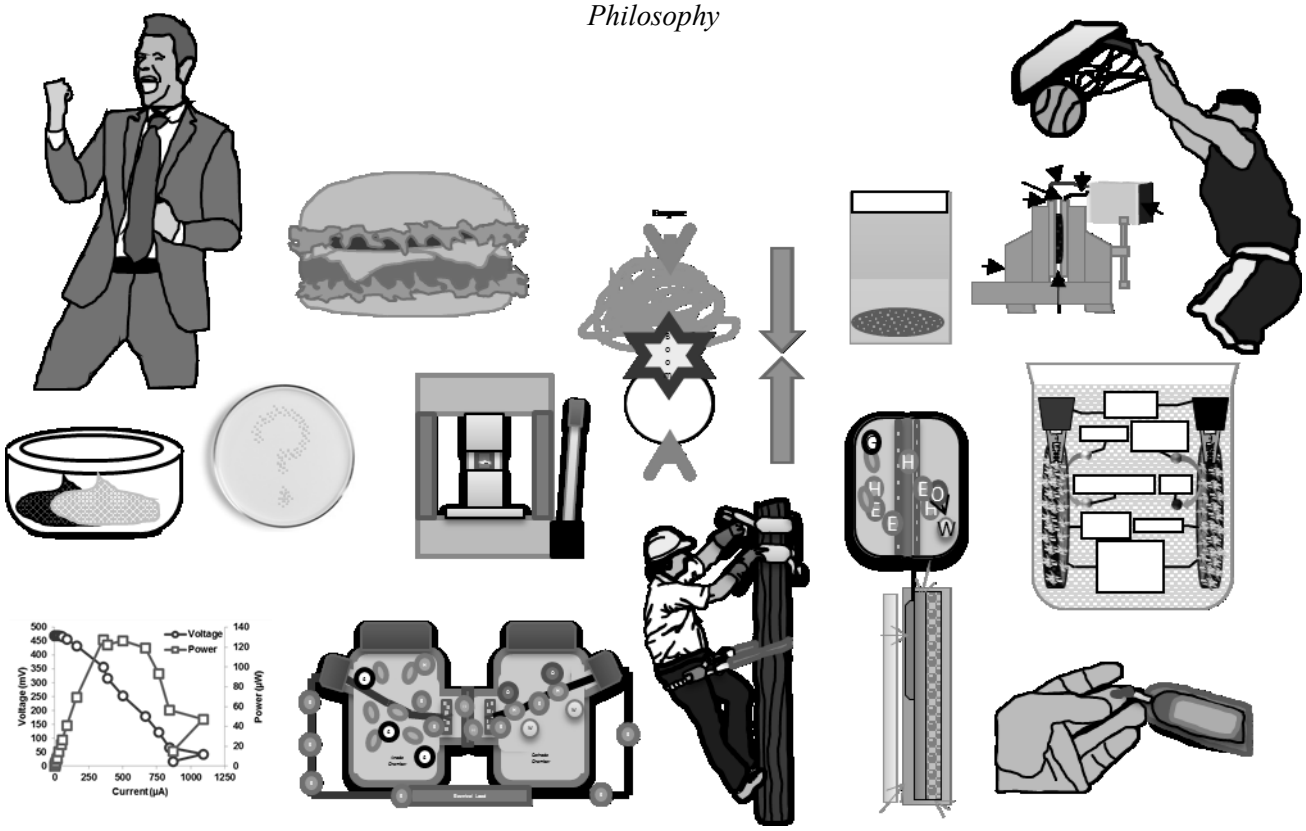

CERTIFICATE OF AUTHORSHIP

I, Daniel Ninio Roxby, certify that the work in this thesis has not previously been submitted for a degree nor has it been submitted as part of requirements for a degree except as fully acknowledged within the text.

I also certify that the thesis has been written by me. Any help that I have received in my research work and the preparation of the thesis itself has been acknowledged. In addition, I certify that all information sources and literature used are indicated in the thesis.

This research is supported by an Australian Government Research Training Program Scholarship.

Signature of Student:

Production Note:
Signature removed prior to publication.

Date: 17 January 2018

ACKNOWLEDGEMENTS

Firstly, I am forever grateful to my parents, Peter and Tess Roxby, my brother Matthew Roxby and our many dogs, for their undying love, support and patience throughout the life of this PhD and my studies. If not for them, I could not go on.

I am appreciative of my supervisor Professor Hung T. Nguyen, Professor and Director for the Centre for Health Technologies, University of Technology Sydney, for taking me on as his student when by traditional standards, I should not have been. I have learnt a lot from his approach to research, innovation and challenges and quick, calm mind. I am also thankful for his support in extracurricular activities and our many geeky gadget chats.

My dearest friends, Daniel Wong and Gladys Cheung and close friends Akane Takana and Zhichao Sheng, you were always a message away whether it be for a complaint, support or a good meal. Thank you so so much.

To the CHT students, it's been a pleasure going through this journey with you all. Our studies have been one thing, but our chats during late nights, food and drinks have been another.

Thanks to Nham Tran and Simon Ting for their efforts and help. From you, I know how to be a better professional. Also thanks to the staff of UTS, especially Steven Su, Gyorgy Hutvagner, Adrian Bishop, Sarah Osvath, Ron Shimmon, Alex Angeloski and Joyce To for their help over the years as well as visiting scholar Pak-Lam Yu.

And finally, and importantly, Huiling Zhou, there are so many words of appreciation for you. The world I know and goals I have now, would be very different if not for you. I will always cherish our WeChats, FaceTimes, travels and many other memories. You have been a source of strength, support and improvement as we faced these PhD and life challenges.

Contents

TABLE OF FIGURES

TABLE OF TABLES

AUTHORS PUBLICATIONS

Published Papers

1. Roxby, D.N., Ting, S.S. & Nguyen, H.T. 2017, 'Polypyrrole RVC biofuel cells for powering medical implants', *Engineering in Medicine and Biology Society (EMBC), 2017 39th Annual International Conference of the IEEE*, IEEE, pp. 779-82.
2. Roxby, D.N., Tran, N., Yu, P.-L. & Nguyen, H.T. 2016, 'Effect of growth solution, membrane size and array connection on microbial fuel cell power supply for medical devices', *Engineering in Medicine and Biology Society (EMBC), 2016 IEEE 38th Annual International Conference of the*, IEEE, pp. 1946-9.
3. Roxby, D.N., Tran, N., Yu, P.-L. & Nguyen, H.T. 2015, 'Experimenting with microbial fuel cells for powering implanted biomedical devices', *Engineering in Medicine and Biology Society (EMBC), 2015 37th Annual International Conference of the IEEE*, IEEE, pp. 2685-8.
4. Roxby, D.N., Tran, N. & Nguyen, H.T. 2014, 'A simple microbial fuel cell model for improvement of biomedical device powering times', *Engineering in Medicine and Biology Society (EMBC), 2014 36th Annual International Conference of the IEEE*, IEEE, pp. 634-7.

Abstract

1. Roxby, D., Tran, N., Yu, P. & Nguyen, H., 'PERPETUALLY POWERING BIOMEDICAL DEVICES WITH MICROBIAL FUEL CELLS', *Australian Biomedical Engineering Conference (ABEC), Melbourne, Australia. Retrieved from, http://www.abec.org. au/wp-content/uploads/2015/10/10.30-Roxbyabstract. pdf.*

NOMENCLATURE

AIMD	Active Implantable Medical Device
Ppy	Polypyrrole
SEM	Scanning Electron Microscopy
MWCNT	Multiwalled Carbon Nanotubes
MFC	Microbial Fuel Cell
SCMFC	Single Chamber Microbial Fuel Cell
DCMFC	Dual Chamber Microbial Fuel Cell
BFC	Biofuel Cell
GEBFC	Glucose Enzymatic Biofuel Cell
RAFT	Reversible Addition-Fragmentation Transfer
RVC	Reticulated Vitreous Carbon
PBS	Phosphate Buffer Solution
LBB	Luria Bertani Broth
TSB	Tryptic Soy Broth
LBA	Luria Bertani Agar
TSA	Tryptic Soy Agar
GPC	Gel Permeation Chromatography
NMR	Nuclear Magnetic Resonance
CV	Cyclic Voltammetry / Voltammogram
GOx	Glucose Oxidase
LAC	Laccase
FTIR	Fourier Transform Infrared Spectroscopy
EP	Electropolymerisation
EI	Enzyme Immobilisation
IC	Increased Conductivity
Glut	Glutaraldehyde
DI	Deionised

ABSTRACT

The most common example of an active implantable medical device (AIMD) is the pacemaker. In 2017, Abbott Laboratories said that 'more than 4 million people worldwide have an implanted pacemaker… and an additional 700, 000 patients receive the devices each year.' Other devices also exist, such as neurostimulators and cochlear implants which are implanted at different ages and whose batteries lives differ such that surgical replacement is required. With further technologies being developed and life expectancy rising, the incidence of this problem will increase.

Current wireless charging and energy harvesting solutions are not ideal. Wireless recharging continues to be researched where issues around alignment, power transfer efficiency and skin heating remain. Importantly, patient anxiety for their device's charge remains but at more regular intervals. Peltier cells can harvest heat energy from the body but must be unfeasibly large. Mechanical energy harvesting with piezoelectric, electrostatic and electromagnetic generators has potential, however, require patient movement or require risky attachment to organs.

Biological fuel cells have the potential to power AIMDs from glucose, using bacteria or enzymes to catalyse the capture of electrons. This study outlines methods to improve the power of both microbial fuel cells (MFCs) and glucose enzymatic biofuel cells (GEBFCs) for AIMDs.

Firstly, MFCs are used to find that positioning electrodes can improve the power output by 5 times as well as that fuel cell stirring can improve power by 1.2 times. These findings have implications where a patient can be upright or lying down, and active or sleeping. Internally, bacteria composition was found to be an important factor in power output, where MFCs that use of a mixed culture could provide 10.27 μW of power whereas a single culture could

provide 5.94 μW and that fuel cell stacking could achieve up to 1.6 V and 39 μW. These findings speak to the size of a MFC and that power density is a significant challenge to implantation.

Alternatively, polypyrrole electrodes were developed for a GEBFC. The method involved a novel combination of RAFT and electro-polymerisation to create a polymer which had a high conversion efficiency of 80.9% and uniform polydispersity of 1.034. The disc electrodes were synthesised through a simple compression method, enabling high enzyme loading and suitability for manufacturing. Further improvements using glutaraldehyde crosslinking and high conductivity silver composites lead to harvesting of 451 mV, 128.2 μW and 1.4 mA and ultimately, an actual medical device is powered.

Whilst there is significant potential, there are some areas for future work. MFCs will require significant work in miniaturization whilst also increasing the power output and making them biocompatible. GEBFCs using polypyrrole will likely also require further biocompatibility work as well as improvements in the conductivity and crosslinking of the material, which will help take care of several issues such as porosity, enzyme leaching, enzyme orientation, biofouling and electron transport.

CHAPTER 1 INTRODUCTION

1. Introduction

1.1. BACKGROUND

When regulatory bodies such as the European Union[1] (European Union 1990) or the FDA[2] in the United States (Federal Drug Administration 2017a) seek to classify implanted medical devices, one particular aspect they look into is whether a device is passive or active. Passive implanted medical devices do not require electrical energy or magnetic fields and may rely on the human body or gravity to perform a particular function. An example of a passive implanted medical device is the artificial joint. Active devices require electrical energy or magnetic fields for their functions and the most well-known of these is the pacemaker[3]. Additionally, the global standard for Active Implantable Medical Devices defines firstly an active medical device as "…Medical device relying for its functioning on a source of electrical energy or any source of power other than that directly generated by the human body…" The standard stipulates that an active implantable medical device is an "…Active medical device which is intended to be totally or partially introduced, surgically or medically, into the human body or by medical intervention into a natural orifice, and which is intended to remain after the procedure…" (AS 2015).

Ongoing statistics show that active implanted medical devices (AIMDs) are being used all over the human body at staggering rates throughout the world. In 2017, Abbott Medical, a major biomedical engineering company, reported that 'more than 4 million people worldwide have an implanted pacemaker… and an additional 700, 000 patients receive the devices each year' (Abbott Laboratories 2017a). Other devices are applied to areas of the body such as the brain, bladder, spine, pancreas, ears and eyes and treatment modalities are generally

[1] The EU regulation covering medical devices is COUNCIL DIRECTIVE 93/42/EEC
[2] The FDA regulation covering medical devices is 21 CFR 862-892.
[3] The EU explicitly describes 'active' and 'passive' devices, whilst the FDA individually mentions for each medical device whether electricity is involve and refers to standards for 'Active' implantable medical devices.

neuromodulation or medication pumping devices, are often combined with some form of sensing and are focused on helping a patient live their life more conveniently or by addressing severe pain. In a separate category is implantable Micro Electrical Mechanical Systems (MEMS) which due to their micro size, may purely be for sensing or may take different approaches to their larger and more traditional counterparts. Some of the technologies have been in use since the early 20th century, whilst others have only been around in the past 5 to 10 years. Broadly speaking, biomedical engineering is considered a major area of investment in the coming years (Japsen 2016). Additionally, other emerging technologies such as robotics, artificial intelligence and big data, all have applications in biomedical engineering, further increasing the likelihood of further devices to come.

Each active medical devices requires a power source. When it comes to active medical devices which are implanted, this becomes a particular issue as one needs to get electricity past the skin and into the device near the organs it is performing functions with or on. The earliest cardiac pacing operations faced issues around electricity supply whereby they ran off mains power supply. The design was such that wires would be inserted into the patient and connected to a laboratory stimulator. The first successful use of this design was on the 30th of January 1957 on a 3-year old girl whose heart had stopped during an operation but who regained heart rhythms and survived the operation. Not long afterwards though on October 31st of the same year, a baby unfortunately died due to hospital power failure (Aquilina 2006).

Current pacemaker technology and other AIMDs use modern Lithium Ion and other high power densities batteries. Nonetheless, the batteries do not last longer than the lifetime of a patient, and it is inevitable that another surgery must take place to replace the battery. Table 1 shows a list of various current AIMDs from Medtronic and how long the battery may last.

At first glance, battery lives of 11 or even 5 years seems fairly reasonable considering they deal with a patients symptoms. In fact when it comes to pacemakers, the 2009 mean age of implantation was in some countries is less than 50 years of age, but mostly above 65 years of age (Mond & Proclemer 2011). The numbers vary though for different devices. For patients with OAB wet symptoms where sacral neurostimulation is a common treatment, the prevalence of symptoms increases with age and more substantially so after 44 years for women and 64 years for men (Sukhu, Kennelly & Kurpad 2016). Deep Brain Stimulators are used to assist with Parkinson's disease symptoms which typically onset at age 60, however early onset can occur for individuals of less than 50 years old (Reeve, Simcox & Turnbull 2014). It is clear that a replacement is imminent for the current generation of AIMD patients, however it is increasingly likely for future generations. Data from the World Bank shows that life expectancy is increasing, where those whom are born now are likely to live 10 years longer than their parents or grandparents, thus further increasing this chance of implant replacement surgery (World Bank 2017). The problem therefore with AIMD batteries and powering technologies likely to increase in the coming years.

Device Type	Name and Manufacturer	Specified Battery Life
Pacemaker	Medtronic Advisor DR A2DR01	6.6-11.8 years (Medtronic 2016b)
Deep Brain Stimulator	Medtronic Activa RC	9 years (Medtronic 2014b)
Sacral Modulator	Medtronic Interstim II 3058	3-5 years (Medtronic 2016e)
Spinal Cord Stimulator	Medtronic RestoreUltra 37712	9 years (Medtronic 2007)
Implantable Cardioverter Defibrillator	Medtronic Visia AF MRI VR SureScan Model DVFB1D1	7.9-11 Years (Medtronic 2015b)

Table 1: Specified Battery Lives for Various Medtonic Biomedical Devices

1.2. MOTIVATION OF THESIS

Amongst various engineering disciplines existing today, biomedical engineering is special in that it enables people to live or to have a better quality of life that they would not otherwise have due to their medical conditions. Without a pacemaker for example, a patient's heart may stop working. Without a cochlear implant, a child may never hear and learn about science or to live a normal life. Biomedical devices have the ability to enable people to live life and to bring about equality. Indeed, perhaps what a child with hearing problems will learn from a teacher with a heart condition will lead them to cure cancer.

The power of biomedical engineering is being felt as it is clear that a large numbers of AIMDs already exist on the market and the trend is for their use to grow into the future. Current battery technology is such that they run out of charge within the lifetime of their patients, such that they require subsequent surgical replacements. Various solutions currently being researched such as wireless recharging or powering and mechanical or thermoelectric energy harvesting require the patient to go to additional efforts to obtain power for their device. Additionally, with life expectancy increasing generation to generation, the problem of powering of AIMDs and their frequent surgical replacement is likely increase in coming years.

Humanity enjoys food and is a major part of daily life and culture. In a physiological sense, it is the power behind a person's ability to live life and perform tasks day to day. In contrast to this, AIMDs helping to accommodate conditions affecting a person's abilities in day to day life are powered by electricity. Whilst many bodily functions use electricity for the nervous system or pacing of the heart, there is an inherent incompatibility existing at this point in history. Biological fuel cells have the ability to convert sugar into electricity, thus having potential to be a bridge between life and the power to live it. Whilst this idea is not new and significant breakthroughs have occurred, much work still needs to be done. As a potential

solution to a significant problem in biomedical engineering, further investigation into the topic is thus warranted.

1.3. OBJECTIVES AND CONTRIBUTION

The aim of this research is to determine approaches for increasing the power output of biological fuel cells which use sugar to electricity for powering AIMDs. The identified gaps in knowledge, as found in the literature review, indicate that whilst there are numerous studies showing various microbial fuel cell reactors for powering AIMDs, it is not understood how they may operate in the medical context and how their operation in the medical context may affect the power output. In regards to glucose enzymatic biofuel cells (GEBFCs), the most recent work has been in the use of compressed multiwalled carbon nanotube (MWCNT) electrodes. A gap however lies in the fact that this method is advantageous in being able to embed large amounts of enzymes into a small electrode but that other conductive and biocompatible materials exist that could be used to overcome the mechanical and immobilisation issues of MWCNTs and could provide good solutions and patient outcomes. It is based on these gaps in the knowledge of biological fuel cells for AIMDs that the outlined objectives are formed and the subsequent findings contributed.

Firstly, key parameters for the operation of microbial fuel cells are contributed as approaches for optimising the power output of MFCs, bearing in mind the medical context. These parameters include how the patient being upright or lying down may affect the power output, how the patient's movement may affect the power output, the MFC reactor type, its size and how this fits into the human body and how the contents of the MFC including bacteria and growth medium and influence of components, may affect the power output. These findings are then investigated by simulation of the conditions in a laboratory environment and the power output assessed via simulated power loads. The body of work suggests that dual chamber microbial fuel cells (DCMFCs) with large membranes containing mixed cultures

more easily obtain significantly higher power outputs, the way a patient moves and sits does contribute to the power output and growth medium composition can increase or decrease power output. These findings contribute to the body of knowledge about how best a MFC may work if designed and implanted for powering AIMDs.

Secondly, we contribute a new approach for improving the power output of GEBFCs. The reversible addition-fragmentation polymerisation (RAFT) technique is used to efficiently (reaction efficiency of 80%) synthesise a uniform polymer (P_d of 1.034), which is then made conductive through Electropolymerisation. The combination of these two techniques is a novel approach not seen in previous literature and is for use with the compression based method for GEBFC electrodes. The material is then characterised for conductivity, electrochemical properties and pseudocapacitance to add to the body of knowledge. Ppy is then used to create the GEBFC electrodes and the GEBFC tested. The GEBFCs using these compressed Ppy electrodes offer the first use of this highly advantageous compression method with Ppy, allowing for high enzyme loading and greater mechanical strength than that seen in previous studies.

Noting (1) the data suggesting that GEBFCs would be more implant appropriate in terms of size and power density and that (2) it would be easier to improve their power output, two factors were further identified which could then improve the power output; namely increased conductivity (IC) and enzyme immobilization (EI).

Lastly, methods to further improve the power output of GEBFCs are contributed. Firstly, composite materials are used, combining both Ppy with either reticulated vitreous carbon (RVC) or silver to increase electrode conductivity. This solution was a novel approach, allowing us to maintain the advantages of the compression methodology and Ppy without direct Ppy manipulation whilst still increasing the conductivity. This increase led to a 5 times

increase in power from the base line as well as a 10 times increase over the MFC power output. EI was also performed via use of the aldehyde groups of glutaraldehyde (Glut) and Ppy leading to further increases from the baseline. Again, this is a novel approach, allowing us to maintain the advantages of the compression approach, whilst avoiding enzyme leaching and achieving the desirable direct electron transfer effect through immobilisation. In particular, by taking advantage of the more porous nature of the silver composite electrodes, more enzymes were embedded and the power achieved was the highest of all experiments and a significant improvement overall. Ultimately from these experiments, a medical thermometer is powered, further showing the potential of the technology.

1.4. STRUCTURE OF THESIS

The structure of this thesis is composed of six chapters including the introduction, literature review, three results chapters followed by a discussion and conclusion section. These are outlined as follows:

- *Chapter 2, Literature Review* presents a review of the literature pertaining to sugar to electricity conversion technologies in the AIMD area. In particular, it investigates the current AIMD market and previous studies aiming to use MFCs and GEBFCs, the various parameters for how they work and each technologies potential for powering AIMDs. For completeness, a history of various AIMDs is also provided in the Appendix section.
- *Chapter 3, Microbial Fuel Cells*, starts by outlining how microbial fuel cells are addressed in this work as oppose to previous studies. The chapter then looks at the materials and methods undertaken in order to see the power producing potential of microbial fuel cells in the context of powering AIMDs and what effect each of the basic operating parameters has. The results are then given from the experiments with these parameters, followed by discussion and conclusion.

- *Chapter 4, Development and Testing of Compressed Polypyrrole Biofuel Cell Electrodes* begins by addressing some of the issues highlighted in the previous chapter, and how if done in a certain way, GEBFCs may be able to help with these problems. The materials and methods are then outlined, before the results are presented in developing a conductive polymer and creating a GEBFC. The chapter finishes off with discussion and conclusions, outlining some of the positive and negative findings of the body of work.
- *Chapter 5, High Power Output GEBFCs through Immobilisation and Increased Conductivity* begins by again addressing some of the issues raised in the previous chapters. Based on the experiments performed up until that point, the GEBFCs were deemed to have greater potential to power AIMDs from glucose and therefore were continued to be improved upon. The materials and methods are outlined, addressing the two main points that could be improved upon. The results are then presented with notable improvements, including the powering of an AIMD. These results are then discussed and concluded upon.
- *Chapter 6, Conclusion and Future Direction* is the final chapter of the thesis in which the body of work as a whole is concluded upon, in particular the many achievements and some of the limitations. Further suggestions on future challenges for the work finish off the chapter.

The thesis also contains an Appendix including parts pertaining to methods which are common in science but not so common in an engineering context, other supporting information and histories of various AIMDs including pacemakers, neurostimulators and cochlear implants.

CHAPTER 2 LITERATURE REVIEW

2. Literature Review

2.1. OUTLINE

This literature review is set out as follows:

- *Current Market for AIMDs*: this section outlines the current major markets for AIMDs including cardiac devices, neuromodulators and intrathecal pumps, cochlear implants and technologies they may become AIMDs in the near future. Within each of these market segments, some statistics are provided, information is given on the major companies as well as smaller start-ups seeking to disrupt the market.
- *Current Technology for Powering AIMDs*: With an understanding of how the development of AIMDs and the current market for them, we look more specifically in this section at how AIMDs are currently powered. This includes batteries, wireless charging through inductive charging and wireless powering links.
- *Research in Powering AIMDs*: This section looks thoroughly at the research of technologies that have the potential to power AIMDs. Whilst wireless charging and powering links are already in use, it still remains heavily researched to this day. Energy harvesting as a broad field is a major area of research and includes thermoelectric harvesting and piezoelectric, electrostatic and inductive energy harvesting. Biological cells are considered energy harvesting technologies, however as the focus of this thesis, they are given separate sections as microbial fuel cells and glucose enzymatic biofuel cells.

Note that for completeness, a *History of AIMDs* is provided in the Appendix section of this thesis. This section reviews the history of AIMDs, looking at the beginnings of the main devices such as the pacemaker and ICD, the deep brain stimulator and the cochlear implant. This section is included with the perspective that in order to understand the current market

and situation for AIMDs as well as the motivations for its existence, one needs to understand how the AIMD market developed.

2.2. CURRENT MARKET FOR AIMDS

Nowadays, whilst AIMDs are continuously researched and improved in research institutions and universities, sales of the devices, and indeed a large amount of R&D is performed by industry or collaborations with industry. To fully understand AIMDs and their current state, we firstly look at who are the major companies in the industry, the market segments and expected trends into the future.

The major segments of the AIMDs market include:

- Cardiac devices, primarily ICDs and pacemakers
- Neuromodulation devices, primarily deep brain stimulators, but also spinal cord stimulators[4]
- Cochlear implants
- Infusion Pumps

2.2.1. CARDIAC DEVICES

The pacemaker is the largest segment of the cardiac devices market and sends electrical signals to contract the muscles of the heart, which in turn helps maintain its rhythmic pumping of blood around the body. In 2017, Abbott Laboratories, a major biomedical engineering company, reported that 'more than 4 million people worldwide have an implanted pacemaker… and an additional 700, 000 patients receive the devices each year' (Abbott Laboratories 2017a). Indeed, the most recent global survey of cardiac pacing in 2009 showed that over 1 million pacemakers were implanted in 2009. Of this number 265 000

[4] The terms neuromodulation and nerve stimulation are used interchangeably.

were replacements of old pacemakers, and 738 000 were pacemakers for new patients (Mond & Proclemer 2011).

Based on sales revenues in annual reports for various pacemaker, ICD and implantable monitoring device manufacturers, the cardiac market in 2016 was worth at least 12 billion US dollars. Medtronic, which is the largest of the biomedical device companies, had the largest sales revenue at 10.2 billion USD (Medtronic 2016f). The other significant players whom are public companies and therefore share their financial data are Boston Scientific with 1.9 billion USD, Livanova with 249.1 million USD and Lepu Medical with 524.22 million USD (Boston Scientific 2016b; Lepu 2016; LivaNova 2016). It should be noted that, up until the end of 2015, St Jude Medical had been a significant player in the cardiac market. St Jude Medical in 2015 had reported a sales revenue of 2.5 billion USD, however due to the time of purchase and accounting period rules, Abbott Laboratories had not reported on its cardiac business unit (originally St Jude Medical) in its 2016 financial results and the 2017 results were not available at the time of writing for all companies. Table 3 showing Abbott's 2017 Three Quarter results indicates that Abbott laboratories is tracking comparably, though down with St Jude's 2016 Three Quarter results. A list of companies selling cardiac devices with where possible, their sales revenues for 2015 and 2016 are shown in Table 2. It is said that in general, doctors and hospitals tend to recommend products from Medtronic, Boston Scientific and St Jude Medical, as these products have vast networks and doctors behind them and significant technical support (Hollmer 2014).

The start-up NeuroTronik is also working in the cardiac space, however not with any of the traditional markets such as pacemakers, ICDs and monitors. Their neuromodulation system seeks to help sufferers of Acute Heart Failure Syndrome. Recently they received $23.1 Million US in their Series B funding round (MedTech Innovator ; Teater 2017).

Company	Cardiac Net Sales / Revenue (USD Millions)	
	2016	2015
Medtronic (Medtronic 2016f)	10,196,000	9,361,000
Boston Scientific (Boston Scientific 2016b)	1,850,000	1,807,000
St Jude Medical (St Jude Medical 2015)	N/A	2,523,000
Livanova (LivaNova 2016)	249.07	52.5
Biotronix	N/A	N/A
Medico	N/A	N/A
Shree Pacetronix (LivaNova 2016; Shree Pacetronix 2016)	68.4	74.7
Vitatron	N/A	N/A
Lepu Medical (Lepu 2016)	524.22	418.55
Total	12,046,842	13,691,545

Table 2: Publicly Available Sales Revenues for 2016 and 2016 of Several AIMD Cardiac Product Companies

Three Quarter Sales Revenue (USD millions)	
Abbott Laboratories 2017	St Jude Medical 2016
511	577

Table 3: St Jude and Abbott Laboratories Three Quarter Sales Revenue (Abbott Laboratories 2017b)

Figure 1: St Jude / Abbott Medical Ellipse VR Implantable Cardioverter Defibrillator Device (St Jude Medical 2014)

2.2.2. NEUROMODULATORS, NEUROSTIMULATORS AND INTRATHECAL PUMPS

Another major market with AIMDs is neuromodulation. Numerous companies have applied the nerve stimulator technology for various applications including pain, depression, epilepsy, obstructive sleep apnea, Parkinson's disease, urinary incontinence and seizures. Medtronic states that to date, over 135 000 people worldwide have had the device implanted for Parkinson's disease (Medtronic 2017c) and 225 000 patients worldwide for sacral neurostimulators (Medtronic 2017f). St Jude Medical stated in 2014 that they had implanted over 45 000 spinal cord stimulator devices across 35 countries (St Jude Medical 2016). Other estimates from the International Neuromodulation Society suggest that as many as 34 000 people undergo surgery for the devices worldwide each year (Thomson 2016).

Figure 2: Illustration of a DBS device and how the leads run up to the electrodes in the brain (Therapeutic Goods Administration (TGA) 2016)

Figure 3: Medtronic Interstim II Implantable Sacral Neuromodulation Device (Medical Expo 2017)

Figure 4: Boston Scientific Precision Montage MRI Spinal Cord Stimulator (Boston Scientific 2017b)

Table 4 shows publicly available sales revenues for numerous neuromodulator technology companies or segments of companies where neuromodulators are embedded, with their associated applications. The market overall is worth at least 8.33 billion USD with Medtronic being the largest player in 2016 by a significant margin at 7.21 billion USD, although this is in part due to its wide coverage of technologies. The second largest player was Boston Scientific with 556 million USD and followed by Livanova with 351.4 million USD.

Medtronic's neuromodulation revenue numbers are also boosted by their implantable drug infusion pumps product 'SyncroMed II' (Medtronic 2017b). This is likely to be only a small part of their market however since doctors tend to prefer neuromodulators (Riemer & Alexander 2016). This is perhaps further supported by the fact that only one other company, Flowonix, has a similar active implantable drug delivery device (Flowonix Medical Inc 2017). Other implantable drug delivery devices do exist from Codman and Shurtleff, but rely on pressure rather than battery powered pumps, and are therefore not included in the scope of this review (Codman & Shurtleff 2017).

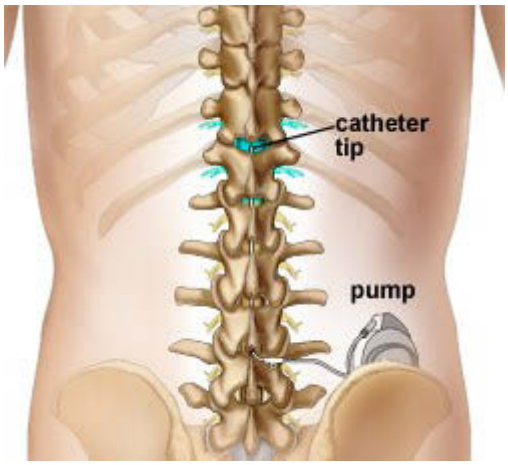

Figure 5: How a intrathecal pump sits within the body (Delhi Pain Management Centre 2017)

Aside from the major players in neuromodulation are several start-up companies who have received sizable funding during their funding rounds. Saluda Medical, which states their product will be 'the first closed loop neuromodulator', are currently running clinical trials throughout Australia, Europe and the Americas, and received in June 2017, $53 million AU during their series D funding round (Saluda Medical 2017b). Similarly, Neuronetics, whose products are for transcranial magnetic stimulation treatment, received $15 million US in 2017 during its series G funding round (NeuroStar 2017), and Axonics received $35 million USD in their series C funding round (Al Irus 2017). For start-ups, these are good results since the later the funding round the better, to reach clinical trials is especially difficult for smaller

companies focused on implants, as well as that hardware based start-ups tend to face particular difficulties.

Company	Neuromodulator Net Sales / Revenue (USD Millions)		Description
	2016	2015	
SetPoint Medical	N/A	N/A	Crohn's disease, Rheumatoid Arthritis, Vagus Nerve Stimulation (Setpoint 2017)
Cyberonics, Livanova	351.41	214.76	Depression and Epilepsy, Vagus Nerve Therapy Stimulation (Cyberonics 2014; LivaNova 2016)
Nevro	0.23	0.07	Depression and Epilepsy, Vagus Nerve Therapy Stimulation (Nevro Corp 2016, 2017)
Neuronetics	N/A	N/A	Depression, Transcranial Magnetic Stimulation (Neuronetics 2017)
Tal Medical	N/A	N/A	Depression, Sleep, Low Field Magnetic Stimulation, Transcranial Magnetic Stimulation, Electroconvulsive Therapy, Transcranial direct or alternating current stimulation, Deep Brain Stimulation (Tal Medical 2016)
Inspire Medical	N/A	N/A	Obstructive Sleep Apnea, Hypoglossal Nerve Stimulation (Inspire Medical Systems 2017)
Imthera	N/A	N/A	Obstructive Sleep Apnea, Tongue Stimulation (Imthera 2017)
Autonomic Technologies	N/A	N/A	Pain, Cluster Headaches, Sphenopalatine Ganglion stimulation (Autonomic Technologies 2015)
Enteromedics	0.79	0.29	Pain, Back and Leg, Spinal Cord Stimulation (EnteroMedics 2016, 2017)
St Jude Medical	N/A	475	Pain, Back, Chronic, Spinal Cord Stimulation and Dorsal Root Ganglion Stimulation (St Jude Medical 2015) (Abbott Laboratories 2017c, 2017e)
StimWave	N/A	N/A	Pain, Back, Chronic, Spinal Cord Stimulation and Dorsal Root Ganglion Stimulation (Stimwave 2017)
Medtronic	7,210	6,751	Pain, Back, Parkinson's Disease, Urinary Incontinence, Spinal Cord Stimulation, Deep Brain Stimulation, Sacral Nerve Stimulation (Medtronic 2016f, 2017e)
Abbott Laboratories*	208	141	Pain, Back, Parkinson's Disease, Spinal Cord Stimulation, Deep Brain Stimulation (Abbott Laboratories 2017b, 2017c, 2017e)
Boston Scientific	556	501	Pain, Back, Parkinson's Disease, Spinal Cord Stimulation, Deep Brain Stimulation (Boston Scientific 2016b, 2017a, 2017c)
Nuvectra	4.16	N/A	Pain, Back, Spinal Cord Stimulation (Nuvectra 2017a, 2017b)

Saluda Medical	N/A	N/A	Pain, Neurostimulation (Saluda Medical 2017a)
Neuropace	N/A	N/A	Seizure and Epilepsy Treatment, No Specific Details Given (Neuropace 2017)
Axonics Modulation	N/A	N/A	Urinary Incontinence, Sacral Nerve Stimulation (Axonics 2017)
Total	$ 8,330.58	$ 482,608.12	

Table 4: Publicly available revenues for 2015 and 2016 for various neuromodulator companies with product categories covered

* As per Table 3, with Abbott Laboratories acquisition of St Jude Medical and accounting period rules, figures shown for Abbott Laboratories are three quarter figures.

2.2.3. COCHLEAR IMPLANTS

Some very interesting research has also been done in the area of bionics, where the bionic ear, better known as the cochlear implant, as well as the bionic eye, which is under development, exist. In principle, both devices use sensors to pick up light or sound, use algorithms to translate them and then using specialised electrodes attached to specific nerves, will send signals to the patient allowing at least improved hearing or sight (Bionic Vision Australia 2017a; Bionics Institute 2017). As of 2012, over 320 000 Cochlear devices were implanted and this grows each year (Eshraghi et al. 2012). Bionic Vision Australia, the developer of the Bionic Eye is currently focused on development of devices catered to people with retinitis pigmentosa and age-related macular degeneration (Bionic Vision Australia 2017b).

A summary of the sales revenue data collected from publicly available information in annual reports for the cochlear implant market is shown in Table 5. Though a much smaller market than cardio or neuromodulation devices, several companies still compete in the cochlear implant space. The Australian company, Cochlear is the largest manufacturer with $1.16 billion US, followed by the Advanced Bionics subsidiary, Sonova with $208.8 million US and the William Demant subsidiary, Otticon Medical with $63.4 million US. The market overall is worth at least $1.4 billion US, based on publicly available financial information.

Company	Cochlear Implant Net Sales / Revenue (USD Millions)	
	2016	2015
Nurotron	N/A	N/A
Advanced Bionics / Sonova (Sonova 2016)	208.8	190
Cochlear (Cochlear 2016)	1,158	942
MED-EL	N/A	N/A
William Demant / Otticon Medical (William Demant 2016)	63.4	60.5
Total	1,430,235	1,192,559

Table 5: Sales revenue data collected from publicly available information in annual reports for the 2016 cochlear implant market

2.2.4. TECHNOLOGIES ON THE HORIZON

Diabetes is estimated by the World Health Organisation to affect 347 million people worldwide by 2030 (Paddock 2014) and an estimated 1.6 million deaths were directly attributed to diabetes in 2015 (World Health Organization 2017). Whilst most diabetes sufferers have Type II (Centres for Disease Control and Prevention 2016), Type I sufferers do make up a sizable portion and have AIMD solutions. The traditional implantable insulin pump, first developed in the 1986 by MiniMed, and allowed for the ability to inject insulin more directly to the peritoneal cavity and liver (Hoskins 2017). Medtronic eventually bought MiniMed and discontinued the product in 2001, but over 450 of the original MiniMed devices still exist worldwide and a new start-up currently in the animal trial phase, PhysioLogic Devices, is still currently working on smaller, wireless and longer lasting insulin pumps (Hoskins 2017; Lord 2017). Additionally, organisations such as the Implantable Insulin Pump Foundation still advocate for their use (The Implantable Insulin Pump

Foundation 2017). In 2017, Medtronic released an artificial pancreas which by using single or dual hormone control, is said to provide approximately 10% improvement for glycaemic control in patients (Haidar et al. 2015). The device, like the insulin pump, is an implant with a tube extending through the skin to an external pouch. It has the ability to inject insulin as per the patient's discretion from a wireless controller (Al Idrus 2017b; Federal Drug Administration 2017b; Hakami 2016) as well as a closed loop function, which will automatically inject insulin as per the patient's glucose levels every 5 minutes. The device is shown in Figure 6 and is currently undergoing clinical trials for Type II patients. Other companies such as Bigfoot Biomedical (Bigfoot Biomedical 2017; Falconer 2016), Insulet (Al Idrus 2017a), Dexcom, Tandem and TypeZero are also working on artificial pancreas devices are expect to release in 2018 (Fiebus 2017). Lastly, continuous glucose monitors also exist from various companies including Senseonics (Eversense 2017), Abbott (Abbott Laboratories 2017d), Dexcom (Dexcom 2017) and Medtronic (Medtronic 2017g).

Figure 6: Photo of the Medtronic MiniMed 670G Artificial Pancreas (Medtronic 2016d)

Lastly is the area of MEMS, where novel micro scale systems are being developed for various different conditions. Some of these devices include Fraunhofer's Hydrocephalus

device to help regular cerebral pressure (Fraunhoffer 2014), the NIBIB's Brain Activity Sensor (NIBIB 2013), EPFL's Blood Analyser (Ecole Polytechnique Fédérale de Lausanne 2013), MIT's Drug Delivery system for vasoconstrictor agents (Cima 2007) and Washington University's implantable heart sensors (Miller 2014) to name a few. Many, if not all of these MEMS devices are still under development, however it hints at the future of AIMDs.

2.3. CURRENT ENVIRONMENT FOR POWERING AIMDS

Current technology to power AIMDs comes in batteries, wireless recharging or a combination of both. The selection of the powering paradigm depends on the powering requirements of the device and the device itself. This determines parameters such as where different parts of the device are placed, the size of the device and how much of a need there is to implant the device. Table 6 shows the powering schemes for different AIMDs and the differences reflect their differing power needs.

Power Scheme	**Devices**	**Notes**
Single Use Batteries	Pacemakers, ICDs, Drug Pumps	Last between 5 to 15 years between implants*
Rechargeable Batteries	Neurostimulators	Daily to monthly recharge for several hours at a time (Medtronic 2017d)
Continuous Wireless Power Transmission	Cochlear Implants	Approximately fortnightly replacement / recharge depending on usage (Jansen 2002)

Table 6: Power Schemes for Various AIMDs as per manufacturers

*See Table 7 for information on different AIMD's batteries and biomaterials

2.3.1. BATTERIES

Battery technology in AIMDs has gone through numerous iterations, always with the concern for improving their longevity. As is shown in the Appendix section showing the history of AIMDs, development in AIMDs has been primarily tied to the pacemaker's success, and a

significant development for the pacemaker was the development of lithium ion type batteries. This occurred in the 1960s and 70s with the work of Wilson Greatbatch who had previously been working on pacemaker circuitry, accidentally stumbling upon a way to lower their power requirements and then later working on the lithium ion battery (Aquilina 2006). Table 7 shows a collection of AIMDs and their battery types, showing that to this day, lithium ion battery technology is still used with the only real difference between the batteries being the type of cathode selected. In general, the types of lithium battery cathode systems found in AIMDs include iodine (Li/I_2), manganese oxide (Li/MnO_2), carbon mono fluoride (Li/CF_X), silver vanadium oxide (Li/SVO) or hybrid cathodes (Li/CF_x-SVO) (Amar, Kouki & Cao 2015). The most current research is focused on flexible batteries which have been used in consumer electronics, but are yet to be used in AIMDs (Gwon et al. 2014; Rahimi-Eichi, Baronti & Chow 2014).

Device Type	Company	Device Name	Chemistry	Reference
Pacemaker	Medtronic	Azure XT DR MRI SureScan W1DR01	Lithium-hybrid CFx silver vanadium oxide	(Medtronic 2016c)
Pacemaker	Medtronic	Advisa DR A4DR01	Lithium silver vanadium oxide with carbon monofluoride	(Medtronic 2013)
Pacemaker	Medtronic	Activa ADDRS1	Single cell lithium-iodine	(Medtronic 2016a)
Pacemaker	Medtronic	Micra MC1VR01	Lithium-hybrid CFx silver vanadium oxide	(Medtronic 2016g)
Pacemaker	Boston Scientific	Altrua 20 S205	Single-cell lithium-iodine	(Boston Scientific 2009)
Pacemaker	Boston Scientific	Accolade	Lithium-carbon monofluoride cell	(Boston Scientific

				2016a)
Pacemaker	Boston Scientific	Formio SR	Lithium-carbon monofluoride cell-silver vanadium	(Boston Scientific 2016a)
Pacemaker	Boston Scientific	Formio DR EL	Lithium-manganese dioxide cell	(Boston Scientific 2016a)
Deep Brain Stimulator	Medtronic	Activa RC 37612 Multi-program neurostimulator	Lithium ion rechargeable	(Medtronic 2014b)
Deep Brain Stimulator	Medtronic	Activa PC Multi-program neurostimulator	Hybrid combined silver vanadium oxide	(Medtronic 2014a)
Deep Brain Stimulator	Medtronic	Activa SC Multi-program neurostimulator	Hybrid combined silver vanadium oxide	(Medtronic 2010)
Sacral Nerve Stimulator	Medtronic	Interstim 3058	Lithium silver vanadium oxide hybrid	(Medtronic 2016e)
Sacral Nerve Stimulator	Medtronic	Interstim 3023	Lithium-thionyl chloride cell	(Medtronic 2016e)
Spinal Cord Stimulator	Medtronic	RestoreSensor 37714 Multi-program rechargeable neurostimulator	Lithium ion rechargeable	(Medtronic 2016i)
Spinal Cord Stimulator	Medtronic	RestoreUltra SureScan MRI Rechargeable neurostimulator	Lithium ion rechargeable	(Medtronic 2016j)
Spinal Cord Stimulator	Medtronic	RestoreAdvanced 37713 Multiprogram rechargeable neurostimulator	Lithium ion rechargeable	(Medtronic 2006)
Spinal Cord Stimulator	Medtronic	PrimeAdvanced SureScan MRI 97702 Neurostimulator	Hybrid combined silver vanadium oxide cell	(Medtronic 2016h)
Cardiac Defibrillator	Medtronic	Visia AF MRI VR SureScan DVFB1D4	Hybrid CFx lithium/silver	(Medtronic 2015a)

			vanadium oxide	
Cardiac Defibrillator	Medtronic	Evera XT DR DDBB1D1 Digital Dual Chamber Implantable Cardio Defibrillator	Hybrid CFx lithium/silver vanadium oxide	(Medtronic 2014c)
Cardiac Defibrillator	Boston Scientific	Venkat Prizm 2	Lithium-silver vanadium oxide cell	(Guidant 2008)
Cardiac Defibrillator	Boston Scientific	Autogen, Dynagen, Inogen, Origen	Lithium-manganese dioxide cell	(Boston Scientific 2015)
Cardiac Defibrillator	Boston Scientific	Incepta, Energen, Punctua	Lithium-manganese dioxide cell	(Boston Scientific 2015)
Cardiac Defibrillator	Boston Scientific	Teligen	Lithium-manganese dioxide cell	(Boston Scientific 2015)

Table 7: Battery Chemistries for Various AIMD Batteries

2.3.2. WIRELESS RECHARGING AND POWERING

Currently, wireless charging is currently used for neurostimulators and wireless powering for cochlear implants. The charging schemes between these two sets of devices are very different, but are designed for convenience to the patient. Neurostimulators typically are charged with a frequency of daily to weekly, depending on the settings set by the physician for the patient's needs. Conversely, cochlear implants are continuously wirelessly transmitted power via RF connection through the skin from an external device when the device is in use.

To understand current neurostimulator charging systems, we look at the charging systems from the two largest neuromodulator manufacturers, Medtronic and Boston Scientific. The Medtronic 37751 Recharger charging system is pictured in Figure 7 and includes a recharger connected to an antenna, shoulder belt and pouch and carrying case. The Boston Scientific Vercise charging system is shown in Figure 8 and works in a similar way but contains a 'charging collar' instead of a belt. The recharger is charged after plugging into the wall and

then with the antenna can be clipped to the belt thus holding the antenna in place and allowing the patient to move whilst charging. The belt can be changed depending on the type of neuromodulator and thus the area of implantation. Medtronic literature suggests that a regular schedule is key to charging their neurostimulator and that it may work for the patient to charge every day for 30 minutes or every 10 to 14 days for 4 hours depending on what their doctor says with their settings and patient preference. The systems contain an antenna and are therefore RF based, induction charging systems (Medtronic 2012). One small difference between the two systems is that the Boston Scientific system also comes with adhesive patches to allow the patient to stick the antenna in place and clip the recharging to clothing instead of using the additional belt (Boston Scientific 2017d).

Figure 7: Person wearing the Medtronic neurostimulator charging device (Medtronic 2017a)

Figure 8: Boston Scientific Vercise Charging System (Boston Scientific 2017d)

Cochlear implants are composed of an external sound processor with microphones and transmitter and an internal component composed of a receiver and electrode array. In contrast to neurostimulators, powering of cochlear implants is through constant RF signals sent transcutaneous via inductive coils within the receiver and transmitter. Due to limited space in this area, the internal component is small and therefore does not have the room for a large battery to power the device. Because of this RF link and the implant area, a magnet exists to help keep the external component in place, without the need for a headband. The external component which sends power through to the internal component is powered by small coin batteries which need regular replacement or charging (Zeng et al. 2008). Both major players in the cochlear implant market, Cochlear and Sonova use the same power scheme (Faltys, Kuzma & Gord 2001; Shaquer 2004).

2.3.3. Design Standards, Compliance and Regulation for AIMDs

Standards, compliance and regulation are significant parts of any product to be designed for a market, however, especially in medical devices where compromises in patient safety can result in significant health issues, if not death of patients. Whilst several bodies exist to create

standards, the International Organization of Standards (ISO) is globally one of the largest in the world, and partners with several organisations globally. Their standards are created from a need in a market, reviewed and updated where necessary every four years and are set by consensus within technical committees comprised of groups of experts from around the world including from academia, industry, non-government organisations, consumer associations and governments (ISO 2018). Whilst global standards are developed, each country or region may customise a standard or may refer to the global version. An example of this occurs in AIMDs where the *AS ISO 14708 Implants for surgery – Active implantable medical devices* where the international version was certified in 2014, the Australian version is certified in 2015 by the ISO's affiliate, *Australian Standards (AS)*.

Whilst global standards are set for medical devices, standards themselves are not law and thus a company developing a product would not necessarily have to comply with them. As such, governments use regulation and regulatory bodies to enforce standards in the design of medical products. In the United States of America, it is the Federal Drug Administration (FDA), in Europe, the European Union (EU) and in Australia, the Therapeutic Goods Administration (TGA) which enforce the standards they wish to enforce in medical devices. Companies must by law follow rules to be able to market and release a product and bear the associated costs (Kucklick 2013).

The primary standard that applies to AIMDs is ISO 14708 Implants for surgery – Active implantable medical devices'. Part 1 is a general standard for all AIMDs and refers to other standards for specific considerations. Several other parts exist for specific AIMDs including pacemakers, neurostimulators, circulatory support devices, infusion pumps, devices for tachyarrhythmia and cochlear implants. Additionally, *ISO 14283 Implants for surgery – Essential principles of safety and performance exists* as a broad standard for implantable medical devices, however AS ISO 14708 Annex B clarifies clauses between these two

standards that could apply to AIMDs. Lastly, a search of the ISO website (http://www.iso.org) will find there are a plethora of standards for medical devices and each of these may also apply for a new device, depending on the nature of the device (AS 2015).

In this section, we briefly outline the different aspects of the general standard ISO 14708-1 and standards for sterilization of an AIMD as it is these that would likely apply to a device proposed in this thesis. Note that also in ISO14708-1 are sections covering items that must accompany the AIMD such as packaging and instructions for the AIMD, however these would not directly affect the design of the proposed device and are therefore not covered here. Lastly, Table 8 is shows all standards referring to and by ISO 14708-1 and thus which may hold relevance (AS 2015).

Standard Number	**Standard Title**
ISO 8601	Data elements and interchange formats -- Information interchange -- Representation of dates and times
ISO 10993-1	Biological evaluation of medical devices -- Part 1: Evaluation and testing within a risk management process
ISO 11607-1	Packaging for terminally sterilized medical devices -- Part 1: Requirements for materials, sterile barrier systems and packaging systems
ISO 14155	Clinical investigation of medical devices for human subjects -- Good clinical practice
ISO 14971	Medical devices -- Application of risk management to medical devices
IEC 60068-2-14	Environmental testing – Part 2-14 Tests – Test N: Change of temperature
IEC 60068-2-27	Environment testing – Part 2-27: Tests – Test Ea and guidance: Shock
IEC 60068-2-47	Environmental testing – Part 2-47: Tests – Mounting of specimens for vibration and similar dynamic tests
IEC 60068-2-64	Environmental testing – Part 2-64: Tests –Test Fh: Vibration, broadband random and guidance
IEC 60601-1	Medical electrical equipment – Part 1: General requirements for basic safety and essential performance
IEC 62304	Medical device software – Software life cycle processes

Table 8 Table of Standards Referred to in ISO 14708-1 (AS 2015)

2.3.3.1. MARKINGS ON THE AIMD

The standard outlines in section 12, that where practical and applicable, the AIMD should bear the following (AS 2015):

- Trade name of the manufacturer
- Model or family name of the AIMD
- Batch or serial number of the AIMD
- Code identifying the manufacturing and year of manufacture

The markings should not rub off after being rubbed with a wet cloth containing water, 96% ethanol and isopropyl alcohol for 15 seconds each sequentially and without undue pressure. The markings should be clearly legible at the time of implantation for positive identification. The code should be readable even without surgical operation, if necessary. Lastly, bearing in mind training and accompanying documentation, any instructions for correct operation or parameter adjustment should be readable on the device to the user and where appropriate, the patient (AS 2015).

2.3.3.2. UNINTENTIONAL BIOLOGICAL EFFECTS

ISO 14708-1 has subsections 14.1 – 14.4 for addressing unintentional biological effects within section 14. Where an AIMD or other enclosed parts is not contained in a hermetically sealed, implantable, container which is impermeable, the device must be sterilized in a terminal way. The theoretical probability of the device having a viable microorganism must be equal or less than 10^{-6}. Further information on terminal processes for sterilization can be found in section 2.3.3.3 Sterilization which outlines relevant standards for various types of sterilization (AS 2015).

Another subsection deals with particulate matter. Specifically, any device which under normal use and which is in contact with body fluids, must not release particulate matter at the time of implantation. The manufacturer must provide testing in which surface-born particular

matter are collected and counted. One particular method using light obscuration particle counting is outlined and is used where there is doubt or dispute. However, the test is in particular for testing the ability of the device to be cleaned and for matter transferred from the packaging, but not for when the device is handled during transportation and storage. It should be carried out under sterile, laminar flow conditions. Further details of the test can be found in the standard, however it involves placing the AIMD in purified water and the water is then tested by passing a laser through the sample and the more light that is passed through and measured, the less particles there are (Beckman 2018). Additionally, specific standards apply for devices being used with the vascular system regarding amount of particles and particle size and the AAMI TIR42 standard is referenced (AAMI 2010). Otherwise, a manufacturer which does not think this test should apply, must conduct a risk assessment outlining another method for determining the count and size of particles (AS 2015).

Parts of an AIMD which are to come into contact with cells, body fluids, biological tissues or to penetrate the body, must also be assessed according to ISO 10993-1. This standard refers to AIMDs which through mechanical wear, fatigue loading or fractures, may generate degradation products. Data must be provided by the manufacturer which shows the biocompatibility of the parts has been demonstrated through either of the following (AS 2015):

a) Analogy with published data
b) Materials selected have been used previously and shown to be clinically biocompatible in a similar application
c) Where other devices already on the market have used the materials (evidence that the materials being used in the new device are traceable to the previously used materials, must be provided)
d) Showing data from published procedures for biological evaluation of parts of AIMDs

Lastly, some AIMDs have added chemicals on their surfaces for medicinal purposes. Where this chemical is a medicinal substance or a medicinal substance derived from human blood or serum, the substance must be declared both safe and beneficial. Data must be provided from appropriate methods showing the quality and safety of the substance (AS 2015).

2.3.3.3. STERILIZATION

Section 14 of ISO 14708-1 also mentions several standards for sterilization of AIMDs which are shown in Table 9. The names of each of the standards are indicative of the processes that are likely to be applied the electrodes if they were to be used. Each method will have its advantages and disadvantages, and present harsh conditions aimed at cleaning and killing any chemicals, biological molecules and organisms (AS 2015).

ISO Number	Title
ISO 11135	Sterilization of health-care products -- Ethylene oxide -- Requirements for the development, validation and routine control of a sterilization process for medical devices
ISO 11137-1	Sterilization of health care products -- Radiation -- Part 1: Requirements for development, validation and routine control of a sterilization process for medical devices
ISO 11137-2	Sterilization of health care products -- Radiation -- Part 2: Establishing the sterilization dose
ISO 11137-3	Sterilization of health care products -- Radiation -- Part 3: Guidance on dosimetric aspects of development, validation and routine control
ISO 17665-1	Sterilization of health care products -- Moist heat -- Part 1: Requirements for the development, validation and routine control of a sterilization process for medical devices
ISO 17665-2	Sterilization of health care products -- Moist heat -- Part 2: Guidance on the application of ISO 17665-1
ISO 17665-3	Sterilization of health care products -- Moist heat -- Part 3: Guidance on the designation of a medical device to a product family and processing category for steam sterilization
ISO 14937	Sterilization of health care products -- General requirements for characterization of a sterilizing agent and the development, validation and routine control of a sterilization process for medical devices
ISO 11737-1	Sterilization of health care products -- Microbiological methods -- Part 1: Determination of a population of microorganisms on products
ISO 11737-2	Sterilization of medical devices -- Microbiological methods -- Part 2: Tests

	of sterility performed in the definition, validation and maintenance of a sterilization process
ISO 25424	Sterilization of medical devices -- Low temperature steam and formaldehyde -- Requirements for development, validation and routine control of a sterilization process for medical devices
ISO 20857	Sterilization of health care products -- Dry heat -- Requirements for the development, validation and routine control of a sterilization process for medical devices

Table 9 Relevant Standards for Sterilization of Medical Devices

2.3.3.4. EXTERNAL PHYSICAL FEATURES

Section 15 of ISO 14708-1 deals with external features of AIMDs. For non-implantable portions of the AIMD, IEC 60601-1, part 9.3 is referenced. This section specifies that where an edge, sharp corner or rough surface can cause injury, it must be avoided. It adds that particular attention should be paid to frame or flange edges and burr removal. Regarding the implantable parts of an AIMD, ISO 14708-1 specifies that any edges or sharp corners that may result in excessive inflammation or reaction, which goes beyond the procedure for implantation, or any rough surfaces which do not serve a purpose, are unacceptable. Compliance in both cases is done through inspection (AS 2015).

2.3.3.5. ELECTRICITY

Section 16 of ISO 14708-1 deals with harm to a patient which may result from electricity. As with other potential causes of harm, any part of the AIMD that is external to the body, must comply with IEC 60601-1, specifically section 8.7. Otherwise, implantable parts of the AIMD must be electrically neutral and have a current density of less than or equal to 0.75 μA / mm^2, except for if the part requires something different for an intended function. Compliance with this is checked through assessment of the design analysis, calculations and test studies (AS 2015).

The standard also applies to insulation of parts. Where implanted leads or catheters have insulating parts for electrical conductors subject to electrical potential differences, the dielectric strength must be withstood to a voltage twice that which is to be applied to the part.

The insulating parts must be preconditioned with immersion in saline solution at 37°C ± 5°C for a minimum of 10 days, then be rinsed and wiped of surface water and have the dielectric test applied and complied with as per the manufacturers specified method (AS 2015).

2.3.3.6. HEAT

Section 17 of ISO 14708-1 refers to protection of the patient from harm caused by heat. The AIMD should not be 2°C above the normal operating temperature of the body (37°C) along the outer surface of the implant when implanted in the absence of external influences or when any single component fails. External influences include MRI, electrosurgery, external defibrillators, ultrasounds and electromagnetic fields. Where a device is intended to supply heat, the clinical effect should be documented in the risk management file (AS 2015).

2.3.3.7. IONIZING RADIATION

Section 18 of ISO 14708-1 outlines what must be done for an AIMD to comply with the standard. If the AIMD contains any radioactive substances, it must be a sealed source, the possible consequent exposure should be justified by the advantages for which the radioactive substances provide and the exposure should be kept to as low as achievable. Compliance is checked for the first case by assessment of the design analysis, supported by test studies. In the second case, assessment of the documentation in the risk assessment file must demonstrate acceptable residual risk. For the third case, compliance is checked by assessment of the manufacturer's calculations and data from test studies (AS 2015).

2.3.3.8. UNINTENDED EFFECTS

Section 19 of ISO 14708-1 deals with unintended effects that may cause harm to a patient by an AIMD. It contains several parts incorporating long term degradation of materials, batteries within AIMDs, component and software failure in AIMDs, any possible side effects of the AIMD, medicinal substances administered by AIMDs and transcutaneous energy transfer to and from AIMDs (AS 2015).

The standard states that for the lifetime of the implant, no unacceptable risk shall result from gradual, long term changes, if any, in the materials of the implant. Compliance is checked with (AS 2015):

a) Analogy with published data
b) Materials selected have been used previously and shown to be clinically biocompatible in a similar application
c) Where other devices already on the market have used the materials (evidence that the materials of the new device being used are traceable to the previously used materials, must be provided)
d) Showing data from published procedures for biological evaluation of parts of AIMDs

Where the AIMD has a power source which is not rechargeable, including a battery or pressure reservoir, an "elective replacement indicator" must be given, which provides warning in advance of the power sources depletion which may result in End of Service (EOS) of the AIMD. The elective replacement indicator signifies the beginning of the recommended replacement time (RRT) in which it is recommended by the manufacturer that the AIMD be replaced. Following the elective replacement indicator, a prolonged service period (PSP) must be defined by the manufacturer, which is the period where the device will continue to operate after the elective replacement indicator, but where it is recommended to be replaced within this period. If the AIMD has a rechargeable battery, information must be provided by the manufacturer on its recharge and replacement. Compliance is shown through calculation and testing results (AS 2015).

In the case of components or software of the AIMD, it must not cause what may result in unacceptable risk. The risk analysis of any component and its failure along with the risk control should be documented in the Risk Management File as per section 5.5.4 of ISO

14708-1. Additionally, software of an AIMD, or software that falls within the definition of an AIMD (see section 1.1), then the AIMD must comply with section 5.2 of ISO 14708-1 which is in regards to the general requirements for risk management. As such, compliance is checked by assessment of the documentation within the Risk Management File (AS 2015).

Typically, there may be unintended side effects of the intended use of an AIMD. However, ISO 14708-1 stipulates that this should not result in an unacceptable risk. Each of the side effects or benefits must be identified by reference to medical practices which are currently used, or where clinical investigations have been conducted in accordance with ISO 14155, an analogy or reference to this investigation can be used. Compliance for unintended side effects is checked through viewing the manufacturer's documentation (AS 2015).

Some medicinal substances that are administered to the body, are not compatible with all administering devices. In ISO 14708-1, where an AIMD is to come into contact with a medicinal substance, it must be designed to be compatible with the medicinal substance. Compliance is checked through assessment of the manufacturer's design analysis, calculations and data from studies (AS 2015).

Lastly, many devices now use wireless energy transfer to help either power the device or charge the battery powering the device. Hence, ISO 14708-1 stipulates that where an AIMD has the intention of using such transcutaneous energy transfer systems, the system should not have unacceptable risk as a result. This should be documented in the risk management file, showing that the residual risk is acceptable in order to show compliance (AS 2015).

2.3.3.9. EXTERNAL DEFIBRILLATORS

Defibrillators for use with emergency situations in which paddles are used to inject an electrical shock to the body are commonplace today and may affect the operation of any

AIMD. Section 20 of ISO 14708-1 covers various points that should be considered for AIMDs in regards to external defibrillators (AS 2015).

When an AIMD is connected to electrodes, the non-implantable part's functions should be designed to ensure that when the patient is defibrillated, that the AIMD is not permanently affected, except in the case where the defibrillator comes into direct contact with the electrodes. For testing of this, IEC 60601-1, section 8.5.5 is referenced (AS 2015).

Similarly, where an AIMD has leads ad electrodes and where the intention is to be implanted in the torso, the parts within the torso should be designed to ensure that when a patient is defibrillated, the functions should not be permanently affected, except where the parts come into direct contact with the defibrillator. To test this, two specific tests are given, (1) a defibrillation test voltage generator is applied with specific test conditions as per ISO 14708-1 and (2) a defibrillator pulse generator producing a truncated exponential waveform with specific test conditions is applied as per ISO 14708-1. Subsequently, the device should not be permanently affected and by reprogramming, settings can be recovered (AS 2015).

2.3.3.10. Electrical Fields Applied Directly to Patient

Section 21 of ISO 14708-1 deals with compliance for AIMDs applying electrical fields directly to a patient. Where the AIMD has parts which are electrically conductive and treats the body electrically, the device should be designed so it is not in the path of the electrical current that is being applied to the body nor within the part of the body being treated. Design calculations are used to check for compliance. Where there is a medical condition that may cause damage to the AIMD, documentation should be given – compliance is checked by seeing the accompanying information. Compliance for specific devices is found in subsequent parts of the standard (AS 2015).

2.3.3.11. Miscellaneous Medical Treatments

Devices of any nature can be affected by different physical phenomena such as shaking or magnetic forces. This very much applies to AIMDs where ultrasounds and MRI are used frequently with the human body for imaging and may affect the AIMD and standards regarding this are covered in section 22 of ISO 14708-1. As such, any AIMD beside leads and catheters must have its design and construction such that when it undergoes diagnostic ultrasonic energy levels, no irreversible change should result. Compliance is checked by a specific test which involves the AIMD being immersed in a water bath and the various surfaces being exposed to ultrasonic beams. After this test, no irreversible damage to any part of the AIMD should be found. In regards to magnetic resonance, a declaration from the manufacturer must be made as to what levels the patient can undergo without unacceptable risk. Reference is also made to ISO/TS 10974 for magnetic resonance and AIMDs (AS 2015).

2.3.3.12. MECHANICAL FORCES

Protections regarding mechanical forces and AIMDs is given in section 23 of ISO 14708-1. In particular, the standard covers drop tests, stress, strain and flexural forces applied to the implantable and non-implantable parts of the system, leads, catheters and connectors. This is summarised as follows (AS 2015):

- Non-implantable parts of an AIMD that may be hand held or portable, must be able to withstand the shocks from mishandling and dropping. A free-fall test must be conducted in accordance with IEC 60601-1, sections 15.3.4.1 and 15.3.4.2, after which the device must operate as per manufacturer specification.
- Implantable parts or parts carried by patients of an AIMD, excluding leads and catheters, must cope with mechanical forces from normal use, including before implantation. Compliance is checked through a vibration test in accordance with IEC 60068-2-47 and IEC 60068-2-64 with specific conditions given for frequency,

acceleration spectral density and its shape and duration, after which the part under test should operate as per the manufacturers specifications.

- Implantable leads or catheters should withstand tensile forces from during and after implantation or replacement, with no physical damage such as fracture or cracking to the body or insulation. Compliance is tested by assessment of the manufacturer's design, calculations and test data.
- Leads to be implanted, having multiple conductive components, must have strain relief from flexural stresses that may occur during or after implantation. Compliance is tested by assessment of the manufacturer's design, calculations and test data.
- Manufacturers must identify any implantable connectors that would be used by physicians to connect the parts of the AIMDs together and their performance identified. Over time or with reconnection, the quality and performance of the connection should not degrade. Compliance is tested by assessment of the manufacturer's design, calculations and test data.
- Since mechanical shocks may occur even during the implantation process, parts of the implantable parts other than the leads and catheters of the AIMD must withstand these shocks. Compliance testing is done in accordance with IEC 60068-2-27 and the shock shape, duration of shock and direction and number of shocks is given, after which, the parts should perform as per the manufacturers specifications.

2.3.3.13. ELECTROSTATIC DISCHARGE

Section 24 of ISO 14708.1 outlines how to deal with electrostatic discharge. The AIMD needs to be designed to ensure that in the event of electrostatic discharge to any electronically powered non-implantable parts of the device, no irreversible damage is done. If an electrostatic discharge does occur, the AIMD should be able to operate in a safe mode that would not result in unacceptable risk and which can be reset to restore function to the original

settings. Compliance is checked by inspection of the risk management file and functional testing. Compliance for specific devices is found in the other parts of ISO 14708 (AS 2015).

2.3.3.14. ATMOSPHERIC PRESSURE CHANGES

Section 25 of ISO 14708.1 outlines what standards an AIMD should meet regarding atmospheric pressure changes. It states that any device shall be capable of withstanding changes in pressure from when a user is in transit or under normal conditions. This is tested by data from the manufacturer in which the device must be placed under 70 kP ±3.5 kP and 150 kP ± 7.5 kP for more than 1 hour where no deformation should be found. Like other sections, standards for specific devices are found in other parts of ISO 14708 (AS 2015).

2.3.3.15. TEMPERATURE CHANGES

Section 26 of ISO 14708-1 covers standards regarding AIMDs and temperature changes. For non-implanted parts of an AIMD that are electrically powered, they must conform to 5.1 of ISO 14708-1 which refers to IEC 60101-1 and requires a risk analysis by the manufacturer for compliance. In regards to the implantable parts, they must be constructed and designed such that no change resulting from temperatures during transport or storage will be irreversible. To test this, in accordance with IEC 60068-2-14, the AIMD must be in its sterile packaging and be subjected to a range of temperatures. The minimum and maximum temperatures are either specified by the manufacturer or will be -10°C ± 3°C and 55°C ± °C with in either case a rate of change in temperature of 1°C ± 0.2°C/min (AS 2015).

2.3.3.16. ELECTROMAGNETIC NON-IONIZING RADIATION

Section 27 covers protections for AIMDs from electromagnetic non-ionizing radiation where it stipulates that where electrical influences such as external electromagnetic fields from malfunction, damage, heating and induced electrical currents in the patient locally should not result in unacceptable risk. Assessment of this in part depends on where the device, including implanted and patient carried parts, is to be used and thus the electromagnetic environment.

Where the device is to be used outside the clinical environment, the European Council Recommendation 1999/519/EC based on ICNIRP Guidelines 1998 should be used. Regardless of the environment however, the risks must be evaluated in design analysis and be a part of the risk control according to section 5.5.4 of ISO 14708-1. Specific guidance for particular devices in given in other parts of the standard (AS 2015).

2.3.3.17. RISK MANAGEMENT

Section 5.5 of AS ISO 14708 has several subsections referring to risk management of AIMDs. Specifically, it refers to Risk Management Policy, Risk management file, Risk management plan and Risk management process. In all cases, it refers to ISO 14971 which is titled *Medical devices – Application of risk management to medical devices (AS 2015)*.

For Risk Management policy, it states that policy that determines acceptable risk and residual risk acceptability is to be defined and documented by the manufacturer, where compliance is checked by inspection of the policy. Regarding the Risk management file, the manufacturer must create one and have entered all the relevant parts as mentioned in other parts of AS ISO 14708, where compliance is confirmed through an index with cross-references between the various parts. For the Risk management plan, it must be established and maintained by the manufacturer as per ISO 14971, however requirements relating to production and post-production collection and review may be excluded. Compliance for the Risk management plan is checked by inspection. The Risk management process must include Risk Analysis, Risk Evaluation and Risk Control as per ISO 14971, where compliance is confirmed by inspection of the risk management policy, conformity to 5.5.3 of ISO 14708 regarding policy and the risk management file contains the required documentation (AS 2015).

2.3.3.18. MISCONNECTION OF PARTS

It may be possible for misconnection of parts to present unacceptable risk with AIMDs. As such, where possible, the design and construction should be such that this is avoided,

otherwise instructions, warnings and markings should be provided. Risk assessment inspection is used for compliance (AS 2015).

2.3.3.19. BIOCOMPATIBILITY OF AIMDS

Biocompatibility of AIMDs is covered by *ISO 10993 Biological evaluation of medical devices*. Depending on the device, all of the following parts of the standard, with their associated tests and compliances may apply (ISO 2009):

- Part 1: Evaluation and testing within a risk management process
- Part 2: Animal welfare requirements
- Part 3: Tests for genotoxicity, carcinogenicity and reproductive toxicity
- Part 4: Selection of tests for interactions with blood
- Part 5: Tests for in vitro cytotoxicity
- Part 6: Tests for local effects after implantation
- Part 7: Ethylene oxide sterilization residuals
- Part 9: Framework for identification and quantification of potential degradation products
- Part 10: Tests for irritation and skin sensitization
- Part 11: Tests for systemic toxicity
- Part 12: Sample preparation and reference materials
- Part 13: Identification and quantification of degradation products from polymeric medical devices
- Part 14: Identification and quantification of degradation products from ceramics
- Part 15: Identification and quantification of degradation products from metals and alloys
- Part 16: Toxicokinetic study design for degradation products and leachables

- Part 17: Establishment of allowable limits for leachable substances
- Part 18: Chemical characterization of materials
- Part 19: Physico-chemical, morphological and topographical characterization of materials (Technical Specification)
- Part 20: Principles and methods for immunotoxicology testing of medical devices (Technical Specification)

The general principles of ISO 10993 section 4 are useful in understanding its application and a summary is given here (ISO 2009):

- Risk management process: as part of ISO 14971, a structured biological evaluation is part of a risk management process.
- Selection of materials: fitness for purpose in the selection of materials regarding characteristics and properties shall be the first consideration.
- Overall biological evaluation: manufacturing materials, additives, process contaminants and residues as per ISO 10993-7, leachable products as per 10993-17, degradation products as per 10993-9, 10993-13, 10993-14 and 10993-15, final product component interactions, final product performance and characteristics and final product physical characteristics.
- Choice of tests and data interpretation: shall take into account chemical composition of the materials.
- Known possible biological hazards: these shall be taken into account for every material and final product. Test results are not a guarantee, thus biological investigations should be followed by observations for unexpected adverse reactions or events during device use.

- *In vitro* or *in vivo* tests: these shall be on end-use applications and conducted according to Good Laboratory Practice or ISO/IEC 17025.
- Re-evaluation of materials or final product: this is necessary where the following occur: (1) changes in source or specification of the material, (2) changes in formulation, processing, primary packaging or sterilization, (3) changes in instructions or storage, (4) changes in intended use of product or (5) evidence of product causing adverse effects.
- Accounting for other factors: this includes mobility and nature of constituent chemicals, other non-clinical tests, post-market experience and clinical studies.

ISO 10993-1 also looks at classification of devices, which then helps to select which particular tests to run. Devices are categorised by the nature of contact with the body and duration of contact with the body. Subcategories for the nature of contact include surface contact devices, external communicating devices and implant devices whilst for duration of contact, categories include limited exposure (up to 24 hours), prolonged exposure (24 hours to 30 days) and permanent contact (exceeding 30 days). Table A.1 of ISO 10993-1 is given in Figure 9 which indicates the selection of tests based on the categories, however the risk assessment of the AIMD will determine other tests for organ specific toxicities, immunotoxicity, reproductive/developmental toxicity, biodegradation, carcinogenicity and chronic toxicity (ISO 2009).

Table A.1 — Evaluation tests for consideration

Medical device categorization by			Biological effect							
nature of body contact (see 5.2)		contact duration (see 5.3) A – limited (⩽ 24 h) B – prolonged (> 24 h to 30 d) C – permanent (> 30 d)	Cytotoxicity	Sensitization	Irritation or intracutaneous reactivity	Systemic toxicity (acute)	Subchronic toxicity (subacute toxicity)	Genotoxicity	Implantation	Haemocompatibility
Category	Contact									
Surface device		A	X [a]	X	X					
		B	X	X	X					
		C	X	X	X					
	Mucosal membrane	A	X	X	X					
		B	X	X	X					
		C	X	X	X		X	X		
	Breached or compromised surface	A	X	X	X					
		B	X	X	X					
		C	X	X	X		X	X		
External communicating device	Blood path, indirect	A	X	X	X	X				X
		B	X	X	X	X				X
		C	X	X		X	X	X		X
	Tissue/bone/dentin	A	X	X	X					
		B	X	X	X	X	X	X	X	
		C	X	X	X	X	X	X	X	
	Circulating blood	A	X	X	X	X				X
		B	X	X	X	X	X	X	X	X
		C	X	X	X	X	X	X	X	X
Implant device	Tissue/bone	A	X	X	X					
		B	X	X	X	X	X	X	X	
		C	X	X	X	X	X	X	X	
	Blood	A	X	X	X	X	X		X	X
		B	X	X	X	X	X	X	X	X
		C	X	X	X	X	X	X	X	X

[a] The crosses indicate data endpoints that can be necessary for a biological safety evaluation, based on a risk analysis. Where existing data are adequate, additional testing is not required.

Figure 9 Table A.1 from ISO 10993-1 on Evaluation tests for consideration (ISO 2009)

2.4. Research in Powering AIMDs

2.4.1. Wireless Charging

One obvious method to help address the powering of active implanted medical lies in wireless recharging of the batteries. In each case, energy is transferred from an external device to an internal one through the skin via methods such as inductive coupling, optical charging and ultrasonics. Whilst as suggested previously, some current AIMDs already use

inductive coupling charging, this area and the other two areas still receive significant attention from researchers around the world.

2.4.1.1. INDUCTIVE COUPLING

Inductive coupling does show some promise, however issues around alignment, size of receiving antenna and the carrier frequency with tissue absorption have been reported (Cao et al. 2012). The technology requires two coils, one implanted inside the body and another in a device outside the body. A varying voltage signal applied to the external coil induces a similarly varying voltage signal on the internal coil due to the magnetic inductive coupling. In such a system, the energy efficiency is of major concern and this is determined by such parameters as the resonant frequency, distance between the coils, alignment and coupling matching between the two coils (Amar, Kouki & Cao 2015).

Care needs to be taken for the frequency for charging AIMDs to be in the low megahertz or kilohertz ranges so as to avoid tissue heating and other side effects (Cao et al. 2012; Ghovanloo & Najafi 2007). In this light, Li et al proposed a 13.36 MHz wireless power transfer system that also includes a reconfigurable resonant regulating rectifier. The proposed system had a maximum power transfer was 102 mW and had an efficiency of 92.6% (Li, Tsui & Ki 2015). Work by Monti et al proposed a system for powering pacemakers that can operate at a high frequency of 403 MHz, delivering up to 1 mW with efficiency of 5.24 % and within safety guidelines (Monti, Arcuti & Tarricone 2015). Another problem for use of this technology with AIMDs is the need for miniaturization. This is a particular issue for devices such as cochlear implants where their efficiency needs to be high since the maximum energy transferred is low due to small coil sizes. Zhao et al proposed an array of coils to help accommodate this, giving a power gain of 16.4 dB (Zhao, Kuo & Niknejad 2017). Other work by Koulouridis et al examines the use of a compact-size planar inverted F-antenna using different frequencies and schemes for powering deeply implanted active medical devices

(Koulouridis et al. 2016). Ho et al also proposes the use of midfield powering to overcome issues of powering deeply implanted medical devices (Ho, Kim & Poon 2013; Ho et al. 2014).

2.4.1.2. OPTICAL CHARGING

Optical charging systems are composed of an implantable photovoltaic cell and an external laser diode unit set at near-infrared wave lengths aimed through the skin toward the voltaic cell. In theory, light does not influence biological tissue significantly below 320 nm, and depending on the wave length, the laser may penetrate deep into the skin (Anderson & Parrish 1981). Like inductive coupling, optical charging systems also have the ability to communicate to the AIMD, however unlike inductive coupling, optical systems may also be more secure (Mosenia & Jha 2017) and there is less risk of electromagnetic interference (Saha et al. 2017). Only recently though has these ideas been formerly characterised as numerous studies have used animal models. Song et al recently used several skin samples from cadavers, finding that the measured power density was influenced by the thickness and tone of the skin, where skin which was thinner and lighter gave the highest power densities of up to 9.05 mW/cm^2 (Song et al. 2017).

Various optical charging and powering systems for AIMDs continue to be developed (Helmers et al. 2015; Liu et al. 2015; Moon, Blaauw & Phillips 2017; Saha et al. 2017). One particular issue with implanting solar cells is the need for biocompatibility. Thin films of epoxy, a long used biocompatible material have been used previously (Goto et al. 2001) however Ahnood et al suggest that diamond encapsulated cells have better light characteristics in addition to biocompatibility, being able to deliver 2.7 mW to an implant. Their device was 1.5 x 1.5 x 0.06 mm^3, giving a power density of 20 mW/mm^3 which is greater than many inductive coupling devices (Ahnood et al. 2016). Shimatani et al have also developed an EMG sensor powered by near-infrared light. The system was implanted in rats

for over 12 weeks and was able to constantly measure EMG signals (Shimatani et al. 2013). Song et al have also created an implantable flexible photovoltaic device, tested in live animal models to power a pacemaker and was able to generate up to 647 μW (Song et al. 2016). Along the same lines, Haeberlin et al have also demonstrated a pacemaker powered by solar cells directly without the need for a battery. The device had no external component and was powered purely by sunlight or indoor lighting (Haeberlin et al. 2015). This method however still suffers from inefficiencies and skin heating issues (Amar, Kouki & Cao 2015).

2.4.1.3. ULTRASONIC CHARGING

Ultrasonic charging systems work by an external ultrasonic generator sending acoustic waves through the skin and body to an implanted ultrasonic transducer. The internal component can operate either in a capacitance or piezoelectric based mode, however the former uses voltages considered too high for implantation (Amar, Kouki & Cao 2015). The technology is considered efficient, can be small, receives no electromagnetic interference and can also communicate data between the internal and external components. Generally the use of ultrasonic waves for the body has been considered safe, however some have reported a burning feeling, possibly due to gas within some cell types heating up (Kennedy, Ter Haar & Cranston 2003). Additionally, whilst one can easily tune the vibration frequency for depth from long wavelengths, the waves spread in a pizza slice like shape, thus affecting areas otherwise not needing to be vibrated (Amar, Kouki & Cao 2015). Numerous studies have been performed for the use of this technology in powering AIMDs (Basaeri et al. 2016; Basaeri, Christensen & Roundy 2016; Basaeri & Roundy 2017; Chang et al. 2017; Chang et al. 2015; Charthad et al. 2015; Moon et al. 2017; Ozeri & Shmilovitz 2014; Shmilovitz et al. 2014; Vihvelin et al. 2016; Wang et al. 2017).

In any case though, if a patient is to be set freer of their medical conditions by a medical implant, the anxiety of their battery running out of charge will still exist, but simply on a

different time line and where they must administer to themselves a fix which therefore still prevents them from getting on with their lives.

2.5. ENERGY HARVESTING

Other research seeking to address this problem has looked at various forms energy harvesting technologies. Energy harvesting seeks to transform latent energy such as mechanical energy through piezoelectric materials, electrostatic generators and electromagnetic generators, heat into electrical energy via Peltier cells and chemical energy through biological fuel cells such as microbial fuel cells and enzymatic biofuel cells. To date, each of these technologies has its issues which affects longevity or power density (Amar, Kouki & Cao 2015). Since biological fuel cells are a key focus of this thesis, they are treated separately in a subsequent section.

2.5.1. THERMOELECTRIC HARVESTING

Thermoelectric harvesting works by using Peltier cells to generate electricity by converting heat energy flowing through the cell. The heat flow is generated by utilising the thermal gradient between the body's internal body temperature and the environmental temperature. The body's internal temperature is changed due to different activities, where the metabolic energy expenditure varies depending on the activity. Table 10 summarises the energy expenditure for different common activities. The body distributes blood throughout the body, allowing it to distribute heat throughout the body as well. Table 11 shows temperatures that can be expected on different parts of the skin. Note that the body through homeostasis, regulates its core temperature to within 36 to 38°C (Zhou et al. 2017).

The maximum temperature difference between where an implant is likely to be placed and the skin is approximately 8K, giving a maximum power output of 180 $\mu W/cm^2$ (Amar, Kouki & Cao 2015). Cascading these devices is possible, but this then faces issues of size as well as the fact that the semiconductors tend to be toxic materials, not to mention that under many environmental conditions, humans tend to where clothing, which brings the skin temperature

closer to body temperature. If there is no clothing achieving this, it tends to be due to warmer weather which again is closer to core body temperature.

Activity	METs
Walking, 2 mph	2.8
Walking, 2.5 mph	3
Walking, 3 mph	3.5
Walking, 3.5 mph	4.3
Walking, 4 mph	5
Jogging, general	7
Jogging, in place	8
Running, 4 mph	6
Running, 6 mph	9.8
Running, 8 mph	11.8
Running, 10 mph	14.5
Running, 12 mph	19
Bicycle, general	7.5
Bicycle, 5.5 mph	3.5
Bicycle, 9.4 mph	5.8
Bicycle, 10-11.9 mph	6.8
Bicycle, 12-13.9 mph	8
Bicycle, 14-15.9 mph	10
Bicycle, 16-19 mph	12
Bicycle, >20 mph	15.8
Home sweeping	2.3-3.8
Mopping	2.5
Cooking	2.5
Making bed	3.3

Table 10: Table from Zhou et al with caption 'Human body energy expenditure for selected physical activities' (McArdle, Katch & Katch 2010; Shephard 2011; Starner 1996; Zhou et al. 2017)

The most famous of the thermal energy harvesting applications is most likely the Seiko watch, which produced 22 μW from a 1.5 K temperature difference, from which its Peltier cell was said to have generated an open circuit voltage of 300 mV (Kishi et al. 1999). Aside from this, many TEG applications have been developed in research such as pulse oximeter (Torfs et al. 2006), EEGs (Leonov et al. 2009; Torfs et al. 2008; Zhang et al. 2013), hearing aid (Lay-Ekuakille et al. 2009), ECGs (Carmo, Gonçalves & Correia 2010; Leonov et al. 2009; Zhang et al. 2013) and EMG (Zhang et al. 2013). Only one application is for an AIMD which is the pacemaker (Watkins, Shen & Venkatasubramanian 2005). Some TEGs designed

for implantation do also exist, including some flexible TEGs (Katic, Rodriguez & Rusu 2016, 2017; Khan, Dahiya & Lorenzelli 2014; Mays et al. 2016; Rojas et al. 2017; Suarez et al. 2017; Yang, Xu & Liu 2014). Other than this, much of the focus of TEG work has been in developing materials and the overall systems around them (Liu et al. 2017; Lu et al. 2016; Oh et al. 2016; Siddique et al. 2016; Wan et al. 2016; We, Kim & Cho 2014; Weber et al. 2006).

Body sites	Minimum time (*h*)	Maximum time (*h*)	Minimum value (°C)	Maximum value (°C)	Mean value (°C)
Foot	15−16	06−07	33.39(0.42)	34.38(0.22)	34.03(0.25)
Hand	14−15	00−01	31.21(0.32)	32.13(0.34)	31.72(0.23)
Thigh	01−02	12−13	33.47(0.46)	34.31(0.43)	33.82(0.42)
Infra	06−07	12−13	33.43(0.23)	34.07(0.19)	33.78(0.18)
Forehead	07−08	18−19	33.89(0.22)	33.23(0.28)	33.58(0.21)
Distal	15−16	06−07	32.30(0.24)	33.25(0.18)	32.88(0.18)
Proximal	07−08	12−13	33.81(0.19)	34.38(0.26)	34.06(0.21)

Table 11: Table from Zhou et al with caption 'Human skin temperature for different body measuring sites under variable ambient temperatures. All the data in the table are with unit °C and the number in the brackets are the standard deviation of the measuring temperatures while the unbracketed value is the mean temperature' (Suarez et al. 2016; Webb 1992; Zhou et al. 2017)

2.5.2. MECHANICAL ENERGY HARVESTING

Mechanical energy harvesting in biomedical applications encompasses several solutions including piezoelectric generators, electrostatic generators and electromagnetic generators (Amar, Kouki & Cao 2015). A summary of the amounts of energy possible from different parts of the body is shown in Table 12.

Electrostatic and electromagnetic generators work to mechanically move an electrostatic electrode against a permanent electrode or a magnetic coil against a permanent magnet respectively, in turn generating an electrostatic potential energy or voltage from magnetic flux. Some interesting work has be performed with both types of systems, including electrostatic generators using the heartbeat and ventricular motion to generate up to 58 μW as well as a MEMS based electrostatic generator that was able to harvest up to 80 μW. From the same beating of the heart, electromagnetic generators have been able to harvest up to 200 μW

and up to 1.1 mW from breathing force within the abdomen and 400 μW from walking (Amar, Kouki & Cao 2015). Aside from specific biomedical examples, mechanical energy harvesters have been designed and can generally be implanted. The best examples of rotary electromagnetic energy harvesters include Piers et al producing 28 W (Peirs, Reynaerts & Verplaetsen 2003), Rome et al producing 7.4 W (Rome et al. 2005), Arnold et al producing 8 W (Arnold et al. 2006) and Donelan et al producing 5 W with up to 63% efficiency (Donelan et al. 2008). Some notable oscillatory electromagnetic energy harvesting studies include Saha et al producing up to 2.5 mW (Saha et al. 2008), Bedekar et al producing 3 mW (Bedekar, Oliver & Priya 2009), Samad et al producing 5.185 mW (Samad et al. 2016), Högberg producing 5 mW (Högberg et al. 2016) and Nico producing 9 mW (Nico et al. 2016). Good high power electrostatic energy harvesting studies include Roundy et al with 116 μW (Roundy, Wright & Pister 2002), Tashiro et al with 35 μW (Tashiro et al. 2002), Sterken et al with 50 μW (Sterken et al. 2003), Chiu et al with 31 μW (Chiu & Tseng 2008) and Choi et al with 35.3 μW (Choi, Han, et al. 2011).

Activity	**Power (*W*)**	**Activity**	**Power (*W*)**
Foot strike	2−20	Blood circulation	~0.9
Ankle motion	~33.4	Respiration	~1.0
Knee motion	~36.4	Elbow motion	~2.1
Hip motion	~38	Shoulder motion	~2.2

Table 12: Table from Zhou et al with caption 'Available energy from human body during daily activities' (Niu et al. 2004; Riemer & Shapiro 2011; Starner 1996)

Piezoelectric generators involve using piezoelectric materials which under stretching or compression, will generate electric charge. Some notable studies in piezoelectric energy harvesting include Kim et al with 39 mW (Kim et al. 2004), Granstrom et al with 45.6 mW (Granstrom et al. 2007), Wan et al with 11mW (Wang et al. 2007) and Pillatsch et al with 21 mW (Pillatsch, Yeatman & Holmes 2012).

Nonetheless, each technology has its problems where in the case of electrostatic generators, the overall power is still low whilst for electromagnetic generators, and it is difficult to manufacture magnets with good properties at the small scale, not to mention that each either requires movement or the potential for interference with key body parts (Amar, Kouki & Cao 2015).

2.6. MICROBIAL FUEL CELLS

2.6.1. HOW MFCS WORK

Microbial fuel cells in a broad sense are able to break down organic substrates such as glucose and generate electricity. The powering of AIMDs is one of many applications proposed for this technology, which includes powering of remote sensors, biohydrogen production, wastewater treatment and biosensing. Figure 10 illustrates the process of electricity generation in a MFC. The most basic MFC which is the dual chamber MFC, is composed of two chambers separated by a proton or cation exchange membrane. In the anode chamber is the analyte, bacteria, organic substrate and anode electrode. In the cathode chamber is a catholyte, cathode electrode and oxygen. The electrodes are connected electrically by an electronic circuit that is to be powered (Logan et al. 2006).

Bacteria break down glucose, and as they grow, they output electrons. These electrons are captured by the anode electrode either directly or indirectly, where the electron then flows through an electric circuit to power a device before arriving at the cathode electrode. During this process, bacteria also output hydrogen which diffuses through the membrane and interacts at the cathode electrode with the oxygen and electrons, creating H_2O (water) (Logan et al. 2006).

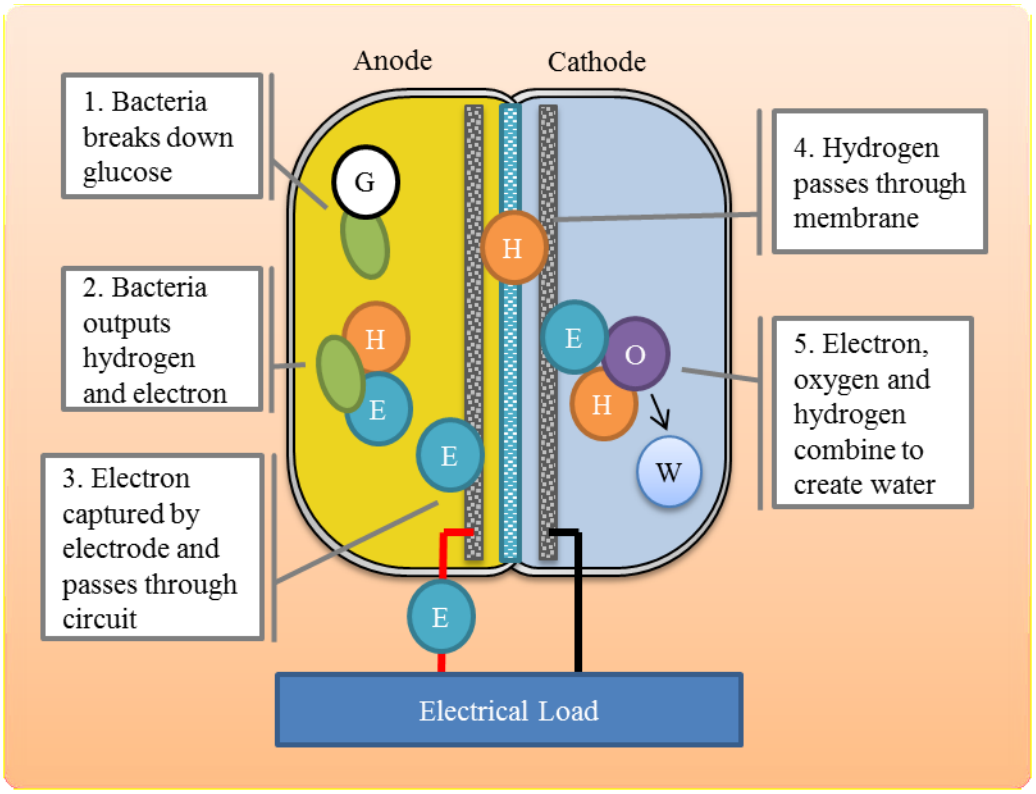

Figure 10: Illustration of how a microbial fuel cell operates

The most common MFC is the H-cell setup like that pictured in Figure 11. It is suitable for testing basic parameters in MFCs such as materials, bacteria and electrolytes. It should be noted that these systems can have high internal resistance, and when testing these basic parameters, electrodes and membranes should be kept to a similar size unless they themselves are being tested (Logan et al. 2006).

2.6.2. Microbe Selection in MFCs

To fully understand the selection of bacteria for MFCs, it is important to firstly understand the mechanisms for which electrons are transferred from bacteria to the anode electrode. One of these methods is indirect where either exogenous mediators are added to the anode chamber or bacteria can produce their own. Bacteria such as *Shewanella oneidensis* (Freguia, Tsujimura & Kano 2010), *Pseudomonas alcaliphila and Pseudomonas aeruginosa (Rabaey et al. 2004)* have been known to produce their own mediators. Direct electron transfer occurs through two mechanisms, the first is via the outer membrane of the bacteria called

cytochrome-C as demonstrated in bacteria such as *Geobacter sulfurreducens (Lovley 2006)* and *Shewanella oneidensis MR-1 (Hartshorne et al. 2007; Shi et al. 2006; Xiong et al. 2006).* Additionally, these bacteria are also known to have extracellular conductive pili, also known as bacterial nanowires (Gorby et al. 2006; Reguera et al. 2005). A list of various bacteria used in MFCs is shown in Table 13, including where possible, their highest current or power densities and electron transfer mechanisms.

Figure 11: Photograph of a H-Cell MFC

Bacteria	**Maximum Current or Power Density**	**Nanowires**	**c-type cytochromes**	**Excreted Mediators**	**Unknown**
Geobacter sulfurreducens (Inoue et al. 2011; Juárez et al. 2009; Mehta et al. 2006; Min, Cheng & Logan 2005; Smith et al. 2014)	3174 mA / m^2	Type IV	c-type cytochrome Z	-	-

Geobacter metallireducens (Holmes et al. 2008; Keller et al. 2014)	40 mW / m^2	-	OmcB and OmcE c-type cytochromes	-	-
Shewanella oneidensis MR-1 (Clarke et al. 2011; Gorby et al. 2006; Leung et al. 2013; Von Canstein et al. 2008)	3000 mW / m^2, 21.3 μA / cm^2	Type II	c-type	Flavins, riboflavins	-
Shewanella oneidensis DSP-10 (Biffinger et al. 2008; Biffinger et al. 2007; Bretschger et al. 2007; Ringeisen et al. 2006)	2000 mW / m^2	-	-	-	-
Shewanella putrefaciens (Clarke et al. 2011; Pandit et al. 2014)	4920 mW / m^3	-	MtrC and OmcA c-type cytochromes	FAD transporter	-
Rhodopseudomonas Palustris (Xing et al. 2008)	2720 mW / m^2	-	c-Type cytochromes	-	-
Thermincola ferriacetica (Marshall & May 2009; Wrighton et al. 2011)	12,000 mA / m^2	-	-	Anthra quinone-2,6-disulfonate	
Pseudomonas aeruginosa (Dietrich et al. 2006; Jayapriya & Ramamurthy 2012; Shen et al. 2014; Von Canstein et al. 2008; Yong et al. 2014)	4310 mW / m^2	-	-	Pyocyanin, phenazine-1-carboxamide	-
Desulfovibrio desulfuricans	233 mA / m^2, 0.51 mW /	-	c-Type cytochromes	-	-

(Kang et al. 2014; Zhao et al. 2008)	cm^2				
Desulfovibrio alaskensis (Keller et al. 2014)	N/A	-	QrcA Transmembrane complexes, Tetraheme cytochrome C3	-	-
Klebsiella pneumonia (Deng et al. 2010)	199 mA / m^2	-	-	2,6-di-tert-butyl-p-benzoquinone	-
Escherichia coli (Goldbeck et al. 2013; Qiao et al. 2008; Zhang et al. 2006)	3390 mA / m^2, 600 mW / m^2	-	-	-	X
Saccharomyces cerevisiae (Prasad et al. 2007; Raghavulu et al. 2011)	282 mA / m^2	-	-	-	X
Lysinibacillus sphaericus (Nandy, Kumar & Kundu 2013)	85 mW / m^2	-	-	-	X
Citrobacter sp. (Xu & Liu 2011)	205 mA / m^2	-	-	-	X
Ochrobactrum sp. (Li et al. 2014; Zuo et al. 2008)	2625 mW / m^3, 89 mW / m^2 708 mA / m^2	-	-	-	X
Clostridium butyricum EG3 (Park et al. 2001; Schröder, Nießen & Scholz 2003)	N/A	-	-	-	X
Desulfuromonas	0.5 mA	-	-	-	X

acetoxidans (Bond et al. 2002)					
Rhodoferax ferrireducens (Chaudhuri & Lovley 2003)	71 mA / m^2	-	-		X
A3 (Aeromonas hydrophila) (Pham et al. 2003)	N/A	-	-	-	X
Desulfobulbus propionicus (Holmes, Bond & Lovley 2004)	28.35 mA / m^2	-	-	-	X
Geopsychrobacter Electrodiphilus (Holmes et al. 2004)	121.43 mA / cm^2	-	-	-	X
Geothrix fermentans (Bond & Lovley 2005)	N/A	-	-	-	X
Acidiphilium sp. 3.2 (Borole et al. 2008)	12.6 mW / m^2	-	-	-	X
Klebsiella pneumoniae L17 (Zhang et al. 2008)	409.71 mW / m^2	-	-	-	X
Thermincola sp. strain Jr (Wrighton et al. 2011)	37 mW / m^2	-	-	-	X
Pichia anomala (Prasad et al. 2007)	2900 mW / m^3	-	-	-	X

Table 13: Various Bacteria Used in MFCs with Maximum Current or Power Density and Electron Transfer Mechanisms

2.6.3. MEMBRANE SELECTION IN MFCS

Most MFCs will require a membrane to separate the two chambers of a MFC (Logan et al. 2006). The primary duty of the membrane is to stop the anode electrolyte from migrating to

the cathode as well as prevent air (in particular, oxygen) from moving in the opposite direction (Rahimnejad et al. 2014). The most common off the shelve membrane is Nafion-117 by Dupont with Ultrex CMI-7000 by Membranes International being a cost effective though less used alternative (Harnisch, Schröder & Scholz 2008; Kim et al. 2007; Logan et al. 2006; Rabaey et al. 2005). Both Nafion-117 and Ultrex are cation exchange membranes. Other materials developed and used for MFC membranes have been ultrafiltration membranes (Kim et al. 2007), course pore filter materials (Zhang et al. 2009), porous fabrics (Fan, Hu & Liu 2007; Zhuang et al. 2009), anion exchange membranes (Kim et al. 2007; Peighambardoust, Rowshanzamir & Amjadi 2010; Zhuang et al. 2012; Zuo, Cheng & Logan 2008), microfiltration membranes (Sun et al. 2009; Zuo et al. 2007), glass fibres (Mohan, Raghavulu & Sarma 2008; Zhang et al. 2009), Zirfon (Pant et al. 2010) and Hyfon (Ieropoulos, Greenman & Melhuish 2010). Aside from these, bipolar membranes, which consist of both cation and anion exchange properties and have been used mostly for high salinity water treatment (Harnisch & Schröder 2009; Zhuang et al. 2012).

Whilst Nafion has been the most common membrane, it does have some problems including issues with its negatively charged sulfonate groups stopping the movement of protons over time (Kelly et al. 2005; Okada et al. 1998; Okada et al. 1997), inconsistent cation transport rates (Chae et al. 2007; Rozendal, Hamelers & Buisman 2006) and instability over 90°C (Ghassemi, McGrath & Zawodzinski 2006; Rowe & Li 2001). Rozendal et al have also investigated Nafion-117's effects on the cathode pH and performance of MFCs. They found that transportation of cations other than protons were found to be the same as the number of electrons that went through the circuit and that electro dialysis was the driving force for cation transport, meaning that electroneutrality was maintained solely by cations, not protons. In the long term, this can lead to acidification in the anode chamber which is not healthy for the bacteria (Gil et al. 2003; Liu & Logan 2004; Rahimnejad et al. 2014; Rozendal, Hamelers

& Buisman 2006). Ghasemi et al found the negative impact of biofouling of the membrane on power output and thus also investigated the performance of pre-treatments of Nafion-117. In their device, biofouling led to a maximum power output of 20.9 mW / m^2 whilst their pre-treated membrane led to a maximum power output of 103 mW / m^2 (Ghasemi et al. 2013).

2.6.4. ELECTRODE SELECTION IN MFCS

The choice of material for the electrode is also quite important since it is at the surface of the electrodes that the bacteria interact with and where chemical reactions take place. In general, it is acceptable to use the same material for both the anode and cathode electrodes (Santoro et al. 2017). Most studies have used the family of carbonaceous and metallic materials for the anode electrodes primarily because they have to varying degrees, the following important characteristics: electrical conductivity, low cost, corrosion resistance, are environmentally friendly, high mechanical strength, biocompatibility and workable surface area. A summary of various materials used as electrodes in shown in Table 14 and photos of the materials are shown in Figure 12.

Name	Description	Reference
Carbon cloth	• High cost • High surface area • High electrical conductivity • High porosity • Flexible and mechanically strong	(Guerrini, Grattieri, et al. 2014; Santoro et al. 2011; Santoro et al. 2012; Santoro, Li, et al. 2013; Zhao et al. 2008)
Carbon brush	• Central 'backbone' is usually titanium, thus guaranteeing good conductivity • Costs decreasing due to ongoing work • Optimal surface to volume ratio • Composed of carbon fibres around titanium core	(Feng, Yang, et al. 2010; Liao et al. 2015; Logan et al. 2007; Santoro, Ieropoulos, et al. 2013a; Santoro, Ieropoulos, et al. 2013b)

Carbon rod	• Low surface area • Affordable • Not often used	(Jiang & Li 2009; Liu, Ramnarayanan & Logan 2004)
Carbon mesh	• Low porosity • Foldable to make 3D structure • If using flow, low durability • Relatively low cost and durability	(Wang et al. 2009; Wu et al. 2017)
Carbon veil	• Porous and 3D • Foldable and robust • Highly porous • Fairly high electrical conductivity	(Artyushkova et al. 2016; Boghani et al. 2014; Gajda et al. 2016; Ieropoulos, Greenman & Melhuish 2008, 2010; Kim et al. 2012; Liu et al. 2010; Winfield et al. 2014; You et al. 2016)
Carbon paper	• Used mostly in small scale due to cost • Expensive • Not porous	(Santoro et al. 2014; Srikanth et al. 2008)
Carbon felt	• Commonly used • Highly porous and electrically conductive • If thick, mechanical strength is good • Fairly reasonable cost	(Calignano et al. 2015; Lv et al. 2012; Roy et al. 2014; Seviour et al. 2015; Zhu et al. 2011)
Granular activated carbon	• Often compressed to help increase conductivity • High surface area • Often used for adsorption of pollutants • Low conductivity	(Jiang et al. 2011; Jiang & Li 2009; Yasri & Nakhla 2017; Zhao et al. 2016)
Granular graphite	• Low cost, high conductivity, high porosity • Low surface area than granular activated carbon due to not activation	(Feng, Lee, et al. 2010; Rabaey et al. 2005) 266

Carbonized cardboard	• Low cost • High electrical conductivity and porosity • 3D material composed of corrugated cardboard	(Baudler, Riedl & Schröder 2014; Kretzschmar et al. 2017; Schrott et al. 2011)
Graphite plate	• High mechanical strength, often used for support • Highly conductive electrically • Low cost relatively • Low surface area and surface to volume ratio	(Dewan, Beyenal & Lewandowski 2008; ter Heijne et al. 2008)
Reticulated Vitreous Carbon	• Unique for its high porosity and high conductivity • Porosity is particular good for biofilm formation • Fragile and expensive	(He, Minteer & Angenent 2005; Lepage et al. 2012)
Stainless steel plate	• Highly conductive • Robust • Cheap • Not porous	(Grattieri et al. 2015; Guerrini, Cristiani, et al. 2014; Guo et al. 2016; Hou et al. 2014; Ketep et al. 2014; Ledezma et al. 2015; Zheng et al. 2015)
Stainless steel mesh	• Highly conductive • Robust • Cheap • Reasonable surface to volume ratio	(Grattieri et al. 2015; Guerrini, Cristiani, et al. 2014; Guo et al. 2016; Hou et al. 2014; Ketep et al. 2014; Ledezma et al. 2015; Zheng et al. 2015)
Stainless steel scrubber	• Highly conductive • Robust • Cheap • Highly porous • Can be made to fit	(Grattieri et al. 2015; Guerrini, Cristiani, et al. 2014; Guo et al. 2016; Hou et al. 2014; Ketep et al. 2014; Ledezma et al. 2015; Zheng et al. 2015)
Silver sheet	• Can be poisonous to bacteria, hence	(Baudler et al. 2015)

	inhibits biofilm formation • Not porous	
Nickel sheet	• Poisonous to bacteria, hence inhibits biofilm formation • Not porous	(Baudler et al. 2015)
Copper sheet	• Poisonous to bacteria, hence inhibits biofilm formation • Not porous	(Baudler et al. 2017; Baudler et al. 2015)
Gold sheet	• Expensive • Not porous	(Baudler et al. 2015)
Titanium sheet	• Expensive • Not porous	(ter Heijne et al. 2008; Zhou et al. 2016)
Carbon fibres	• Often formed by electrospinning • Some are activated	(Chen, He, et al. 2011; Chen et al. 2012; Chen, Hou, et al. 2011; He et al. 2011; Karra et al. 2013)

Table 14: Various materials used as MFC electrodes (Santoro et al. 2017)

2.6.5. IMPLANTABLE MFCS

A steady flow of research continues to be performed in the application of MFCs to the powering of AIMDs. Some of the most prominent work has involved mini scale MFCs for implantation with the intestines and colon. Aside from these, work has been is in microfluidic devices where different designs and materials continue to be experimented with and urine MFCs.

In 2010, Han et al, as part of the Liu lab, presented a MFC which they proposed could be implanted within the human large intestine to utilize its contents. In their experiments, they simulated such conditions as the intestinal fluid, dissolved oxygen levels, temperature and pH. The device is shown in Figure 13 and is a large rectangular box shape made of plexiglass with a volume of 125 mL, containing an activated carbon fibre cloth anode and a carbon

paper cathode. In a long term experiment, the voltage slowly rose to peak at around 300 hours to nearly 300 mV with a 500 Ω resistance. The maximum power density was measured to be 73.3 mW / m^2, as well as a maximum open circuit voltage of 552.2 mV and the maximum current density was 225.6 mA / m^2. The voltage monitored until the voltage stabilised is shown in Figure 14 and the polarisation and power curves are shown in Figure 15 (Han, Yu & Liu 2010).

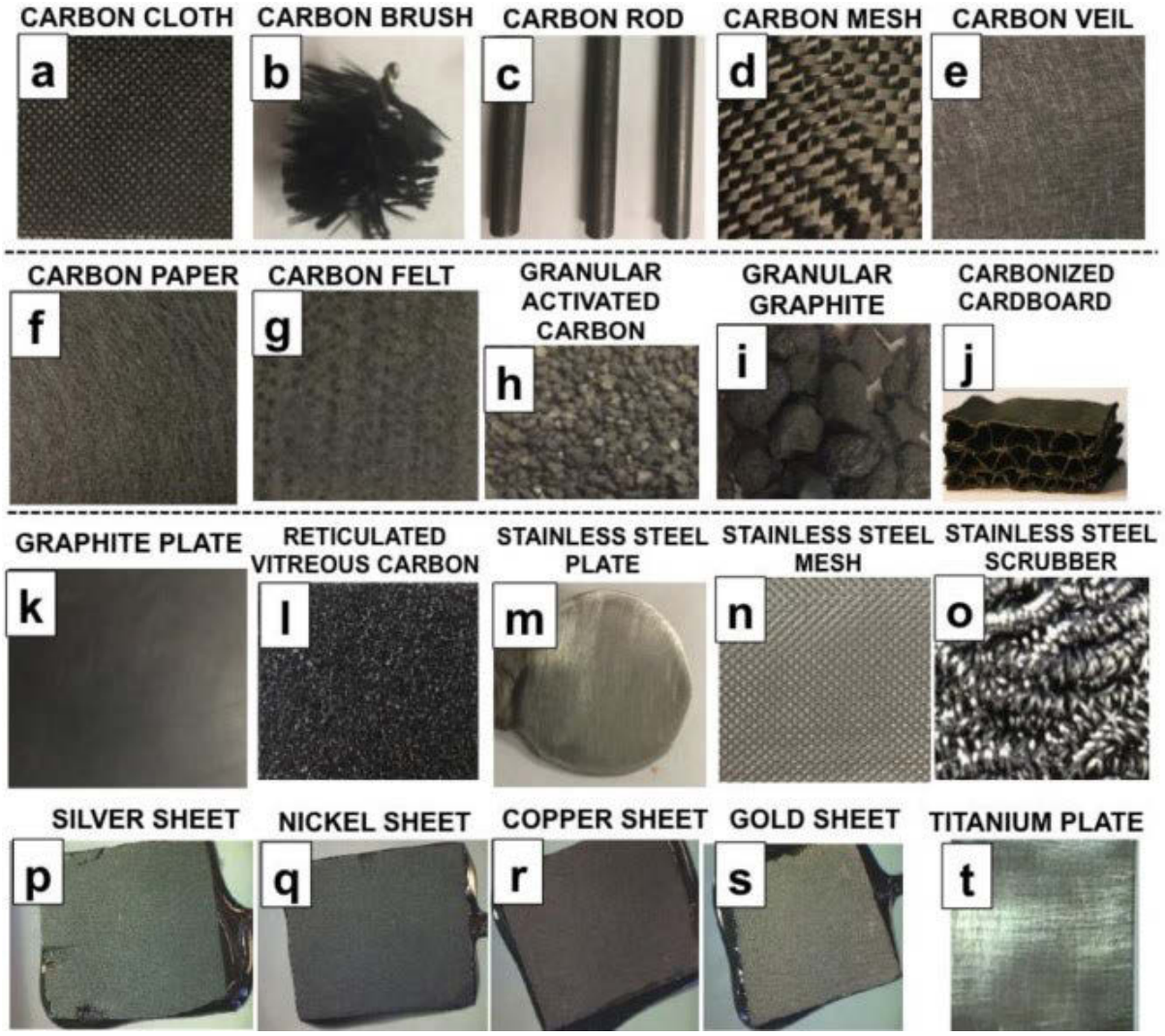

Figure 12: Photos of Various Materials Used as Microbial Fuel Cell Electrodes (Santoro et al. 2017)

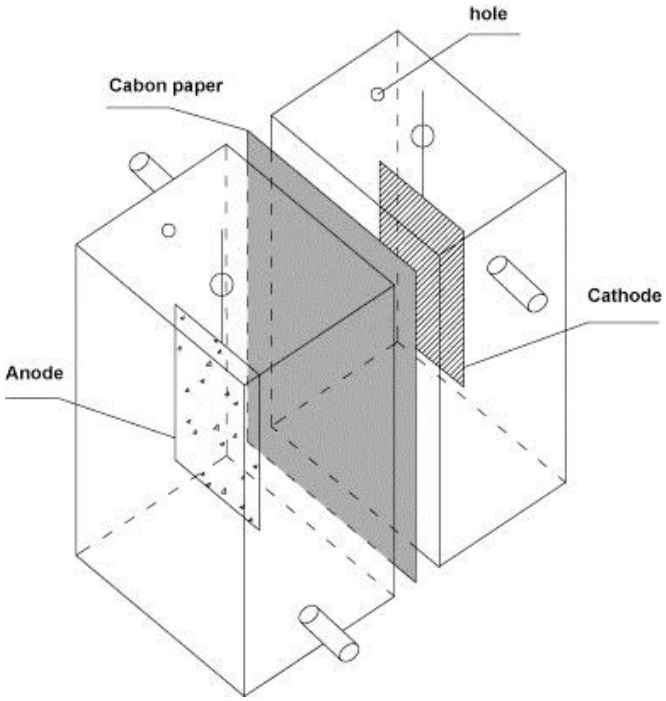

Figure 13: 'Schematic of prototype MFC' from Han et al (Han, Yu & Liu 2010)

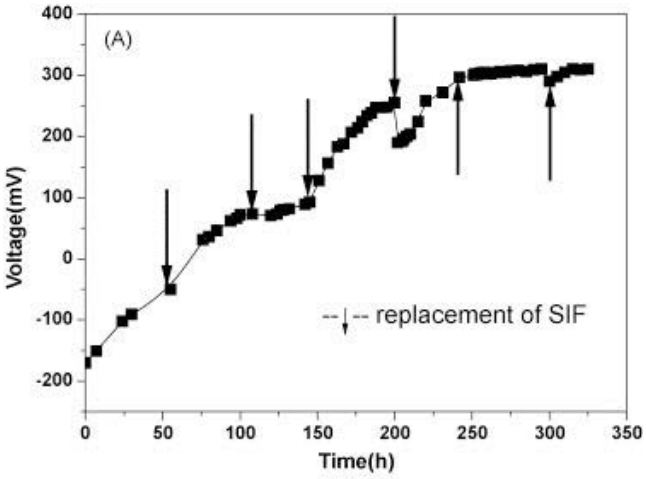

Figure 14: 'Voltage outputs of MFC with external resistance of 500 Ω during initial several cycles. (Arrows showed the replacement of SIF at the end of each cycle.)' from Han et al (Han, Yu & Liu 2010)

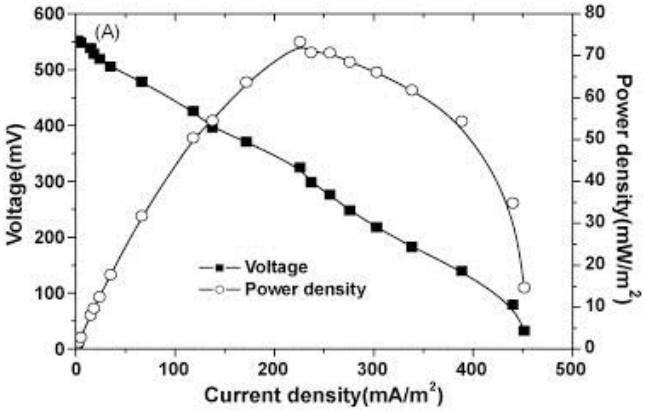

Figure 15: 'Voltage generation of MFC in a typical cycle at stable state (external resistance of 300 Ω)' from Han et al (Han, Yu & Liu 2010)

The Liu lab continued this work in 2013 when Dong et al conducted similar experiments with a redesigned implanted MFC for the human colon and with simulated colonic fluids. The device is said to have taken biocompatibility into consideration by the shape of the device as seen in Figure 16, as well as the use of such materials as pyrolytic carbon, carbon fibre and carbon nanotubes. Whilst both the 2010 and 2013 devices were meant for continuous use, only the 2013 device was experimented in this mode with both batch and continuous voltages over time shown in Figure 17. The maximum power density measured was 11.73 mW / m^2 at an internal resistance of was 800 Ω. The polarization and power curves are shown in Figure 18 (Dong et al. 2013).

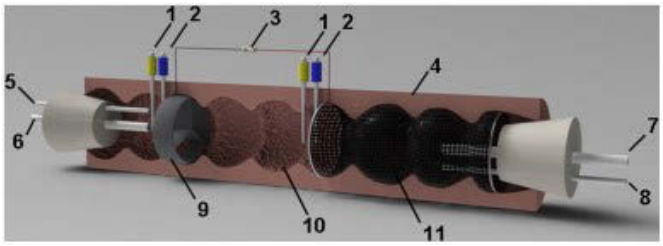

Figure 16: 'The new MFC configuration design simulated colonic environment as power supply for IMDs. 1: ORP transducer; 2: pH transducer; 3: external resistance; 4: simulated transverse colon; 5: feed inlet; 6: sampling port of cathodic area; 7: sampling port of anodic area; 8: liquid outlet; 9: cathodic plate; 10: simulated colonic haustra; 11: anodic plate' from Dong et al (Dong et al. 2013)

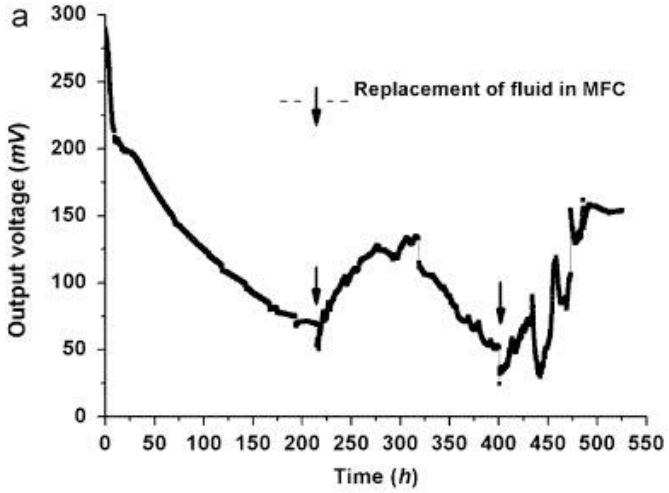

Figure 17: 'Voltage outputs of the experimental MFC. Batch operation stage (arrows showed the replacement of simulated colonic contents; A), continuous-operation stage (B)' from Dong et al (Dong et al. 2013)

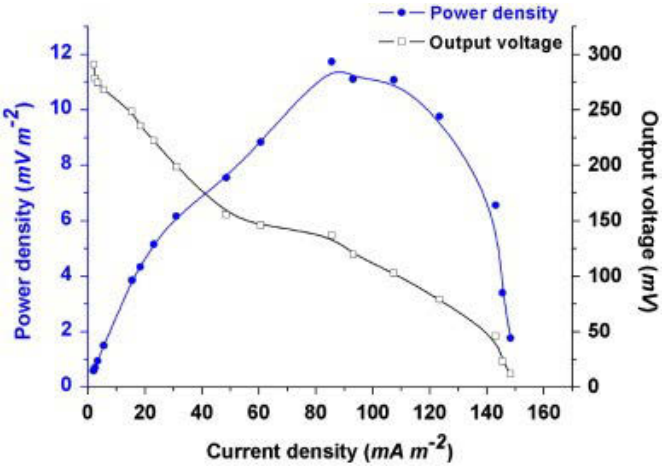

Figure 18: 'Polarization curves performed stably in continuous-flow operation from' Dong et al (Dong et al. 2013)

More recently, Yuming & Hongyan experimented further with the idea of using colonic fluids in microbial fuel cells by assessing the effect that different illnesses would have on the performance of a microbial fuel cell. In a continuous fed, H-cell setup, simulated fluids for diarrhoea, constipation, changes in diet, fever and a combination of fever and diarrhoea were tested. The fuel cell had volumes of 400 mL per chamber with a membrane with an area of 38.465 cm^2 and carbon cloth anode and cathode. The results of the experiments are summarised in Table 15. If this represented one person, then the average power measured

would be 15.34 mW or 51.18 mW / m^2 which should be enough to power many AIMDs (Yuming & Hongyan 2017).

Simulated Condition	Feeding Rate (mL / L)	Temperature (°C)	Open Circuit Value (mV)	Internal Resistance (Ω)	Maximum Power Density (mW / m^2)	Power (mW)
Diarrhoea	31.2→62.4 →124.8→31 .2	37	647.3	100	36.89	11.07
Constipation	31.2→15.6 →6.0→31.2	37	748.7	85	58.68	17.6
Change of Diet	31.2	37	734.4	120	42.77	12.83
Change of Diet	31.2	37	809.2	80	74.02	22.21
Fever	31.2	37→39→43→ 37	704.7	100	43.53	13.06
Diarrhoea	31.2→124.8 →31.2	37→43→37	704.7	100	43.53	13.06

Table 15: Adapted from Yuming & Hongyan table with caption as 'The Effects of Colonic Inner Environment on Microbial Fuel Cell Performance ' (Yuming & Hongyan 2017)

Aside from colonic fluids, blood based MFCs have also been experimented with where the objective was to determine the suitability of blood as a catholyte. Wang et al used H-cell MFCs, bovine rumen from a dairy cow serving as both the source of bacteria and analyte, carbon cloth was used as the anode and carbon paper was used as a cathode electrode. Red blood cells were added at 1, 2, 5, 10 and 12.5% concentrations to the MFC's cathode and the fuel cell was run at the internal human body temperature of 37°C. Between these different values of red blood cells, the maximum power density varied between 27.7 to 45.8 mW / m^2 and the open circuit value varied between 495 and 527 mV. The authors suggest that whilst there is enough power for a pacemaker, the device is still too large for implantation, and that

blood contains white blood cells and platelets as well as red blood cells, which would likely cause fibrin formation around non-compatible materials (Wang 2014).

A microfabricated MFC has also been fabricated by Siu et al from the material polydimethylsiloxane (PDMS) with gold micropillar structured electrodes. An exploded view of the device is shown in Figure 19 where the overall size of the device is 1.7 x 1.7 x 0.2 cm, the weight is 0.5 grams and the size of the micropillars is 40 µm. The device, using dual chambers, gold electrodes and the bacteria *Saccharomyces cerevisiae*, was able to generate a maximum current density of 30.2 µA / cm^2, maximum open circuit voltage of 488.1 mV and a maximum power density of 401.2 nW / cm^2 from a 15 µL drop of blood (Chiao 2008). Chiao also has a patent on this device (Chiao, Lin & Lam 2007).

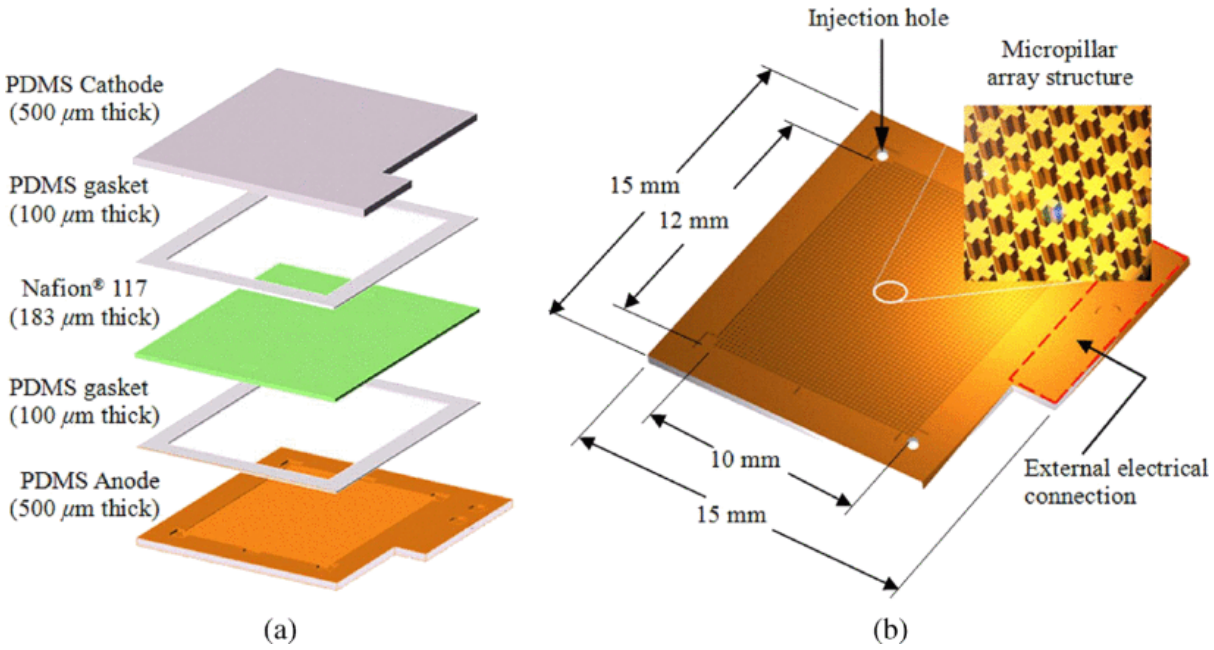

Figure 19: Figure from Chiao et al with caption 'Exploded view of the fuel cell structure: (a) PDMS MFC assembly and (b) the PDMS electrode with micropillar structures' (Chiao 2008)

In 2008, Mink et al designed a 1.25 µL MFC. The device used a mixed bacteria culture fed with acetate that had a multi walled carbon nanotube anode and carbon cloth cathode with a ferricyanide mediator. The device produced a maximum power output of 19.6 mW / m^2 and a

maximum current of 197 mA / m^2 and had a low internal resistance, being tested with a 100Ω resistance (Mink et al. 2012).

Another microfluidic device has also been tested by Mardanpour et al. The device was composed of poly methyl methacrylate, a nickel plate as the anode, carbon cloth as the cathode, used the bacteria *Escherichia coli* and used glucose and urea in human blood or urine as the substrates. Their choice of *Escherichia coli* is based on the way that it is not pathogenic, but does have exoelectrogenic properties. In the studies, the glucose fed MFC was able to achieve the highest power density of 5.2 μW / cm^2 and the highest open circuit voltage was 459 mV. Interestingly, the device cost less than 1 US dollar, which adds to the potential of micro-sized MFCs for powering electronic devices (Mardanpour & Yaghmaei 2016).

As previously mentioned, *Shewanella oneidensis* is another bacteria known for its exoelectrogen capabilities. Qian et al used this bacteria in a microfluidic MFC in 2009 to generate significant power at the time. The device is a stacked device composed of a PDMS cathode chamber, carbon cloth cathode electrode, followed by proton exchange membrane, a gold anode electrode and a SU-8 anode chamber, all fabricated on a silicon chip. As the anolyte, the microbial growth medium is used, whilst for the catholyte, Fe(III) is used. An illustration and photo of the MFC is shown in Figure 20. The fuel cell was able to generate 0.15 μW / m^2 and 6.7 μA / m^2 of power and current respectively. Unfortunately, the device was only able to generate an open circuit voltage of 48 mV and so it would not be able to turn on any electrical devices. Polarisation and power curves for the device are shown in Figure 21 (Qian et al. 2009). Ringeisen et al have also used *Shewanella oneidensis* in a millilitre size MFC, generating 24 mW / m^2 and 44 mA / m^2 for the power density and current density respectively with graphite felt electrodes (Biffinger et al. 2008; Biffinger et al. 2007;

Ringeisen et al. 2006). The fuel cell is shown in Figure 22, the voltage over time is shown in Figure 23 and the polarisation and power curves are shown in Figure 24.

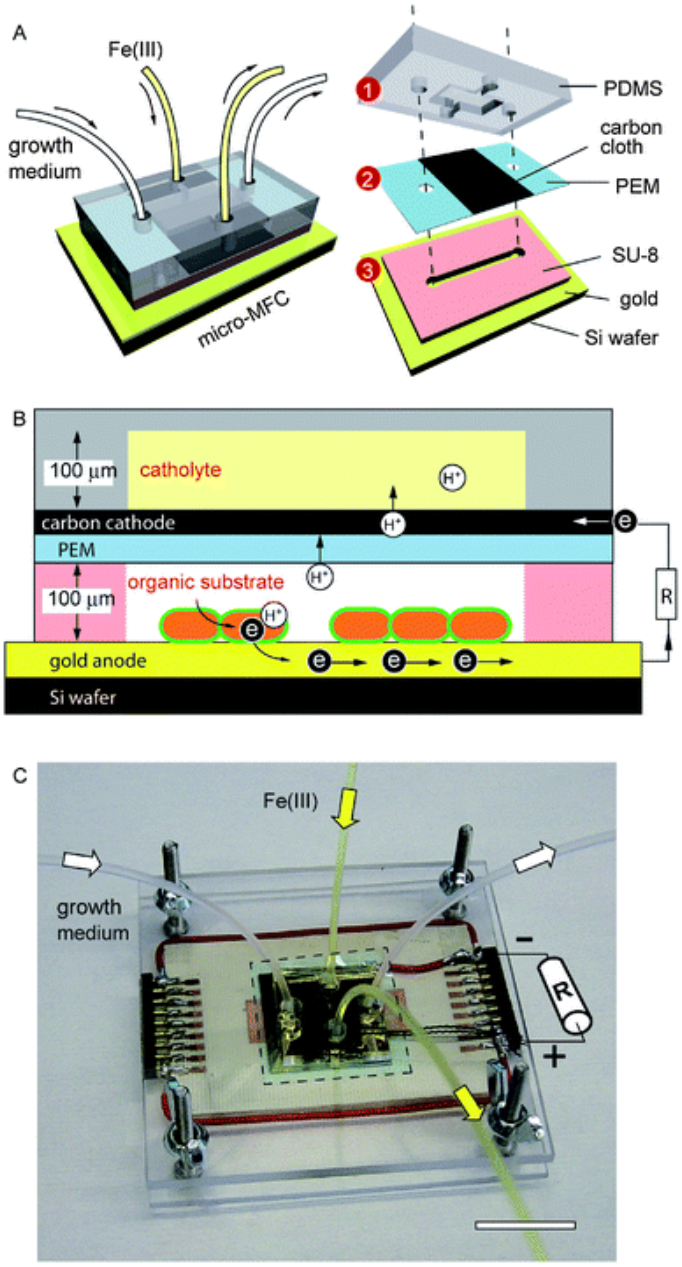

Figure 20: Figure from Qian et al with caption 'Micro-MFC design and assembly. (A) Schematic representation of the MFC components. Arrows indicate microfluidic flow pathways of electrolytes; dashed lines indicate the alignment of components for anolyte flow. (B) Operating principles of a MFC. Bacteria in the anode chamber (white) metabolize organic feedstocks and produce protonsand electrons that are subsequently conducted to the cathode chamber (yellow) via PEM and an external circuit, respectively. (C) Photograph of a micro-MFC device filled with electrolytes. The signs denote the cathode and anode of the fuel cell, and a dashed line indicates the PEM. Scale bar is 2 cm' (Qian et al. 2009).

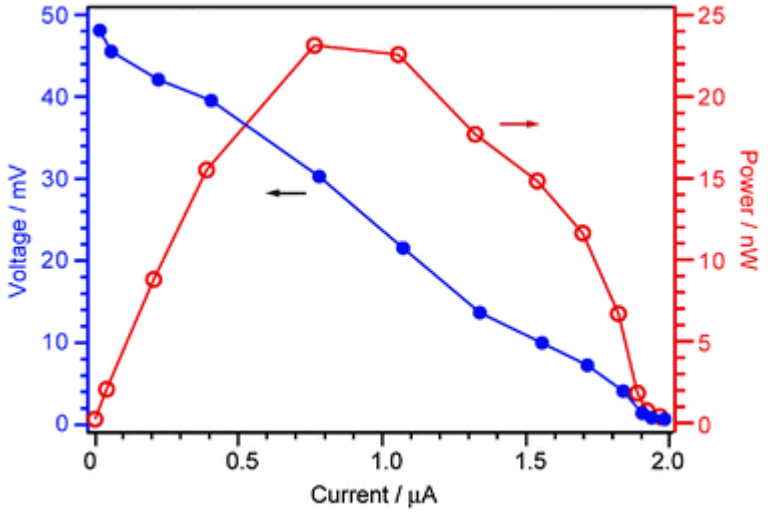

Figure 21: Figure from Qian et al with caption 'MFC polarization curve (blue) and power output (red) measured as a function of current' (Qian et al. 2009).

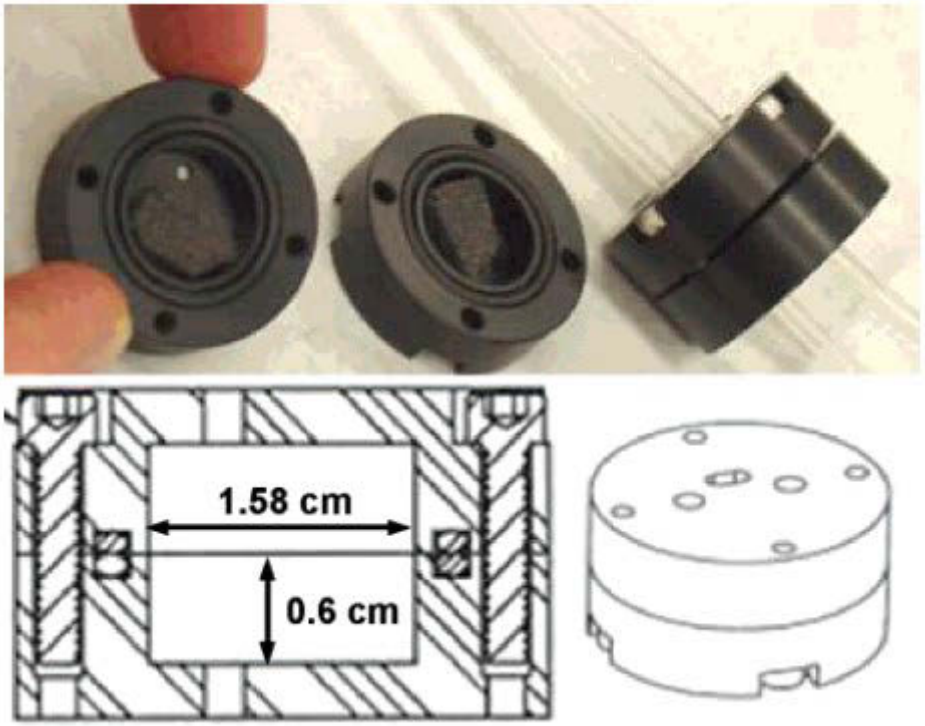

Figure 22: Figure from Ringeisen et al with caption 'Mini-MFC with cross sectional and top views' (Ringeisen et al. 2006)

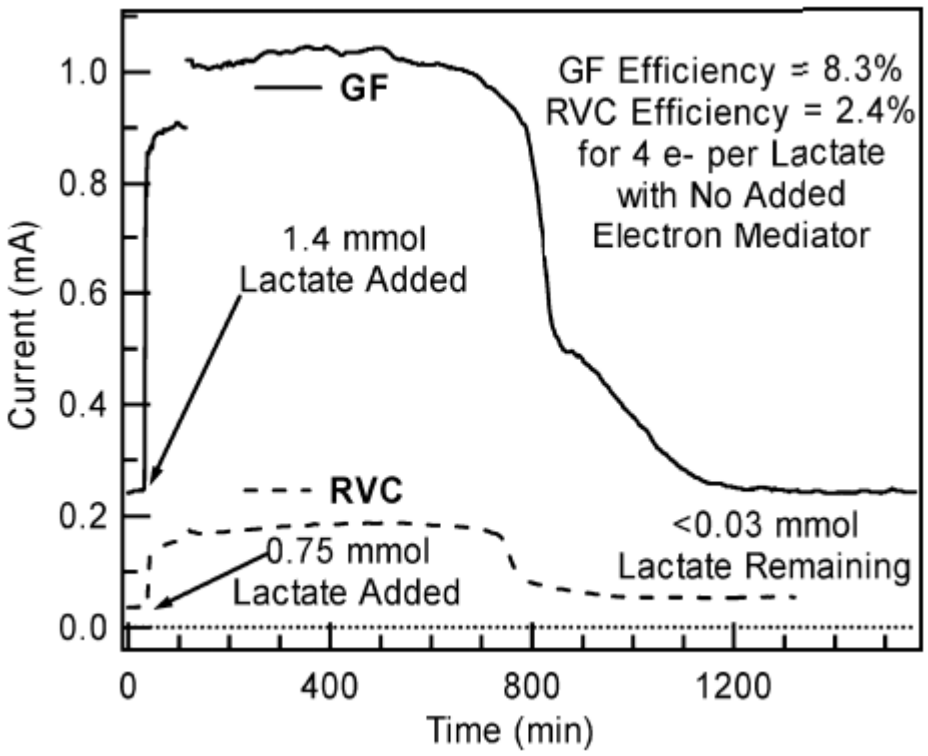

Figure 23: Figure from Ringeisen et al with caption 'Calculated Coulombic efficiency deduced from current at maximum power versus run time for GF (ss) and RVC (- - -) for cultures without exogenous mediators' (Ringeisen et al. 2006)

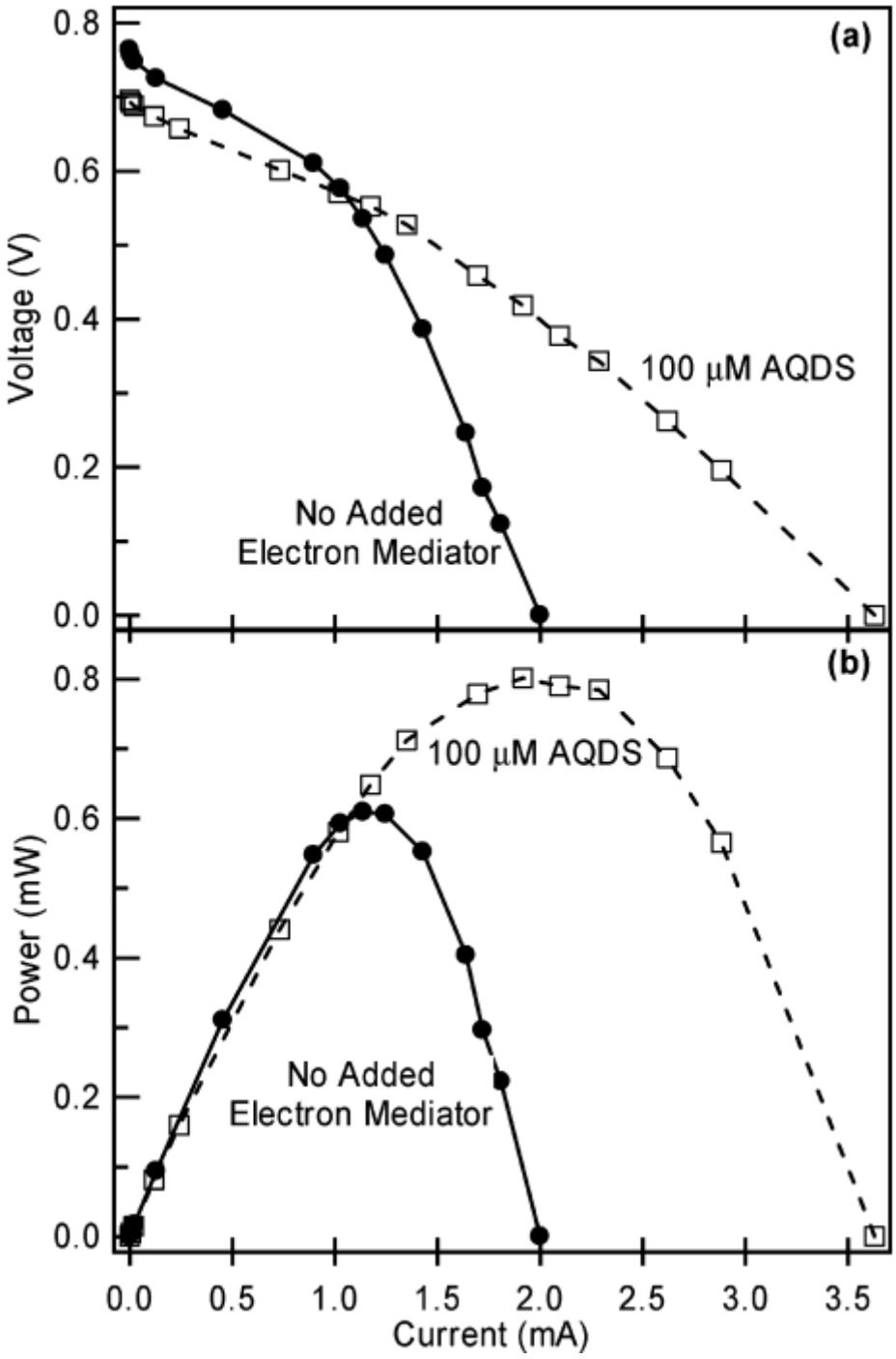

Figure 24: Figure from Ringeisen et al with caption ' (a) Current and (b) power versus run time for the miniMFC for DSP10 (ss) and Bacillus sp. (- - -) cultures without exogenous mediators' (Ringeisen et al. 2006)

The use of biofilms has also been a feature in microfluidic MFCs for powering AIMDs. Work by Choi et al highlights that due to the micro size of microfluidics devices and other factors, their power output is low. Biofilms, having been a significant breakthrough for macro scale MFCs as a good method for improving power output. The study used the bacteria *Geobacter*

sulfurreducens with a MFC composed of PDMS and glass channels (see Figure 25) along with a Nafion 117 membrane. The thickness of the PDMS was controlled to 10, 20, 55 and 155 µm, to help control the thickness of the biofilm formed. The authors state that when the thickness was less than 55 µm, the current and power density were both significantly limited. Nonetheless, a sizable power density of 95 µW / cm^2 was measured and the power and voltage curves are shown in Figure 27 (Choi & Chae 2013; Choi, Lee, et al. 2011). Additionally, Parra et al used *Geobacter sulfurreducens* in a microfluidic MFC. The fuel cell was composed of gold electrodes however it was larger at 350 µL and had a large internal resistance of 300 kΩ. Despite this, it was able to generate a power density of 12 µW / cm^2, a current density of 60 µA / cm^2 and an open circuit voltage of over 600 mV (Parra & Lin 2009). A photo and diagram of the fuel cell is shown in Figure 27.

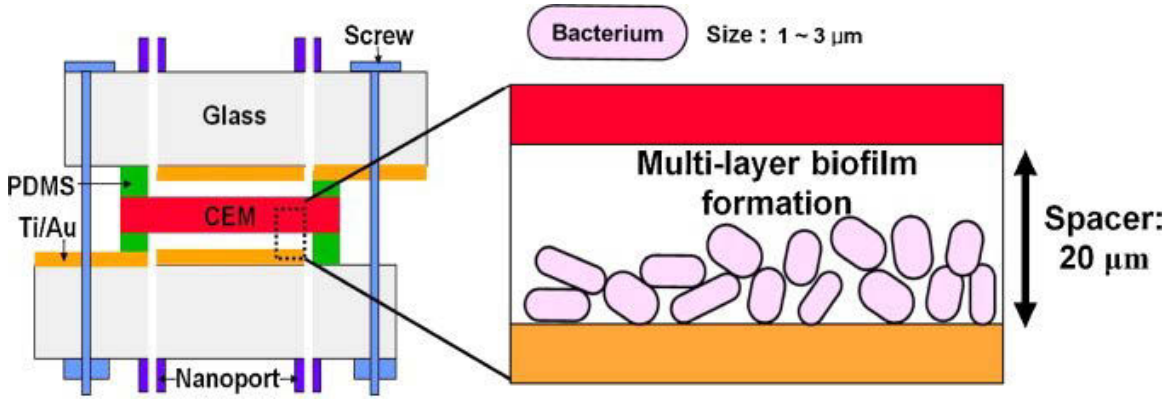

Figure 25: Figure from Choi et al with caption 'Cross-sectional view of a micro-scale microbial fuel cell (MFC); space constraints (20 µm-tall anode chamber) by a photolithographically defined PDMS layer. The anode and cathode chambers were formed between the glass chips and CEM (cation exchange membrane). The PDMS layer is a spacer to define the height of anode and cathode chambers to limit the bacterial biofilm formation' (Choi & Chae 2013)

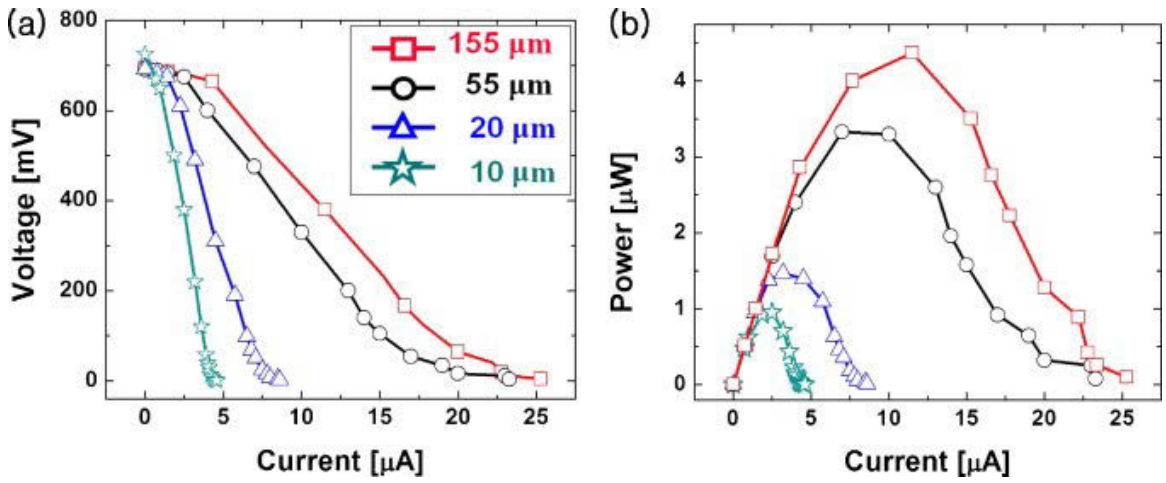

Figure 26: Figure from Choi et al with caption '(a) Polarization curve and (b) power output of the MEMS MFCs with four different thicknesses of the PDMS spacers, measured as a function of current. The values are derived and calculated based on the maximum current value at a given external resistance (910k, 482k, 270k, 150k, 66k, 33k, 15k, 10k, 7k, 2.6k, 1k, 428, 333, and 150 Ω)' (Choi & Chae 2013)

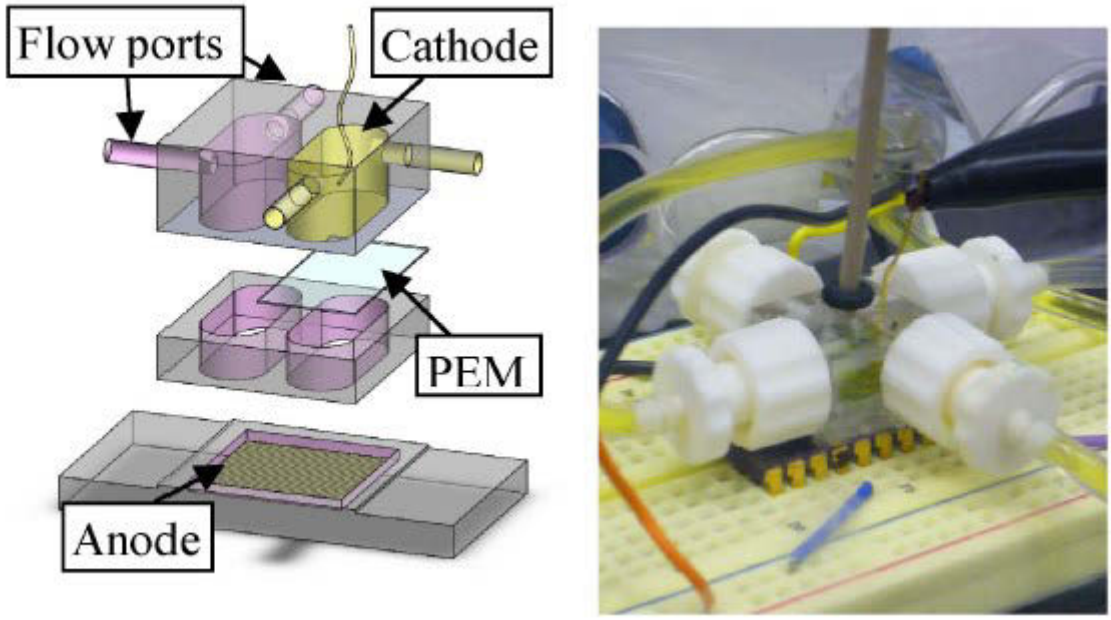

Figure 27: Figure from Parra et al with caption '(a) Exploded view of the MEMS MFC. Anolyte and catholyte circulate through corresponding chambers separated by a Nafion membrane. (b) Fuel cell experimental setup using potassium ferricyanide as electron sink at cathode' (Parra & Lin 2009)

Lastly, several urine MFCs have been designed where the bacteria and substrate are obtained from human urine. These MFCs are not specifically designed for implantation, however given their use of human urine, with additional work, their application may to the powering of AIMDs may be added as an application (Ieropoulos, Greenman & Melhuish 2013;

Santoro, Ieropoulos, et al. 2013a; Santoro, Ieropoulos, et al. 2013b; Shreeram, Hassett & Schaefer 2016; Winfield et al. 2015; Winfield et al. 2014; You et al. 2016).

2.6.6. OTHER CONSIDERATIONS IN MFCS

A common variation of the dual chamber microbial fuel cell is the single chamber fuel cell. In this reactor setup, as the name suggests, only one chamber exists and is filled with an electrolyte, bacteria, organic substrate and electrodes. A key advantage of this reactor design is its simplicity and lower cost since proton exchange membranes and the changes in creating the bridge to accommodate it can be costly as well as that membranes undergo biofouling (Ghasemi et al. 2013; Logan et al. 2015; Rahimnejad et al. 2014). The downside however is that since bacteria can and in many cases prefer to output electrons directly to oxygen rather than a metallic electrode, the electric circuit may never receive the electrons for its power (Logan et al. 2006).

Further variations on the single chamber MFC exist in the form of air cathode type MFCs. In this setup, the anode chamber of a DCMFC is kept the same, however the cathode electrode is placed directly against the cathode side of the membrane or is a separator itself. Such a design requires good air flow since one useful characteristic of a liquid catholyte is diffusion and being able to carry the required chemicals directly to the electrode. Alternatively, the cathode electrode may sit in a single chamber with the anode electrode but may be wrapped in a membrane. These designs have provided good power outputs (Fan, Hu & Liu 2007; Feng, Lee, et al. 2010; Feng, Yang, et al. 2010; Liu & Logan 2004; Logan et al. 2007; Pant et al. 2010; Sun et al. 2009; Zhu et al. 2011), however in terms of powering an AIMD, their designs still present challenges, particularly in providing adequate air flow. It may well be difficult to obtain oxygen at all within the human body, therefore to provide increased oxygen levels to accommodate an air cathode would be difficult.

In general, when compared to GEBFC, MFCs are considered more stable, long term and robust due to the bacteria. Bacteria grow slowly whereas enzymes react almost instantly. Bacteria are adaptable, so the conditions, within limits, can be adapted to, whereas enzymes are more susceptible to conditions such as temperature and pH. However, bacteria are living organisms that are known to be pathogenic for humans and they require some of the system energy for their own use (Logan et al. 2006). Conversely however, bacteria can completely breakdown glucose, and have a wider range of substrates, giving the system overall, more energy.

2.7. GLUCOSE ENZYMATIC BIOFUEL CELLS

2.7.1. HOW GEBFCS WORK

GEBFCs work in a similar way to microbial fuel cells, except the catalyst that begins and ends the process is enzymes as shown in Figure 28. A GEBFC is composed of a single chamber, anode and cathode electrodes, anodic and cathodic enzymes, electrolyte, glucose, oxygen and the electronic circuit connecting the electrodes. The anodic enzyme begins by interacting with the glucose, unlocking the electrons. The electrons are captured by the anode electrode, power the electronic circuit and flow through to the cathode electrode. The anode reaction, when interacting with glucose, results in gluconolactone and hydrogen as by-products. At the cathode electrode, the cathodic enzyme interacts with the hydrogen, oxygen and electrons, transferring off the electrons and creating water (H_2O) (Cosnier, Le Goff & Holzinger 2014).

Glucose has the ability to provide up to 12 electrons per molecule, although generally it is incompletely oxidised to gluconolactone, giving only two electrons and two protons. Oxygen partakes in a four electron, four proton reduction reaction. With these reactions, GEBFCs are well suited to use in powering AIMDs. To maximise BFC output, overpotentials must be

minimised and efficient and selective use of available glucose and oxygen is required (Cosnier, Le Goff & Holzinger 2014).

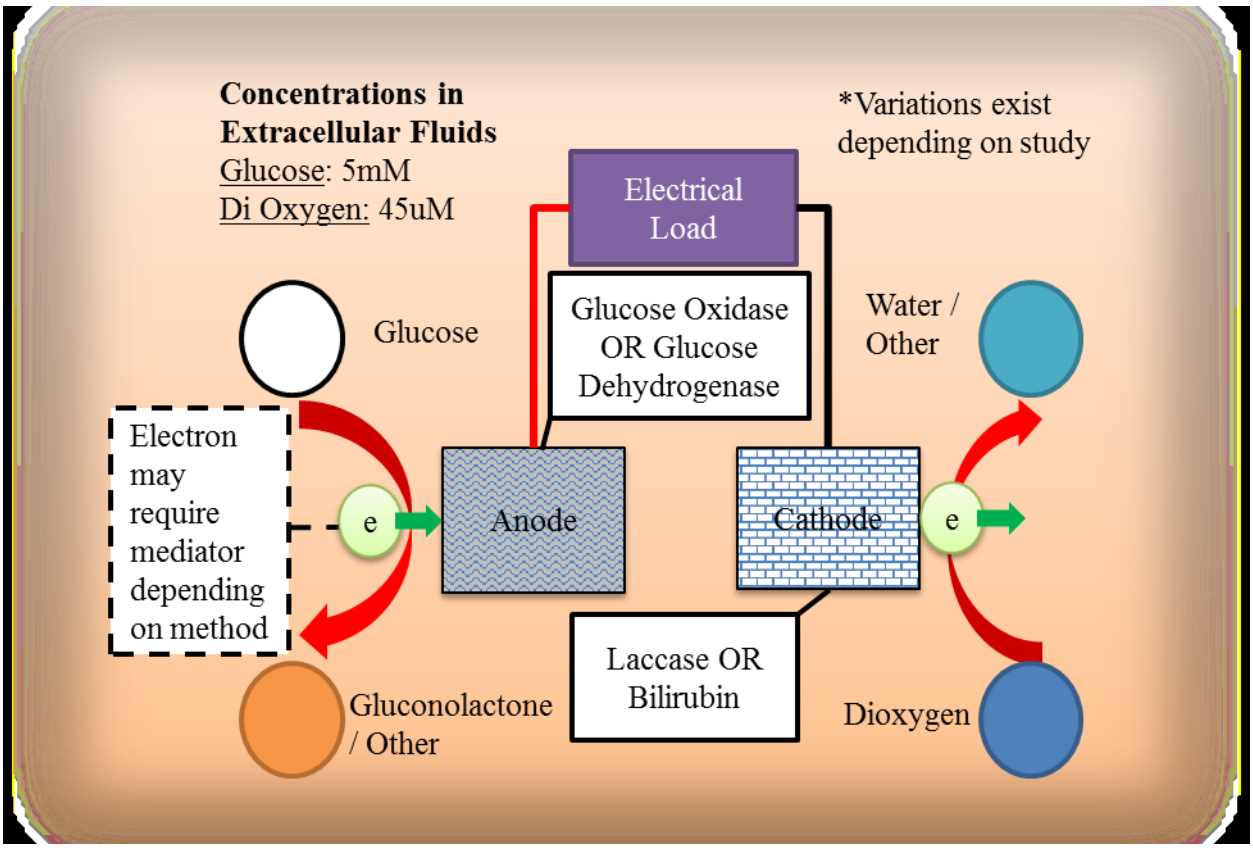

Figure 28: Diagram Illustrating How GEBFCs Work

2.7.2. Enzyme Selection in GEBFCs

The choice of enzymes and materials to conduct the electrons to and from the circuit is of critical importance. Usually in GEBFCs, the anode enzyme is either glucose oxidase (GOx) or glucose dehydrogenase (GDH) and the cathode electrode is either laccase (LAC) or bilirubin (BLR). In particular for the anode electrode, GOx from *Aspergillus niger* is used for its high specificity toward β-D-glucose found in physiological fluids. Enzymes chosen for biocathodes tend to come from the multicopper oxidase family, which has a mononuclear copper centre where the electron transfer from the electrode takes place, and a type 2 / type 3 trinuclear centre, where water is created from oxygen reduction (Cosnier et al. 2016). Specific organisms where LACs and bilirubin oxidases (BOD) are extracted from can provide

T1 copper centres with high redox potentials (Le Goff, Holzinger & Cosnier 2015; Mano & Edembe 2013).

Choice of these enzymes is now well established and provides nearly 1 V at open circuit since GOX and GDH oxidise glucose at – 0.4 V and -0.1 V respectively, and LAC and BOD reduce oxygen at + 0.6 V and + 0.55 V respectively (Cosnier et al. 2016). Whilst these are well established choices, work continues to be done with these enzymes to improve density and stability. For the cathode electrode, the controlled orientation of LAC and bilirubin oxidase has received significant attention recently (Blanford et al. 2009; Blanford, Heath & Armstrong 2007; Bourourou et al. 2013; Cracknell et al. 2011; Dos Santos et al. 2010; Giroud & Minteer 2013; Karaśkiewicz et al. 2012; Lalaoui, De Poulpiquet, et al. 2015; Lalaoui, Le Goff, et al. 2015; Le Goff, Holzinger & Cosnier 2015; Lopez et al. 2014; Mano & Edembe 2013; Meredith et al. 2011; Murata et al. 2009; Nazaruk et al. 2010; So et al. 2014; Sosna et al. 2010; Sosna et al. 2012; Tominaga, Ohtani & Taniguchi 2008). Attention for the anode electrode enzymes has focused on improved DET to GOx through the use of CNT based materials. This is due to the way that GOx is a large molecule (160 kDa and 8 nm average diameter) (Bankar et al. 2009; Wilson & Turner 1992) along with its active site being deeply embedded. Another method based on compression of CNTs and enzymes together (see below) has been used for DET, however much of the enzyme leaches out and thus does not remain in a DET position (Cosnier et al. 2016). One strategy has been to use electrode materials with FAD attached, then GOx that has had FAD removed (Patolsky, Weizmann & Willner 2004; Xiao et al. 2003). Unfortunately, there is not much of this FAD removed GOx available (Cosnier et al. 2016). A good strategy which offers tuneable redox potentials has been in the use of osmium based hydrogels and quinones (Forster et al. 2004; Kumar & Leech 2014; Milton et al. 2015) and is hydrophyllic, allowing for diffusion of substrates and by products (Heller 1992). Numerous other studies have also used osmium based hydrogels

and variants in different ways (Barrière et al. 2004; Barrière, Kavanagh & Leech 2006; Conghaile et al. 2013; Gao et al. 2010; Mano, Mao & Heller 2002; Ohara, Rajagopalan & Heller 1993; Rengaraj, Kavanagh & Leech 2011; Vigolo et al. 2000; Zafar et al. 2010).

2.7.3. MATERIAL SELECTION IN GEBFCS

To create a pathway for conduction from the enzymes to the electrode material, two options are available including either mediated or direct electron transfer (MET or DET respectively). MET uses other molecules to transport the electrons from the enzymes to the conductive material, whilst DET occurs when the electrons are directly transported from the enzyme redox centre directly to the conductive material. The MET process inherently contains more overpotentials due to more electron transfer steps, however the DET process is usually harder to achieve (Cosnier, Le Goff & Holzinger 2014). To create these two processes, appropriate materials and methods must be chosen. As can be seen in subsequent paragraphs, much of the work has used carbon nanotubes in one of their various forms, or bucky paper which is composed on CNTs. Methods with these materials have been primarily through compression or filtration respectively.

CNT fibres have also shown potential as a material for GEBFCs for their ability to form electrocatalytic electrodes with high surface area, porosity and miniature size. 14 $\mu W / cm^2$ power densities have been reported by Zheng et al from electrospun-nanofiber-based GEBFCs where the fibres were made of collagen and CNTs for both the anode and cathode (Zheng et al. 2014). A similar strategy was also used by Cosnier et al for LAC wiring and involved the electrospinning and annealing of polyacrylonitrile-CNT fibres leading to current densities of 100 $\mu A / cm^2$ (Barrière, Kavanagh & Leech 2006). Lastly, Baughman et al were able to obtain a maximum power density of 2.18 mW / cm^2 with an open circuit voltage of 700 mV from a yarn spinning process that uses a twisting method to introduce mediators and enzymes to the fibres (Kwon et al. 2014; Lima et al. 2011).

Conductive polymers are another material that can and has been used as an electrode material in GEBFCs. EP, one of two methods for synthesising conductive polymers, is a common method to immobilise enzymes and mediators through encapsulation. Using this method Brunel et al was able to obtain 27 μW / cm^2 from GOx entrapped with 8-hydroxyquinoline-5-sulfonic acid hydrate as the anode and LAC entrapped with 2,2′-azinobis (3-ethylbenzothiazoline-6-sulfonate) diammonium salt as the cathode in polypyrrole films (Brunel et al. 2007). Likewise, Crepaldi et al was able to obtain up to 130 μW / cm^2 by entrapping polyamidoamine dendrimers attached to GOx with ferrocenium hexafluorophosphate as a mediator in polypyrrole films (Crepaldi et al. 2014). Enzymes have also been immobilised through crosslinking. Kim et al showed that a three step process of adsorption, precipitation and crosslinking of enzymes on polyaniline films was able to achieve a maximum power density of 292 μW / cm^2 (Kim et al. 2011; Kim et al. 2014). Schubert et al covalently bound pyrroloquinolinequinone-dependent glucose dehydrogenase to polyaniline films and used a bilirubin MWCNT gold electrode to produce voltages of 680 mV and maximum power densities of 65 μW / cm^2 (Schubart, Göbel & Lisdat 2012). Christwardana et al has also used a layer-by-layer approach of CNTs, polyaniline, enzymes and Glut as a crosslinker, providing up to 290 μW / cm^2 (Christwardana & Kwon 2015). A more unique use of polymers for GEBFCs has been by Kim et al who created polypyrrole nanowires (Kim, Kim & Yoo 2009). This method was able to increase the power density by two orders of magnitude due to increased surface areas and enzyme loading over a film type electrode. Lastly, an interesting use of polymers has been with the combination of GEBFCs and capacitors by Kizling et al and Pankratov et al (Kizling et al. 2015; Kizling et al. 2016; Pankratov et al. 2014).

2.7.4. IMPLANTABLE GEBFCS

The use of GEBFC technology for implants has been thoroughly explored for the past two decades however, the first mention of the technology for powering implants was in 1967 when Warner and Robinson first reported an abiotic catalysing glucose fuel cell intended to run from glucose in body fluids. Their fuel cell used an unbuffered 10% glucose solution and had a maximum power density of 165 μW / cm^2 (H. Warner 1967). A year later, Wolfson et al reported a dual chamber GEBFC for powering a pacemaker achieving 3.5 μW / cm^2. The device was setup such that it was not implantable since the chambers were separate and the anode chamber was purged of oxygen, although good work had been performed in exploring glucose concentrations, buffer capacity and pH (Wolfson et al. 1968). Several other studies were performed in the decades up until the early 2000s, including some work by the large biomedical engineering company Siemens (Kerzenmacher et al. 2008).

Some of the more notable MET based implantable GEBFCs were first conducted in early 2000s by Mano and Heller. Their work used the wiring of glucose and copper oxidases, electrically connected by osmium redox hydrogels. Laboratory experiments led to voltages as high as 800 mV using micro sized electrodes implanted into a grape, and on average, 540 mV and 2.4 μW (Forster et al. 2004; Mano, Mao & Heller 2002).

From 2010 onwards, significant work was done in the way of DET based GEBFC electrodes. Their electrodes were made by mixing graphite particles, ubiquinone redox mediator, GOx and catalase powders for the anode and graphite particles, quinhydrone and polyphenol oxidase powders as the cathode. These mixtures were then mechanically compressed via a mould into disc like shapes and a wire connected with conductive glue. The discs were placed face to face and inserted individually into two sets of dialysis bags and then both in a Dacron sleeve with the wires protruding. The dialysis bags helped prevent the enzymes and redox mediators from escaping the vicinity of the electrodes, whilst the Dacron sleeves helped to

make the overall device biocompatible for implantation into a Wistar rat. Several milligrams of enzymes and mediator were used and was the first demonstration of GEBFC generating power from and within an animal (Cinquin et al. 2010).

In 2011, Zebda et al further improved on the work of Cosnier et al by using multiwalled carbon nanotubes. The use of MWCNTs enabled voltages of 0.95 V and high power outputs of 1.3 mW / cm^2 and when two GEBFCs were connected together in series, over 3 mW was measured (Zebda et al. 2011). This work was later continued in 2013 with the implantation of the electrodes into rats where the electrodes were placed in a silicon tube, encapsulated in both a dialysis bag and Dacron bag and implanted into the rat. The GEBFC was connected to a buck converter which could both turn on an LED and power a digital thermometer. During the powering of these devices, the rat was able to move freely due to the way the team had surgically implanted the device and wires (Zebda et al. 2013). The team has also subsequently used the biocompatible molecules chitosan and genipin to immobilise the enzymes and was able to use the electrodes after six months in storage (El Ichi et al. 2015). The general consensus of this work however is that there are issues in (1) the need for large amounts of enzymes, (2) with the large thickness of the discs, diffusion becomes a problem, (3) the electrodes become brittle, especially when exposed to solutions and (4) the porous structure is limited by the interconnection of nanotubes (Cosnier et al. 2016).

At the same time, numerous other GEBFCs have been developed and implanted in numerous other living organisms by the Katz group including in clams (Szczupak et al. 2012), snails (Halámková et al. 2012), insects (Rasmussen et al. 2012), lobsters (MacVittie et al. 2013) and rabbits (Miyake et al. 2011). These works use premade compressed multiwalled carbon nanotubes in the form of bucky paper which is functionalised with pyrenebutanoic acid succinimidyl ester (PBSE) to attach PQQ-dependant glucose dehydrogenase for the anode and LAC for the cathode. By combining several implanted GEBFCs in clams or lobsters and

stacking them in series or parallel, Katz et al was able to power several different electronic devices including an electric motor (Szczupak et al. 2012), watch and pacemaker (MacVittie et al. 2013). Due to tissue conductivity however, they reported that it was not possible to implement these stacked setups in one living organism. Bucky paper has some distinctive advantages over compressed CNTs in that they are better held together due to van der Waals interactions and CNT interlocking. Whilst they are still brittle like compressed CNTs when exposed to solution, they tend to be denser and less prone to falling apart (Cosnier et al. 2016). Other work using bucky paper shows significant promise for the material (Hussein et al. 2011; Hussein, Urban & Krüger 2011; Katz & MacVittie 2013; Villarrubia et al. 2014).

2.7.5. CONSIDERATIONS IN GEBFCS

Cosnier et al highlight significant challenges to overcome in the sterilization and biocompatibility aspects of GEBFCs. Sterilization refers to the cleanliness of the implant from any chemicals and other organisms that could cause sickness to the patient. Industrial sterilization techniques for biomedical implants are well developed and include autoclaving with high pressure steam, high temperature dry heat (usually higher than 140°C), ethylene oxide gas sterilization, gamma or x-ray sterilization or exposure to chemicals such as sodium hydrochloride, formaldehyde or ozone. None of the aforementioned studies, including those which have performed implantation, have had these industrial sterilization techniques used, and any of the techniques is likely to result in enzyme loss due to their sensitivity. Biocompatibility refers to if the materials would cause a major inflammatory or toxicity response. Whilst Dacron bags have been used in some studies, and others have proposed coating the electrodes with biocompatible polymers, these increase the overall size of the device and decrease diffusion of glucose and oxygen toward the electrodes (Cosnier et al. 2016).

Cosnier et al also notes that the power in GEBFCs is a function of several parameters to do with the enzymes including the mass embedded, electrical wiring to the active site of the enzyme, supply of fuels to the enzyme and the long term stability of the enzyme. The MWCNT electrodes studied by the Cinquin group, typically have large amounts of enzymes compressed with them (Cosnier et al. 2016). MWCNTs also have a hydrophobic outer wall nature leading to good enzyme adsorption as well as a high specific surface area. This leads to good electron transfer along higher porosity and interfacing with enzymes respectively (Cosnier, Le Goff & Holzinger 2014).

The long term stability of enzymes is a particular concern since they are known to be fragile to conditions such as pH, humidity and temperature. Enzymes have their highest reactivity at a particular pH, humidity and temperature and slowly drop off in reactivity with increases or decreases away from these values (Bankar et al. 2009). Researchers are happy to deal with some losses, and those conditions within physiological fluids give acceptable losses, however enzymes can still breakdown in response to high biocatalytic turnover or in response to other metabolites within the fluids. Additionally, for GEBFC setups requiring MET or non-immobilised enzymes that may leach out, this will not only compromise long term stability but harm the organism or patient (Cosnier et al. 2016). Biofouling of the electrodes, has also been known to be an issue (Amar, Kouki & Cao 2015). Some studies have had long term stability reviewed, though only one was in vitro where only a few measurements were made over a 9 to 11 day period (Cinquin et al. 2010). Other studies have looked at the *in vitro* performance of GEBFCs where for example, 75% of the original power of microneedle device was measured 60 hours after operation (Valdés-Ramírez et al. 2014). Another device which used sweat, measured 65% of the initial measured value after a 10 hour period (Falk et al. 2014). Over a continuous discharge of 24 hours, Bilewicz et al reported a 20% loss from the initial power of 131 $\mu W / cm^2$ (Karaśkiewicz et al. 2012). In a miniature flow based

biofuel cell run for 30 days, a half-life of 8 days was measured (Du Toit & Di Lorenzo 2015). Lastly, two studies by Cinquin et al have used EI to improve stability or storage to at least 6 months (El Ichi et al. 2015; Reuillard et al. 2015).

2.8. RESEARCH GAP AND PROPOSED STRATEGY

To appropriately conduct an innovative research study, it is important to identify the gap in the research having read all current literature within the field. This section will outline some of the issues found within the literature which align with the aforementioned objectives of the thesis, then outline the proposed strategy that is studied within this thesis, as a solution to the found issues.

Several MFC devices have been studied for powering active implanted medical devices. Devices by Dong et al and Han et al have shown the potential of MFCs using intestinal fluids. Chiao et al has shown the potential of miniaturised microfluidic MFC devices being powered off as little as 1 drop of blood as well as Siu et al showing the potential of a PDMS microfluidic device with the exoelectrogen bacteria *Shewanella oneidensis MR-1*. Yuming & Hongyan presented interesting results in the simulated response of implanted MFCs to sick patients and Wang et al presented an interesting idea for use of blood as a catholyte.

As great and interesting as these studies have been, a gap exists at a fundamental level for determining the exact approaches and optimisations for improvement of power output in implanted MFCs. More specifically, these studies have directly designed implanted MFCs or have directly experimented with ideas, however have not experimented with optimisations for fundamental MFC design features which will heavily influence the overall design.

In this thesis, we propose that several of the fundamental parameters which dictate the outputs of MFCs be experimented with, as a means of understanding and improving power

output. In particular, we take the distinct approach of having a biomedical perspective, to see what implications these optimisations have in a biomedical context.

This being the case, consider when a patient is asleep or awake, or when a patient is active or stationary. Analytes and cathalytes are liquids affected by gravity and other mechanical forces and the MFCs power will respond to these forces accordingly. A difference between MFCs and other powering technology solutions for AIMDs is that MFCs have living organisms. Accordingly, what bacteria we choose and feeding them appropriately is an important optimisation. A device and its size is also a factor, since current AIMDs have to be specific sizes for implantation. The design of the device is thus important since whilst certain features such as membrane size and MFC stacking may allow us to increase the power output, they may make the device larger.

In our experiments, we propose the following approaches for improvement of power output in MFCs for powering AIMDs:

- Optimisation of the orientation of the electrodes which corresponds to the lying down and upright positions of a patient.
- Stirring and static MFCs, corresponding to active and non-active patients.
- Mixed and single culture MFCs, looking at their power output difference, but also pathogenicity implications.
- Testing of standard growth mediums such as LBB and TSB, and what effect this may have on the power output.
- DCMFCs, SCMFCs and membrane sizes, looking at effect reactor type and subsequently membrane size has on the power output and size of the device.
- Stacking of MFCs, and whether the trade-off in power output and size will have implications on the size of the device.

- Broadly, simplicity in design as a means, since technical complexity presents challenges to actual implementation of the technology.

Two broad gaps exist within GEBFCs for powering AIMDs, primarily in regard to the conductive materials used in electrodes and the loading of enzymes. As outlined in the literature review, the three main materials that have been used in GEBFC electrodes has been bucky paper, which is composed of MWCNTs, MWCNTs themselves and conductive polymers.

Methods using of conductive polymers for connection to enzymes have involved mostly either electropolymerisation for encapsulation of enzymes, or adsorption based techniques. The key issue with these techniques is through these methods, the amount of enzymes loaded is low. As outlined in work by Cirpan et al, a key feature of their high power density electrodes has been their ability to load high amounts of enzymes, to allow more concurrent extraction of electrons from glucose.

Additionally, encapsulation and adsorption methods have issues in terms of stability since it is inevitable that physically, enzymes will leach out from the electrode by these methods. Hence, whilst conductive polymers have significant potential for use in GEBFCs, current methods for their use have shortcomings for enzyme loading and stability.

Secondly, whilst the work by Cirpan et al was able to load high amounts of enzymes, it used MWCNTs, this material is known to have issues with mechanical stability when exposed to solution, as outlined in reviews mentioned in the literature review. Additionally, as shown in work by Zebda et al, their compressed MWCNT electrodes have high porosity. This would usually be a positive aspect, however with the compression method, whilst MWCNTs and enzymes are compressed into a small space, the porosity means they are not confined to this small space and thus can still leach out. Both these issues have been confirmed by our own

experiments and the reason for the use of membranes for mechanical encapsulation of the enzymes to the MWCNTs and for strengthening of the electrodes.

We hence present the following as a means for improvement of GEBFC power output, again with a biomedical perspective:

- Use of the compression method, previously used with MWCNTs. This allows for simplicity in method, allowing for potential use in manufacturing of the electrodes.
- Given the mechanical issues related to MWCNT, a conductive polymer should be used with the compression method. It should be observed therefore what differences mechanically may exist and what effect the use of the method and material has on the power output.
- Since enzyme leaching is not necessarily specific to MWCNTs, strategies for enzyme immobilisation will be developed. Keeping in mind simplicity in method, the use of glutaraldehyde, a commonly used crosslinker for cells to substrates in microscopy can be used. Experiments on enzyme leaching and the effect on power output can be observed.
- MWCNTs have higher conductivities than conductive polymers. As such, improvements in conductivity which still maintain the simplicity of the compression method should be addressed by way of polymer composite materials. These accordingly need to be characterised electrochemically and for conductivity.

Lastly, by way of an energy harvester electronic circuit or directly, a medical device should be powered.

CHAPTER 3

MFC PARAMETER OPTIMISATION FOR IMPROVED POWER OUTPUT

3. MFC Parameter Optimisation for Improved Power Output

3.1. INTRODUCTION

Microbial fuel cells use bacteria to break down organic substrates and then capture the electrons from the bacteria output through a specialised fuel cell setup. Particular inputs and outputs, namely the sugar as a common organic substrate and electricity as an output, make them applicable to many applications such as wastewater monitoring and energy recovery, open water buoy electricity supply and AIMD powering to name a few.

This chapter is concerned with the parameters involved in microbial fuel cells and how they affect the power output in the biomedical context of AIMDs. Many of the past studies, whilst achieving high power output, have investigated ideas or devices which may not be suitable for implantation into the human body due to various reasons such as the microbe used or the design of the reactor. Other reactors have been designed and experimented with for implantation, but were based on hefty assumptions and have not holistically looked at how they work within the human body, thus leaving them in the conceptual and prototype stages of development.

We seek to solve this problem, in this chapter, by experimenting with the fundamental parameters affecting the operation of microbial fuel cells, how they may sit within the context of accompanying a medical device for implantation into the human body and ultimately how they may influence power output. Typically a user will be moving around during the day by standing and walking, whilst at night will lie down. This could therefore affect the chambers or how electrodes sit within the chamber or chambers of the MFC. A powering scheme of this nature is likely to involve charging a capacitor or battery to buffer the MFC's electrical output which may be intermittent. Part of this intermittent nature comes from the need to feed and grow the bacteria and thus knowing how they react when given sugar, the different

amounts of bacteria and the resultant electrical output is important. A major consideration is also the reactor type with single and dual chamber MFCs. Much work has been done with SCMFCs to improve their power output, however their layouts may not be suitable for implantation and can be complex. Dual chamber designs require more components, can be physically larger and are more costly as a consequence, but the basic design may provide a more appreciable base level of power with less work.

This chapter starts by stating the materials and methods used in the experiments. Some aspects of the methods are unique to MFCs and are outlined specifically here including how all the components of the MFC were put together and setup and which parameters were tested. Some other methods are more basic and general scientific laboratory techniques and can be found in the Appendix section. The results of the experiments are then presented, separating them by reactor type and go firstly into the single chamber MFC experiments including the electrode configuration, stirred and static SCMFCs and inoculation size. The chapter then proceeds to present results on the dual chamber MFCs, in particular showing results from mixed culture DCMFCs, the effect of different growth media in DCMFCs, the influence of the membrane size on DCMFCs and then finishing off on the stacking of DCMFCs. The experiments are designed to test how much power may be provided based on how the MFC may sit within the human body. The results focus on the power producing capabilities, since the objective of this thesis is to determine the ability of biological fuel cells to power AIMDs from glucose. The chapter then finishes off with a discussion of the results and methods with conclusions being drawn, based on what we know from the work established within this chapter.

3.2. MATERIALS

The list of materials is as follows:

Product Name	Manufacturer / Supplier	Product Code
Shewanella oneidensis MR-1	ATCC – American Type Culture Collection	700550
Tryptic Soy Broth	BD	211825
Luria Bertani Broth	BD	244620
Tryptic Soy Agar	BD	236950
Reticulated Vitreous Carbon	Goodfellow	073-784-76
Conductive Silver Epoxy	CircuitWorks	CW2400
Titanium Wire	VWR	ALFA00362.G1
Heat Shrink	JayCar Electronics	WH5525
DCMFC 25 mm	Adams & Chittenden Scientific Glassware	100.25.3
DCMFC 40 mm	Adams & Chittenden Scientific Glassware	100.40.3
Membrane	Nafion	Nafion-117

Table 16 List of Materials Used in the MFC Experiments

3.3. METHOD

3.3.1. PREPARATION OF CHEMICALS

Phosphate buffer saline (PBS) was prepared from tablets whilst Trypic Soy Broth (TSB), Luria Bertani broth (LBB) and Tryptic Soy Agar (TSA) were purchased in dehydrated powder form and were used in the following concentrations:

- TSB: 30 g / 1 litre*
- TSA: 40 g / 1 litre*

- LBB: 25 g / 1 litre*

These were dissolved in 18.2 Ω milliQ DI water and autoclaved at 121°C for at least 15 minutes. The PBS, TSB and LBB were stored at room temperature and sealed until required. The TSA was poured into Petrie dishes whilst still warm under sterile conditions and stored, upside down, in a 4°C refrigerator until required.

3.4. MICROBE AND GROWTH CONDITIONS

Shewanella oneidensis MR-1 was taken from laboratory stocks and used to create streak plates on TSA which were then grown for 16 to 18 hours at 30°C. From these plates, to ensure genetic similarity between bacteria within a MFC, a single colony was picked from the streak plate and added to a TSB culture. In the case of SCMFCs, several 2mL tubes of TSB were used, whereas in the case of DCMFCs, a 50 mL culture was used. In either case, the TSB cultures were left in an incubator, shaking at 200 R.P.M. for 16 to 18 hours.

For SCMFCs, either 0.5, 1 or 2 mL of the TSB cultures, depending on the experiment, were added to the growth chamber. In the case of DCMFCs, drop plating was used and CFU counting performed to ensure each inoculation was approximately 10^8 CFU / mL. Subsequently, 100 μL of the TSB culture was then added to the anode chamber of the DCMFC and voltage monitoring begun.

3.5. MFC MATERIALS

3.5.1. SINGLE CHAMBER MFCS

To create the chamber for the SCMFC, 100 mL beakers were chosen for which lids were made of aluminium foil. The electrodes were Reticulated Vitreous Carbon (RVC) and were cut to a size of 30 x 30 x 0.5 mm size and have an approximate surface area of 0.02775 m^2. Titanium wire which had a diameter of 0.5 mm was insulated with electrical tape. The wire was connected to the electrodes by wrapping the wire around and multimeter was used to

ensure the resistance of the connection was approximately 20 Ω. The SCMFC was then autoclaved at 121°C for 20 minutes as a whole with sterile 100 mL TSB being added afterwards, followed by inoculation and voltage monitoring.

3.5.2. DUAL CHAMBER MFCS

The H-Cell MFC glassware was autoclaved at 121°C for 20 minutes. The anode chamber was filled with either 100mL of sterile TSB or sterile LBB, depending on the experiment and the cathode chamber filled with 100mL of sterile PBS at pH 7.0. The separating membrane was Nafion-117 which was cut to a circular diameter of either 25 mm or 40 mm as shown in Figure 29.

The wire was connected to the electrodes with conductive silver epoxy and a hot air gun was used to dry the paste. A multimeter was used to ensure all electrodes had approximately 20 Ω resistance for consistency in measurements of the MFC outputs. The other end of the wire was then inserted in to the screw terminal of the data logger. See Figure 30 for a photo of the electrode and wire assembly. The assembled wire with electrodes and membrane was exposed to UV for 10 minutes each side in a class II hood for sterilization purposes before use. A photo of the DCMFC is shown in Figure 31.

Figure 29: Nafion-117 Cut to either 25 or 40 mm Diameter for use as a Membrane in the DCMFC

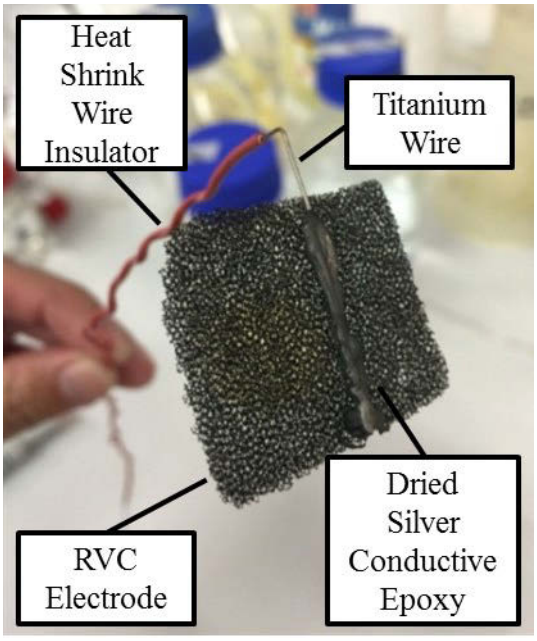

Figure 30: Close up with Heat Shrink Wrapped Titanium Wire Connected to the RVC Electrode via Silver Conductive Epoxy

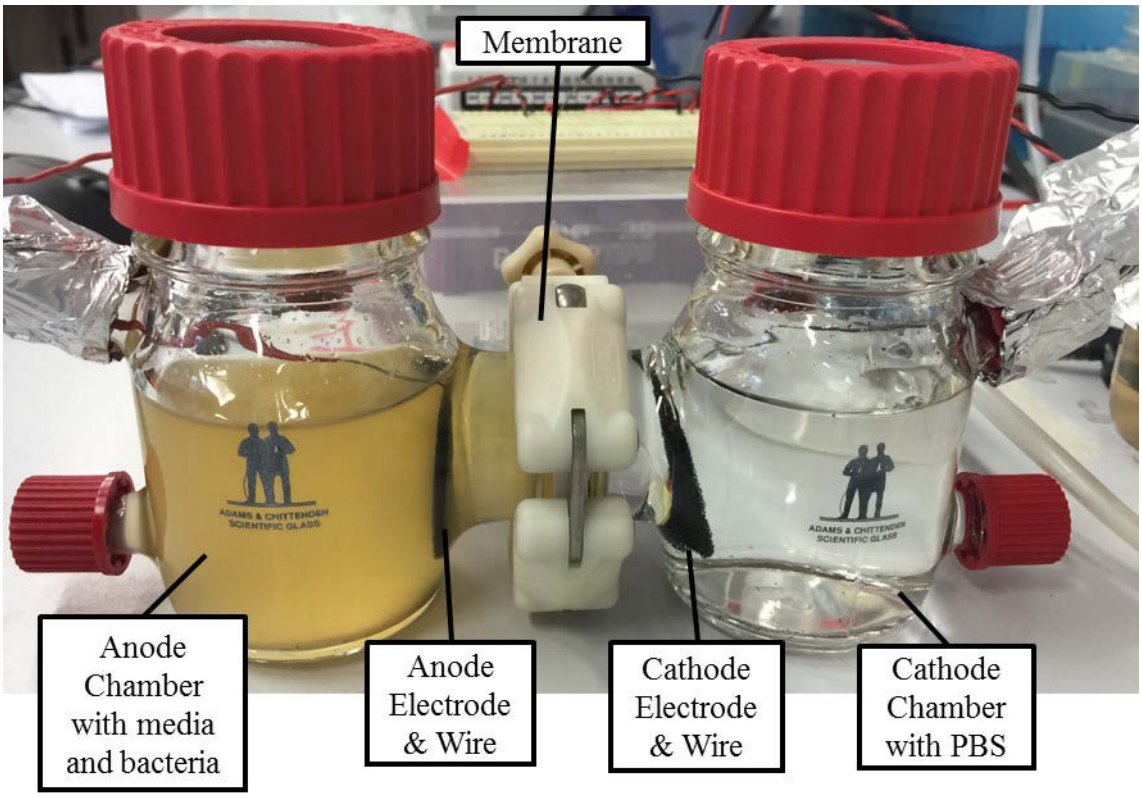

Figure 31: Annotated Photo of a DCMFC Used in Experiments

3.6. MEASUREMENT SETUP

The voltage output of the MFCs was monitored by a National Instruments USB-6009 in differential measurement mode, driven by a custom built LabView program on a Windows

PC. A screenshots of the LabView programs can be found in the Appendix section. The cathode electrode was taken as the positive, and the anode electrode taken as the negative, as per convention. The output voltage of the MFCs was monitored for 6 to 7 days and logged every 10 seconds in to a spreadsheet for later analysis.

After the 6 to 7-day open circuit period, various resistances starting from close to open circuit to close to short circuit were connected to the MFCs. An exact list of resistances used can be found in the Appendix section. To effectively and quickly connect the DCMFC, resistors and data logger together, an electrical breadboard was used and was raised on a plastic box to prevent the analyte and catholyte leaking through the wire insulation. With each change in resistance, the voltage was left to stabilise for 10 minutes and the average of the final 60 seconds was taken for the polarisation curves.

Output current was calculated by Ohm's law (V=IR) and the area and volumetric maximum current and power output are referred to the electrode surface area and total combined chamber volume respectively. The internal resistance of each of the fuel cells is determined to be the resistance at the peak power since peak power occurs where the source and external resistance are equal. For each LBB and TSB MFC experiment, each was run in triplicate under the same room temperature and humidity.

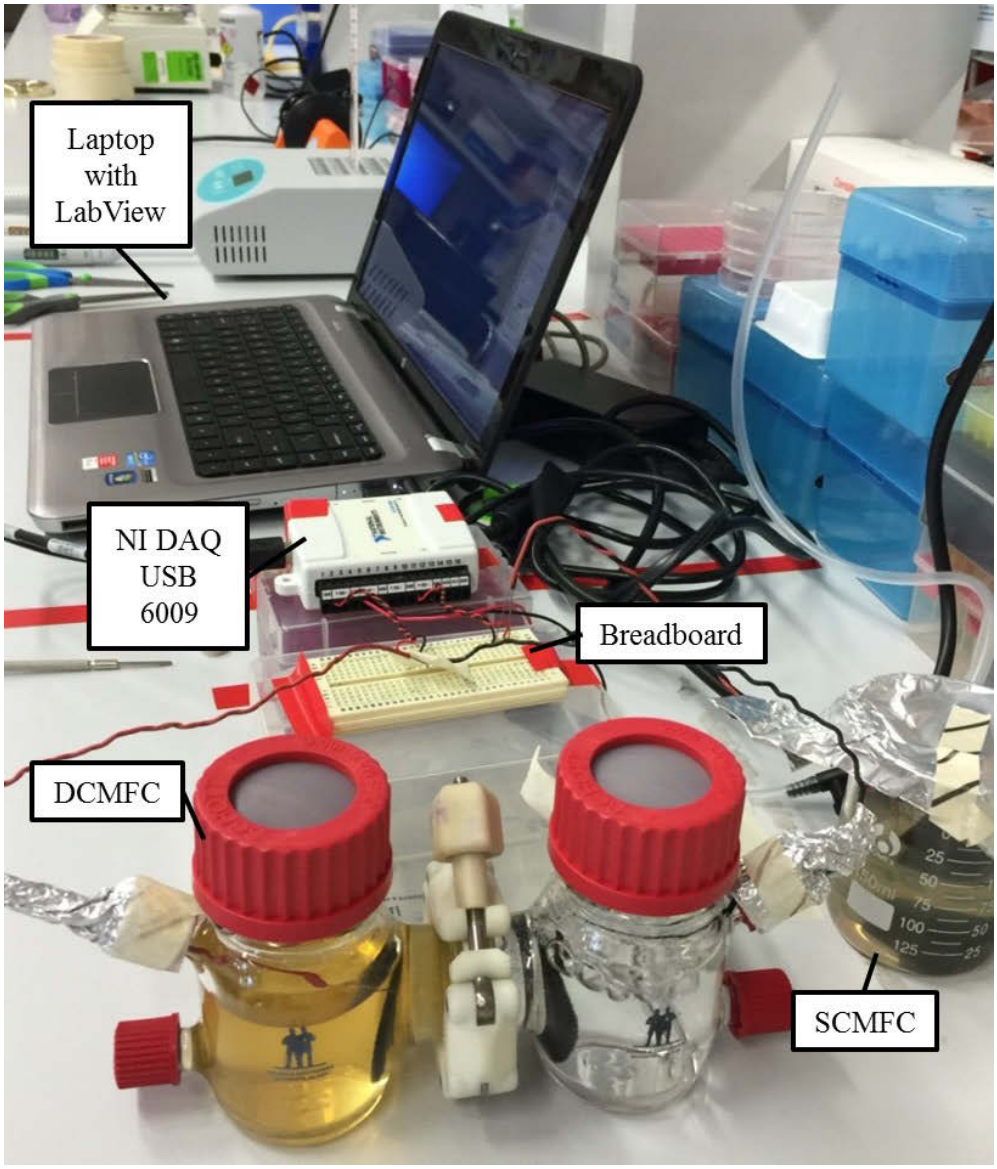

Figure 32: Annotated Measurement Setup during DCMFC Monitoring

3.7. Biomedical Implant Based Experimental Conditions

3.7.1. Single Chamber MFCs

If MFCs are to be used with an AIMD, it is likely that the overall fuel cell will undergo changing conditions as the patient goes about their daily life. These conditions may affect the output of the MFC itself and as such should be tested. If a person is standing up or laying down, the result is that the electrodes will be orientated differently. This is therefore tested in which the electrode configurations are shown in Figure 33 and are designated as 'Top-Bottom' and 'Side-by-Side'.

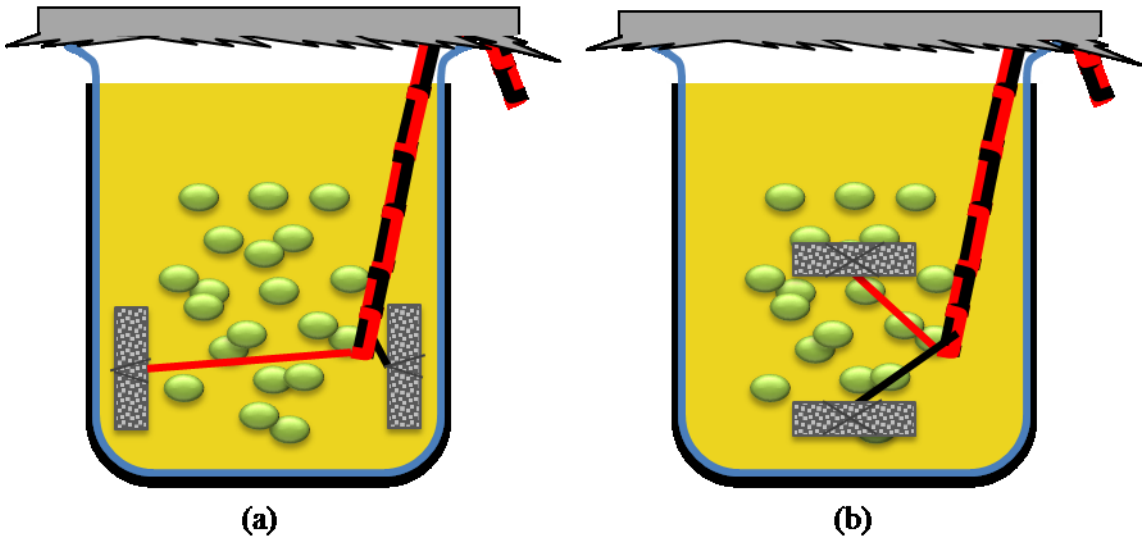

Figure 33: SCMFC Electrode Configuration - (a) Side-by-Side and (b) Top-Bottom

A particular purpose of AIMDs is to allow patients to be unburdened from their medical conditions, and thus go about their daily lives. In doing this, they are likely to be moving around and stopping. The MFC is filled with liquids and bacteria which typically respond to stirring and this condition will change with the patient's movement if implanted. To test what effect this movement and non-movement may have on the MFC electrical output due to stirring, gently stirred and unstirred SCMFCs were compared. Stirring was induced with a magnetic stir bar and plate.

Lastly, the electrical output of the MFC is determined by the amounts of bacteria inside the chamber. The population of the MFC grows to the size proportionate to the space they have to grow, consuming the nutrients depending on their concentration. As such, different starting inoculations of bacteria were tested including 0.5 mL, 1 mL and 2 mL and the resultant voltage monitored.

3.7.2. Dual Chamber MFCs

Another parameter that can be tested with MFCs is their chamber setup. Dual chamber MFCs have more parts but may have a higher overall power output which may make them a good candidate for powering AIMDs. One of these parts is at the centre of a DCMFC, between the

two chambers, the membrane, that allows the exchange of hydrogen between the two chambers. To test the effect the size of the membrane has on the electrical output of DCMFCs, 25 mm membranes and 40 mm membranes were tested to see which may be better for powering AIMDs, noting that both a smaller the device and high power output are desirable.

The bacteria themselves have a major influence on the overall power output of MFCs. To further elucidate their effect, *Shewanella oneidensis MR-1* was mixed with other common lab bacteria to form a community of bacteria and their electrical output monitored. A community of bacteria may exist say in the gut of a patient, which as past literature suggests, is a possible place for implantation. Additionally, there are many common nutrient solutions that *Shewanalla oneidensis MR-1* can grow in. To test what effect that this may have on the electrical output of DCMFCs, the DCMFCs were inoculated with Luria Bertani broth and Tryptic Soy Broth.

Lastly, often when powering electronic devices, several batteries are connected in series or parallel to boost their voltage or current respectively. To test how the DCMFCs may behave in this setup, 4 DCMFCs were connected in series, parallel and in a hybrid of these connections. Once the 6 to 7 day open circuit period, and polarisation and voltage curves experiments of the above were completed, the DCMFCs for each experiment were left for their voltages to recover and then connected together in either series, parallel or a hybrid of series and parallel as shown in Figure 34 and polarisation and voltage curves were conducted.

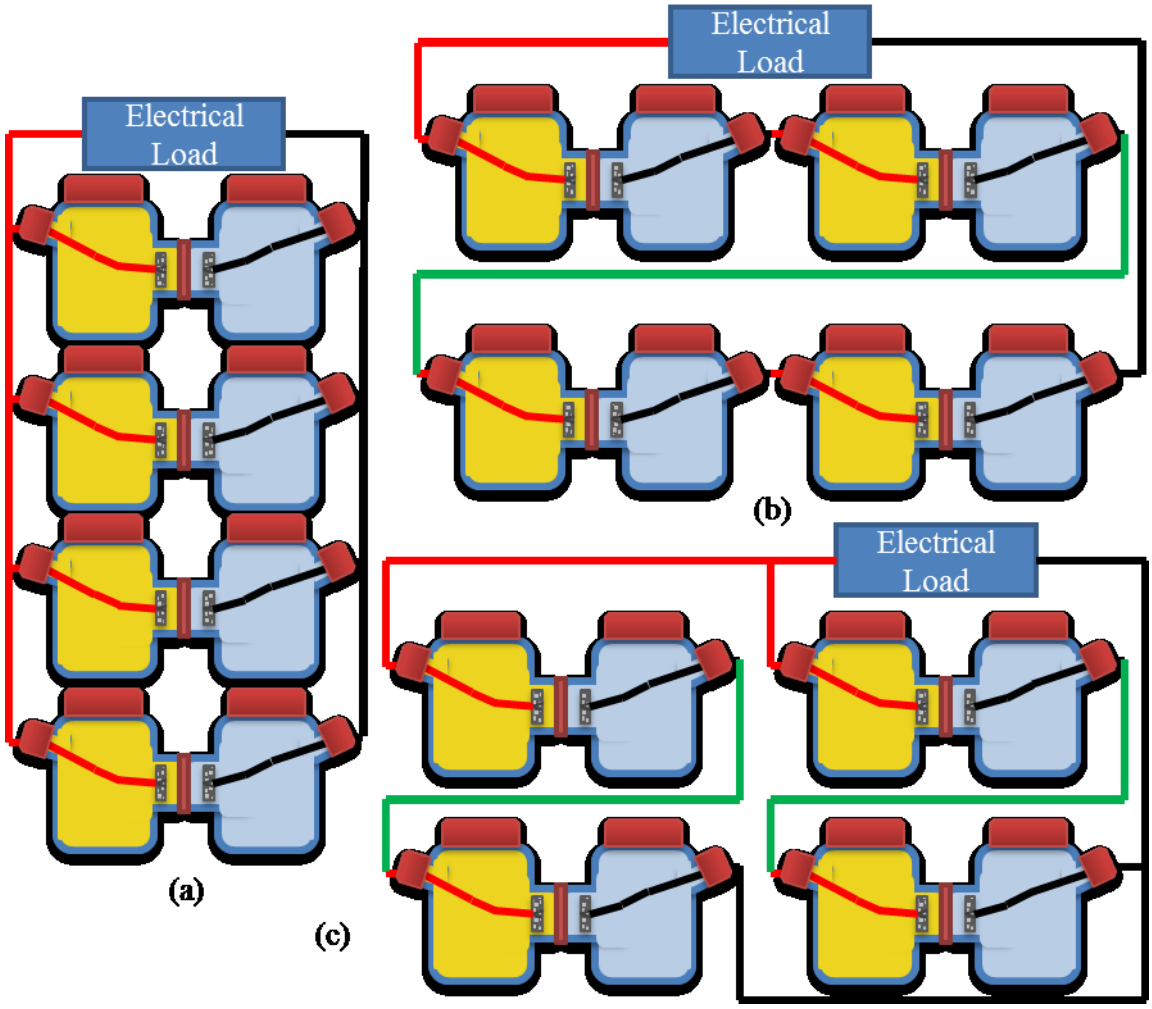

Figure 34: Different Connection Types for Arrays of DCMFCs (a) Parallel, (B) Series and (C) Hybrid of Series and Parallel

3.8. Results

3.8.1. Single Chamber Fuel Cells

3.8.1.1. Electrode Configuration

To test what effect the configuration of the electrodes had on the power output of SCMFCs, SCMFCs were setup with two different electrode configurations as outlined in Figure 33. The recorded voltage output across a 3.9 MΩ resistance is shown in Figure 35 with 5 hours of data recorded. The peak voltage for the Side-by-Side SCMFC was 69.34 mV giving 17.78 nA of current and a power output of 1.23 nW occurring at time 2.2 hours. The peak voltage for the Top-Bottom SCMFC was 156.88 mV with a current of 40.23 nA and output power of 6.31 nW occurring at time 2.62 hours.

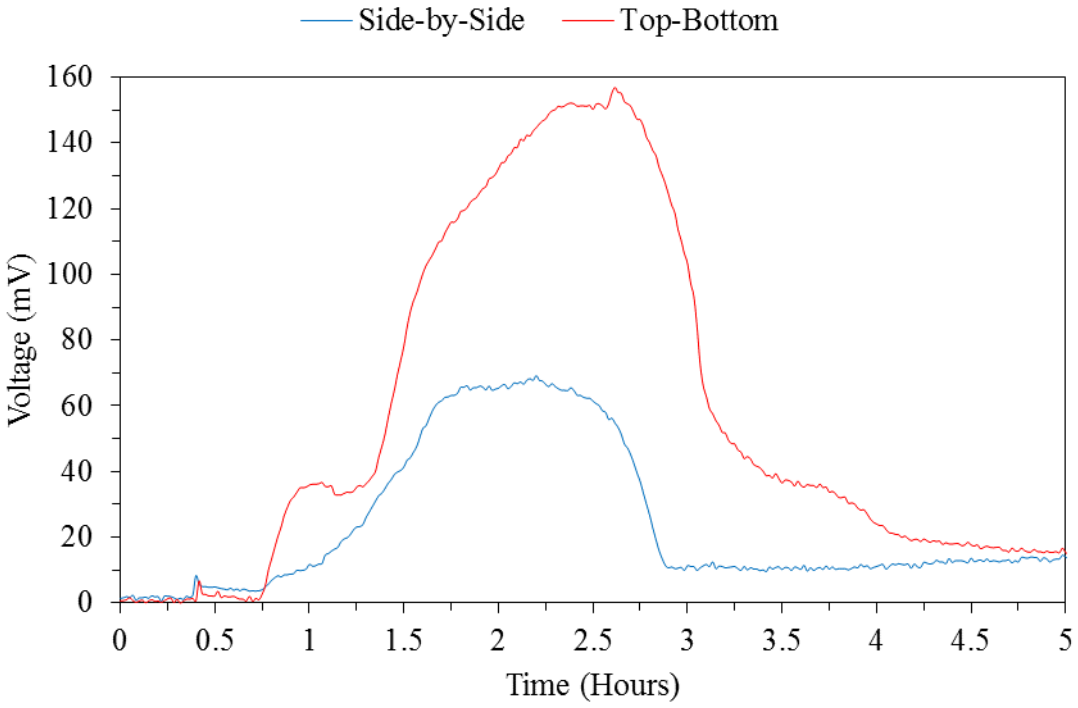

Figure 35: Recorded Voltages across a 3.9 MΩ Resistor for Side-By-Side and Top-Bottom Electrode Configurations in SCMFCs

3.8.1.2. STIRRED AND STATIC SCMFCS

Figure 36 shows the recorded voltages for SCMFCs in which one set of SCMFCs had stirring induced in the chambers, whilst the others were left static. The static SCMFC had a peak voltage of 182.30 mV with output current of 50.96 nA and output power of 8.52 nW occurring at time 2.98 hours. The stirred SCMFC showed a higher output voltage of 198.75 mV, output current of 50.96 nA and an output power of 10.13 nW occurring at time 2.3 hours. The stirred SCMFC does peak earlier and on average also outputs a higher voltage at 85.80 mV whereas the static SCMFC outputs an average of 67.73 mV.

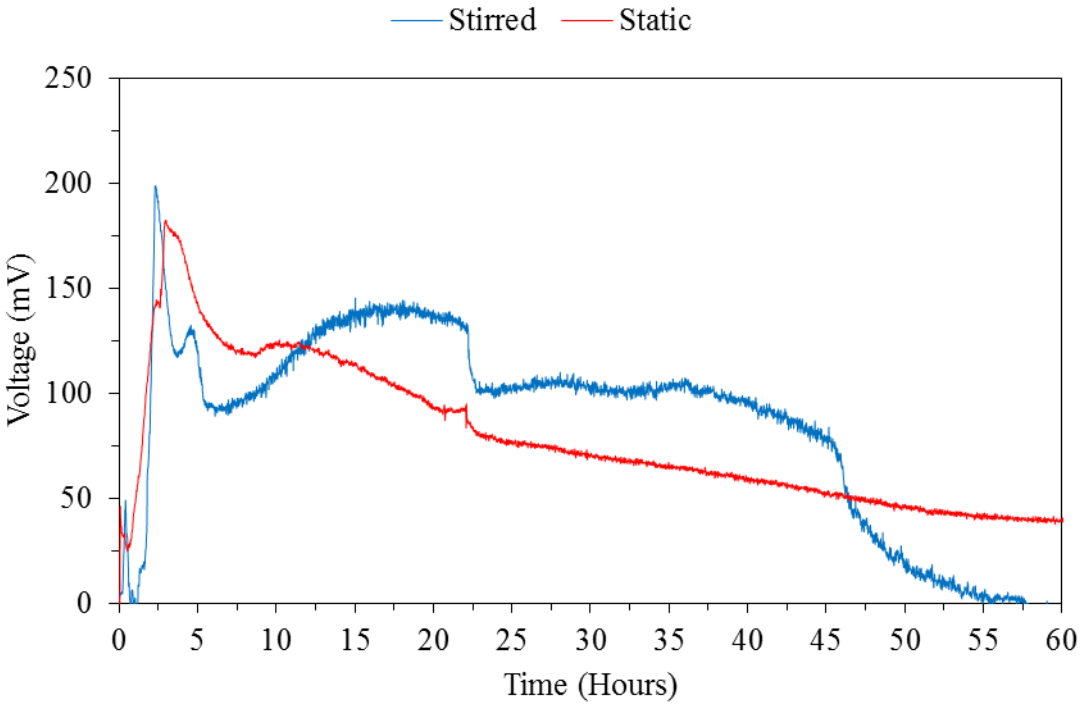

Figure 36: Recorded Voltages across a 3.9 MΩ resistance for stirred and static SCMFCs

3.8.1.3. SCMFC INOCULATION SIZE

Voltages recorded for SCMFCs with different inoculations sizes of 0.5 mL, 1 mL and 2 mL are shown in Figure 37. The SCMFC with 0.5 mL inoculation had the lowest voltage output, peaking at 11.96 mV, with a current of 3.07 nA and a power of 0.04 nW at time 14.98 hours. This is compared to the 1 mL inoculated SCMFC which had a peak voltage of 70.21 mV, an output current of 18 nA and a output power of 1.26 nW at time 4.23 hours. Lastly, the 2 mL inoculated SCMFC had a peak voltage of 77.89 mV, a peak current of 19.97 nA and a peak power of 1.56 nW occurring at time 3.12 hours.

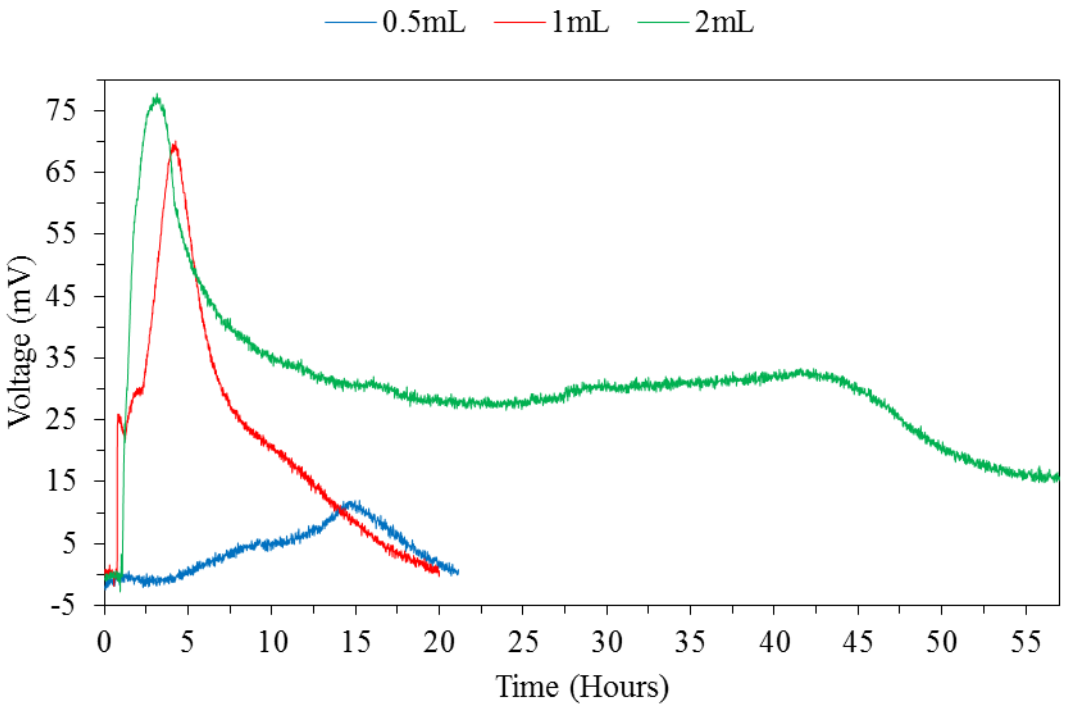

Figure 37: Recorded Voltages across a 3.9 MΩ Resistance for SCMFCs with 0.5 mL, 1 mL and 2 mL Starting Inoculations

3.8.2. Dual Chamber Microbial Fuel Cells

3.8.2.1. Mixed Culture DCMFC during the 6 to 7 Day Open Circuit Period

Open circuit voltages recorded over time for the DCMFCs with LBB as the nutrient growth solution, 25 mm membranes and with either mixed or single culture are shown in Figure 38. The initial period where little or no voltage is recorded is the lag phase of growth for each of the cultures before the voltages begin to climb. The slight notch in the mixed culture DCMFC between day 1 and day 2 can also be seen in other voltage curves. After this notch, the mixed culture DCMFC voltage climbs at a faster rate than the single culture before steadying to the same rates as that of the single culture. By the end of the 6 to 7 day open circuit growth period allowed for the DCMFCs, the voltage for the single culture was found to be 457.68 mV whilst for the mixed culture it was found to be 491.17 mV.

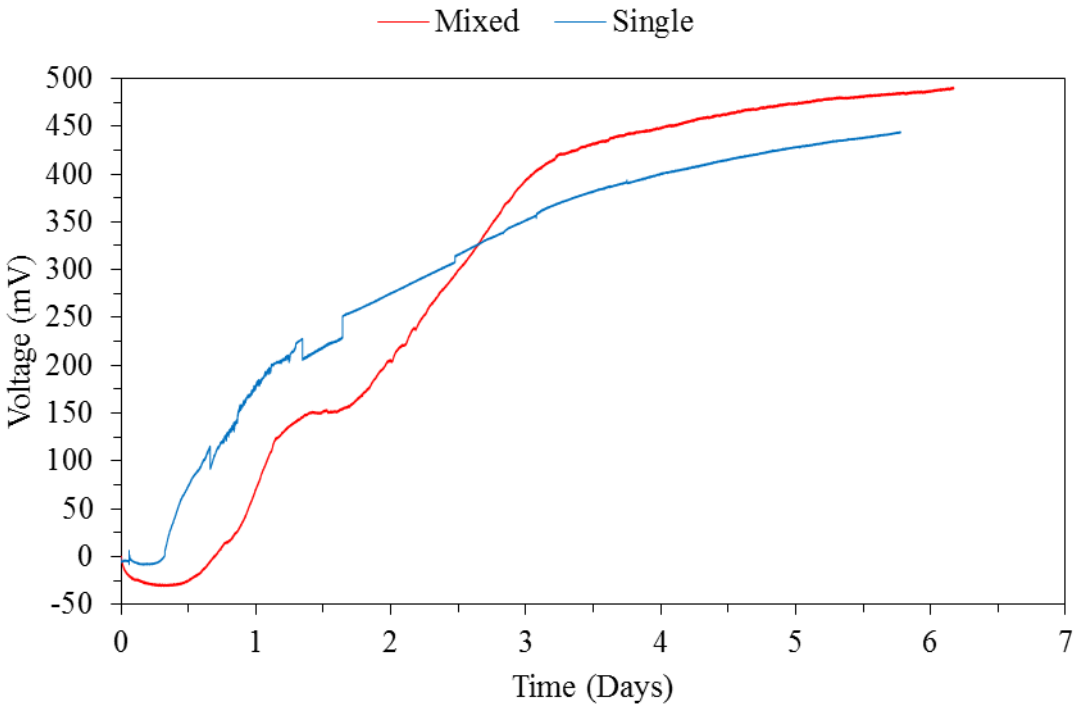

Figure 38: Open Circuit Voltages for Mixed and Single Culture DCMFCS for the 6 to 7 Day Period

3.8.2.2. MIXED CULTURE DCMFC POLARIZATION AND POWER CURVES

The Single and Mixed Culture DCMFC polarisation curves are shown in Figure 39. Values ranged between 491.17 mV at 0.13 µA to 31.5 mV at 70.95 µA for the Mixed Culture DCMFC, and 457.68 mV at 0.12 µA to 15.81 mV at 52.68 µA for the Single Culture DCMFC. The Mixed Culture DCMFCs appear better able to produce a higher voltages at open circuit and on average as well as higher short circuit currents.

Figure 40 shows the power curves for the Mixed and Single Culture DCMFCs which are taken after the 6 to 7 day open circuit period. The peak power for the Mixed Culture DCMFC was found to be 10.27 µW at 37 µA. This was almost twice as high as the Single Culture DCMFC peak power of 5.94 µW at 24.37 µA. Based on these peak powers, the internal resistances are 7.5 kΩ and 25.4 kΩ respectively.

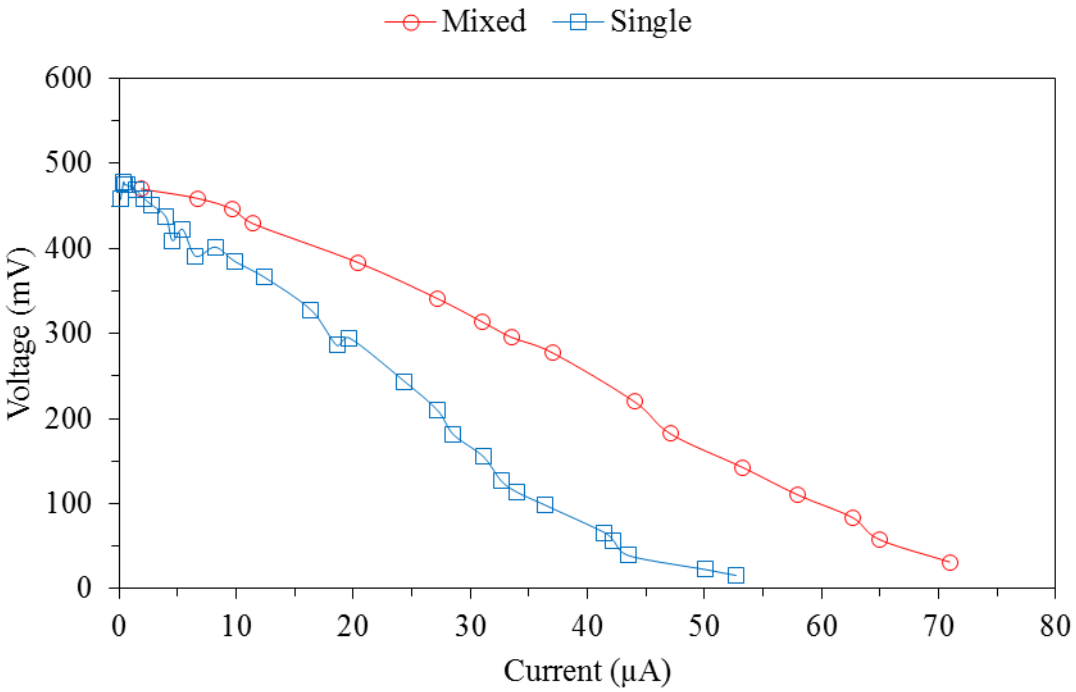

Figure 39: Polarization Curve for Mixed and Single Culture DCMFCs

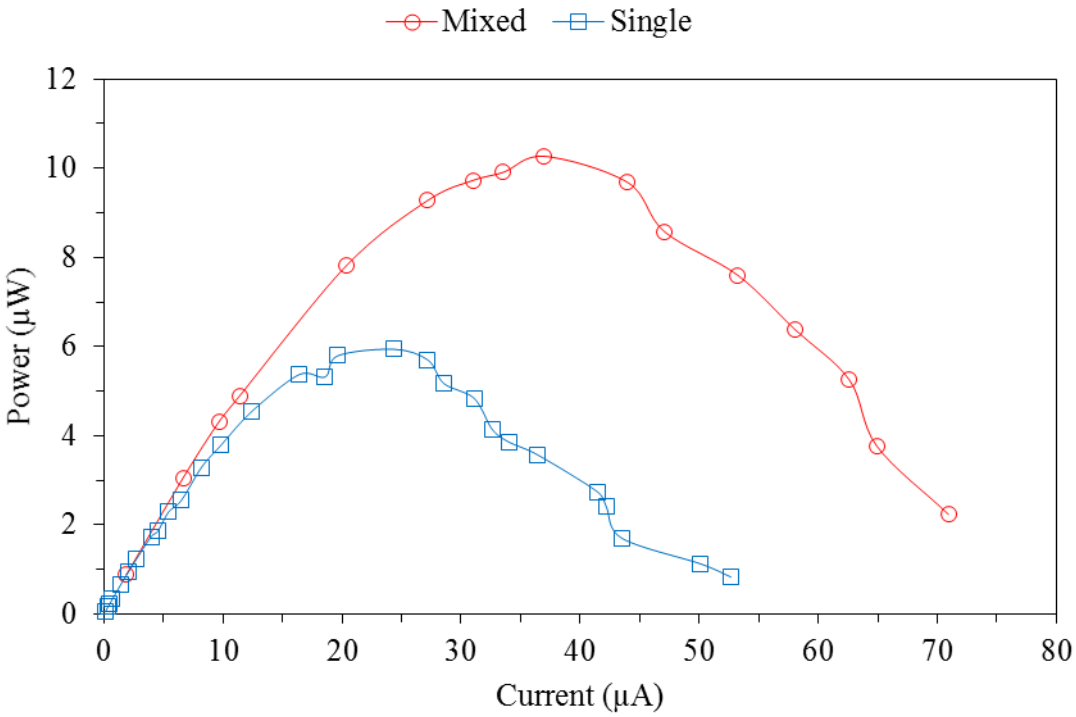

Figure 40: Power Curves for Mixed and Single Culture DCMFCs

3.8.2.3. Identification of Mixed Culture Microbes

As a first step toward identifying the microbes within the mixed culture DCMFC, streak plates from the anode chamber were created and grown. A close up image of the plate can be

seen in Figure 42. Whilst *S. oneidensis MR-1* does dominate the plate, there are two other cultures which are different in colony morphology to *S. oneidensis MR-1* which have 'Large Milky' and 'Sharp Yellow' morphology and are hence called these.

To help distinguish each of the colonies, gram staining, catalase testing and oxidase testing were performed. Both colonies were found to retain crystal violet indicating they are both gram positive, and both were also positive during the catalase testing, indicating the colonies are either aerobic or facultative anaerobes. The large milk colony was found to be positive for the oxidase testing and the sharp yellow colony was negative. Lastly, a negative result of the sharp yellow colony for the oxidase testing indicates that the microbes are from the *Enterobacteriaceae* family whilst a positive result the large milky colony is of one of either of the following (Acharya 2012):

- *Pseudomonas spp*
- *Vibrio cholerae*
- *Neisseria spp*
- *Campylobacter spp*
- *Helicobacter spp/ Haemophilus spp.*
- *Aeromonas spp*
- *Alcaligens*

Microscope images of the two colonies were also taken and are shown in Figure 41. The large milky colony shows rod shaped microbes which are short, do not show any particular arrangement on the slides and may be spore forming. The sharp yellow colony shows coccus shaped microbes that are tiny in size and again show no particular arrangement or clustering on the slides.

Other tests performed included a McClonkey Agar, Horse Blood Agar and an API Biochemical Test and were inconclusive. Based on the data taken however, it seemed that the bacteria found in the mixed culture DCMFCs were likely bacteria found on the human skin or in the lab and could be a *Staphylococcus* or *Pseudomonas*. No further identification was undertaken as the colonies did not seem to provide significantly more power than the single culture *S. oneidensis MR-1* DCMFCs, and therefore were not to be used in subsequent experiments.

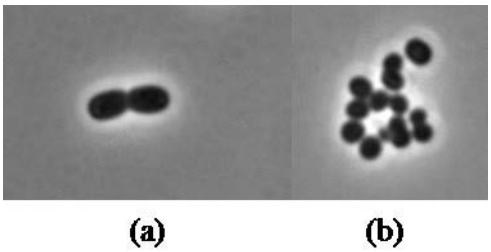

Figure 41: Microscope images of two colonies of the Mixed Culture DCMFC other than *S. oneidensis MR-1* (a) Large Milk, (b) Sharp Yellow.

3.8.2.4. LBB AND TSB DCMFCS DURING THE 6 TO 7 DAY OPEN CIRCUIT PERIOD

LBB and TSB DCMFCs were run for a 6 to 7 day period in open circuit with their voltage monitored and are shown in Figure 43. The LBB DCMFC during this period reached a peak of 464.557 mV, whilst the TSB DCMFC reached a peak of 332.86mV. Aside from a difference in the peak voltages, there is also a major difference in the voltages in the first two days of running. The TSB DCMFC's voltage rises quickly in the first day to almost 200mV and slowly climbs to its peak by day 6. In contrast, the LBB DCMFC is largely inactive in the first day and only begins to steadily rise from day 2 onwards.

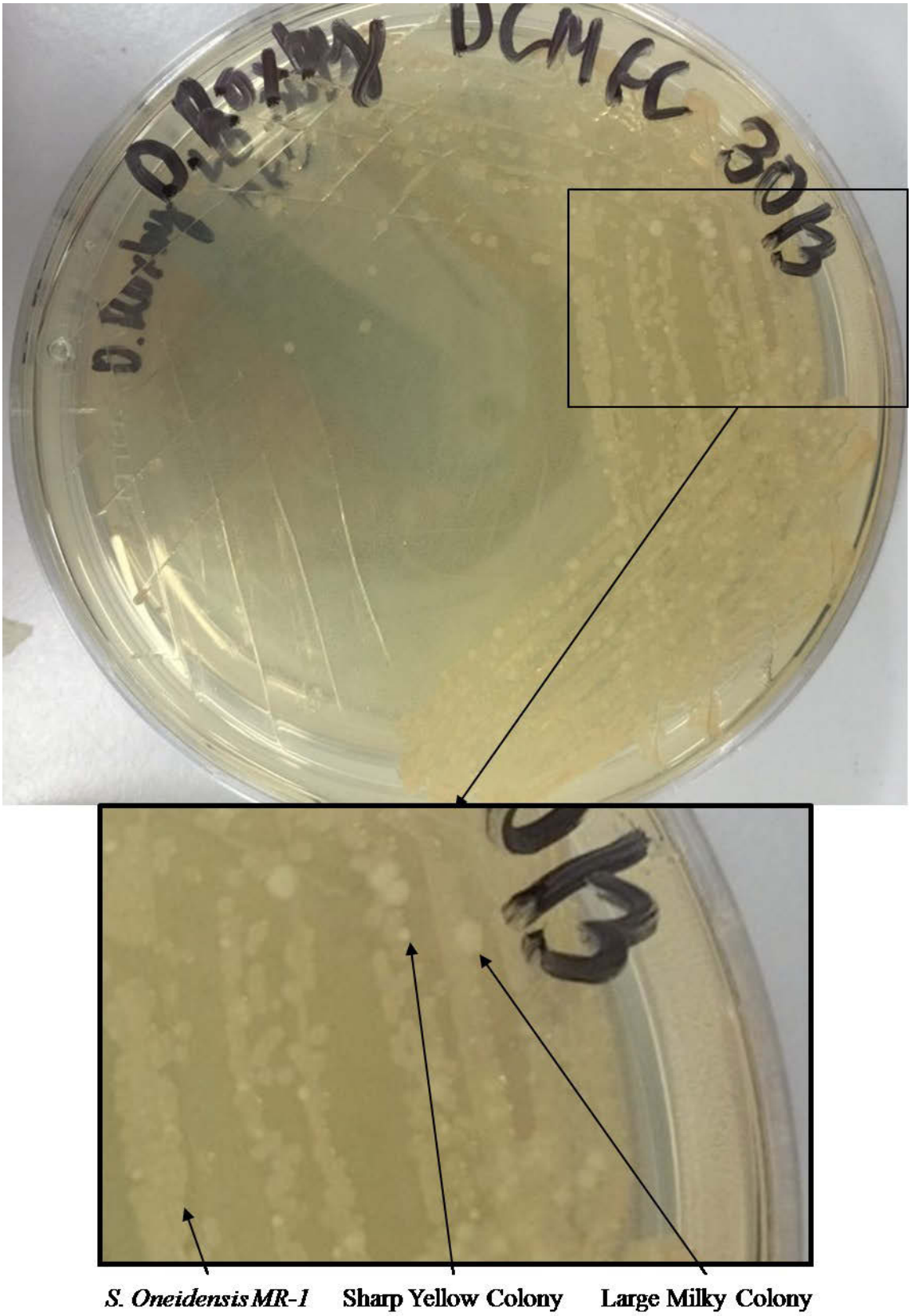

Figure 42: Close up of streak plate for identifying mixed culture of DCMFC

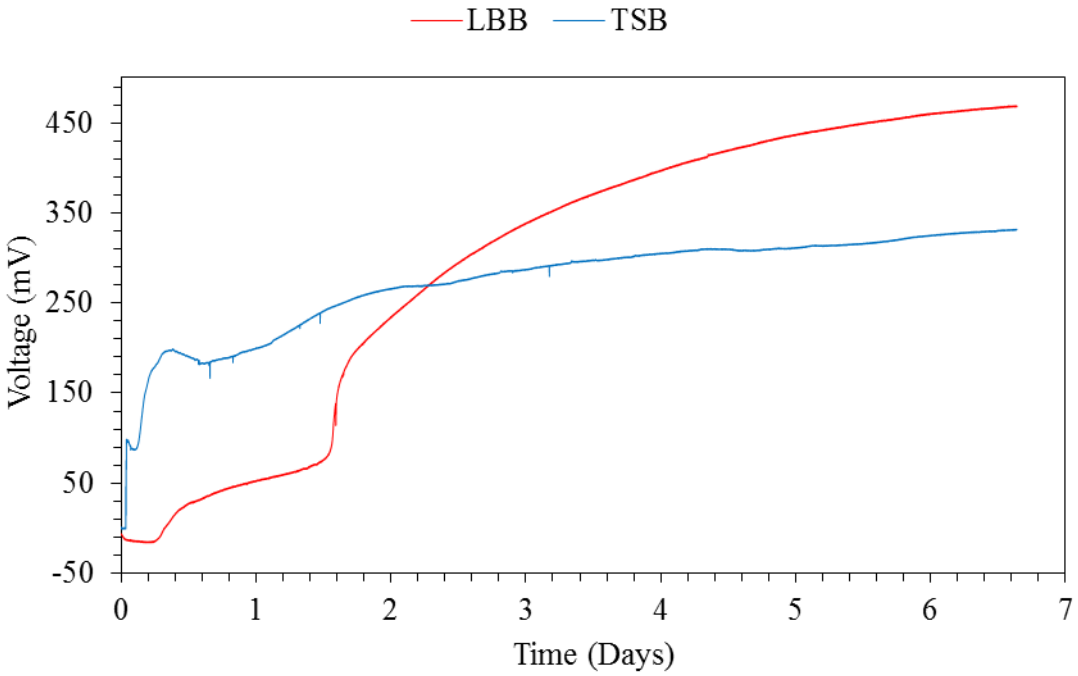

Figure 43: Open Circuit Voltages for LBB and TSB DCMFCS for the 6 to 7 Day Period

3.8.2.5. TSB AND LBB POLARIZATION AND POWER CURVES

The TSB and LBB DCMFC polarisation curves are shown in Figure 44. Values ranged between 451.02 mV at 0.115 µA to 70.8 mV at 70.8 µA for the LBB DCMFC, and 328.82 mV at 0.084 µA to 13.42 mV at 16.37 µA for the TSB DCMFC. Given that all components are the same between the two DCMFCs, it would appear that either the microbial population grown from the LBB supports higher voltage output than TSB, or perhaps there is some other chemical difference.

Figure 45 shows the power curves for the LBB and TSB DCMFCs which are taken after the 6 to 7 day open circuit period. The peak power for the TSB DCMFC was found to be 1.23 µW at 11 µA. This is approximately 8 times lower than the LBB DCMFC peak power of 9.68 µW at 34.31 µA. With these peak powers, the internal resistances are determined to be 10 kΩ and 8.2 kΩ respectively.

It is known that pacemakers can be powered from as little as 30 µW of power, and therefore neither of the TSB and LBB DCMFCs has the capability to power a pacemaker. Additionally,

the peak power occurs as a voltage of 109.99 mV for the TSB DCMFC and 281.31 mV for the LBB DCMFC. These voltages by themselves are too low to be able to turn on any devices.

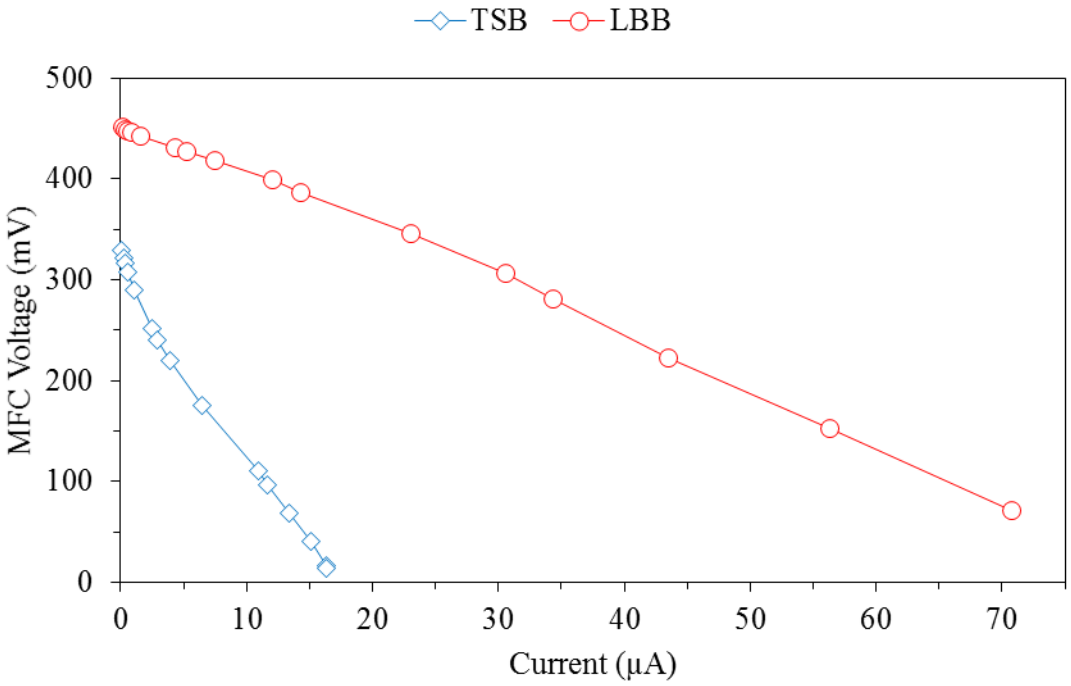

Figure 44: Polarisation Curves for TSB and LBB DCMFCs

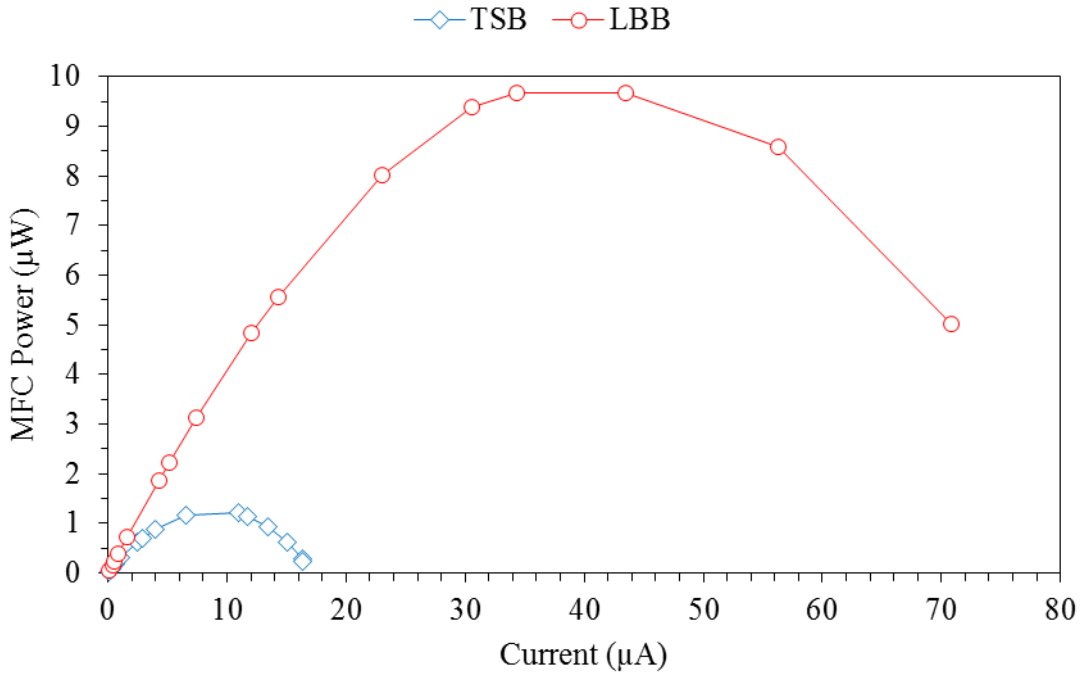

Figure 45: Power Curves for TSB and LBB DCMFCs

3.8.2.6. INFLUENCE OF MEMBRANE SIZE ON POWER OUTPUT OF DCMFCS

One of the needs of a membrane is to allow the sole movement of hydrogen in to the cathode chamber from the anode chamber, to both maintain optimum growth pH in the anode, but also to complete the reaction at the cathode electrode. The size of the membrane may influence how much hydrogen moves through to cathode electrode and thus how much current is generated if there is more electrons allowed off the cathode electrode during the reaction. To test this, 25 mm and 40 mm diameter membranes we experimented with and the voltage and power outputs measured. Only LBB DCMFCs were used as these previously provided the best power output.

Figure 46 shows the open circuit voltages of LBB DCMFCs during the 6 to 7 day period. There is minimal difference in the voltages aside from the first 2 days where the voltage of the 25 mm diameter membrane DCMFC increases faster to approximately 200 mV than the 40 mm diameter membrane DCMFC. Most notably, after the 6 to 7 day open circuit period, the voltages are approximately the same.

In Figure 47 is the polarisation curve for the two different sizes membrane DCMFCs. The voltages at open circuit are both at approximately 450 mV, however we see that as various resistances are connected, lowering the voltage and increasing the current output, we see that for similar voltages, the larger membrane DCMFC is able to output higher current. As a comparison, for the 25 mm membrane DCMFC, at 155.535 mV, 31.107 μA is sustained, whereas the 40 mm membrane DCMFC sustains 56.307 μA at 152.03 mV.

The difference in output current, resulting from the difference in membrane size also has further downward affects. Specifically, the difference in output power shown in Figure 48 is significantly larger. The 25 mm membrane DCMFC was able to provide a maximum of 5.94 μW of power at 243.73 mV and 24.737 μA, whilst the 40 mm membrane DCMFC provided a

maximum of 9.68 µW of power at 281.31 mV and 34.306 µA. This meant the internal resistances were 10 kΩ and 8.2 kΩ respectively.

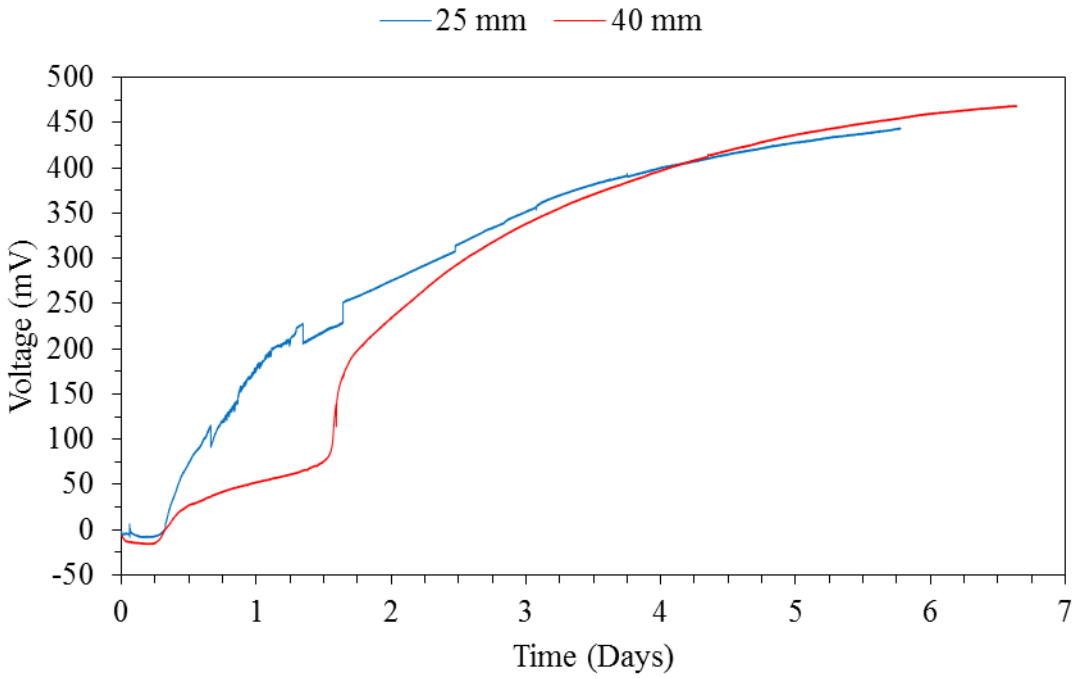

Figure 46: Open Circuit Voltages for 25 mm and 40 mm Membrane DCMFCs for the 6 to 7 Day Period

3.8.2.7. ARRAYS OF DCMFCS

Following experiments with DCMFCs on parameters such as the growth medium and the size of the membrane, placing DCMFCs in different array connections was then tested as shown in Figure 34. The series and parallel connections were first tested, as these are common types of connections. It was expected that depending on the type of connection, that different increases in current and voltage would be seen. The parallel-series hybrid connection was borne out of a need to improve both the current and voltage concurrently.

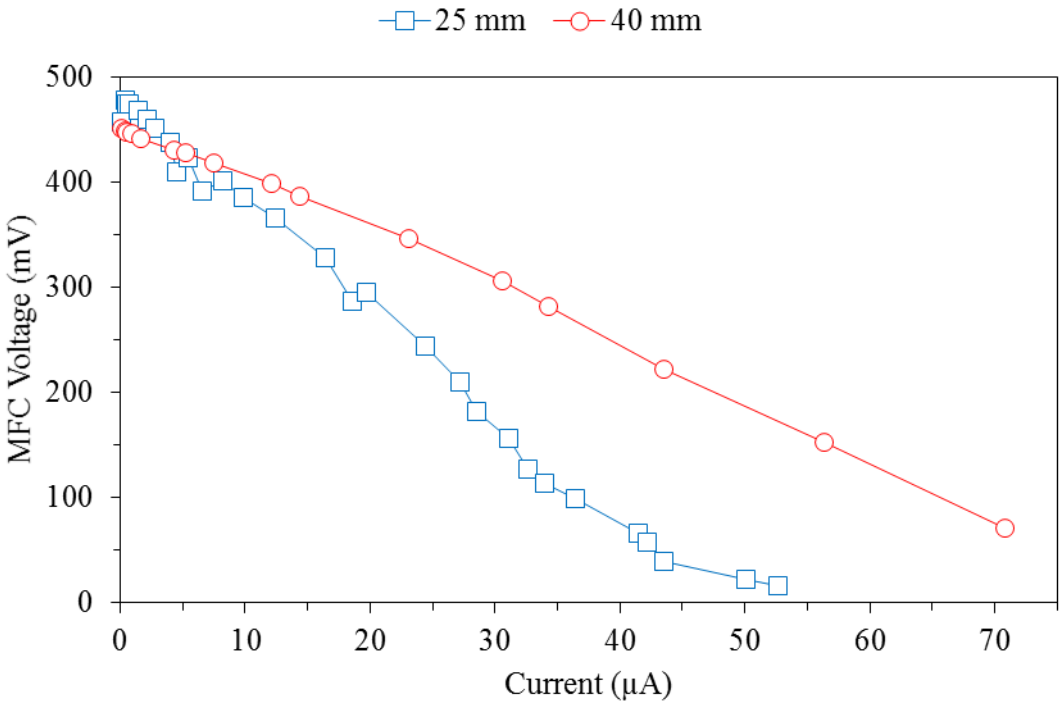

Figure 47: Polarisation Curve FOR 25 mm and 40 mm Membrane DCMFCS

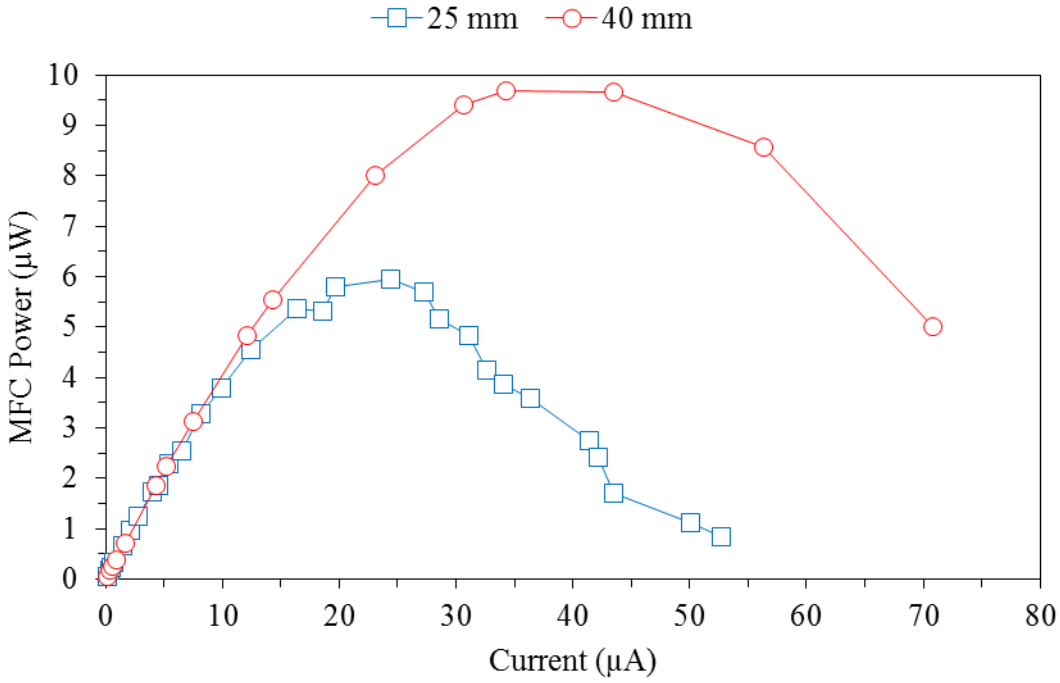

Figure 48: Power Curves for 25 mm and 40 mm Membrane DCMFCs

The polarisation curve for the arrays of DCMFCs is shown in Figure 49. The series array starts at approximately 1619.38 mV and provides a peak measured current of 69.69 µA. The parallel connected array starts at a voltage of 490.559 mV and a peak current of 378.667 µA.

The hybrid parallel-series connected array sits in the middle of both, giving an open circuit voltage of 913 mV and a measured peak current of 261.89 µA. The power curve for DCMFCs in arrays is shown in Figure 50. The peak power for the series, parallel, parallel-series and single LBB DCMFC are 39.069 µW at 765.534 mV and 51.0356 µA, 63.47 µW at 251.935 mV and 251.953 µA, 54.645 µW at 527.91 mV and 103.511 µA and 9.68 µW at 281.31 mV and 34.31 µA respectively. The internal resistances for each array are 15 kΩ for series, 1 kΩ for parallel, 5.1 kΩ for parallel-series and 8.2 kΩ for the individual LBB DCMFC.

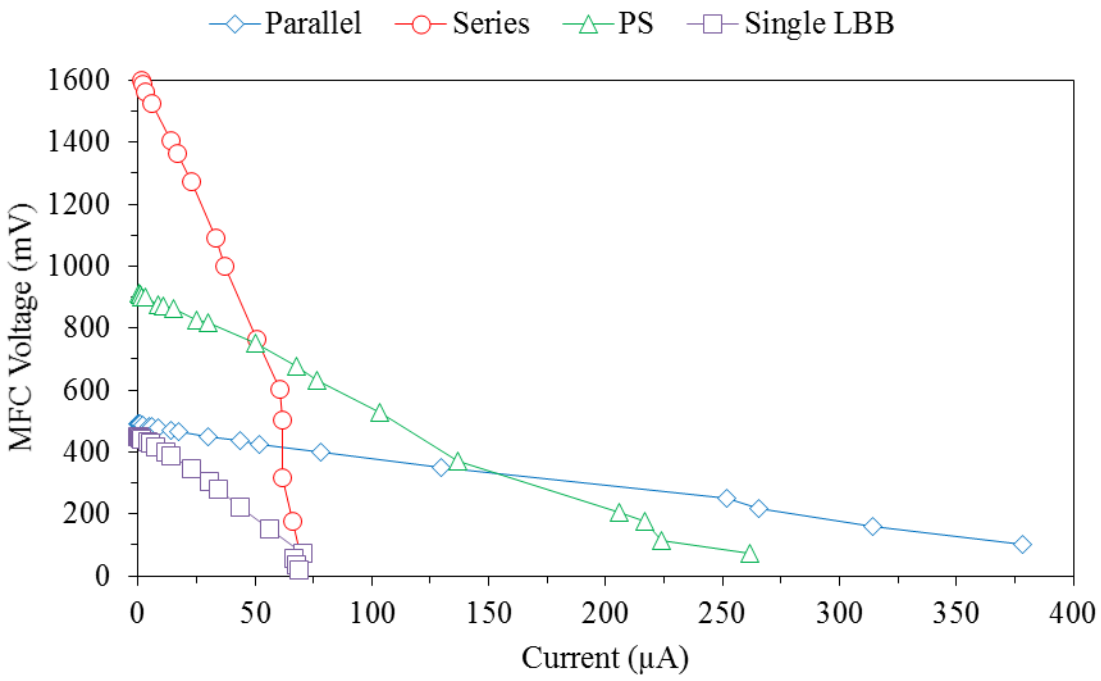

Figure 49: Polarisation Curves for Parallel, Series, Parallel-Series and a Single LBB DCMFC

3.9. Discussion and Conclusion

To determine methods for improving the power output of Microbial Fuel Cells, both single and dual chamber MFCs were experimented with and within each, various different parameters. In the SCMFCs, parameters tested included electrode configuration, stirring and inoculation size, and in DCMFCs parameters included mixed versus single culture, growth media, membrane size and stacking connections.

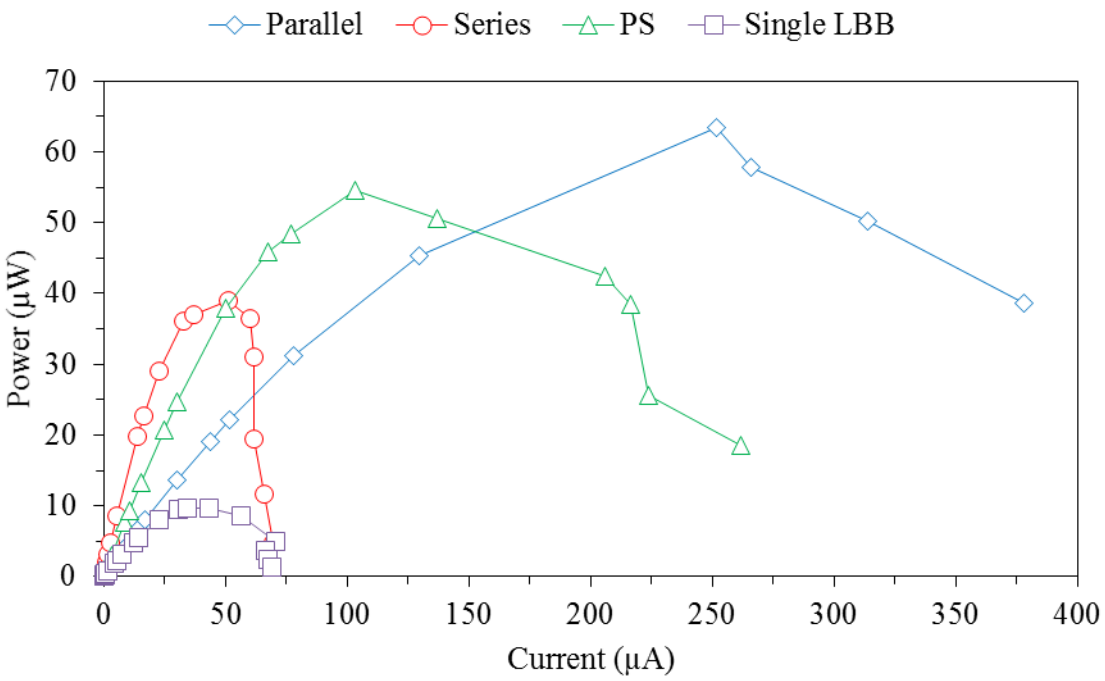

Figure 50: Power Curve for Parallel, Series, Parallel-Series and a Single LBB DCMFC

The SCMFC results first tested the electrode setup and what effect that this may have on the power output. The idea here being that a patient moves around, standing or sitting up as well as laying down and therefore the electrode position changes. In a Top-Bottom configuration, the voltage was over 2-times higher than the Side-by-Side configuration. As the bacteria float, they fall onto the electrodes under the Top-Bottom configuration and generate more electrical output when they come in contact with the electrode. This is less likely to happen with the Side-by-Side configuration.

When testing the SCMFCs with different inoculation sizes, initial spikes of electrical output were measured and the lower the inoculation volume, the lower the voltage measured. It is the case that the smaller volumes needed time to grow in population before they could generate higher voltages. Alternatively, these inoculation volumes may be too high, and small volumes may need to be tested.

The third parameter in SCMFCs, stirring versus static SCMFCs, also gave some interesting results. The stirred SCMFC gave the higher voltage between the two and the highest overall voltage between all SCMFCs of almost 200 mV. This was expected since usually, stirring does increase microbial growth and chemical reactions, which in a MFC, may result in more voltage, current and power.

The voltages overall from the SCMFCs had been a challenge up to this point, and to obtain a result of nearly 200 mV through stirring showed improvement. This result places SCMFCs in contention with other energy harvesting technologies such as mechanical harvesting which require movement from the user to harvest energy. With these and further optimisations, SCMFCs can power AIMDs.

Results of the DCMFC were significant improvements again on the SCMFCs. In the first test of the DCMFCs, mixed culture DCMFCs and single culture DCMFCs were tested. The mixed culture DCMFCs gave significantly higher power at over 10 μW and an open circuit voltage of almost 500 mV. Attempts were made to identify the different microbes in the culture, however in the end this was not completely. The streak plates showed that most of the microbes present in the culture were *S. oneidensis MR-1* and subsequent experiments showed that similar amounts of power were also measurable from other conditions. Additionally, since one of the potential identification candidates for the bacteria is *Pseudomonas*, the likelihood of this eventually being implanted in the human body is unlikely due to its many issues in clinical contexts. The potential of DCMFCs was shown, giving significant voltages and power outputs. Nonetheless, the bacteria are likely to have come from human skin, and this all suggests the potential for use of the bacteria of the human body like say from the gut, for use in implantable MFCs.

To further experiment with DCMFCs, the effect of common growth media was tested. At the end of the 6 to 7 day open circuit period, the LBB DCMFC had a voltage approximately 40% higher than the TSB DCMFC. In MFCs, electrons are transported from the bacteria to the electrode either indirectly or directly, where directly offers higher power output capabilities. In the direct case, this occurs when particular bacteria have DET mechanisms such as nanowires pili or cytochromes which come as a survival response to less favourable conditions for the bacteria. LBB, whilst being considered a general growth media for bacteria, is still less nutrient rich than TSB. In studies using optical density measurements, we found that TSB cultures had higher growth than cultures grown in LBB. The fact that it is less nutrient rich makes it less favourable condition to the bacteria and is a cause for the direct electron transfer mechanisms, thus leading to increased power output.

Given the aforementioned, it would make sense that if we made conditions more unfavourable for the bacteria, that they may be able to produce more power. A common growth media with fewer nutrients is M9 and this was used, supplemented with glucose as a carbon source, to test this idea. Neither voltage nor any bacterial growth was measured in the M9 DCMFCs after the 6 to 7 day open circuit period. M9 has a similar set of ingredients to a specialised mixture used for the MFC microbe *G. sulfurreducens* (Bond & Lovley 2003). The lack of growth and voltage output suggests limitations with *S. oneidensis MR-1*.

The membrane size of a DCMFC has been shown to influence the current and power, but have no effect on the voltage output. Theoretically, the fuel cell potential can be calculated by analysing each electrode as half cells reactions with each having their own voltage potential. This equation has two parts where the first part sets the voltage of the electrode due to its composition and is measured relative to hydrogen and the second part is related to the reaction itself. The reaction is about the supply of electrons to the electrode and perturbs the standard electrode voltage from its ideal value (Bard & Faulkner 2000).

Under open circuit conditions, this value would remain unaffected by a change in membrane, as a smaller or larger membrane affects how many protons are exchanged from the anode to cathode electrode and under open circuit, there is no requirement for electron supply thus no perturbation from the standard electrode voltage. When a load is connected causing current to flow, protons which diffuse through the membrane will eventually react with the cathode electrode. A smaller membrane will act as a bottleneck, as it will limit the amount protons which eventually react with the electrode and limit the current. Figure 51 illustrates this idea.

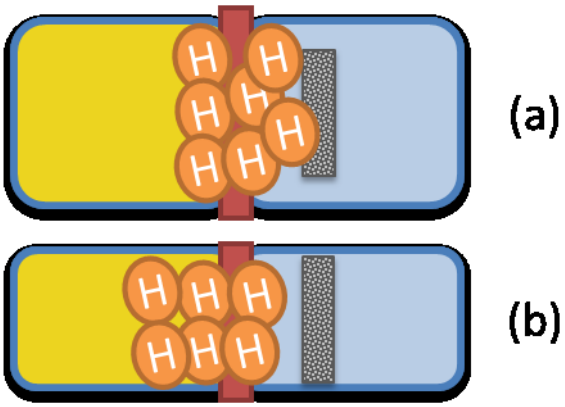

Figure 51: (a) a larger membrane, enabling more hydrogen through at any one time (b) a smaller membrane, creating a bottle neck of hydrogen needing access to the cathode electrode

Connecting power sources in series or parallel will typically boost the voltage or current respectively, whilst also either increasing or decreasing the internal resistance respectively. Experimental data shows a similar effect has occurred, where for the series connection, 4 DCMFCs connected together multiplied the individual voltage of 451.02 mV by almost 4 times to 1619.38 mV. In parallel connection, we see an increase in current from 69.11 µA to 378.167 µA, coming as a result of both the 4 sources of current, and the lowering of the internal resistance. In order to increase both the voltage and current, the parallel-series connection was experimented with, resulting in a boost in voltage from 451.02 mV to 913 mV and an increase in current from 69.11 µA to 261.89 µA. The higher voltage was a significant step, since this is well within the operating range of various electronic devices.

The changes in internal resistance are also interesting, since there is an inverse relationship between the internal resistance and the maximum power output. Decreasing the internal resistance leads to a higher maximum power output which also lead to a wider operational current range. Internal resistance of a MFC is known to come from multiple sources including the conductivity of solution, membrane size, contact resistances and distances between electrodes to name a few. In terms of reactor design then, an individual DCMFC can have its maximum power output increased if the reactor is designed to lower the internal resistance.

The typical approach to boost a voltage in electronics is to use a step up converter which takes what voltage and current is available, and usually sacrifices some of the current to boost the voltage. Despite the increases in voltage, current and power in the DCMFCs over the SCMFCs, connecting a step up converter evaluation board, the LTC3109 to either of the arrays did not help. The voltage of the arrays was within the range required for the evaluation board to operate, however in all cases the voltage of the arrays quickly dropped as it could not sustain the high current required for the board to be able to charge and output a higher voltage.

The datasheet of the LTC3109 gives a minimum value of 6 mA for the device to begin and without any load connected. In the parallel connection, which gives the highest amount of current possible from 4 connected DCMFCs, the maximum output current was less than half of 1 mA. The LTC3109 was the best of this class of electronics at the time of purchase, however newer ICs have since been released which may be able to handle the current and power ranges that these DCMFCs are capable of.

Irrespective of whether the DCMFC arrays or the energy harvesting ICs were able to power an AIMD or not, the fact remains that the DCMFCs are at least 200 mL (200 cm^3) in volume,

which is twice the size of the SCMFCs. Coin batteries, which are the existing technology for powering many AIMDs, has a volume of approximately 1 cm^3. The DCMFCs are also larger than the devices to power. For example, the pacemaker, the Medtronic Adapta a has a volume of 17.81 cm^3 (Medtronic 2016a). Miniaturization and power density are therefore major challenges for MFC technology to power AIMDs.

If miniaturization were to be worked on within MFCs, there are still limitations with the bacteria in two ways. Firstly, in hospitals around the world, there is a constant battle to try maintain sterile environments to ensure that during surgical procedures that patients are not infected (Levy 1998; Pires et al. 2017; Rodríguez-Rojas et al. 2013). A literature search will find that whilst some people have been infected with *S. oneidensis*, there is limited literature available on its potential infectious affects, however evidence suggests *Shewanella oneidensis* has antibiotic resistance building genes (Fredrickson et al. 2008; Heidelberg et al. 2002; Holt, Gahrn-Hansen & Bruun 2005; Janda 2014; Janda & Abbott 2014; Korenevsky et al. 2002; Yang et al. 2009; Yousfi et al. 2017). Existing implantable batteries very clearly do have highly toxic materials but can be contained. In contrast however, bacteria as a living organism can be pathogenic and thus actively seek to survive and will spread and harm others if required. We previously discussed the idea of placing bacteria under difficult conditions to help them to grow to output electrons. The particularly pathogenic bacteria such as *P. aeruginosa* and *Staphylococcus* have distinguishing features allowing them to survive in harsh conditions such as limited nutrient supply, acidic or basic pH and pili allowing them to spread to new places that others cannot. In a sense then, to increase power output from bacteria is to increase their pathogenic properties and thus in this point in history where the field of antibiotics is having its issues, the idea of implantable bacteria is hardly passable.

The second challenging issue is the characteristic of bacteria to grow to a population size proportional to the space they are growing in and their nutrients (Willey, Sherwood &

Woolverton 2008). There is inherent an upper limit then to the amount of bacteria that may be able to be implanted and thus an upper limit on the energy generation possible. This is in addition to the need to devise a way to be rid of the toxic metabolites of the bacteria or else the bacteria themselves will eventually die from their own waste. This waste management system would need additional space to what is already required.

The use of MFCs to generate electricity from sugar is still a compelling idea. A solution which appropriately takes the advantages of this idea without the disadvantageous power density and pathogenicity issues is certainly future work for this field. It is notable that the 'guts' of bacteria provide it with many functions allowing them to live and output electrons but also many of the aforementioned problems. The following chapters discuss methods to leverage this idea.

CHAPTER 4 COMPRESSED POLYPYRROLE ELECTRODES FOR GLUCOSE ENZYMATIC BIOFUEL CELLS

4. Compressed Polypyrrole Electrodes for Glucose Enzymatic Biofuel Cells

4.1. INTRODUCTION

In the previous chapter, we investigated various parameters involved in improving microbial fuel cell power output, and how they affect the power output in the context of powering AIMDs. This was on the basis that many studies may not be appropriate for implantation or their design intent was for implantation but have not fully considered all aspects and thus may not be appropriate. Some of the parameters and contexts investigated include the orientation of electrodes and the effect the orientation of the electrodes has on power output, since a patient is lying down or standing or sitting upright. It is hoped that with medical technology that a patient can live a more normal life and therefore at least be somewhat active. This being the case, a fuel cells electrolyte may be stirred or static. The reactor type also has an influence on the overall device design, since a single chamber is simpler to arrange but requires greater complexity to achieve high power output. Alternatively, a dual chamber design's baseline power output may be higher but it is a more complicated and costly design. The amounts of bacteria as well as the nutrients that are fed to them also has particular importance since it is implanted and thus much harder to fix.

In experimenting though, we found that even when combining several DCMFCs together, the best power output that could be achieved was a little over 60 μW with 4 large 200 mL DCMFCs. This was not quite enough to power a device, even with a step up converter, and it was not considered ideal to implant bacteria. Bacteria themselves are living and thus require part of the energy from the sugar, and are usually infectious making it a difficult proposition to deliberately implant them. Inside the bacteria are enzymes which are what extracts the electrons from the glucose sugar and if this were used directly, rather than the bacteria, the issues surrounding microbial fuel cells toxicity and operating energy requirements can

potentially be bypassed. This kind of fuel cell is the other type of biological fuel cell called enzymatic biofuel cells.

The key component of an enzymatic biofuel cell is the electrodes which contain both the enzymes and a conductive material to conduct the extracted electrons off to the electric circuit. Many studies have taken this approach but the methods used constrain them to only using small amounts of enzymes through complicated methods. One promising method uses a very simple approach which is to directly compress the conductive material and enzymes together to form tablet like electrodes with multiwalled carbon nanotubes wrapped in cellulose membranes to help keep the enzymes within the compressed conductive matrix (Zebda et al. 2011). This compression method is very similar to that used in medical tablets and therefore is simple, highly manufacturable and allows large amounts of the constituent chemicals such as the conductive materials and enzymes to be compressed densely into a small space, allowing for high enzyme loading for high concurrent electron transfer, as well as DET.

In this chapter, we take a slightly different approach which has its own distinct advantages. It is clear that the electrodes are key, but the selection of an appropriate conductive material is required. Polymers are able to be made to be conductive, biocompatible and enzymes can be directly immobilised, all through functionalization. The focus of this chapter is to test the potential of conductive polymers as an alternative material for use in compression method for improving power output in GEBFCs. In particular, we focus on the monomer synthesis, RAFT polymerization of the monomer, EP to graft the polymer and make it conductive, creation of the compressed polypyrrole (Ppy) electrodes and subsequent GEBFC studies.

The chapter is thus laid out as follows: we begin with the materials and methods, going into as much detail as possible about the various steps in the experiments. Much of the work done

is with the development of the monomer and polymers, but ultimately culminates in the main focus which the creation of the electrodes and the GEBFC itself. We then go into the results, giving several NMRs, GPCs and conversion ratios for the monomer and polymers, as well as electrochemical studies of the formed material. The compressed GEBFC electrodes are then formed and tested in which power is generated from sugar through the compressed polypyrrole matrix electrodes.

4.2. MATERIALS

Product Name	**Manufacturer / Supplier**	**Product Code**
3-Thiophenemethanol	Sigma Aldrich	332399
Dry triethylamine	Sigma Aldrich	T0886
Polypyrrole (Ppy, conductivity 10-50 S/cm)	Sigma Aldrich	577030
Calcium chloride	Sigma Aldrich	212946
Dry diethyl ether	ChemSupply	EA012-2.5L
Distilled Methacryloyl Chloride	Merck	64120
Sodium Hydroxide	ChemSupply	SL178
Flake Silver	Johnson Matthey	FS2
Reticulated Vitreous Carbon	Goodfellow	073-784-76
Platinum Foil	Goodfellow	PT000261 332-547-93
Acetonitrile	ChemSupply	AH1008
Tetrabutylammonium tetrafluoroborate	Sigma Aldrich	86896
Silver Wire	Sigma Aldrich	327026
Pyrrole	Sigma Aldrich	131709
4-Cyano-4-	Sigma Aldrich	758353

(phenylcarbonothioylthio)pentanoic acid N-hydroxysuccinimide ester		
4,4′-Azobis(4-cyanovaleric acid)	Sigma Aldrich	11590
1,4-Dioxane	Sigma Aldrich	296309
Laccase from *Tramates versicolour*	Sigma Aldrich	38429
Glucose oxidase from *Aspergillus niger*	Sigma Aldrich	G2133

Table 17 Various materials used for the Chapter 4 experiments

4.3. METHOD

4.3.1. PREPARATION OF CHEMICALS

3-Thiophene methanol, dry triethylamine, copper chloride, dry triethylether, distilled acryloyl chloride, sodium hydroxide, calcium chloride, Polypyrrole (Ppy, conductivity 10-50 S/cm), Glucose oxidase (GOx) from *Aspergillus niger*, Laccase (LAC) from *Trametes Versicolor*, Polypyrrole (Ppy, conductivity 10-50 S/cm) and Phosphate Buffer Solution (PBS) tablets were purchased from Sigma Aldrich and used as is. Glucose was purchased from Ajax Chemicals. Deionised water was filtered through a MilliQ machine at 18.2 MΩ.

4.3.2. SYNTHESIS OF 3-METHYLTHIENYL METHACRYLATE (MTM)

The synthesis of MTM was adapted from Çirpan et al (Çirpan et al. 2002) where as best as practically possible, proportions stated in the methods section for concentrations were matched. Under a chemical hood, 6.35 grams (55.59 mmol) 3-thiophene methanol, 8.13 grams (80.33 mmol) triethylamine, a pinch of dry copper chloride and 35 mL of diethyl ether was mixed together in round bottom flask on a magnetic stirring plate to make ‘mixture 1’. Again in the chemical hood, 12.39 mL methacryloyl chloride (113.98 mmol, 11.91 ml) was mixed with 35 mL diethyl ether and left for 10 minutes to settle, creating ‘mixture 2’.

A rubber cap was added to mixture 1 with a needle inserted, then bathed in ice to keep it as close to 0°C as possible and mixture 2 was slowly added drop wise via a syringe to mixture 1

over the course of 2 hours. With each addition of mixture 2, vapour rose from mixture 1 and the needle allowed for the pressure to be released. An illustration of the procedure is shown in Figure 52.

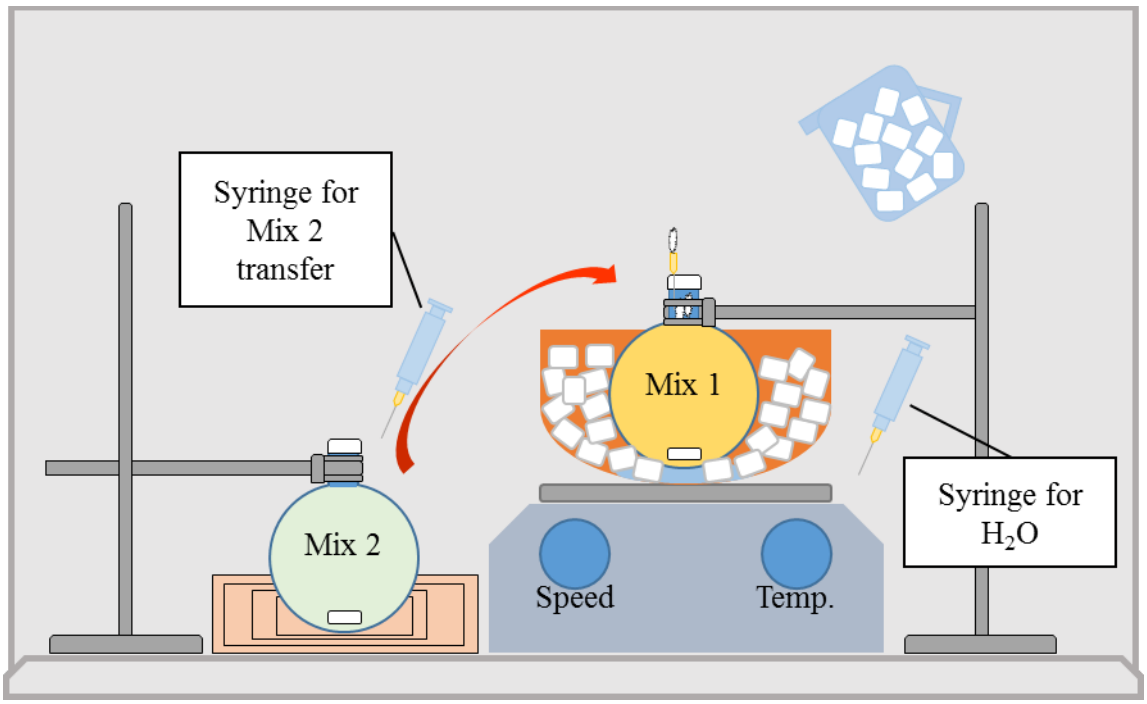

Figure 52: Illustration of the method followed for the synthesis of 3-Methylthienyl Methacrylate

Following the addition of mixture 2 to mixture 1, the triethylammonium chloride was filtered off with a silica gel column with additional diethyl ether added to the round bottom flask to further remove it and to help extract as much as possible from the silica gel column. The solvent was then evaporated with a rotary evaporator to make it more concentrated but not to completely remove the solvent altogether.

A 1:1 mixture was then made of dichloromethane and 2M sodium hydroxide. This was mixed with filtered mixture 1 for 12 hours overnight in the hood. The dichloromethane-sodium hydroxide mixture was mixed at a volume 10x that of the measured residue. This was then added to a separating column and washed twice with milliQ 18.2 MΩ DI H_2O, where the organic layer was taken after carefully allowing separation for at least 1 hour but up to 1 day.

This step removed most of the H_2O, however to further remove it, calcium chloride was used and then was filtered out with filter paper.

Where required due to time limitations, the mixtures were left in their glassware, wrapped in aluminium foil to avoid light and stored at 4°C for no more than an overnight period.

4.3.3. INITIAL CALCULATIONS

The mass calculations for the RAFT agent and initiator are based on the molecular weight, mass of MTM used and an appropriate ratio depending on the length of the chains of polymers desired. Note that MTM's theoretical molecular weight is 182.242 grams / mole.

Inputs:

Category	Description	Symbol	Value
Desired Ratios	Monomer to RAFT Agent	R_{MtoR}	100:1 (Ratio)
	RAFT Agent to Initiator	R_{AtoI}	5:1 (Ratio)
Molecular Weights	RAFT Agent	M_{MW-R}	376.45 grams / mole
	Monomer	M_{MW-MTM}	182.242 grams / mole
	Initiator	M_{MW-I}	280.28 grams / mole
Solvent and Monomer Concentrations	Monomer Concentration	C_M	1 M
	Dioxane Solvent Volume	V_D	3.49 mL

Table 18: Relevant Symbols and Values for RAFT Polymerisation Calculations

4.3.4. RAFT POLYMERIZATION OF MTM

The RAFT agent selected was 4-Cyano-4-(phenylcarbonothioylthio)pentanoic acid N-hydroxysuccinimide ester and the initiator was 4,4′-Azobis(4-cyanovaleric acid) on the basis of their suitability and availability.

With the relevant symbols and values listed in Table 18, we firstly determine the amount of moles of the monomer:

Monomer in moles = Mass Used / Molecular Weight

= 182.242 / 0.6372

= 0.003496 moles

The amount of RAFT agent in moles, which is based on the ratio given above is determined to be:

RAFT agent in moles = Monomer in moles / Monomer to RAFT Ratio

= 0.03496 / 100

= 0.00003496 moles

The RAFT agent in mass to be weighed out is then:

RAFT Agent Mass = RAFT Molecular Weight x RAFT Agent in moles

= 376.45 x 0.00003496

= 13.162 mg

We determine the initiator moles and weight in the same way:

Initiator in moles = Monomer in moles / RAFT to Initiator Ratio

= 0.00003496 / 5

= 0.000006992 moles

RAFT Agent Mass = Initiator Molecular Weight x Initiator in moles

= 280.28 x 0.000006992

= 19.6 mg

4.4. EXPERIMENTAL WORK

After mathematically determining the amounts of chemicals required, all chemicals were weighed out into glassware cleaned by ethanol, acetone and air drying. All chemicals were weighed out into small vials except for the initiator which having a small weight, was weighed 10x its desired weight into 1 mL of solvent. The polymerisation was reacted in a small round bottom flask with a rubber septum. The RAFT agent and monomer were directly added to the round bottom flask whilst the initiator dissolved in solvent was added as a 0.1 mL volume.

The round bottom flask was then capped with a rubber septum and degassed with N_2 gas. A needle is used to bubble the N_2 gas ensuring it is close to the bottom of the flask and the pressure is maintained, for one hour, whilst another needle is inserted into the septum to allow oxygen and N_2 gas to escape.

Once the flask had been degassed, it was left in an oil bath at 75°C with light stirring induced in the flask to allow the RAFT polymerisation reaction to occur for 7 hours. After the 7 hour period, the flask was left at -4°C to prevent further reaction. The resultant mixture containing Poly(MTM) was purified via precipitation by first dissolving the polymer in diethyl ether and centrifugation at 4000 RPM for 8 minutes after 3 steps.

4.4.1. ELECTRO-COPOLYMERIZATION TO POLY(MTM)-PYRROLE GRAFT COPOLYMER

To create the conductive copolymer, Ppy was grafted onto Poly(MTM) through EP. The electrolyte was 0.05 M *p*-toluene sulfonic acid in acetonitrile with 0.02 M pyrrole, the working and counter electrodes were platinum foil (12.5 x 25 x 0.1 mm) and the reference electrode was silver wire (diameter 0.5 mm). 10 mg of poly(MTM) was dissolved into 200 μL of dichloromethane (DCM) and was deposited onto one side a platinum foil. The DCM was allowed to dry off before repeating the deposition for the other side of the platinum foil. The potentiostat was a CH Instruments CHI660E in potentiostatic mode set to 1.1 V and was left until a black film formed on the working electrode. The charge passed was monitored throughout the experiment.

4.4.2. MONOMER AND COPOLYMER ANALYSIS

All NMR spectra were taken to determine chemical structure with an Agilent 500 MHz NMR instrument set for hydrogen using $CDCl_3$ as the solvent. GPCs were taken to determine polymer molecular weight in a Waters GPC system against a polystyrene standard with dimethylacetamide (DMAC) as the solvent.

4.4.3. ELECTRODE PREPARATION AND CHARACTERIZATION

The electrodes were prepared in a simple compression method in which 100 mg Ppy powder was weighed, added to a FTIR KBr pellet press and then 8 tonnes of mechanical force was applied. These electrodes were then electrochemically characterized via cyclic voltammetry with a Pine Research WaveDriver 10 potentiostat in which the compressed Ppy electrode was the working electrode, the reference electrode was Ag/AgCl electrode, the counter electrode was platinum foil and the electrolyte was phosphate buffer solution (0.001 M, PBS). Note that in this case, PBS was chosen to characterize the electrode over TBAFB and acetonitrile as the GEBFC experiments used this and thus this solvent would most accurately represented the electrochemical conditions of the GEBFC. The pseudocapacitance was calculated from

the equation C = A / (2.SR.R) where C is the specific capacitance, A is the area under the CV curve, SR is the Scan Rate and R is the scan range as per Patil et al (Patil et al. 2013).

4.4.4. GLUCOSE ENZYMATIC BIOFUEL CELL STUDIES

The electrodes prepared for the GEBFC studies were similar to that of the previous section, except that in addition to Ppy, enzymes were also weighed and added prior to adding them to an FTIR KBr pellet press and applying 8 tonnes of mechanical force. The anode electrode was composed of 100 mg Ppy and 100 mg GOx from *Aspergillus niger* and the cathode electrode was composed of 100 mg Ppy and 100 mg LAC from *Trametes versicolor*.

To prepare the GEBFC, D-glucose was stirred via a magnetic stir bar and plate into 50 mL of 0.001 M PBS to a concentration of 100 mM in 50 mL glass beakers. The aforementioned electrodes were clipped with alligator clips, connected to voltage monitoring data acquisition software via cables and then dipped into the prepared glucose PBS solution and the voltage monitored. The data acquisition hardware was a National Instruments DAQ USB-6008 and the software was LabView running a customised computer program which updated a live display every second and logged to an Excel spreadsheet every 10 seconds. The GUI and LabView program can be found in Appendix section.

With the GEBFC running in open circuit and being monitored, to establish the power producing capabilities of the GEBFC, after some time a breadboard was inserted between the GEBFC and the DAQ to enable the connection of resistances. Since the GEBFC was in open-circuit and had no current running, resistances began at a high resistance practically close to open circuit and then sequentially lowered in resistance toward short-circuit. With each change, the voltage was monitored and allowed to settle before being logged. A full list of the resistances can be found in Appendix section. An illustration of the GEBFC setup in shown in Figure 53.

4.5. Results

4.5.1. Development of MTM Monomer

To create electrodes composed of conductive polymer, a thiophene based monomer was first synthesised via esterification with methacryloyl chloride of 3-thiophene methanol prior to RAFT polymerisation and EP. The NMR spectra of the monomer after purification are shown in Figure 55. Peaks occur at 7.3 and 7.1 which are hydrogens on the thiophene ring, 6.1 and 5.8 which are vinyl hydrogens, 5.2 which relates to formaldehyde, 2.0 and 1.6 PPM which relate to methyl groups. The peaks corresponding to each part of the MTM molecule are shown in Figure 54. After purification, the monomer was weighed to be 5 grams, which as compared to the mass of 3-thiophene methanol used for the experiment of 6.35 grams gives a yield of 78.78 %.

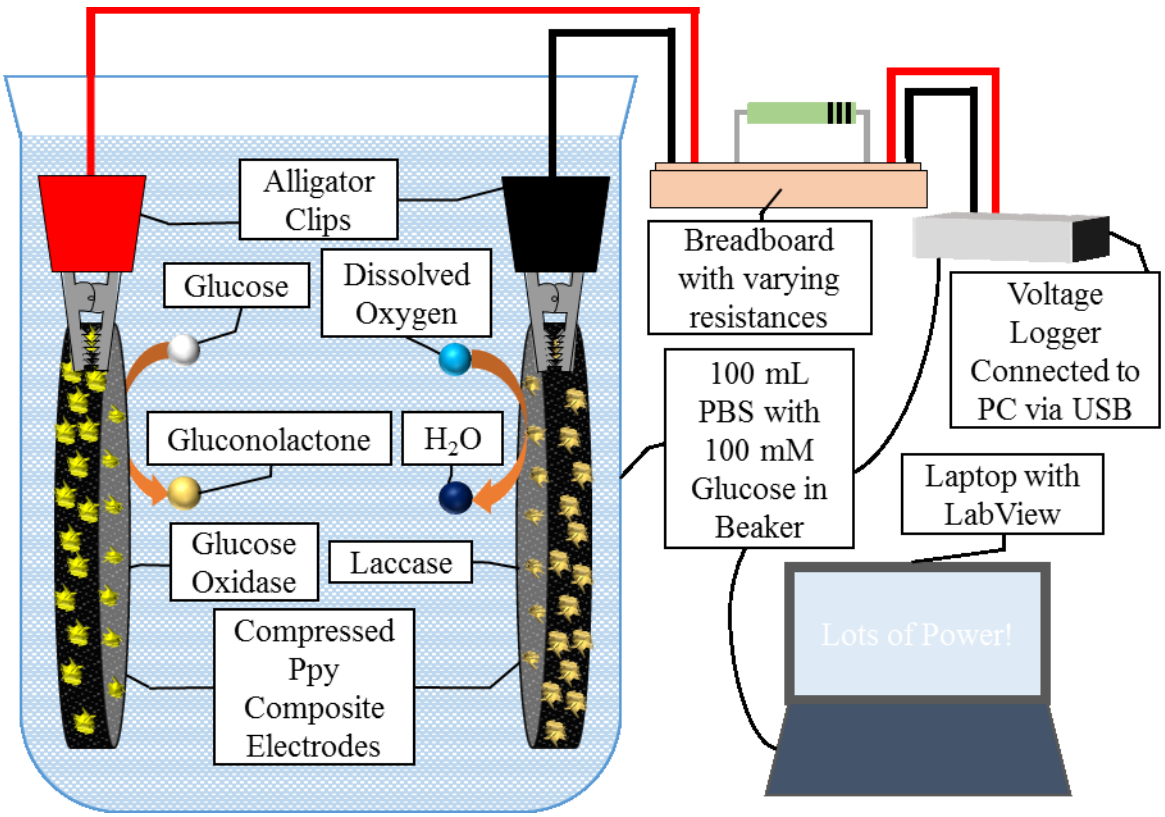

Figure 53: GEBFC Schematic

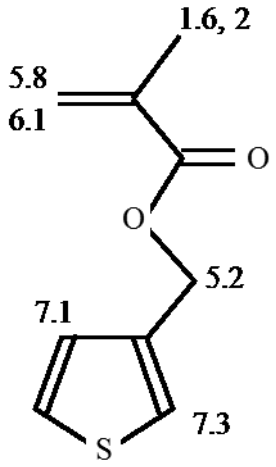

Figure 54: MTM Monomer with Correspondingly Labelled NMR Peaks

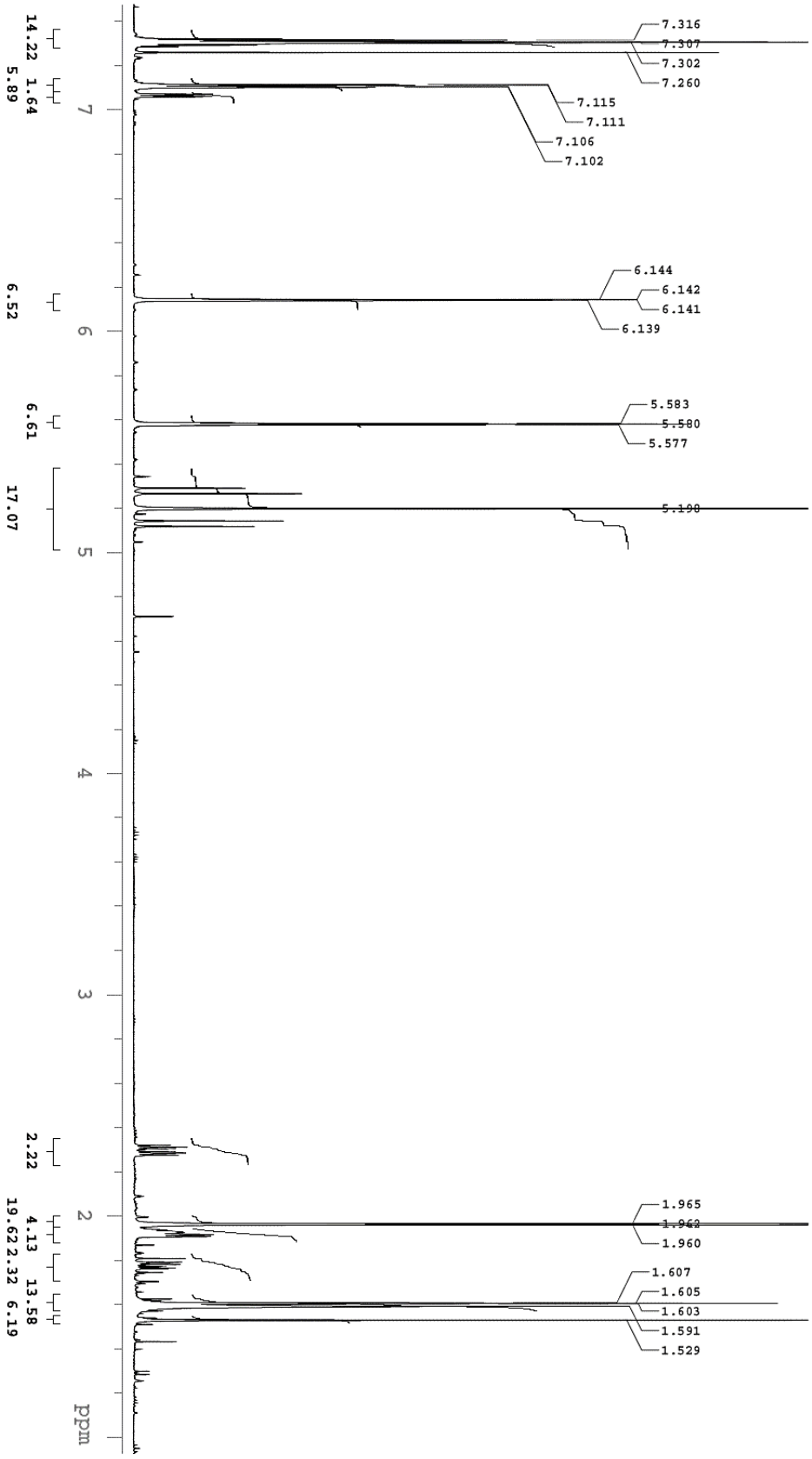

Figure 55: NMR Spectra of Purified MTM Monomer Synthesised via esterification of 3-thiophene methanol via methacryloyl chloride

4.5.2. RAFT POLYMERIZATION OF MTM

Following the synthesis of MTM, RAFT polymerisation was used to create poly(MTM) to create a polymer which would form the basis for the grafting on of pyrrole through EP. The method shown in the previous section was followed with a NMR taken before purification of the crude polymer for calculation of conversion % whilst both NMR and GPC were taken after purification was performed.

The NMR for the crude batch directly after the polymerisation of MTM is shown in Figure 56 and a table of integrals from the analysis software is shown in Table 19. We calculate the conversion as per the following two methods:

Method 1…

$$Conversion\ \% = \frac{Polymer\ Peak}{\left(Polymer\ Peak + (2 \times Monomer\ Peak)\right)} \times 100$$

$$= \frac{1.37 + 1.06 + 1.98}{\left(1.37 + 1.06 + 1.98 + (2 \times 0.233)\right)} \times 100$$

$$= 90.44\%$$

Based on this we calculate the molecular weight of the polymer…

$$M_{nNMR1} = \left(\frac{Conversion\ \%}{100} \times M_{nMonomer} \times Monomer\ to\ RAFT\ Ratio\right) + M_{nRAFT-Agent}$$

$$M_{nNMR1} = \left(\frac{90.44}{100} \times 182.242 \times 100\right) + 376.45$$

$$M_{nNMR1} = 16858.96\ grams/mol$$

Method 2…

$$Conversion\ \% = \frac{Polymer\ Peak}{\left(Polymer\ Peak + (2 \times Monomer\ Peak)\right)} \times 100$$

$$= \frac{0.747 + 0.81 + 0.42}{\left(0.747 + 0.81 + 0.42 + (2 \times 0.233)\right)} \times 100$$

$$= 80.925\%$$

Based on this we calculate the molecular weight of the polymer…

$$M_{nNMR2} = \left(\frac{Conversion\ \%}{100} \times M_{nMonomer} \times Monomer\ to\ RAFT\ Ratio\right) + M_{nRAFT-Agent}$$

$$= \left(\frac{80.925}{100} \times 182.242 \times 100\right) + 376.45$$

$$= 15124.40\ grams/mol$$

The NMR results for the purified Poly(MTM) sample are shown in Figure 57. Peaks at 7.26 PPM, 7.212 PPM and 7.012 PPM are identified as the thiophene ring structure, 4.923 PPM is 2H, 3.704 PPM is residual 1,4-dioxane, 1.758 PPM is the 3H, 1.570 PPM is residual H_2O and peaks at 1.252, 1.221, 1.208 and 1.193 PPM are from the RAFT end group.

Figure 58 shows the signal measured from the GPC instrument taken against a polystyrene standard. The polymer parameters M_n and M_w which are the weight average molecular weight and the number average molecular weight respectively were measured to be 10 416 grams / mole and 10 776 grams / mole respectively. Calculating the polydispersity, PDI, through equation PDI = M_w/M_n we find PDI = 1.034.

Number	Start (PPM)	End (PPM)	Integral Value (Signal Intensity / PPM)
1	7.34523	7.27539	0.747
2	7.26043	7.22052	0.811
3	7.22052	7.16066	0.42
4	7.12075	7.07086	0.233
5	7.07086	7.03594	0.205
6	7.03594	6.9661	0.406
7	6.16295	6.0981	0.23
8	5.60922	5.51443	0.234
9	5.3099	5.08043	0.892
10	4.99064	4.831	0.859
11	4.15755	3.98794	1.383
12	3.87819	3.78839	0.454
13	3.7435	3.62876	69.169
14	3.62876	3.55892	1.738
15	3.55892	3.51901	0.55
16	2.83059	2.38661	5.379
17	2.38661	2.20702	5.071
18	2.00249	1.93764	1.063
19	1.93764	1.85284	1.372
20	1.85284	1.70318	1.976
21	1.61339	1.56849	0.65
22	1.53856	1.48867	0.686
23	1.45874	1.34899	0.381
24	1.11453	0.954896	1.463
25	0.954896	0.755354	2.777
26	0.755354	0.605698	0.85

Table 19: Integral Values from NMR analysis software for the crude batch of Poly(MTM)

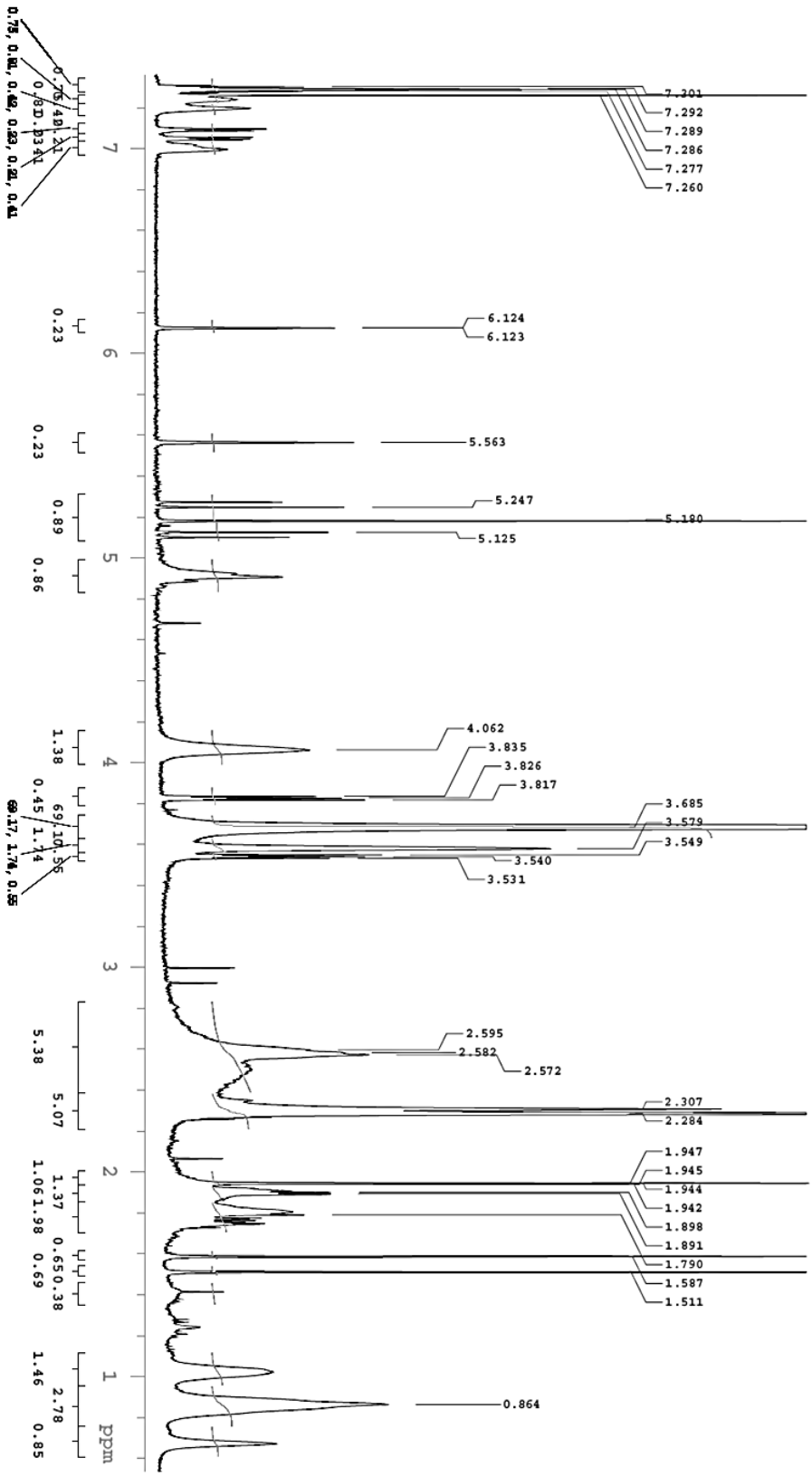

Figure 56: NMR Spectra of Crude Poly(MTM) Polymer Synthesised via RAFT Polymerization. Note: due to limitations in the NMR analysis software, annotations of some peaks were added.

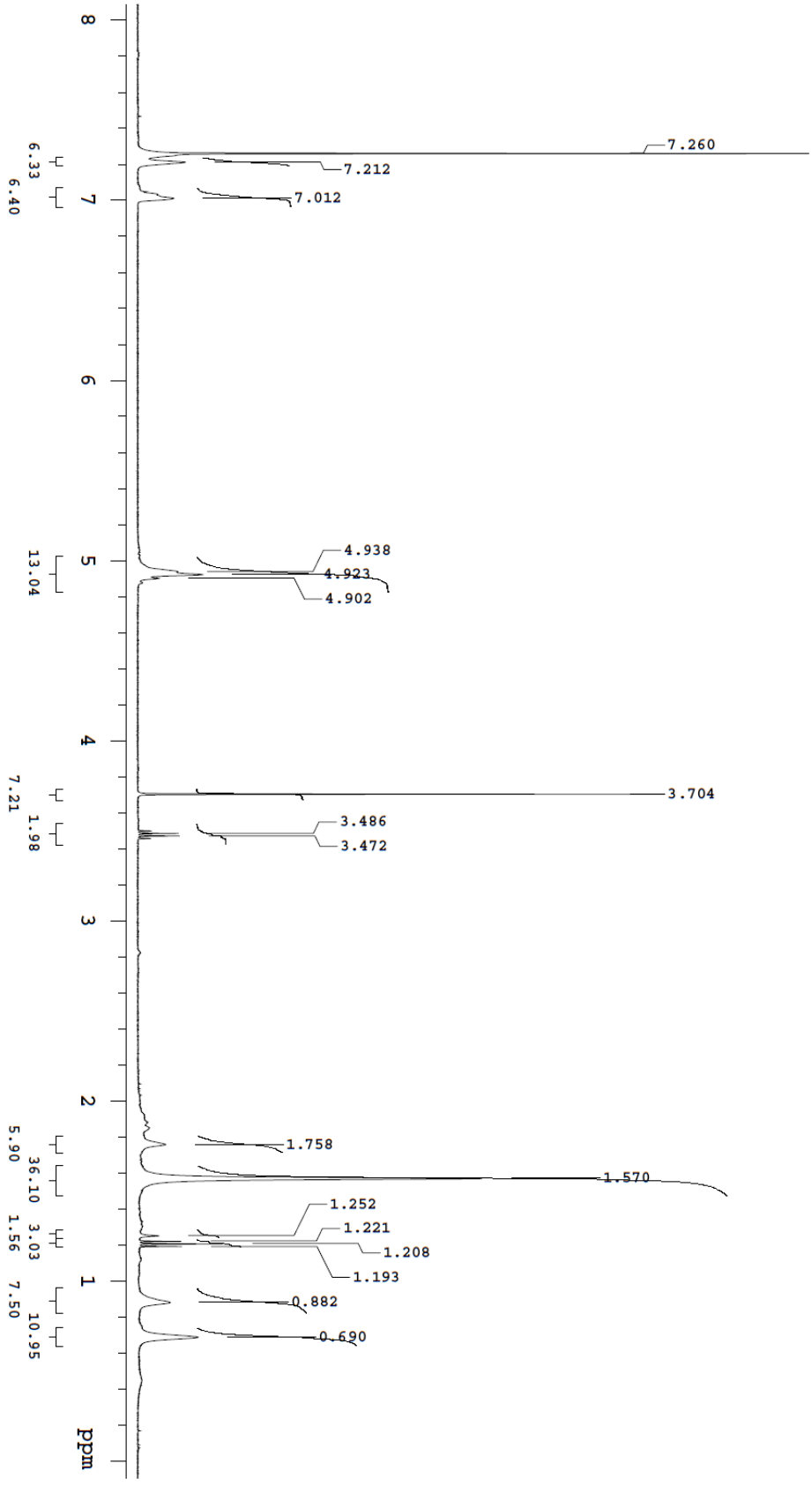

Figure 57: NMR Spectra of Purified Poly(MTM) Polymer Synthesied via RAFT Polymerization

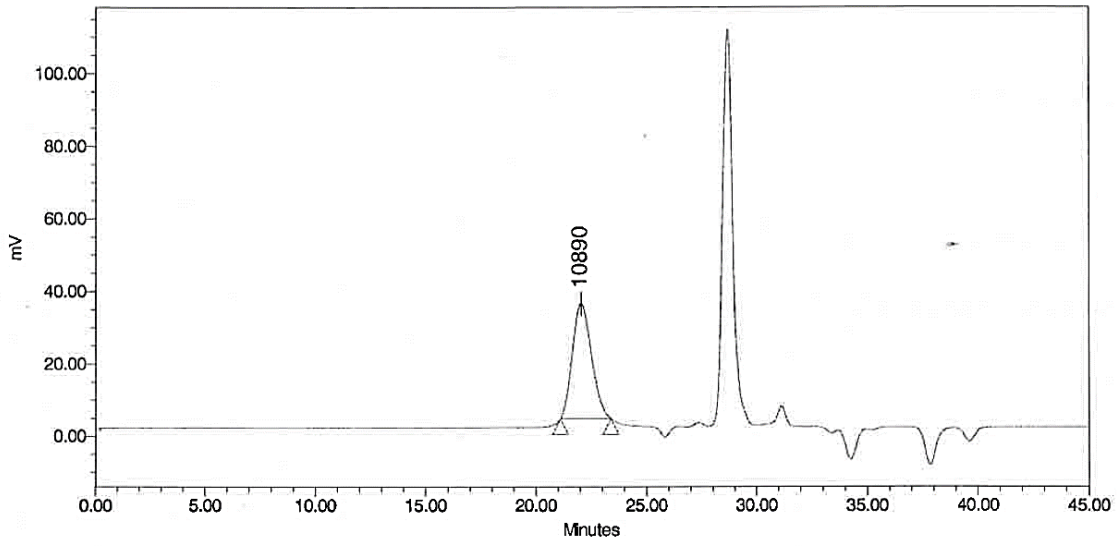

Figure 58: GPC Signal for Poly(MTM) With PolyStyrene Standard

4.5.3. ELECTROPOLYMERISATION AND PYRROLE GRAFTING OF POLY(MTM)

In the final step to create the conductive polymer, pyrrole was grafted onto Poly(MTM) through galvanostatic EP. The voltage was held for almost 7 hours to generate a thick film of conductive polymer and the charge passed is shown in Figure 59 with the total charge passed being 16.84 C. A photo of the film is shown in Figure 60 with the thick film on both sides of the platinum foil electrode.

The CVs are shown in Figure 67 for scan rates from 20 mV/s to 100 mV/s. No distinct peak is shown in any of the scans and is likely due to pseudocapacitance. Plots of the CVs at the lower scan rates of 8, 9, 10 and 11 mV/s in Figure 65 more clearly show the rectangular shape typical of pseudocapacitive materials during CVs. A plot of the decreasing capacitance with increasing scan rate is shown in Figure 63.

Subsequent to the EP and CVs, the polymer was scrapped off and weighed where less than 10 mg of mass was measured. To use this as part of a compression based method, several more milligrams of conductive polymer would be required. Hence, further experiments use premade Ppy purchased from Sigma Aldrich.

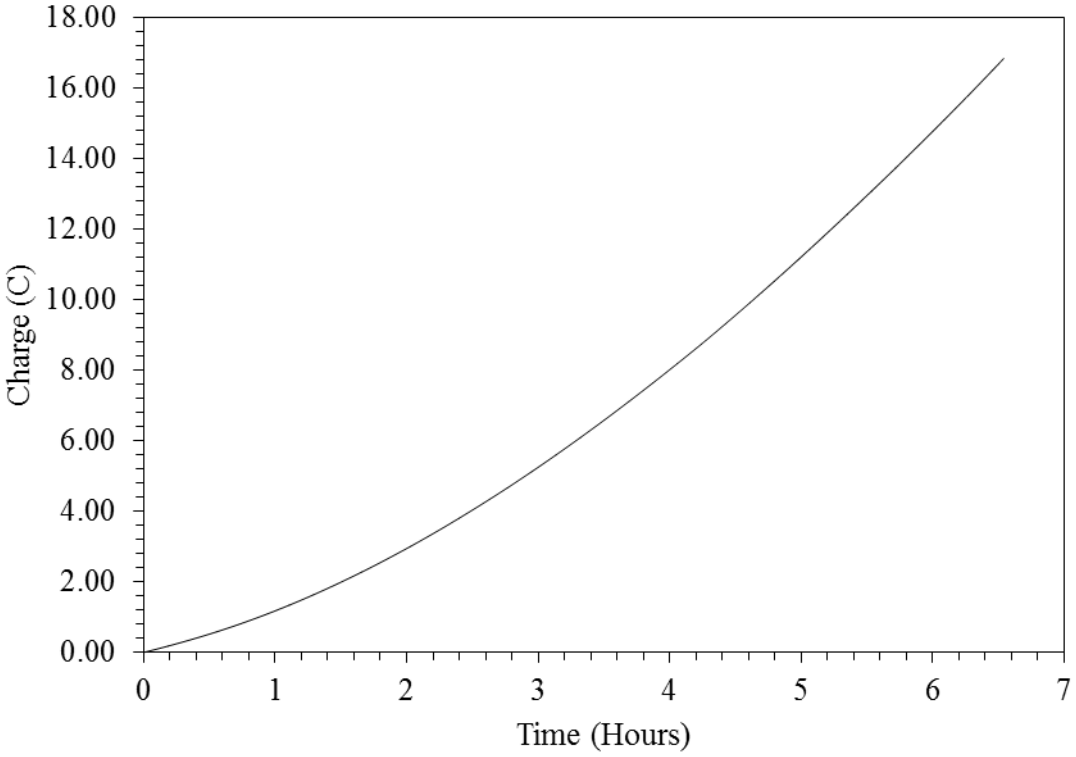

Figure 59: Charge Passed During the EP

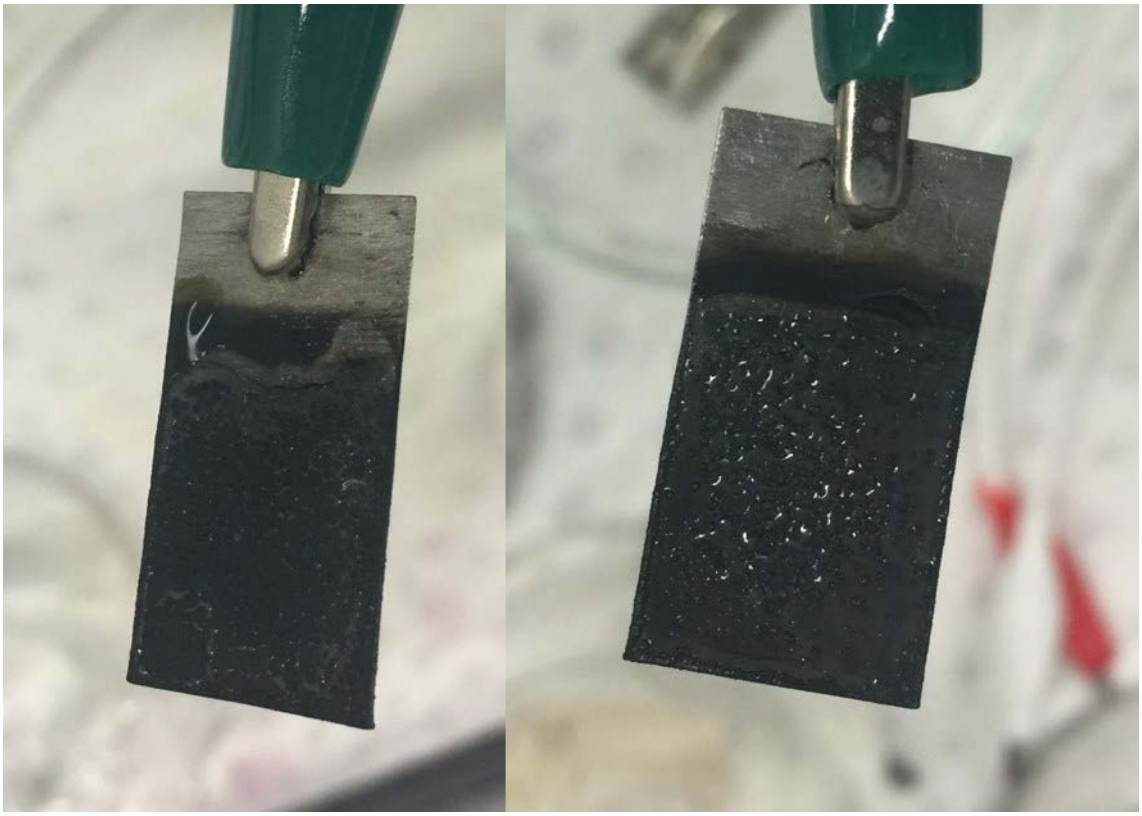

Figure 60: Photos of the Poly(MTM)-Pyrrole film as a result of the EP on the Pt electrode

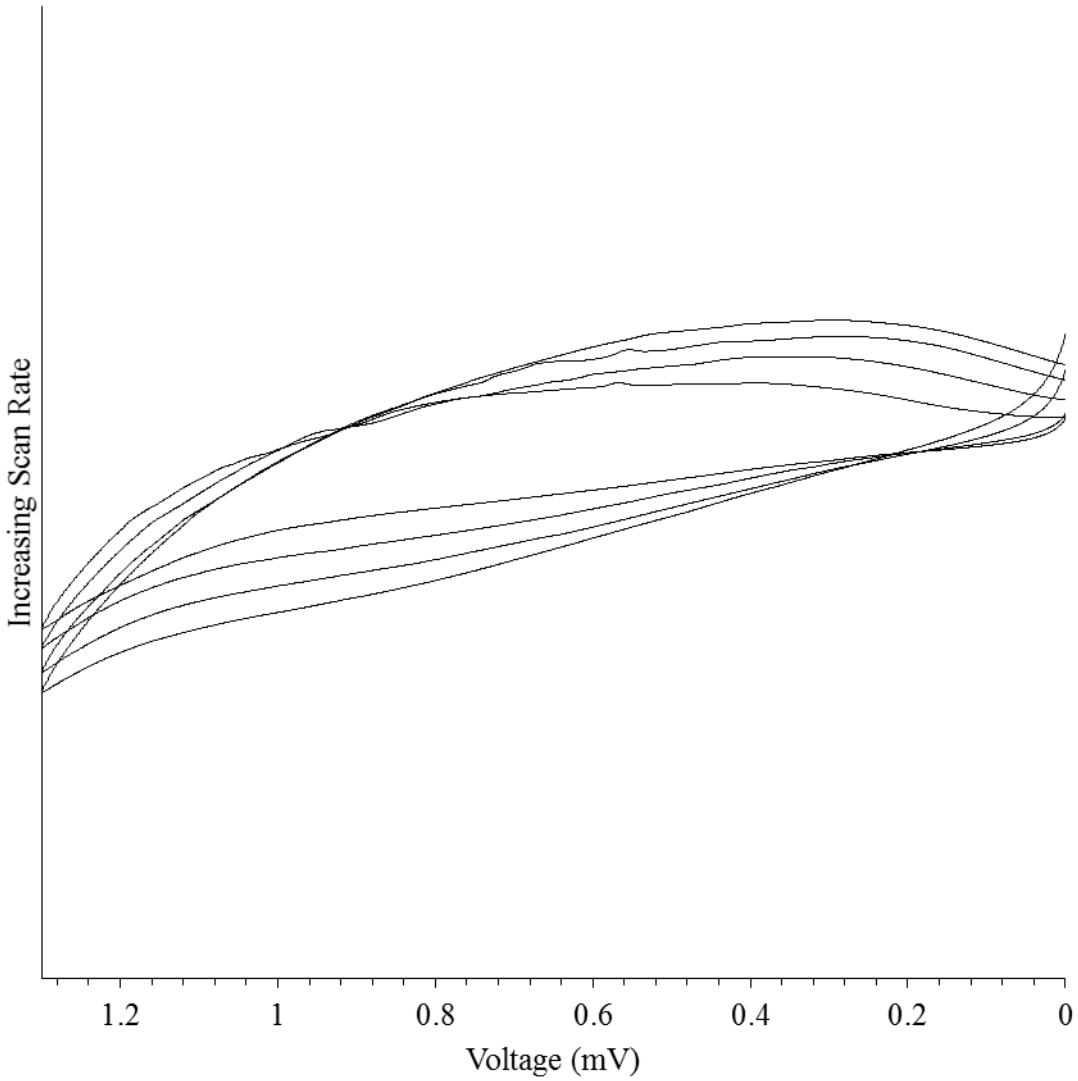

Figure 61: CV of Poly(MTM)-Pyrrole at 8, 9, 10 and 11 mV/s showing rectangular shape, indicating pseudocapacitance

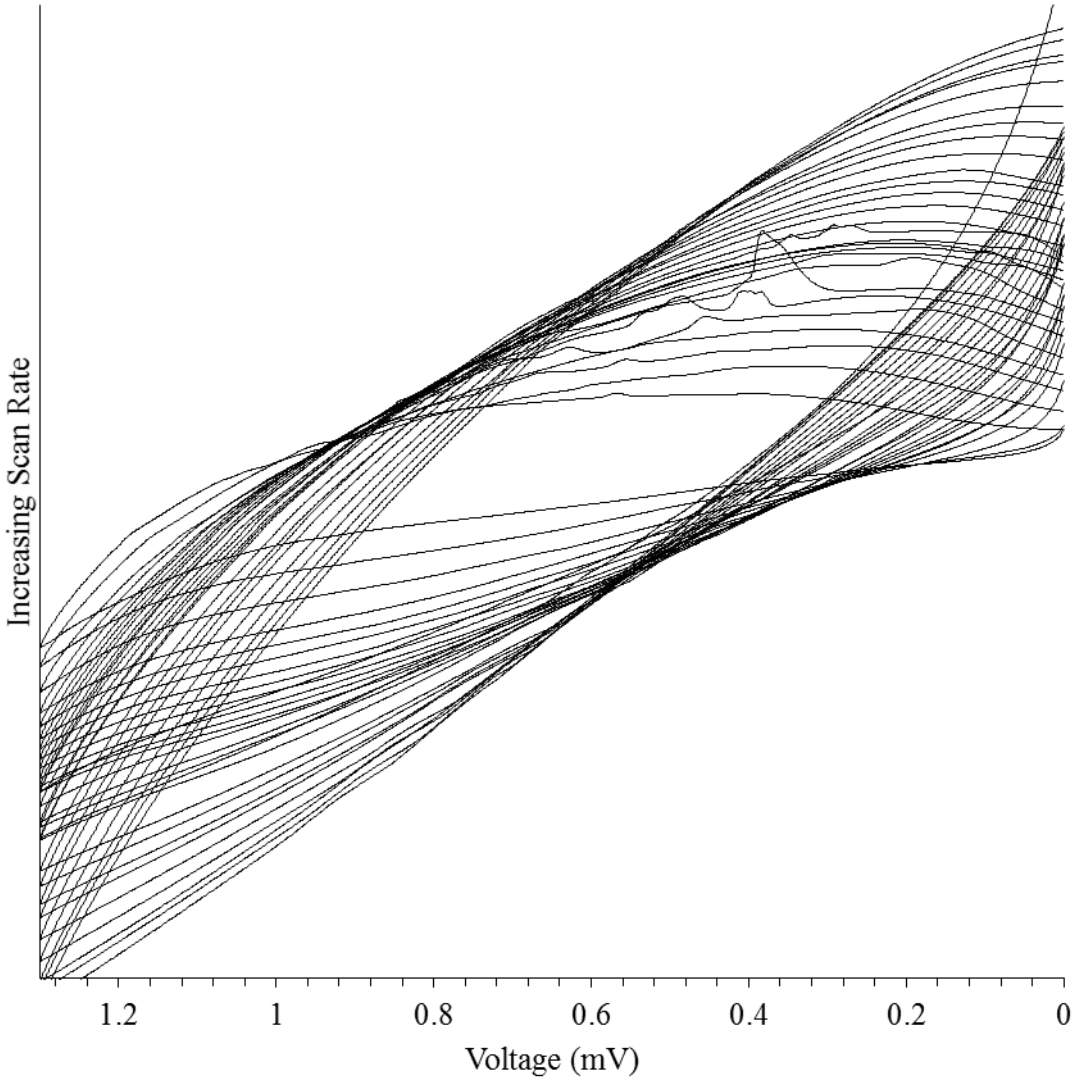

Figure 62: CV of Poly(MTM)-Pyrrole

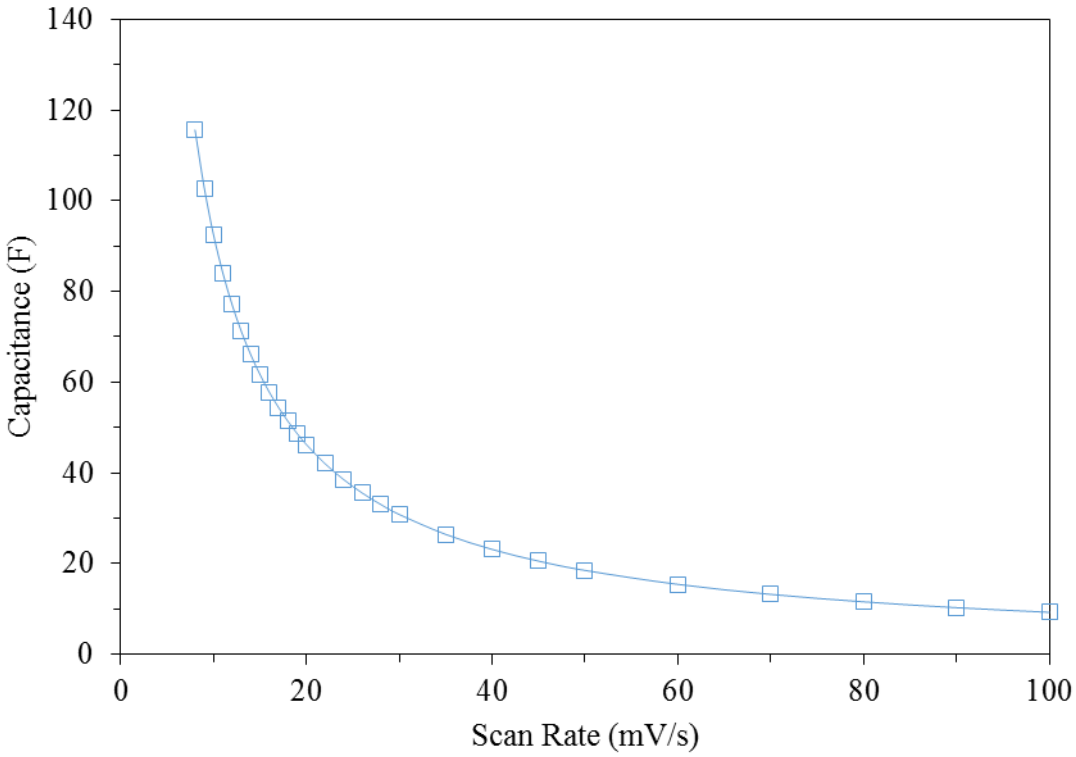

Figure 63: Pseudocapacitance of Poly(MTM)-Py taken from CVs

4.5.4. Electrode Fabrication and Characterization

When the Ppy powder was weighed and compressed, the result was small coin like electrodes shown in Figure 64. The electrodes had a diameter of 1.31 cm and a thickness of 0.5 mm as measured by a calliper. The electrodes were solid, small discs that could be broken apart, but needed some force to do so.

Figure 64: Photos of the compressed Ppy electrodes

To electrochemically characterize the electrodes and ensure they were electrochemically similar to the conductive polymer developed in the previous sections, CVs were obtained for the compressed electrodes. Figure 65 shows the faint rectangular shape of the compressed Ppy electrodes at a low scan rate of 10 mV/s, whilst Figure 66 shows CVs with increasing scan rates of up to 1000 mV/s. Figure 67 shows the measured capacitance from the electrodes and its decreasing values with increasing scan rate.

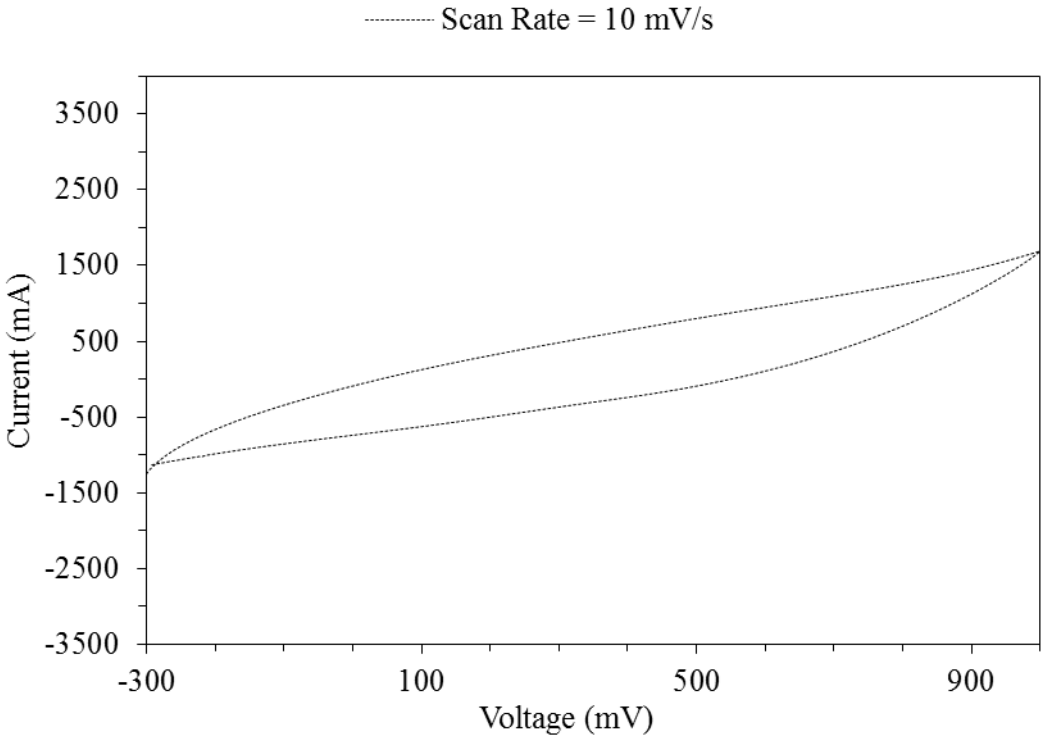

Figure 65: Near Rectangular shape of the compressed Ppy electrode showing some pseudocapacitance

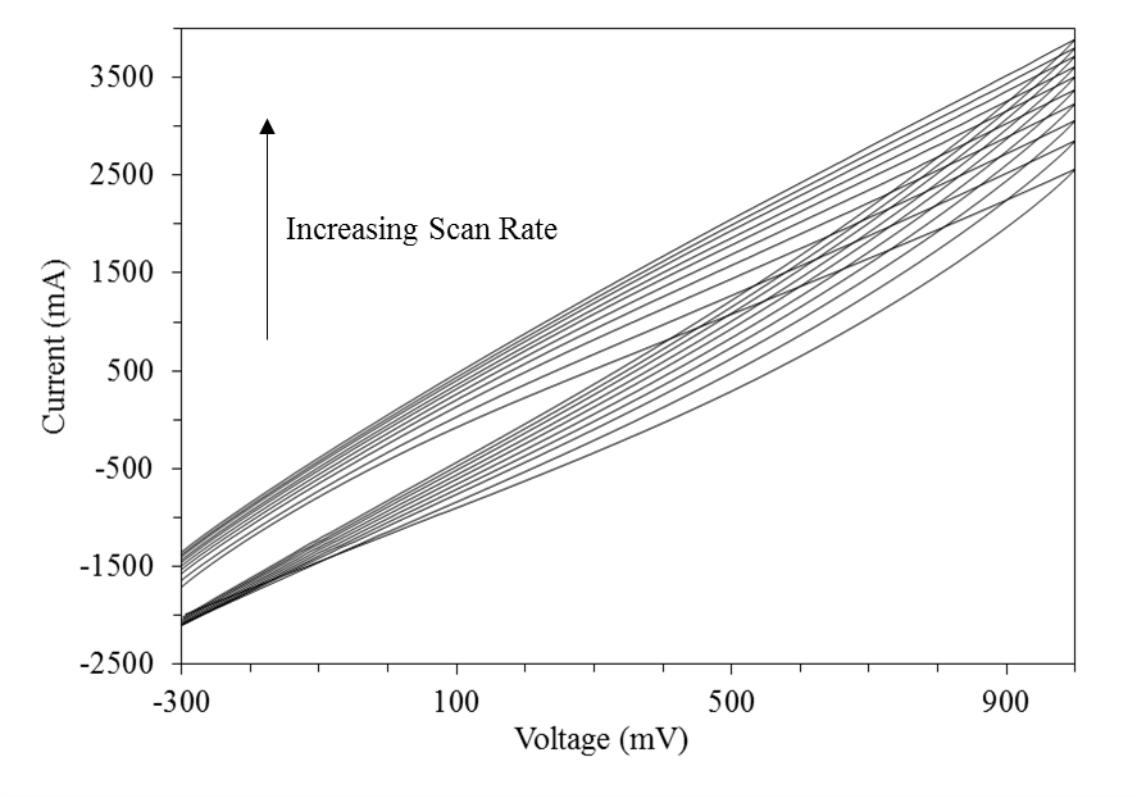

Figure 66: CVs of the compressed Ppy electrodes

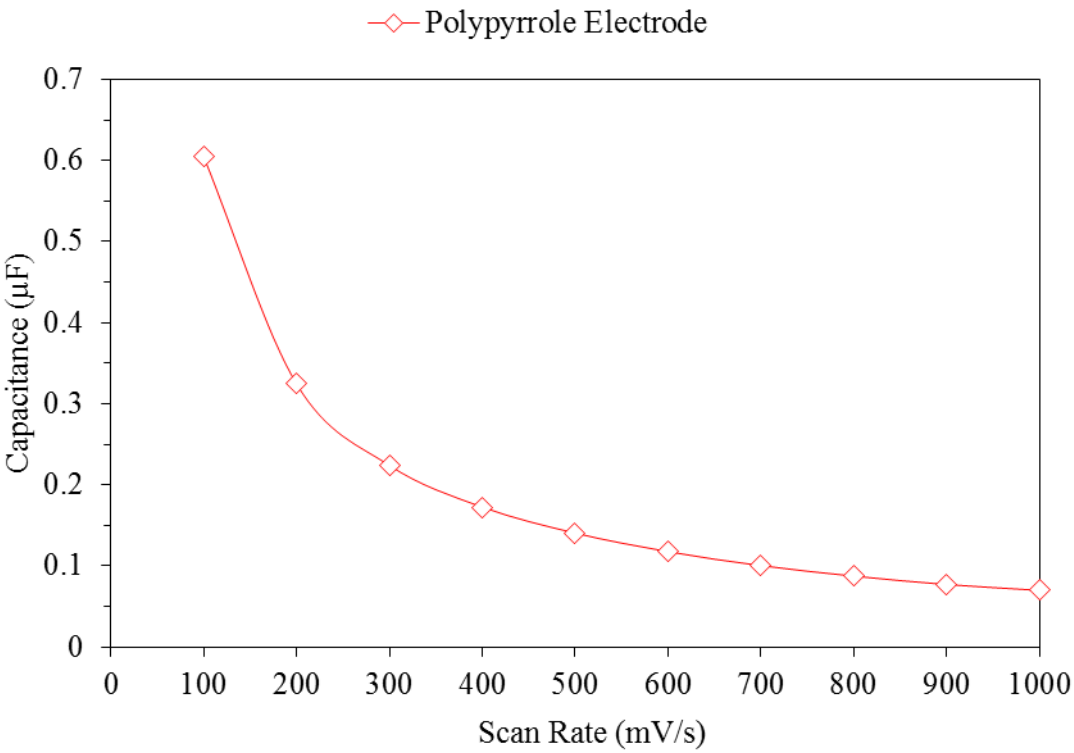

Figure 67: Pseudocapacitance of the Ppy electrode

4.5.5. BIOFUEL CELL ELECTRICAL OUTPUT

Following the electrochemical characterization of the compressed Ppy electrodes, Ppy was mixed with GOx for the anode and LAC for the cathode, connected to a DAQ and dipped in a glucose PBS solution. The voltage generated as a result of this is shown in Figure 68. The peak voltage reached was 212.83 mV which occurred at approximately 9 minutes. After this peak, the voltage stabilized to between 60 and 80 mV for the hour after the peak.

To test the power producing capabilities of the Ppy electrode GEBFC, resistances were connected and the voltage measured. Figure 69 shows the measured voltages in response to resistances where for the high resistances, the voltage dropped quickly to about 40 mV before the GEBFC was able to handle current output. The maximum current output was 224.5 μA.

From the measured voltages and currents, power was also calculated and are shown in Figure 70. A peak power of 2.24 μW was measured at a voltage of 23.74 mV and 87.92 μA. The internal resistance determined as the resistance at the maximum power is 270 Ω.

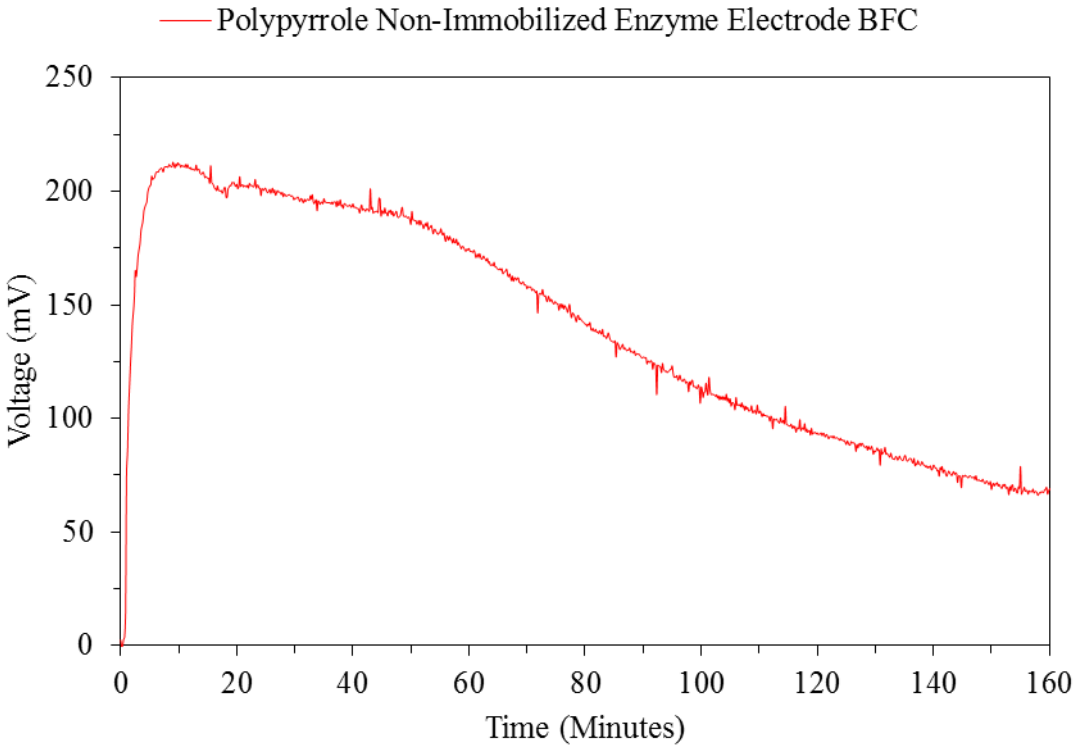

Figure 68: Voltage of time for compressed Ppy electrode GEBFCs

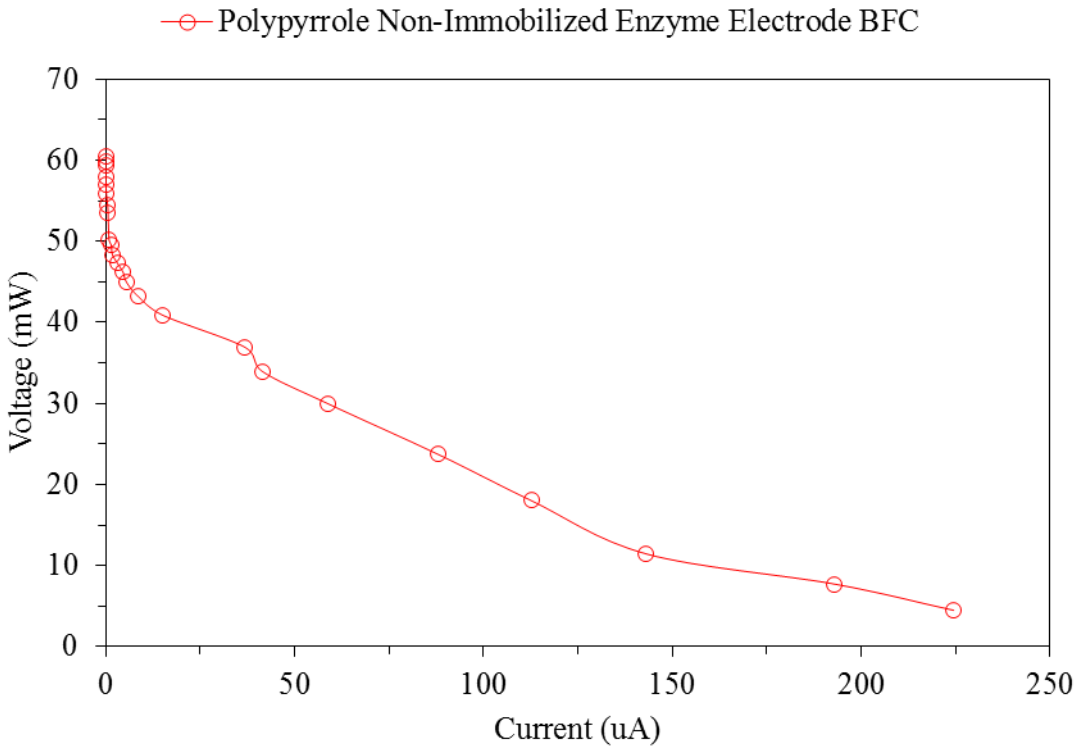

Figure 69: Polarization Curve for GEBFCs containing non-immobilised enzyme electrodes

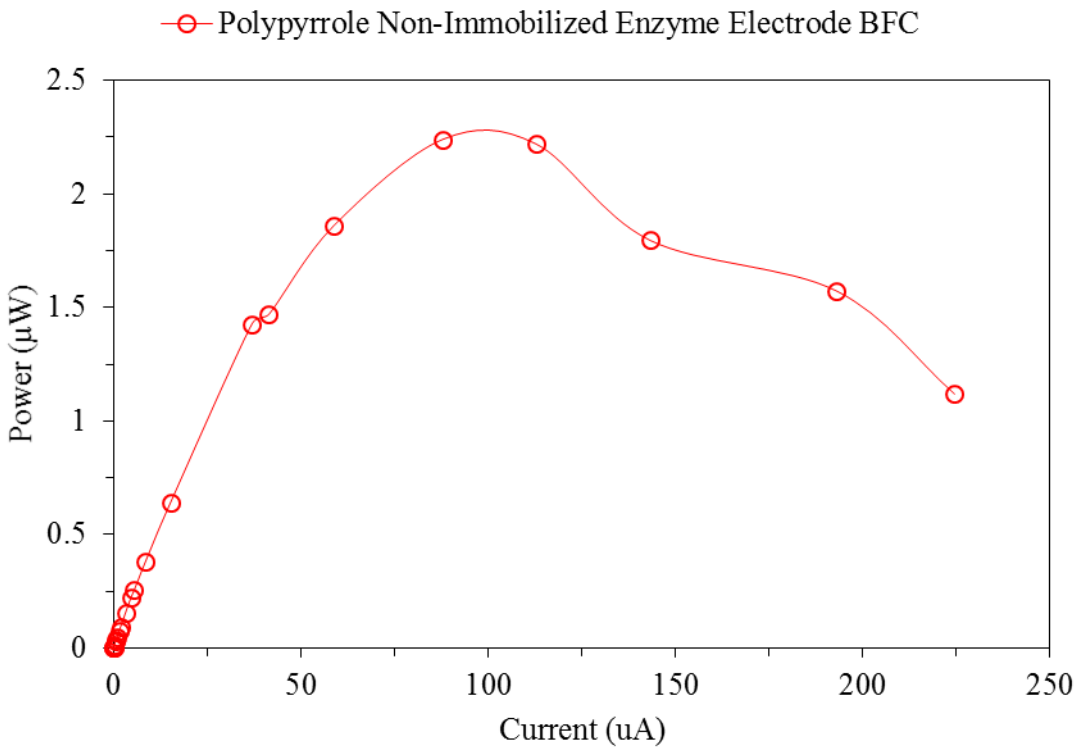

Figure 70: Power curve for GEBFCs with non-immobilised enzyme electrodes

4.6. Discussion and Conclusion

In order to create compressed conductive polymer electrodes, the conductive polymer poly(MTM)-pyrrole was first developed, involving the synthesis of monomer 3-methylthienyl methacrylate, its RAFT polymerization followed by its EP with pyrrole. Prior to the synthesis of MTM, the original intent was to use acryloyl chloride rather than methacryloyl chloride. This was changed for two reasons: firstly, during the synthesis of MTA, low yields of less than 50% occurred and this was due to MTA's sensitivity to hydrolysis. It was also found that upon passing Poly(MTA) through the columns of the GPC, very little polymer was detected. Whilst all attempts were made to avoid H_2O in samples, many reagents still do contain some H_2O and extra efforts and resources would have had to have been devoted to this. One of the objectives of the project was to create a system that was cost effective and simple, and further processing was not desired. Secondly, timing issues arose whereby it would take at least 6

months to source another bottle of acryloyl chloride, whereas it was possible to obtain methacryloyl chloride within weeks.

During the synthesis of MTM, some small practical issues did occur. Specifically with the solvent being diethyl ether for Mixture 1, it tended to evaporate easily, even with ice. The ice and rubber seal help a lot to contain the mixture, however additional diethyl ether was added from time to time. Preventing the mixture from drying out is difficult but important as otherwise residue forms at the bottom which is a combination of the desired monomer and unreacted species and is difficult to remove from a round bottom flask, resulting in a reaction that is overall inefficient and wasteful. In the end, a high yield of almost 80% was achieved, and it is believed that with successive attempts at the reaction, this number could be improved.

RAFT polymerisation had been developed originally to create chains of polymers that were more uniform and specific in length compared to other existing methods. The original paper by Çirpan et al (Çirpan et al. 2002) which synthesised Poly(MTM) used free radical polymerisation where they synthesised two Poly(MTM)s, namely PMTM1 and PMTM2. Their GPC results were molecular weights of 73 000 grams / mol and 133 000 grams / mol respectively and polydispersities of 2 and 2.1 respectively. In addition to this, conversion yields of 33% and 21% were given by Cirpan et al. Table 20 shows highly uniform molecular weights, near ideal polydispersity and consistently higher yield results. Clearly RAFT offers improvements in process which are advantageous for obtaining more uniform polymers from more efficient and more cost effective processes. This is the best known results for polydispersity and conversion efficiency for this polymer known to the author.

Batch Number	GPC Measured Molecular Weight (grams / mol)	Polydispersity	Yield (%)
Poly(MTM)2	9479	1.081	79.66
Poly(MTM)3	9144	1.149	82.17
Poly(MTM)4	10 416	1.034	80.93

Table 20: GPC Results of Poly(MTM) from RAFT Polymerisations

In the final step toward synthesising the conductive polymer, poly(MTM) was grafted with pyrrole by first casting the polymer onto Pt electrodes and then applying voltages in a 3-electrode potentiostat setup. To ensure a good yield at the end of the experiment, several different strategies were implemented. When first performing the experiment, only 1 mg of poly(MTM) was cast with DCM. We thus increased the amount to 10 mg and was difficult to cast onto the Pt foil due to its size. Following this, we then tried to coat both sides of the Pt foil, allowing for more time to dry to avoid any poly(MTM) coming off, however the overall size of the electrode was still a problem. We finally tried successive layers of poly(MTM), which did help, however it was difficult to achieve a uniform film which stuck to the electrode. If the bottom layer or layers had dried, an application of a fresh layer would still dissolve the bottom layers.

After depositing poly(MTM), when the electrode was placed in the electrochemical cell for EP, after a short time the film, whilst it did not dissolve, did begin to drip off the electrode into the electrolyte. Nonetheless, as can be seen in Figure 60, a small amount of conductive polymer was synthesised. The photo shows the characteristic black colour of pyrrole based conductive polymers and also characteristically, the film did not dissolve is any of the common laboratory solvents including dichloromethane, ethanol, methanol, acetone, DI

water, acetonitrile, dimethyl sulfoxide (DMSO), diethyl ether, tetrahydrofuran and chloroform. When weighed, the polymer was less than 10 mg. As can be seen in the GEBFC electrode fabrication, 100 mg of polymer was used per electrode since the powder is compressed down, creating the desired conductive polymer matrix, mixed in with the enzymes. This was then the reason to switch to a commercial conductive polymer that could be purchased in higher quantities. Nonetheless, this is the best of the author's knowledge, the first successful use of both RAFT polymerisation and EP to create a conductive polymer. It is also firmly believed that this conductive polymers is suitable for use in a GEBFC, and therefore is included here.

Whilst synthesising monomers and polymers are important steps in the process, the creation of the electrodes themselves was the ultimate goal. Figure 64 shows small coin like electrodes which are reasonably firm but under force can break. Additionally, in switching to the commercial Ppy, CVs were obtained on both conductive polymers to ensure electrochemical similarity. The synthesised conductive polymer could be used for the electrodes, except for the purposes of this project it was not viable. Both CVs shown in Figure 61 and Figure 65 for poly(MTM)-pyrrole and Ppy respectively, have the near rectangular shapes which characteristically show pseudocapacitance, and which mask the redox peaks. One difference does exist however in the amount of capacitance, which for a smaller amount of conductive polymer, the poly(MTM)-pyrrole has 9.24 F of capacitance at 100 mV/s versus 0.6 μF for the commercial Ppy at the same scan rate. This is not considered to be a problem however since with the exception of one study (Kizling et al. 2015; Kizling et al. 2016), GEBFC electrodes have not been known to have pseudocapacitance, and thus perhaps less is best. At the same time however, pseudocapacitance can also be seen as a good property to have. It should be highlighted at this point that commercial Ppy is synthesised by chemical oxidative methods rather than by potentiostatic or galvanostatic methods thus

electrodes are not required (Sigma Aldrich 2017). It is the electrodes that cause the bottleneck in the amount of conductive polymer made and future studies wishing to create conductive polymer may wish to consider this.

With the electrodes fabricated and electrochemically tested, the next step was to test them within a GEBFC itself. Figure 68 showing the open circuit voltage output of the GEBFC is positive, however the peak voltage was only 212.83 mV, occurring at 9 minutes time before stabilising to between 60 and 80 mV. For an open circuit voltage, this shows there is room for improvement, especially when compared to the MFC voltages shown in Figure 72 of voltages almost as high as 500 mV. When comparing the polarization and power curves however, there is more positive news in that the current output range of the GEBFC is much higher, at over 200 μA which is over two times higher than the MFCs. The peak power was still low however at 2.24 μW, 40 mV and 87.92 μA which would not be in the operating range of any devices.

In the MFCs, the voltage did not stabilise until approximately 6 to 7 days whereas for the GEBFCs, the voltage peaked and began to decrease within 1 hour. There are two factors which are contributing to this: the first is enzyme leaching, the second is the reaction rates of enzymes. Figure 71(a) shows a photo of the GEBFC running, (b) showing a close-up in which a stream of yellow appears to be falling from the electrode and (c) shows the end result of the enzyme leaching. The purpose of the compression of Ppy to create the electrodes is the direct electron transfer between the enzymes and Ppy due to their close proximity. If the enzymes leach out however, then they are not in close proximity and electrical output is slowly lost. Regarding reaction rates of enzymes (see Appendix for calculations), GOx and LAC have reaction rates of 100 000 μmol / min and 500 μmol / min respectively. Assuming concentrations of glucose and oxygen of 5000 μmol and 6.25μmol, if there are ideal conditions for the reaction, then it could take less than 1 minute for all substrates to be

consumed. The short time that the voltage output then, based on enzyme leaching and fast reaction time of enzymes is expected.

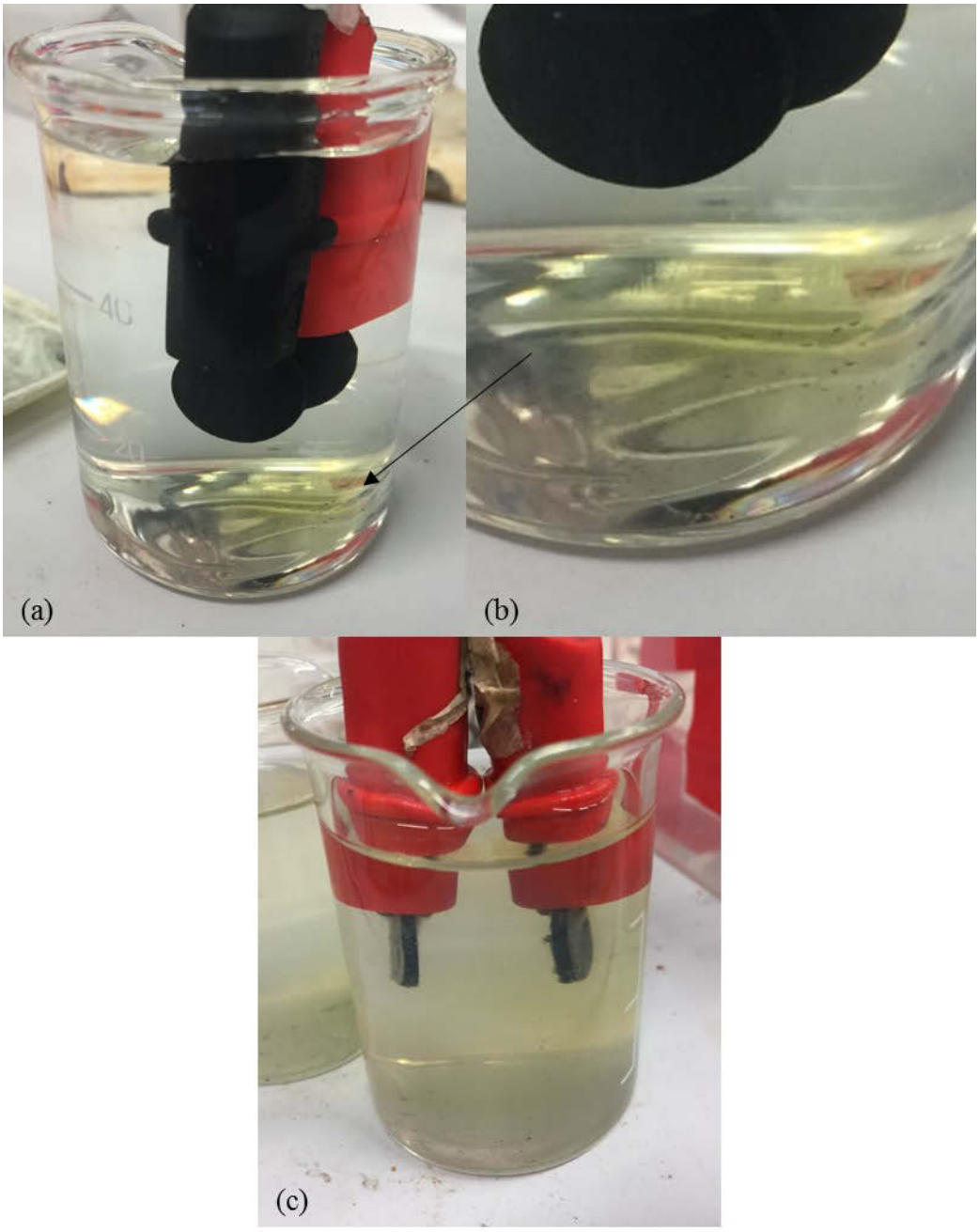

Figure 71: (a) Photo of GEBFC running with enzymes leaching out. (b) Close up of the enzymes leaching out of the GEBFC electrodes. (c) End result of enzyme leaching from the GEBFC compressed Ppy electrodes.

As can be seen in Figure 72, optimisation was performed to determine what may be the best ratio of polymer to enzyme. Ideally the optimisation could theoretically be performed by comparing the sizes of each of the molecules, however the size of the commercial Ppy is not

provided by Sigma Aldrich and therefore it was determined through experimentation. This is important since it is the enzymes which are extracting the electrons from the glucose, although conversely it is the Ppy which act as a conduit for the electrons to the circuit to and from the enzymes. If the enzymes do not have contact with Ppy, then the extracted electrons will not flow through to the circuit as electricity leading to the result that an excess amount of enzymes does not result in optimum voltage. If there is a greater proportion of Ppy to enzymes, then the voltage is also low. This may be due to Ppy blocking contact between the enzymes and glucose molecules.

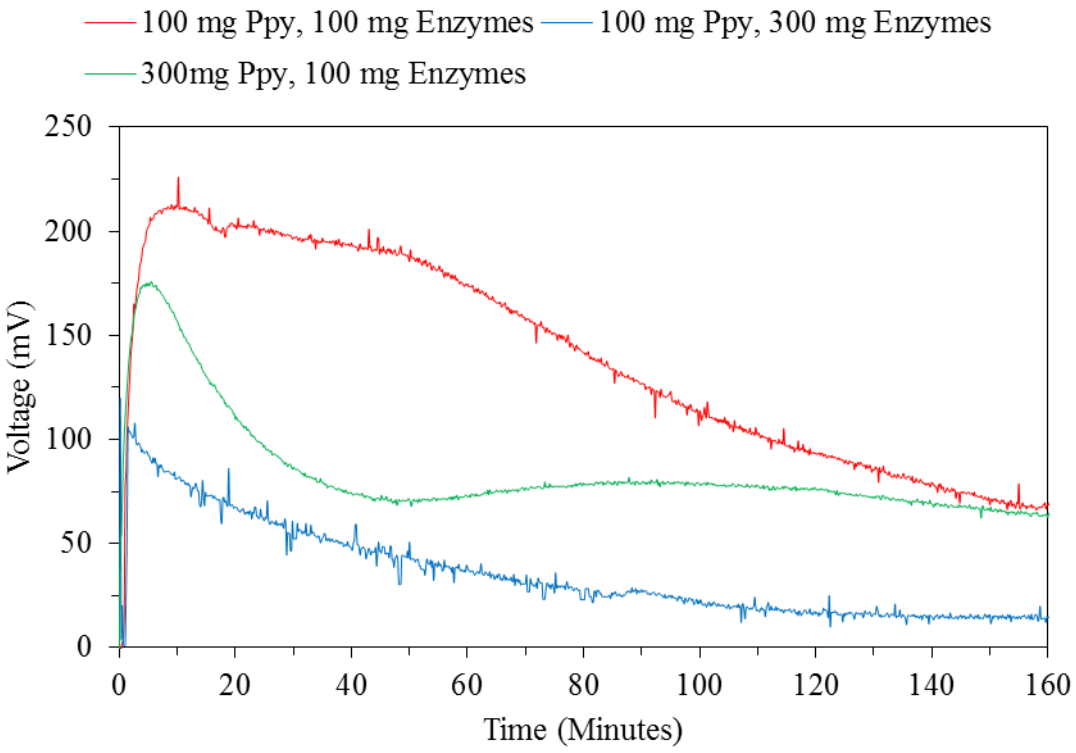

Figure 72: Voltages Over Time for GEBFC with Different Ratios of Ppy and Enzyme within the Electrodes

The results in this chapter are very positive, containing the synthesis of a monomer, which is then RAFT polymerised and a voltage applied to it to create a pyrrole based conductive polymer. Novel combination of RAFT polymerisation and EP, with high conversion rates and polydispersity were excellent results. These were improvements in process over previous studies in efficiency of the synthesis of the monomer and polymer. To better create the

volume within the GEBFC electrodes, the project continued forward with a commercial Ppy, which was electrochemically similar to the synthesised poly(MTM)-pyrrole. From this commercial polymer, a simple compression method create the electrodes was used. This simplicity should not be under rated, since in manufacturing for high volume like for AIMDs, this is a highly valued. Not only this, but the electrodes are only 1.2 cm in diameter, meaning they are well suited to being implanted in terms of size and the method also allows for high enzyme loading. The electrodes were then placed into a glucose solution and were able to produce electricity. Again, this was a novel use of an interesting material, conductive polymer Ppy and of the compression method. The use of Ppy over MWCNTs has proven to be stronger in that upon exposure to solution, the electrodes did not fall apart in the same way that the MWCNT compressed electrodes did. These electrodes provided improvements over the MFCs in that they were smaller, were able to harvest more current and have greater manoeuvrability in terms of being able to make them biocompatible and implantable. They also have room for improvement in voltage compared to both the previous MFC electrodes and to what is required to power electronic devices. Additionally, the enzymes leach out, lowering the overall voltage output and stability. An analysis of this problem and some solutions are provided in Chapter 5.

CHAPTER 5 HIGH POWER OUTPUT THROUGH IMMOBILIZATION AND INCREASED CONDUCTIVITY

5. High Power Output GEBFCs through Immobilization and Increased Conductivity

5.1. INTRODUCTION

In the previous two chapters, we assessed two types of biological fuel cells which are able to generate electricity from sugar as a possible solution for powering AIMDs. In looking at microbial fuel cells, we have investigated the factors influencing their power output such as electrode configuration, stirred and static SCMFCs, inoculation size, reactor type, culture type, electrolyte type, membrane size and arrays of DCMFCs and assessed these in a biomedical context. When testing GEBFCs, the parameters are quite different and essentially required a method to load large amounts of enzymes into dense conductive material matrix electrodes. This was achieved by the development of a conductive polymer, and compression of a conductive polymer directly with enzymes to create the electrodes.

It is important to recognise that a major consideration for the transition between the two technologies was that MFCs containing bacteria, have particular biocompatibility and toxicity issues, depending on design, they must be more self-contained and are larger, and that in terms of energy efficiency, bacteria must use some of the energy from glucose for their own livelihood. Enzymes are a part of the overall process that allows bacteria to digest glucose and output electrons, and in GEBFCs we can directly use these enzymes. Having now quantified both technologies, we can see that with microbial fuel cells, 9.68 μW at 281.31 mV and 34.31 μA of electricity was generated with an individual 200 mL DCMFC and with GEBFCs of which are 2 coin like electrodes, 2.24 μW at 23.74 mV and 87.93 μA of electricity was generated. Since the objective is to implant one of these technologies with an AIMD, it is helpful to look at the overall size of the device. An MFC must remain contained, to help ensure the bacteria do not escape and infect the patient as well as a large chamber to house the bacteria, whilst for the GEBFC, once the enzyme leaching is taken care of, and

once the material is made biocompatible, may need only be the electrodes themselves. Regardless however, the experiments thus far have been at a 50 mL capacity. On this basis then, the power is per mL for an individual MFC is 0.0484 μW/mL compared to 0.0494 μW/mL for GEBFCs. Similarly, comparing the currents at the peak power where an energy harvesting circuit is most likely to extract power, the MFCs measure at 0.1715 μA/mL and the GEBFCs at 1.758 μA/mL. Additionally, energy harvesting circuits more easily cope with low voltages than low currents. GEBFCs therefore have an advantage being slightly more power dense and can provide greater current.

Despite this fact, there is still room for improvement with the GEBFC electrodes. The voltage for these electrodes peaked at over 200 mV, but comparing this even to the MFC voltages, is approximately half. The Ppy being used has a stated conductivity of 10 to 50 S/cm in compressed pellet form (Sigma Aldrich 2017). MWCNTs, which have been used as compressed electrodes for GEBFCs, have a conductivity of in the ranges of $10^6 – 10^7$ S/m (Zhang 2017) which is significantly higher than that of Ppy. Further, lowering internal resistances in fuel cells can lead to higher power outputs. Improving the conductivity then of the electrodes may help to improve the electrical output. Additionally, as we have also seen from Figure 71, the enzymes had a tendency to leach out of the electrodes, and may be a reason for why the voltage longevity is not ideal. Immobilization of the enzymes then is another clear area that could be worked on. This would create greater stability in power output of the electrodes by anchoring the enzymes to the Ppy conductive matrix.

In this chapter, the focus is on improving on the power density of the compressed Ppy electrodes. To address issues around enzyme leaching, we use the aldehyde groups of Glut to form amide bond linkages with the amine groups of the Ppy and enzymes, creating a chemical imide bonds between them. To improve the conductivity of the electrodes whilst still maintaining the chemical functionality of Ppy, we blend Ppy with reticulated vitreous

carbon (RVC) and silver to create Ppy composites. By combining these two features, the power output is greatly improved.

The chapter is laid out as follows: we begin by outlining the materials and methods used to create both the improved conductivity and immobilization of the electrodes, characterize these features and the running of GEBFCs with electrodes with applied improvements. We then go into the results, firstly dealing with enzyme immobilization (EI), followed by the increased conductivity (IC) improvements and then combine both EI and IC improvements. We then discuss these results, actually attempt to power a medical device and draw some conclusions.

5.2. MATERIALS

Product Name	**Manufacturer / Supplier**	**Product Code**
Polypyrrole (Ppy, conductivity 10-50 S/cm)	Sigma Aldrich	577030
Flake Silver	Johnson Matthey	FS2
Reticulated Vitreous Carbon	Goodfellow	073-784-76
Platinum Foil	Goodfellow	PT000261 332-547-93
Acetonitrile	ChemSupply	AH1008
Tetrabutylammonium tetrafluoroborate	Sigma Aldrich	86896
Silver Wire	Sigma Aldrich	327026
Laccase from Tramates versicolour	Sigma Aldrich	38429
Glucose oxidase from *Aspergillus niger*	Sigma Aldrich	G2133
Glutaraldehyde (70% solution)	Sigma Aldrich	G7776

Table 21: List of Chemicals Used for EI, IC and Corresponding GEBFC Studies

5.3. METHOD

5.3.1. PREPARATION OF CHEMICALS

Laccase (LAC) from *Trametes Versicolor*, Glucose oxidase (GOx) from *Aspergillus niger*, Polypyrrole (Ppy, conductivity 10-50 S/cm), Glutaraldehyde (Glut, 70% solution), Tetrabutylammonium tetrafluoroborate (TBAFB) were purchased from Sigma Aldrich and used as is. Silver wire was also purchased from Sigma Aldrich and a 5 cm piece was cut from the roll for use. The Pt foil and Reticulated Vitreous Carbon (RVC) were purchase from Goodfellow where the Pt foil was cut into 2 equal pieces and the RVC was crushed into a fine powder prior to use. The silver flakes were obtained from Johnson Matthey, D-glucose from Ajax Chemicals and Deionised H_2O filtered through a milliQ machine at 18.2 MΩ and used as is.

5.3.2. COMPOSITE ELECTRODE PREPARATION FOR IMPROVED CONDUCTIVITY

As per the methods section of Chapter 4, the electrodes were prepared with a simple compression method keeping the manufacturability and high enzyme loading advantages of the method in mind. An outline of the relevant powders mixed together is shown in Table 22 for each of the experiments where RVC and silver were added to increase the overall conductivity of each electrode. Mixing was performed in a standard laboratory plastic weigh boat or glass vial and stirred with a spatula until visual uniformity was observed. The sample was then added to a FTIR KBr pellet press with which, 8 tonnes of mechanical force was applied to the sample, creating coin like electrodes pictured in Figure 63. Where GOx or LAC is added to the electrode either directly or through EI, the electrode is considered either the anode or cathode respectively.

	Ppy (100 mg)	**RVC (50 mg)**	**RVC (100 mg)**	**Silver (5 mg)**	**GOx/ LAC (50 mg)**	**GOx/ LAC (100 mg)**
Ppy with Immobilised Enzyme Electrode	x				x	
Ppy-RVC with Immobilised Enzyme Electrode	x	x			x	
Ppy-Silver with Immobilised Enzyme Electrode	x			x	x	
Ppy with Non-Immobilised Enzyme Electrode	x					x
Ppy-RVC with Non-Immobilised Enzyme Electrode	x		x			x
Ppy-Silver with Non-Immobilised Enzyme Electrode	x	x		x		x

Table 22: Weights of Chemicals for Electrode Mixtures

5.3.3. Conductivity Measurements

The conductivity of the electrodes was measured with an Agilent U3402A in 4-probe measurement mode on the compressed Ppy and Ppy composite electrodes in the absence of enzymes. The electrodes were inserted and clamped between two highly conductive silver disc electrodes and the conductivity determined from the resistance measurement as per equation $\rho = RA/l$ where ρ is the conductivity in S/cm, R is the measured resistance Ω, A is the contact area of the electrode in cm^2 and l is the thickness of the electrode in mm. An illustration of the measurement setup in shown in Figure 73. The forced exerted on the electrodes was slowly increased until the conductivity stabilised.

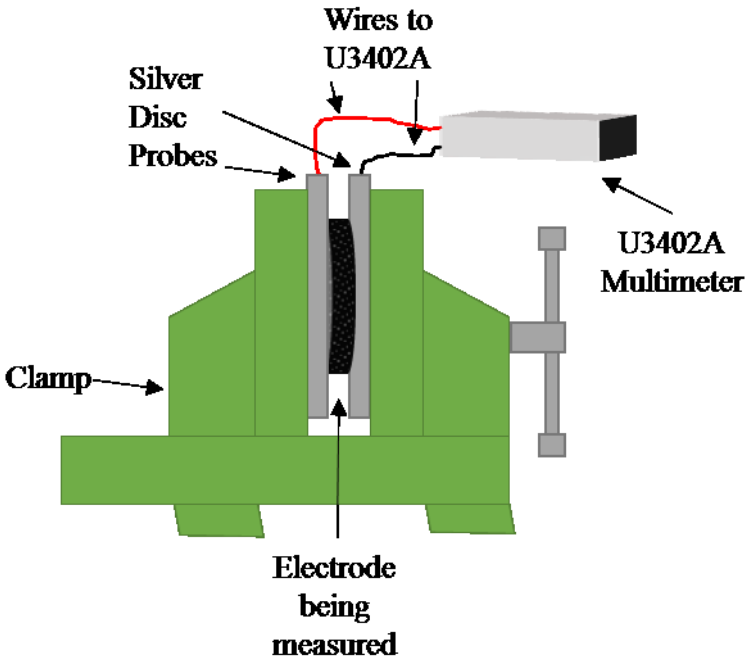

Figure 73: Illustration of the Conductivity Measurement Setup

5.3.4. Enzyme Immobilization Procedure

To create a direct physical anchor and connection between the surface of the compressed Ppy electrodes and the enzymes, Glut was used as a crosslinker, as adapted from Jugović et al (Jugović et al. 2016). The powders were mixed as per Table 22 and were compressed to create compressed electrodes in the absence of enzymes. The electrodes were then thoroughly covered with an excess of Glut and left to incubate for 1 hour before being rinsed with DI

H_2O to remove unreacted Glut. Vials were prepared with 50 mg of either GOx or LAC in 2mL of PBS and the electrodes added and left to incubate on a bench top shaker for 20 hours in room temperature at 210 RPM. The electrodes were then again washed of unreacted enzymes with DI H_2O and used as is. A diagram of the procedure is shown in Figure 74.

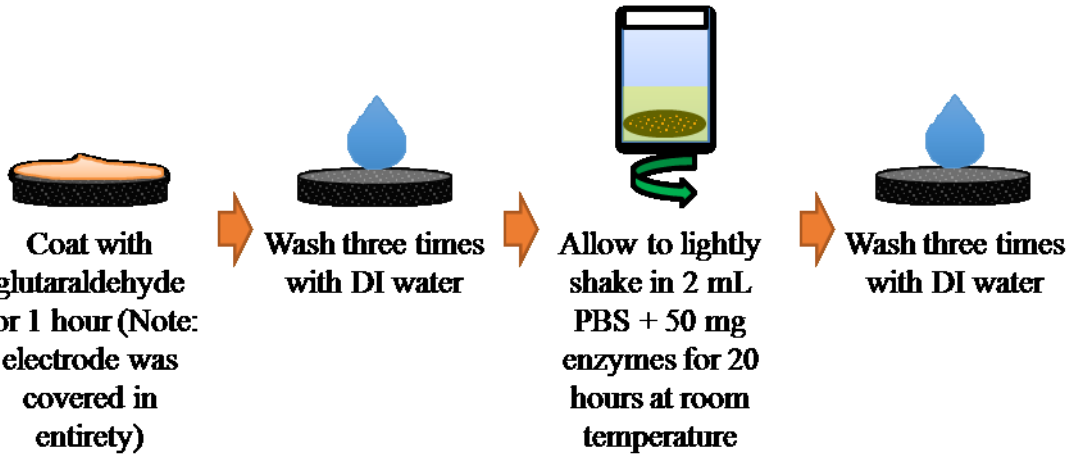

Figure 74: EI Procedure

5.3.5. FTIR Analysis

To confirm the presence of the crosslink between the Ppy surface, Glut and the enzymes, Fourier Transform Infrared (FTIR) spectra were obtained. Scans were taken at different stages of the process including the bare Ppy compressed electrode, after Glut treatment and after enzyme treatment. DI H_2O was used after each treatment to ensure excess Glut or enzyme solution was washed clear and this was followed by freeze drying to ensure no H_2O remained. A Nicolet 6700 Spectrometer with ATR attachment was used, where the background noise was first measured and then a total of 64 scans and their average taken with the measured noise being subtracted from the average. Spectra were measured between 4000 and 600 cm^{-1} and are shown in absorbance.

5.3.6. Biofuel Cell Studies

Refer to the 4.4.4 Glucose Enzymatic Biofuel Cell Studies methods section for the Biofuel Cell Studies Methodology.

5.4. RESULTS

5.4.1. ENZYME IMMOBILIZATION TO IMPROVE POWER OUTPUT

5.4.1.1. FTIR ANALYSIS SHOWING CROSSLINKING OF ENZYMES TO ELECTRODE SURFACE

The FTIR spectra for the Ppy electrodes at different stages are shown in Figure 75 including (a) bare compressed Ppy electrodes, (d) after Glut treatment, cleaning and drying and (c) and (b) with Glut and GOx and LAC treatments respectively. Figure 75(a) contains peaks for C-C stretching, C=C stretching, C-N stretching, C-H out-of-plane vibration and Ppy ring vibrations which correspond to peaks 1624, 1505, 1422, 1076, 989 and 731 respectively (Li et al. 2012; Nascimento & Oliveira 2015; Patro & Wagner 2016; Ruhi & Dhawan 2014).

The Glut treated spectra, shown in Figure 75(d), includes the peaks at 1624, 1505, 1422, 1076, 989 and 731 which are those from Ppy, but with the addition of peaks at 1709 and 2852. These additional peaks correspond to Aldehyde C-H and Aldehyde C=O respectively, along the Glut molecule. There is also a very faint peak at 3329 which corresponds to O-H stretching of the H bonds (Baghayeri 2015; Patro & Wagner 2016).

Figure 75(c) and (b) show the FTIR spectra for the Ppy electrodes with GOx and Lac immobilised by Glut respectively. The aldehyde peaks at 1709 and 2852 are barely visible as expected, due to the treatments in which a reaction takes place between the enzyme amines and the Glut. The fact that they are barely visible suggests that what remains is likely to be unreacted or unwashed residue. Strong peaks at 3300 are from the N-H stretching resulting from the presence of enzymes (Baghayeri 2015; Patro & Wagner 2016).

A 1516 peak which is in the enzyme treated samples in Figure 75(b) and (c) but which cannot be found in the Glut treated sample in (d) is the N-H in-plane bending and polypeptide chain N-N stretching modes of amide II. Lastly, C-C stretching vibrations from the Ppy seen in all four spectra are shielding the 1650 and 1643 peaks which are usually assigned to the amine I

C==O stretching of the peptide bonds of enzymes and imine bonds respectively (Baghayeri 2015; Patro & Wagner 2016; Wang, Turhan & Gunasekaran 2004).

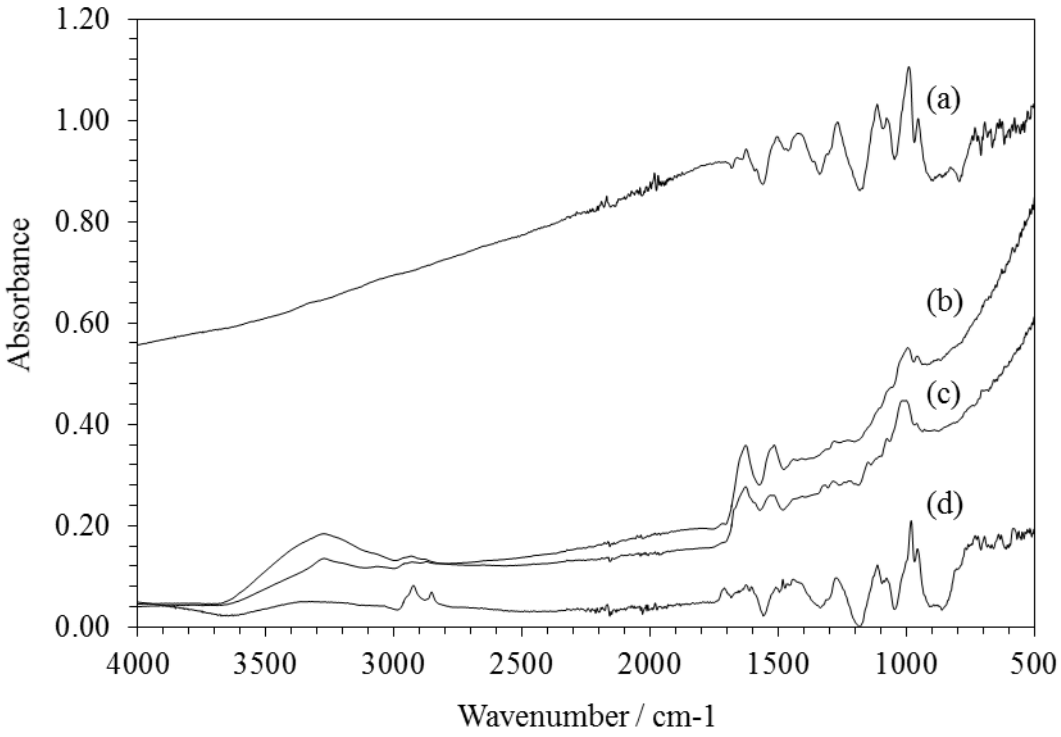

Figure 75: FTIR spectra for (a) Ppy, (b) Ppy with crosslinked LAC, (c) Ppy with crosslinked GOx and (d) Ppy with bonded Glut.

5.4.1.2. BIOFUEL CELL USING IMMOBILISED ENZYMES ELECTRODES

Once the compressed Ppy electrodes were treated with Glut and enzymes for immobilization, the electrodes were placed into a GEBFC setup. Figure 76 shows the open circuit voltage over time before the polarization and power curves were obtained. A peak voltage of 212.5 mV was measured which was at the very end of the time period at 153 minutes as the voltage steadily grew.

After the open circuit voltage settled in the Ppy immobilised enzyme electrode GEBFCs, polarization and power curve data was sampled and are shown in Figure 77 and Figure 78 respectively. The open circuit voltage was measured to be 184.7 mV and this voltage was sustained by the GEBFC for up to 3.29 μA before the voltage dropped with increasing

current draw. The peak current drawn from the GEBFC was 396 µA, although with a voltage of 7.92 mV. The maximum power measured from the GEBFCs was 16.36 µW with 127.5 mV and 127.5 µA giving an internal resistance of 1000 Ω.

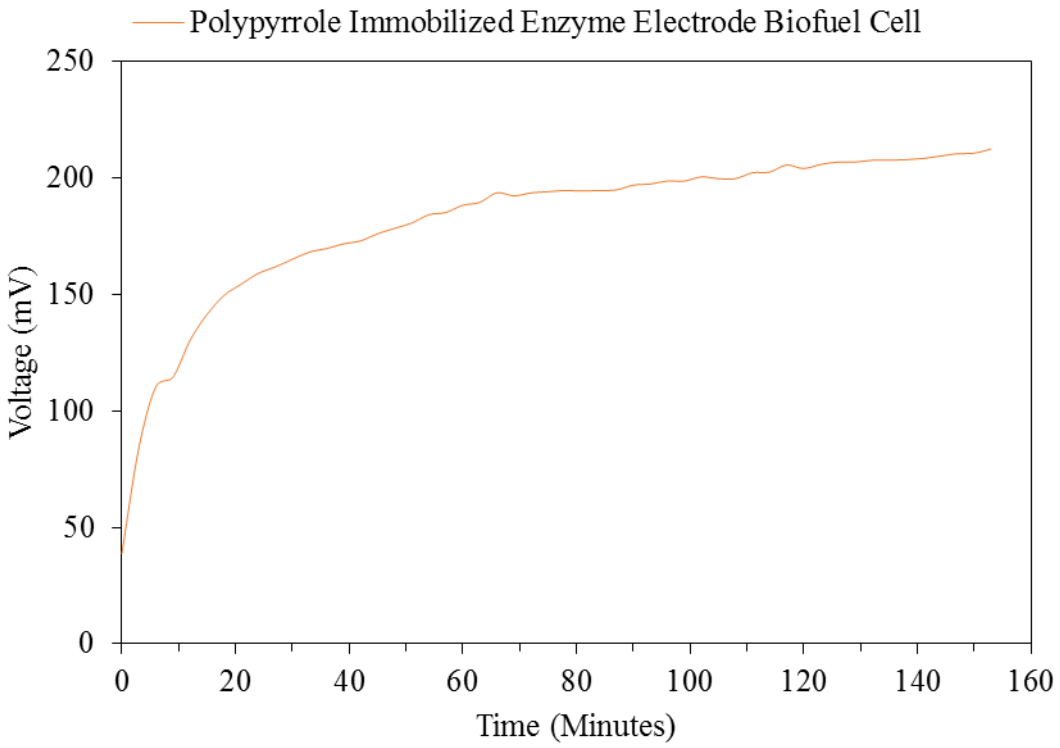

Figure 76: Voltages Over Time for Compressed Ppy Electrodes with Immobilised Enzymes in GEBFCs

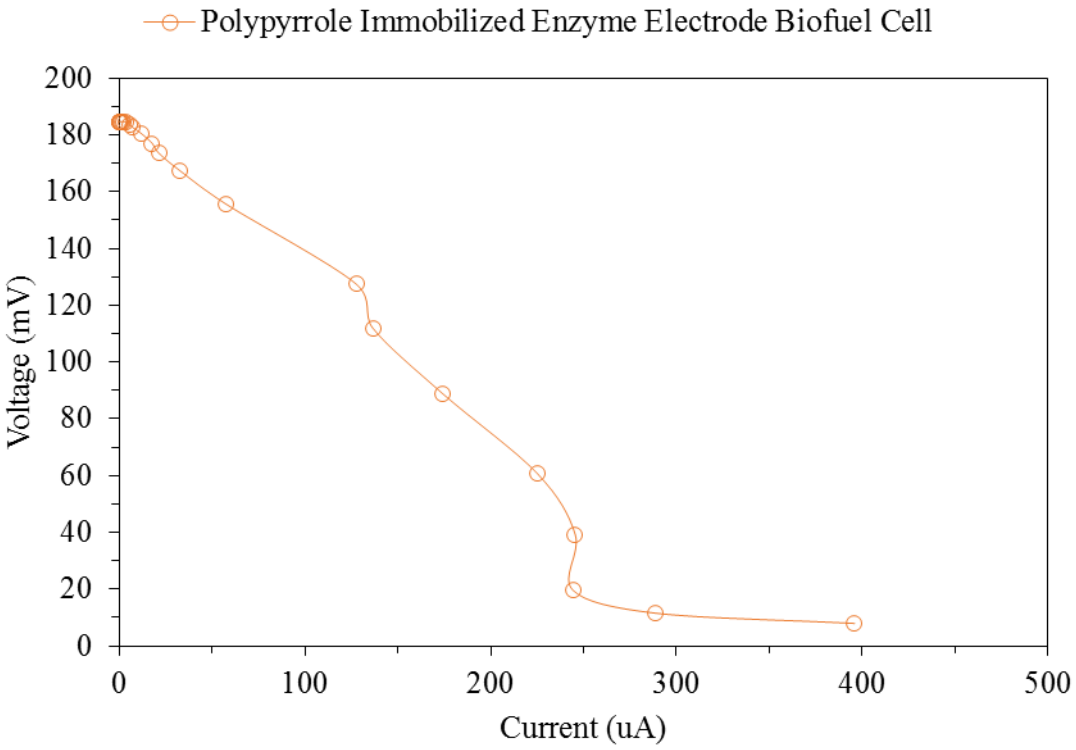

Figure 77: Polarization Curve for a GEBFC Containing Compressed Ppy Electrodes with Immobilised Enzymes

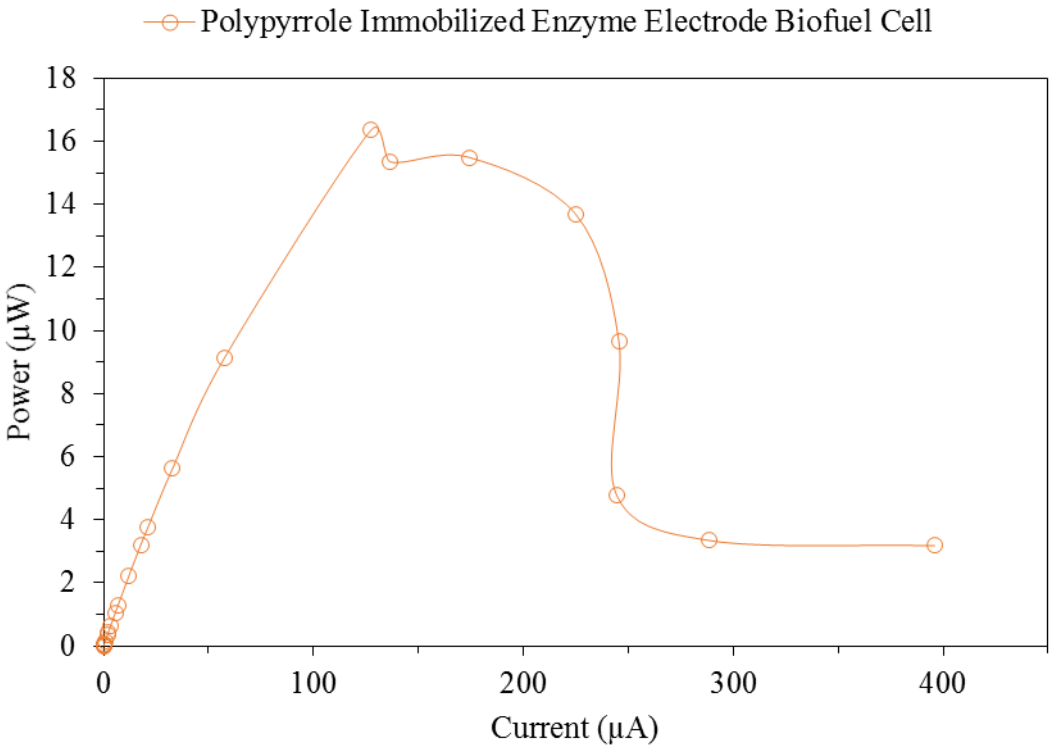

Figure 78: Power Curve for GEBFCs with Compressed Ppy Electrodes with Immobilised Enzymes

5.4.2. Increasing Electrode Conductivity through Ppy Composites

5.4.2.1. Electrode Conductivity

The express purpose of mixing Ppy with RVC and silver was to increase the overall conductivities of the electrodes. The measured conductivities from the Agilent U3402A in 4-probe mode of the electrodes are shown in Figure 79 and are measured without enzymes. Ppy has a conductivity of 2.59 mS/cm, Ppy mixed with 50 mg RVC has a conductivity of 5.99 mS/cm, Ppy mixed with 100 mg RVC has a conductivity of 14.83 mS/cm and Ppy mixed with silver has a conductivity of 61.8 mS/cm.

5.4.2.2. Electrochemical Characterization

In creating composite material electrodes, cyclic voltammetry was performed to assess the electrochemical nature of the electrodes since the addition of RVC and silver may introduce electrochemical changes. Figure 80 and Figure 82 shows CVs for the Ppy-RVC and Ppy-silver composite electrodes respectively, at a scan rate of 10 mV/s between -300 mV and 1000 mV. For the Ppy-RVC composite, this lower scan rate shows a slightly rectangular shape, indicating an imperfect pseudocapacitance in the material. Figure 81 and Figure 83 show the CVs for each of the electrodes for scan rates of 100 to 1000 mV/s.

Figure 84 shows pseudocapacitance for each of the electrodes, including for the Ppy electrode from Chapter 4.5.4 Electrode Fabrication and Characterization, shown here for comparison and reference. At the scan rate of 10 mV/s, the pseudocapacitances are 6.04 nF, 7.47 nF and 0.28 nF for the Ppy, Ppy-RVC composite and Ppy-silver composite electrodes respectively. The figure shows a clear dependence on the scan rate, in which the higher scan rates result in lower capacitances.

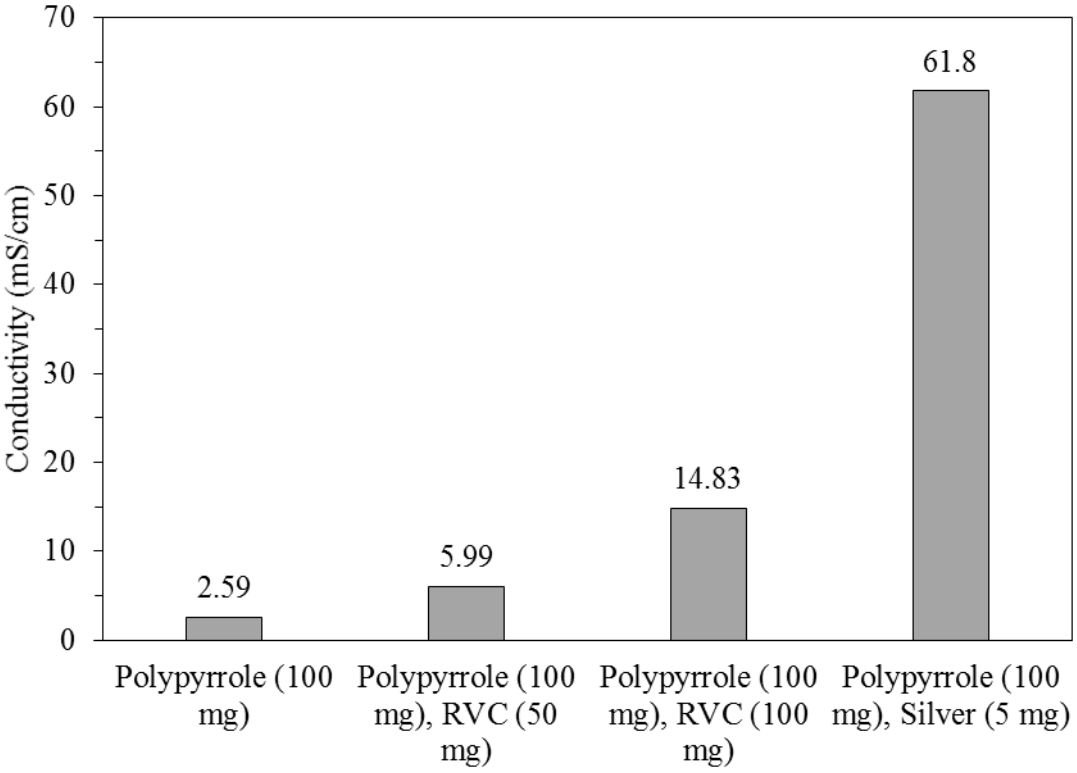

Figure 79: Conductivities of the Ppy composites

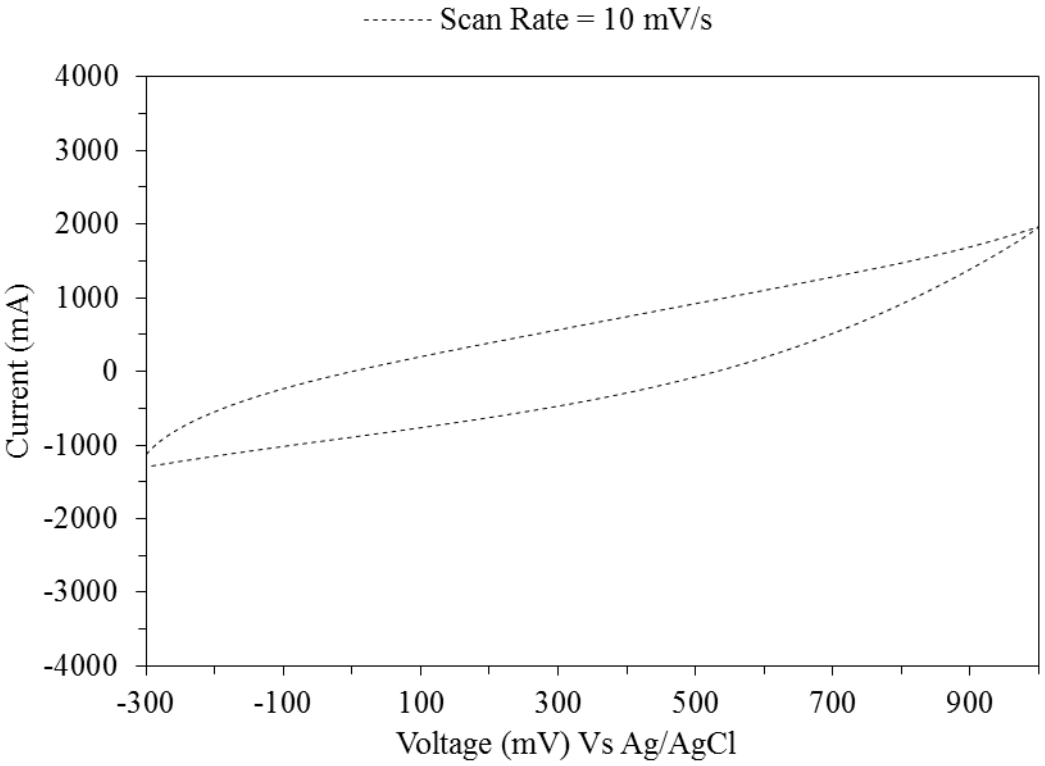

Figure 80: CV for a Compressed Ppy-RVC Electrode at a Scan Rate of 10 mV/s

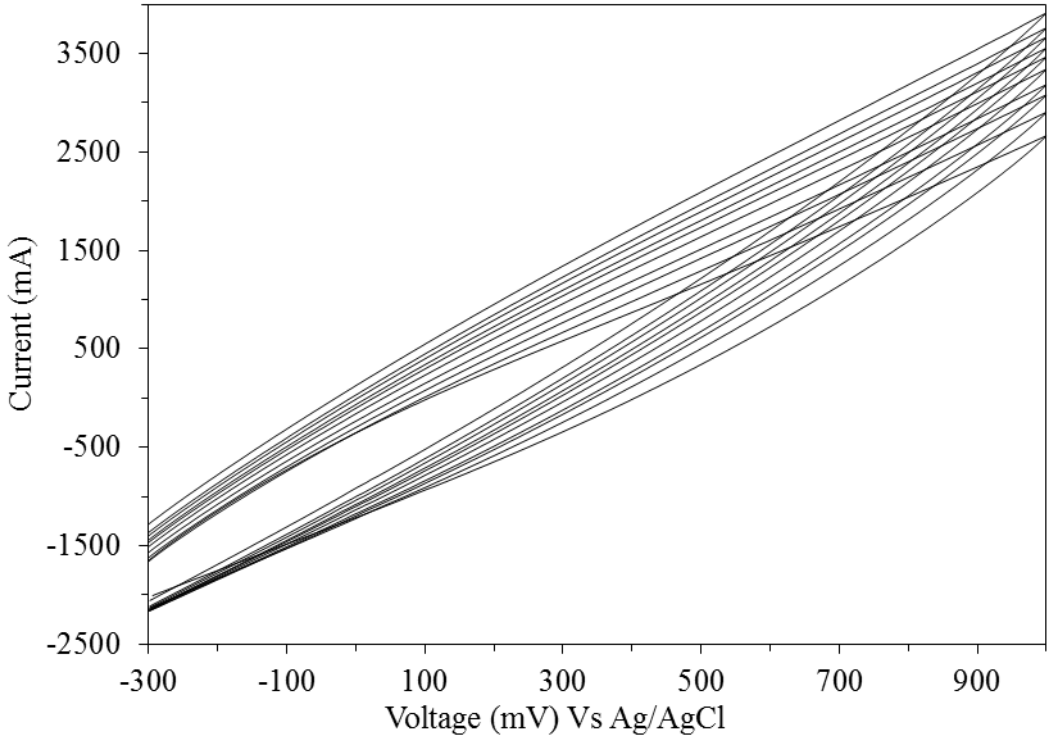

Figure 81: CVs for a Compressed Ppy-RVC Electrode at Scan Rates from 100 to 1000 mV/s

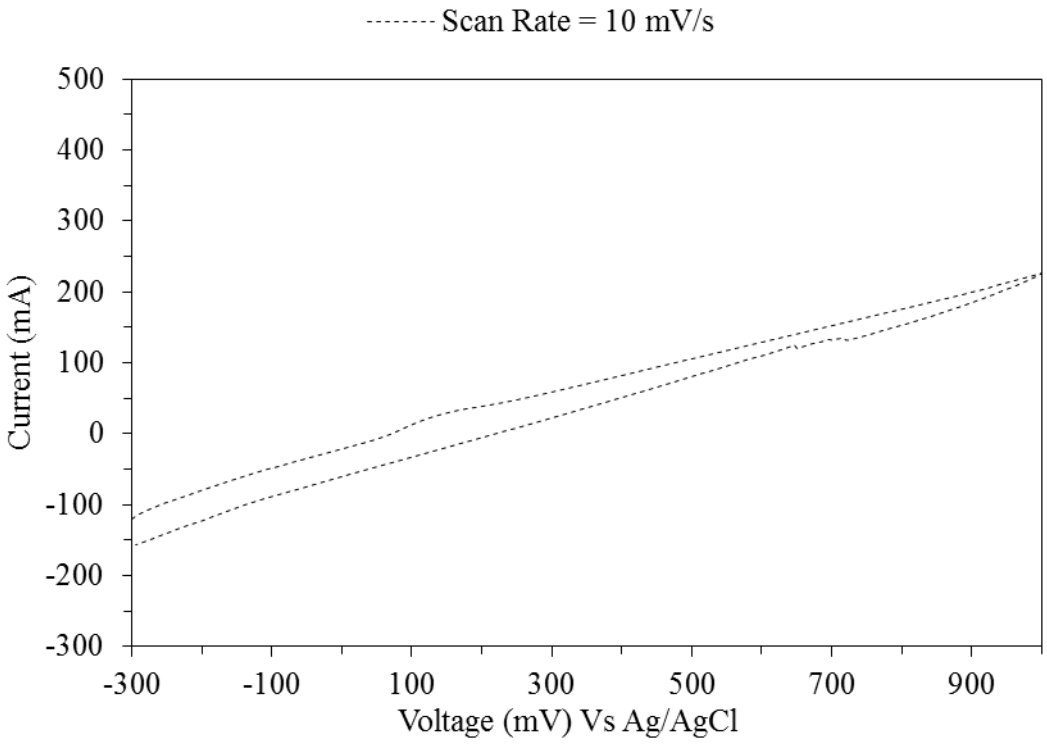

Figure 82: CV for a Compressed Ppy-Silv Electrode at a Scan Rate of 10 mV/s

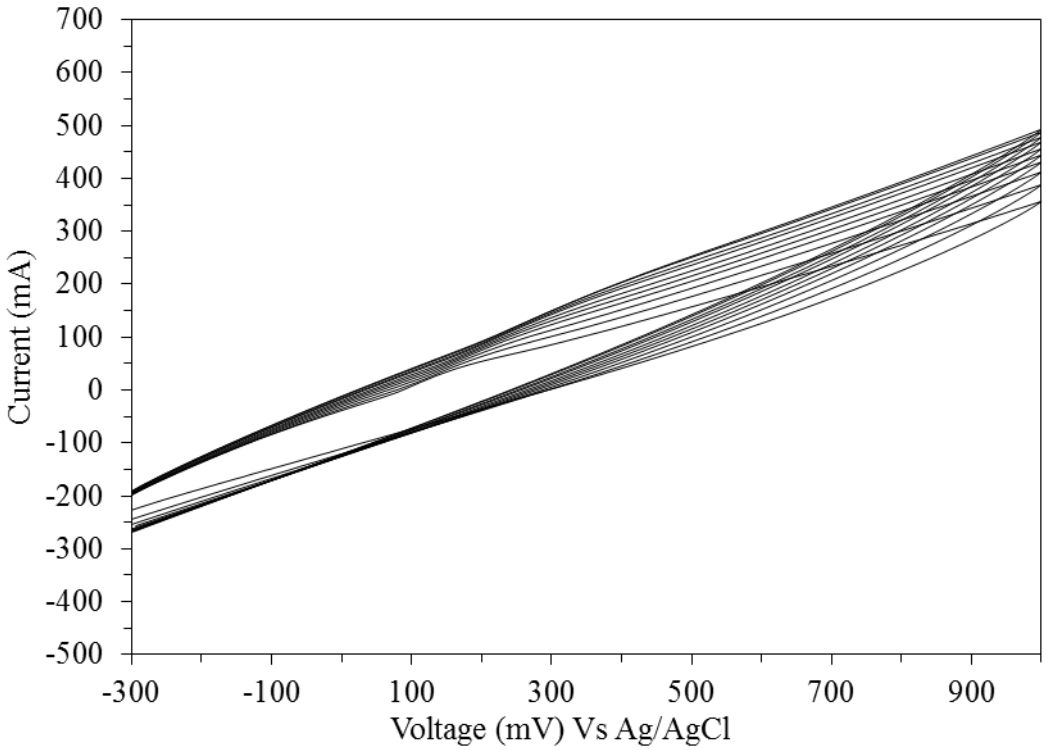

Figure 83: CVs for a Compressed Ppy-RVC Electrode at Scan Rates from 100 to 1000 mV/s

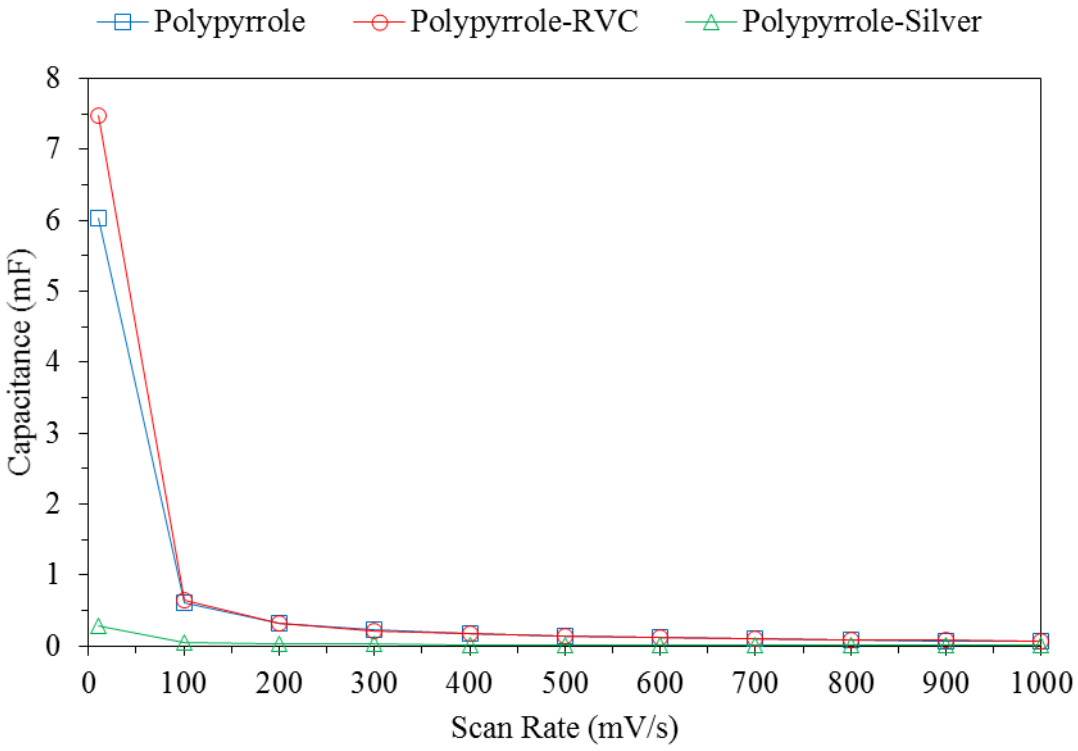

Figure 84: Pseudocapacitances of Ppy Electrode Composites for Different Scan Rates

5.4.2.3. Biofuel Cells with Increased Conductivity Polypyrrole Composite Electrodes

After the compressed Ppy composite electrodes were characterised for their conductivity and electrochemical behaviour, the materials were used in GEBFC setups. Figure 86 shows the voltage over time for the Ppy-RVC composite electrodes and the Ppy electrodes (shown here as a baseline and originally in Chapter 4.4.4 Glucose Enzymatic Biofuel Cell Studies). As can be seen, the voltage climbs to a peak open circuit value of 475.51 mV at the very end of the period before the polarization curve and power curve experiments are performed.

Likewise, the Ppy-silver composite materials compressed for use in GEBFCs was also tested and the open circuit voltages are shown in Figure 85 with the plain Ppy electrode voltage data as a baseline. The peak open circuit voltage measured was 459.26 mV which again was measured at the end of the open circuit value period, prior to the polarisation and power curve experiments.

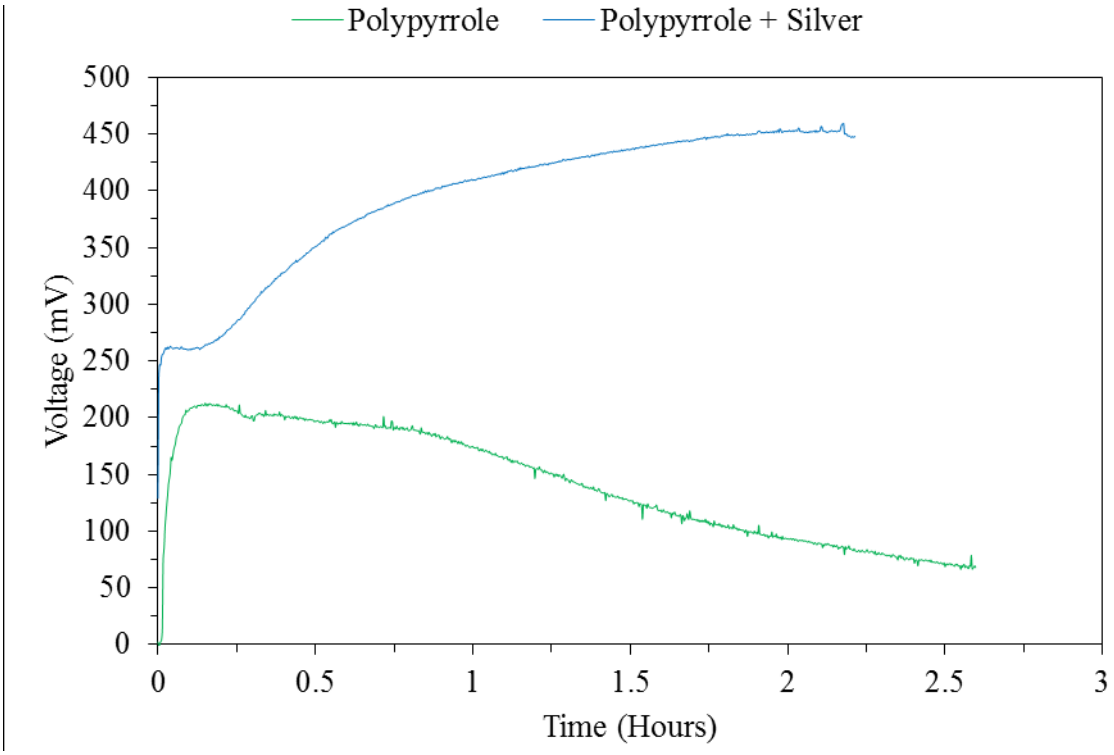

Figure 85: Voltages over Time for GEBFCs containing compressed Ppy and Ppy-silver composite electrodes

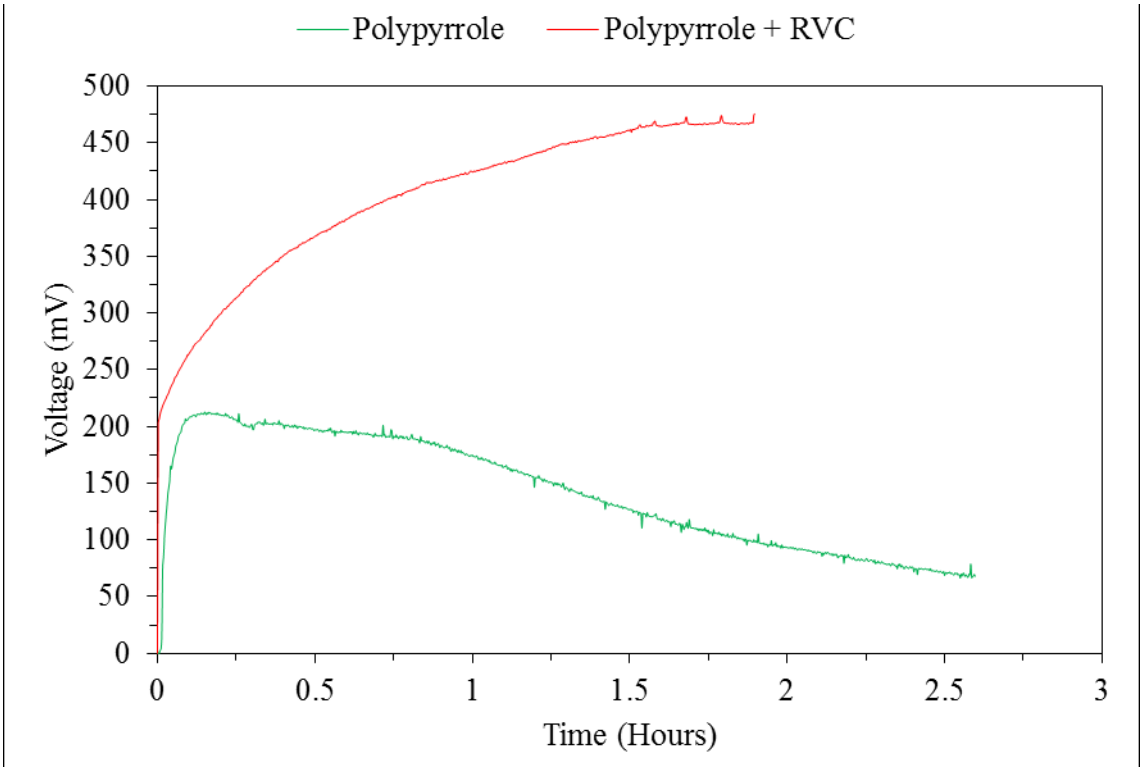

Figure 86: Voltages over Time for GEBFCs containing compressed Ppy and Ppy-RVC composite electrodes

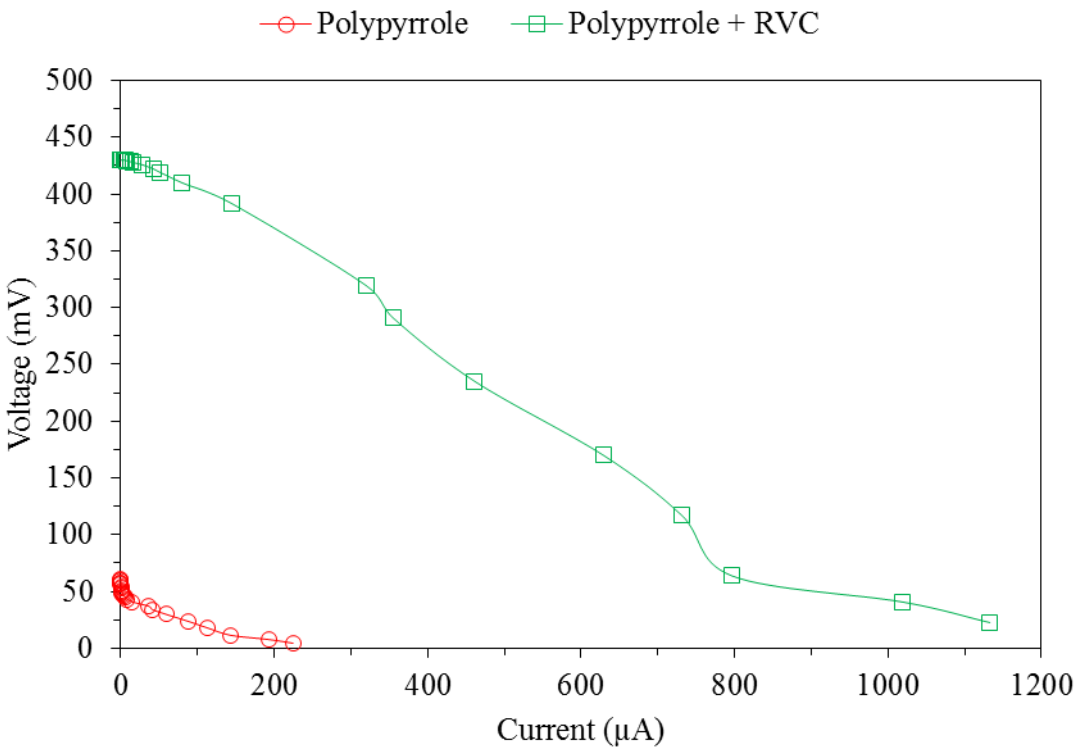

Figure 87: Polarization Curve for GEBFCs containing Ppy electrodes and Polpyrrole RVC composite electrodes.

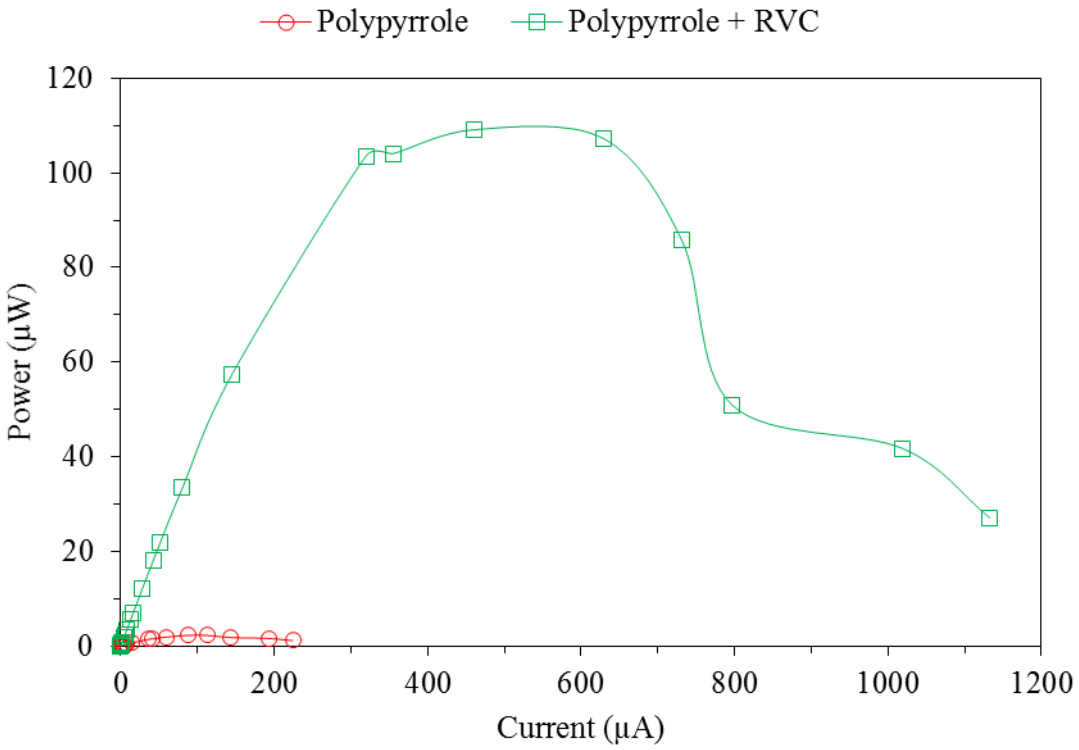

Figure 88: Power Curve for GEBFCs Containing Ppy Electrodes and Ppy and RVC Composite Electrodes.

When the voltage had stabilized in the GEBFCs containing Ppy and RVC composite electrodes, the polarization and power curves shown in Figure 87 and Figure 88 were obtained respectively. The open circuit voltage was 429.85 mV which was able to be maintained up until 5.24 µA before the voltage began to drop as more current was drawn with decreasing resistance. The maximum current drawn from the circuit was 1.13 mA and the maximum power was 109.14 µW at a voltage of 235.15 mV and a current of 461.08 µA, giving an internal resistance of 510 Ω.

Likewise, when the voltage stabilized in GEBFCs with Ppy and silver composite electrodes, Figure 89 and Figure 90 show the polarization and power curves data that was collected. The open circuit voltage was 463.7 mV and this was held for up to 0.56 µA before the voltage dropped with increasing current draw. The maximum current drawn was 739.25 µA and the maximum power was 95.99 µW measured at a voltage of 221.05 mV and 433.43 µA giving an internal resistance of 510 Ω.

5.4.3. Biofuel Cells Using Ppy Composite and Immobilised Enzyme Electrodes

Once the effect of increasing electrode conductivity and immobilizing enzymes was tested in GEBFCs individually, the combined effect was tested as shown below.

5.4.3.1. Voltage Over Time

Figure 91 shows the voltages over time for the GEBFC containing the Ppy and RVC composite electrodes for both with immobilised enzymes and with non-immobilised enzymes shown in the previous section for reference. The GEBFC with immobilised enzymes showed an unusually unstable voltage compared to the non-immobilised enzyme version. The peak open circuit voltage measured was 558.7 mV occurring at approximately 12 minutes. The voltage appears almost instantaneously and the average voltage over the 56 minutes of monitoring prior to the polarization and power curves was 512 mV.

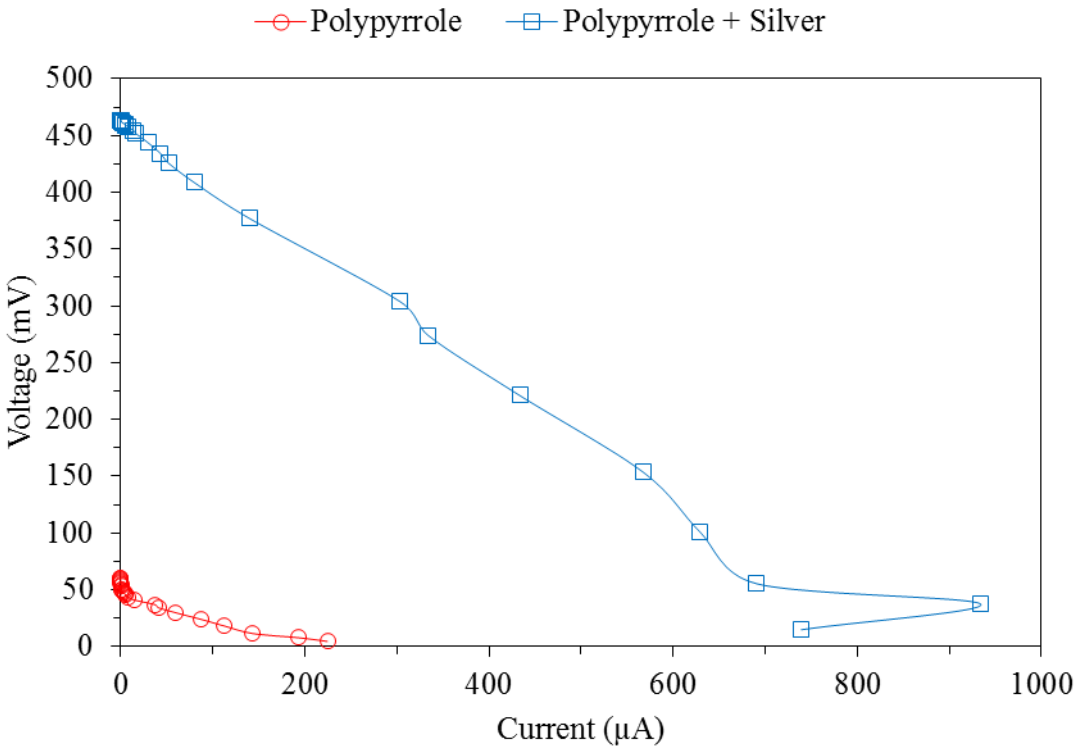

Figure 89: Polarization Curve for GEBFCs Containing Ppy electrodes and Ppy and Silver Composite Electrodes.

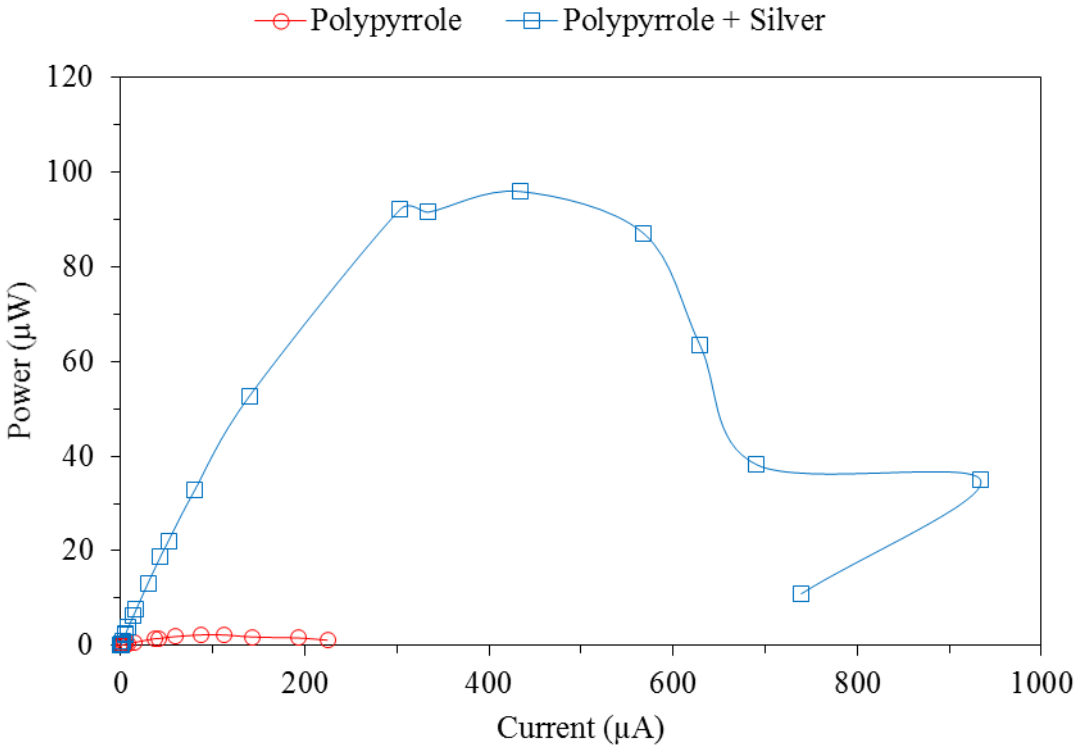

Figure 90: Power Curve for GEBFCs Containing Ppy Electrodes and Ppy and Silver Composite Electrodes.

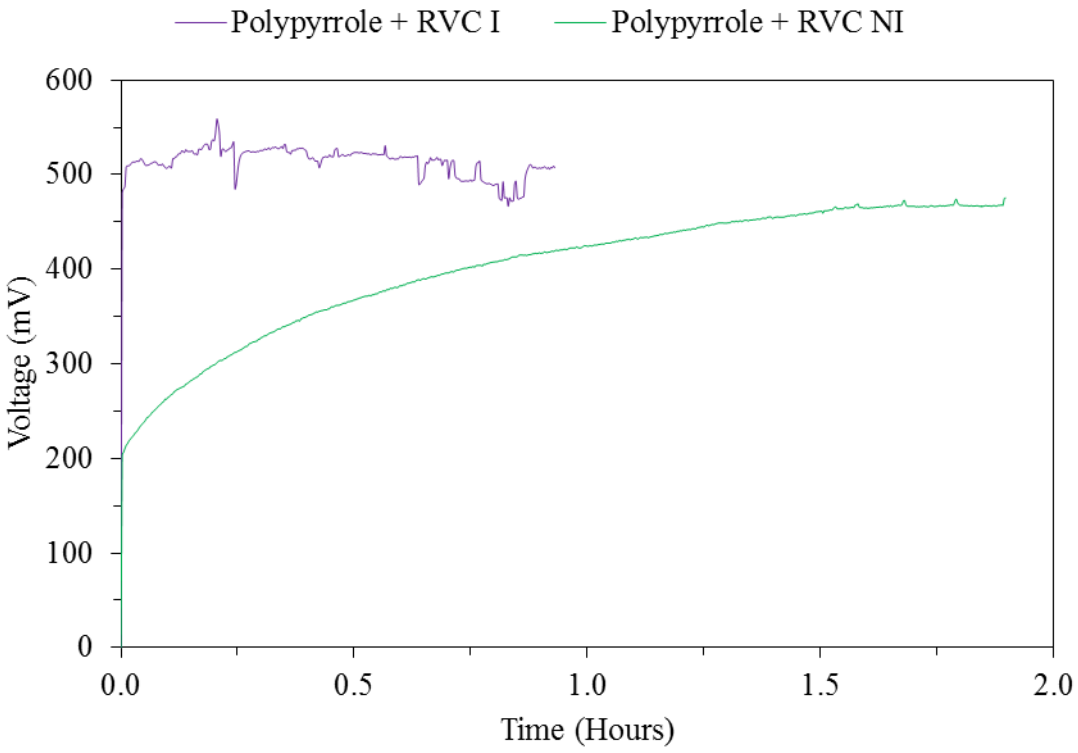

Figure 91: Voltages over Time for GEBFCs with Ppy and RVC Composite Electrodes with Non-Immobilised and Immobilised Enzymes

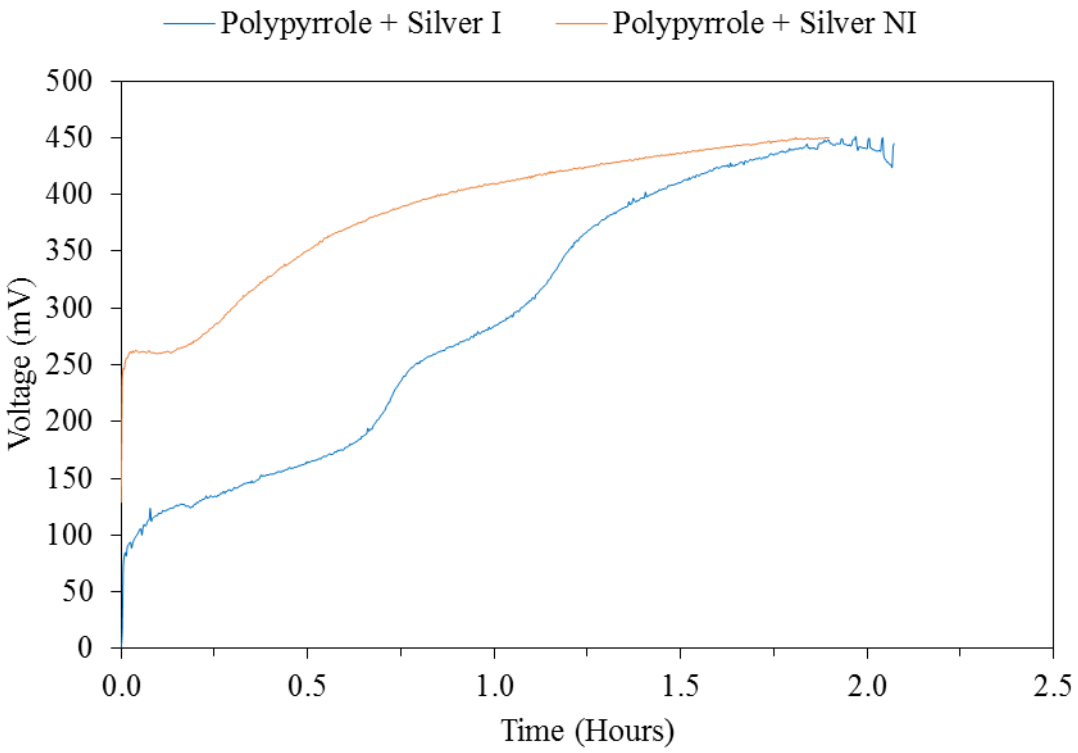

Figure 92: Voltages over Time for GEBFCs with Ppy and Silver Composite Electrodes with Non-Immobilised and Immobilised Enzymes

The voltages measured from a GEBFC using Ppy and silver composite electrodes with both immobilised and non-immobilised enzymes (shown in the previous section and here for reference) in start-up mode, prior to the polarization and power curves are shown in Figure 92. The voltage climbs to a peak of 451.02 mV which occurs at time 118 minutes which was toward the end of the measurement. The voltage rose quite slowly and was similar to the non-immobilised voltage of time curve.

When the voltages of the Ppy and RVC composite electrode electrodes with immobilised enzymes had stabilized, polarization and power curves were obtained and are shown in Figure 93 and Figure 94 respectively. The open circuit value measured was 522.05 mV and this could not be sustained at any current. The voltage continued to be unstable but above 500 mV up until a current draw of 8.94 µA where eventually the peak current measured was 533.63 µA. The peak power measured was 35.8 µW measured at a voltage of 189.15 mV and a current of 189.15 µA, giving an internal resistance of 1000Ω.

5.4.3.2. Polarization and Power Curves

The polarization and power curves were once again performed on the Ppy and silver composite electrodes with immobilised enzymes after the open circuit voltage was stabilised and are shown in Figure 95 and Figure 96 respectively. The open circuit voltage measured was 416.7 mV which remained stable up until 0.11 µA. The peak current measured was 1.24 mA and the peak power extracted was 128.2 µW at a voltage of 185.85 mV and a current of 688.33 µA, giving an internal resistance of 270 Ω.

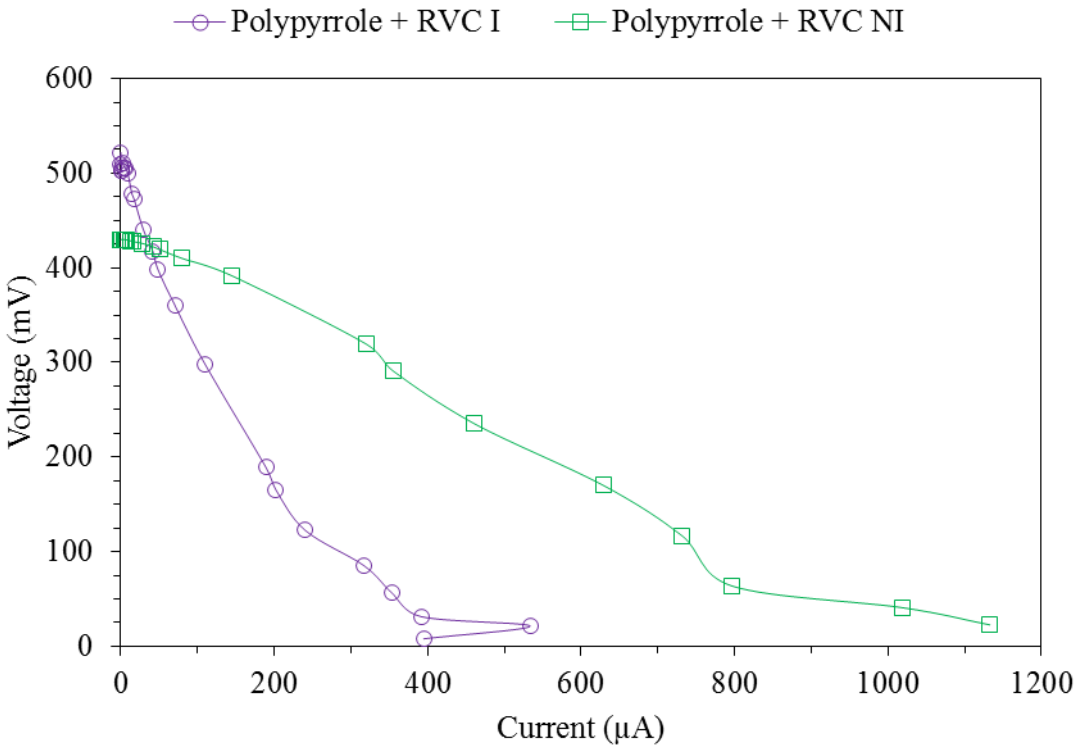

Figure 93: Polarization Curves for GEBFCs containing Ppy and RVC Composite Electrodes with Immobilised and Non-Immobilised Enzymes

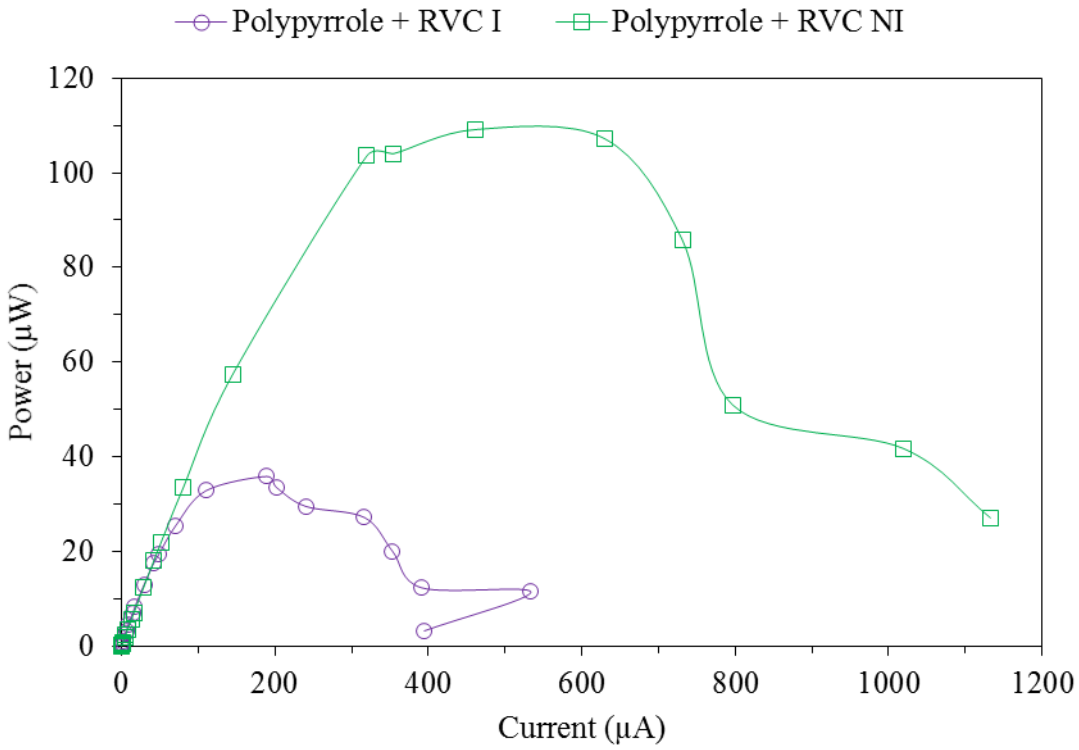

Figure 94: Power Curves for GEBFCs containing Ppy and RVC Composite Electrodes with Immobilised and Non-Immobilised Enzymes

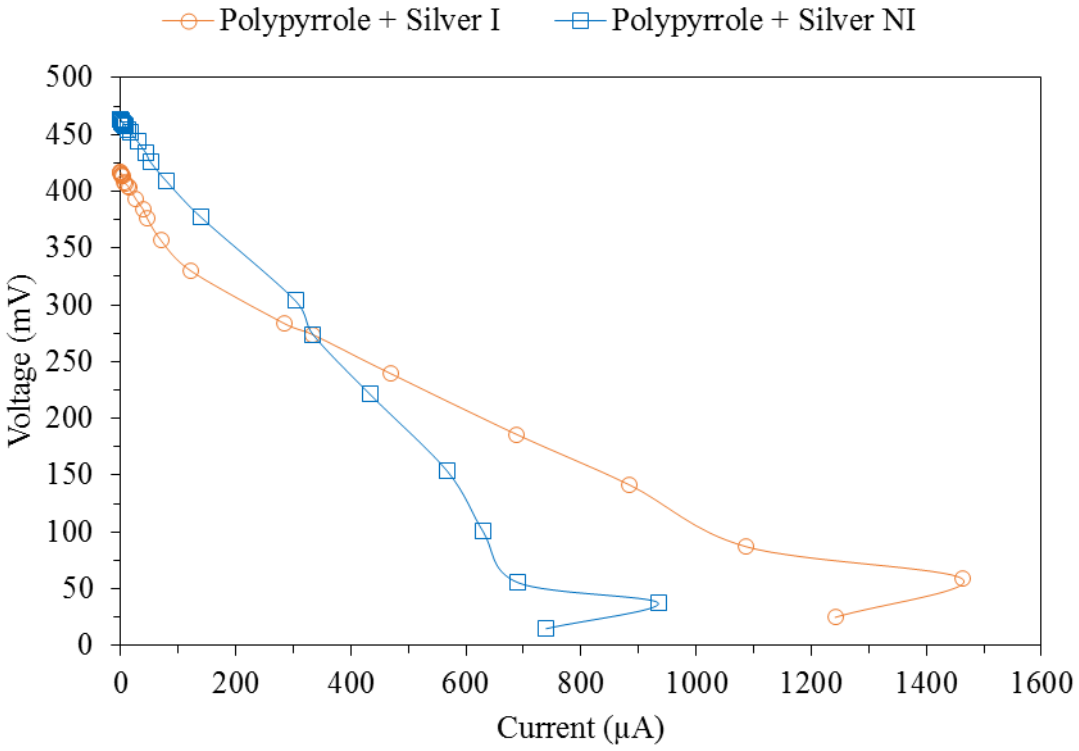

Figure 95: Polarization Curves for GEBFCs containing Ppy and Silver Composite Electrodes with Immobilised and Non-Immobilised Enzymes

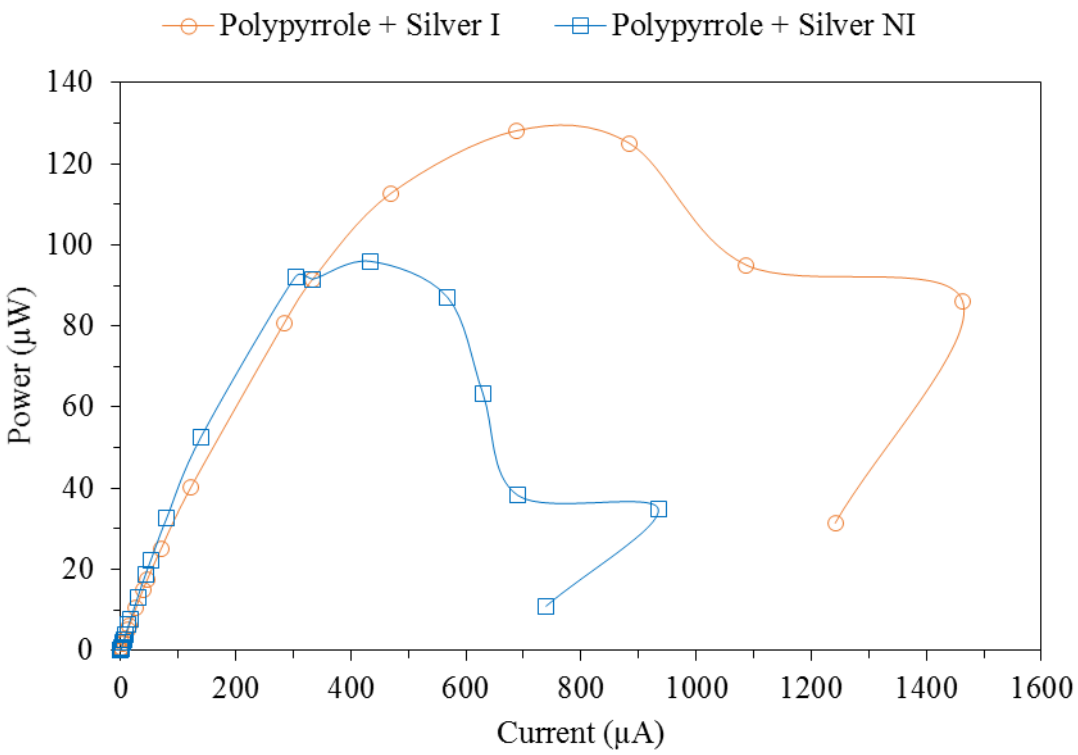

Figure 96: Polarization Curves for GEBFCs containing Ppy and Silver Composite Electrodes with Immobilised and Non-Immobilised Enzymes

5.5. Discussion and Conclusion

This chapter has presented experiments proving two possible solutions to improving power output in compressed Ppy electrodes for GEBFCs. Specifically, that by increasing the conductivity in the Ppy electrodes and by immobilizing enzymes on the surface of the electrodes, the power output against the standard plain Ppy electrodes can be improved.

When comparing the open circuit voltage of the electrodes with Ppy and enzymes compressed together to the compressed Ppy with surface immobilised enzymes, the maximum voltage was practically the same at 212.83 mV for the former compared to 212.5 mV for the latter. However, as was previously mentioned, the voltage is less than a half of this for the non-immobilised enzyme electrodes after 160 minutes, whilst for the immobilised version, the voltage steadily builds. This is due to how the enzymes leach out of the electrode in the non-immobilised electrodes, but are directly attached in the immobilised electrodes.

When comparing the polarization and power curves of the non-immobilised and immobilised Ppy electrodes, we also see large differences. The maximum current output of the immobilised enzyme electrodes is almost double that of the non-immobilised enzyme electrodes with 396 μA compared to 224.5 μA. The maximum power is also quite different, with a maximum of 16.36 μW for the immobilised enzyme electrodes, compared to 2.24 μW for the non-immobilised enzyme electrodes.

However, whilst the immobilised enzyme electrodes out-compete the non-immobilised enzyme electrodes in many ways, the internal resistance of the non-immobilised enzyme electrodes was lower at 270 Ω compared to 1000 Ω. More importantly, a major reason for EI was the way that the voltage of the non-immobilised enzyme electrodes suffered from enzyme leaching, as shown in Figure 71. The voltage of the immobilised version did not seem to suffer from this issue as there was no visible enzyme leaching into the PBS glucose electrolyte solution.

It should be noted though that despite the overall success of the use of Glut as a crosslinker, there are some issues. Ideally, if we knew the amount of amine groups along the Ppy chains, then we could optimise the amount of Glut used, rather than adding large amounts to achieve the ‘in excess’ condition. It is likely that waste amounts of Glut were used in order to achieve the crosslinking. This is in fact a problem with Ppy in that it is incredibly difficult to dissolve (Nalwa 1999), leading to it being difficult to work with. This being the case, neither NMR or GPC analysis could be performed with the Ppy, and Sigma Aldrich as the manufacturer of the product, was not aware of the molecular weight or other useful information of the Ppy (Curlevski 2017). Indeed neither of the manufacturing methods for Ppy which include chemical oxidative polymerisation and EP, are polymer chain length control methods and the chain length is usually not a concern for conductive polymers.

Aside from the immobilization of enzymes on the surface of the compressed Ppy electrodes, we also mixed the Ppy and enzyme powders with either RVC or silver before compression, to increase the conductivity of the electrodes. The increases in conductivities were confirmed via 4-probe resistance measurements and the trends were in line with other studies in which the conductivity of RVC or glassy carbon is 200 S/cm^2 (Baker & Bragg 1983) and the conductivity of silver is 6.3 x 10^7 S/cm^2 (Serway & Gordon 1998). With the stated conductivity of Ppy from the manufacturer data being 10 to 50 S/cm^2 (Sigma Aldrich 2017), it is reasonable to expect that a mixture of Ppy and RVC is more conductivity than Ppy and that a mixture of silver and Ppy is more conductive again, as seen in the results.

Before experimenting with the IC electrodes, the mixing of composite materials to be used for electrochemical means such as in electrodes necessitates testing the electrochemical properties first through cyclic voltammetry. In the previous chapter, no peaks could be measured and this is due to the thickness of the electrodes. Typically when CVs are performed with Ppy, Ppy is in a film form (Kizling et al. 2015). At low scan rates for the Ppy and the Ppy-RVC composites, the presence of a small amount of pseudocapacitance was detected but not in the Ppy-silver composite. Pseudocapacitance has been detected in Ppy previously although (Kizling et al. 2015; Kizling et al. 2016) the lack of it in the Ppy-silver composite is due to the way in which capacitance usually exhibits itself along with resistance. With this being the case, the IC of the Ppy-silver composite may alter the charge-discharge characteristics of the electrode. Nonetheless, the charge and discharge characteristic was measured, indicating the material is appropriate and useful as an electrode material.

When the composite material electrodes were used with non-immobilised enzymes in a GEBFC setup, the results were positive. For the Ppy-RVC composite electrodes, the open circuit voltage measured was 475.51 mV. Similarly, the Ppy-silver composite electrodes also had a high voltage of 459.26 mV as compared to the plain Ppy electrodes, which had a peak

voltage of 212.83 mV. In both cases then, with the increase in conductivity, the open circuit voltage was doubled. These increases are also seen in the polarisation and power curves where the peak current was 1.13 mA and 739.25 μA and the power 109.14 μW and 95.99 μW for the Ppy-RVC and Ppy-silver composites respectively. Compared to the Ppy electrodes which had 224.5 μA of current and 2.24 μW of power, this is a marked improvement.

With both the IC in Ppy GEBFCs and the EI working individually, we then tested electrodes where both electrode improvement features were present. During the open circuit testing with the Ppy-RVC composite electrodes, the voltage was unusually unstable. Nonetheless, the voltage rose immediately rather than slowly as with other GEBFCs and a peak of 558.7 mV was measured with an average value of 512 mV across the one hour of open circuit testing before the polarization and power curves were obtained. This is a further improvement on the 475.51 mV peak open circuit voltage measured from the Ppy-RVC composites with non-immobilised enzymes. The Ppy-silver composite electrodes with immobilised enzymes did not show a similar improvement in open circuit voltage. The voltage was 451.02 mV for the immobilised enzyme version, which is close, but still lower, than the 459.26 mV measured for the non-immobilised version.

Whilst during the open circuit testing, the Ppy-RVC electrodes provided a higher voltage, the results were different for the polarization and power curves. When resistances were connected to the immobilised enzyme Ppy-RVC electrodes, the maximum power extracted was 35.8 μW and the peak current that could be outputted from the GEBFC was 533.63 μA. This is a decrease from the non-immobilised electrode equivalent which measured a peak power of 109.14 μW and maximum current of 1.13 mA. Looking at the Ppy-silver electrodes however, we see that this is reversed where the immobilised enzyme electrodes provide an increased power output compared to the non-immobilised version. A peak power of 128.2

μW was measured and a maximum current of 1.469 mA for the immobilised enzyme electrodes, compared to 95.99 μW and 739.25 μA for the non-immobilised electrodes.

Several possible reasons can be offered for this difference in trend between the different IC electrodes with immobilised and non-immobilised enzymes. The first is that when immobilizing the enzymes, they are only immobilised on the surface of the electrodes and this sets an upper limit on the amount of enzymes that are immobilised. This is the basis for why only 50 mg of enzymes is used during the EI, whilst for the non-immobilised electrodes, 100 mg of enzymes are used. The 100 mg is mixed and compressed with the rest of the electrode and is perhaps why the Ppy-RVC non-immobilised enzyme electrodes provide more power, but does not explain the electrical performance of Ppy-silver immobilised enzyme electrodes. One possible reason lies in the porosity of the materials which can be seen in the SEM images in Figure 97, Figure 98 and Figure 99 for the compressed Ppy, Ppy-RVC and Ppy-silver electrodes respectively.

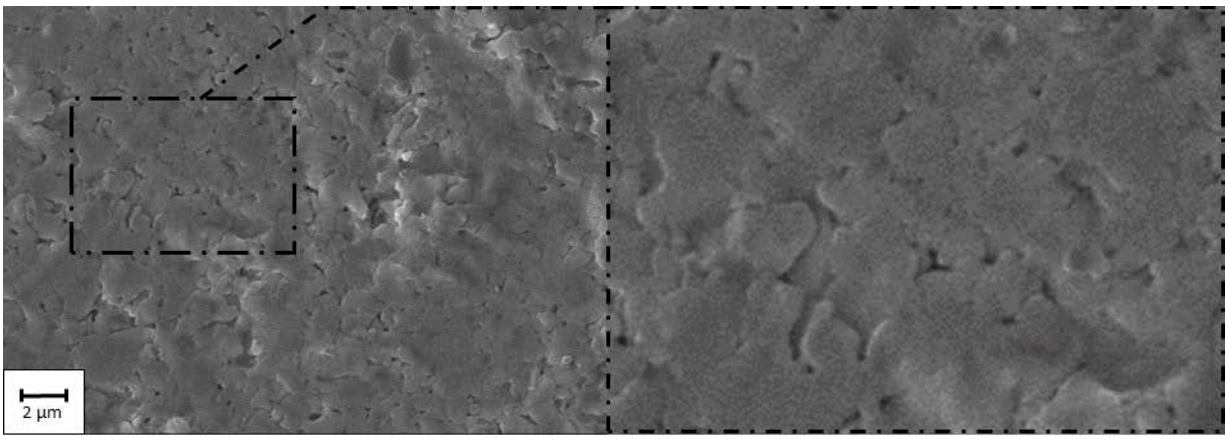

Figure 97 SEM micrograph of a compressed Ppy electrode

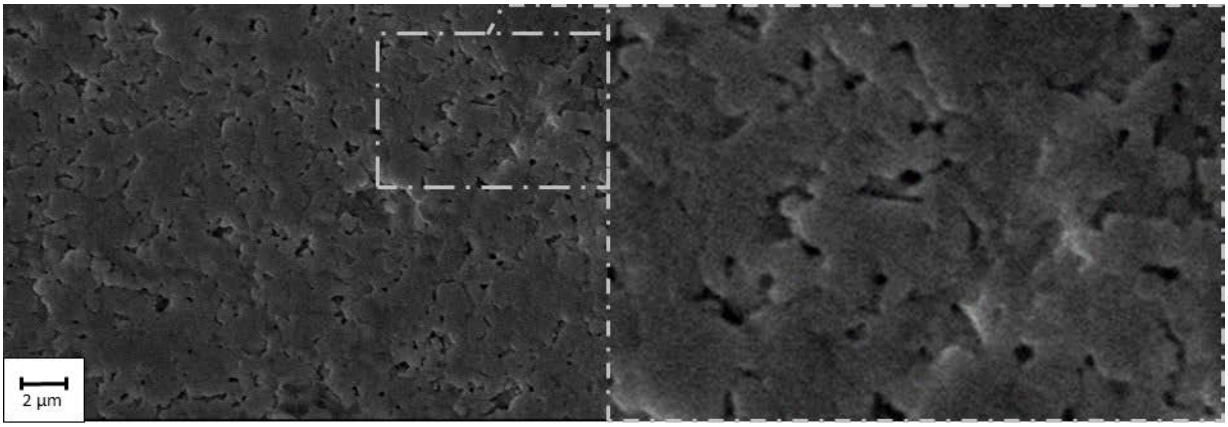

Figure 98 SEM micrograph of a compressed Ppy-RVC electrode

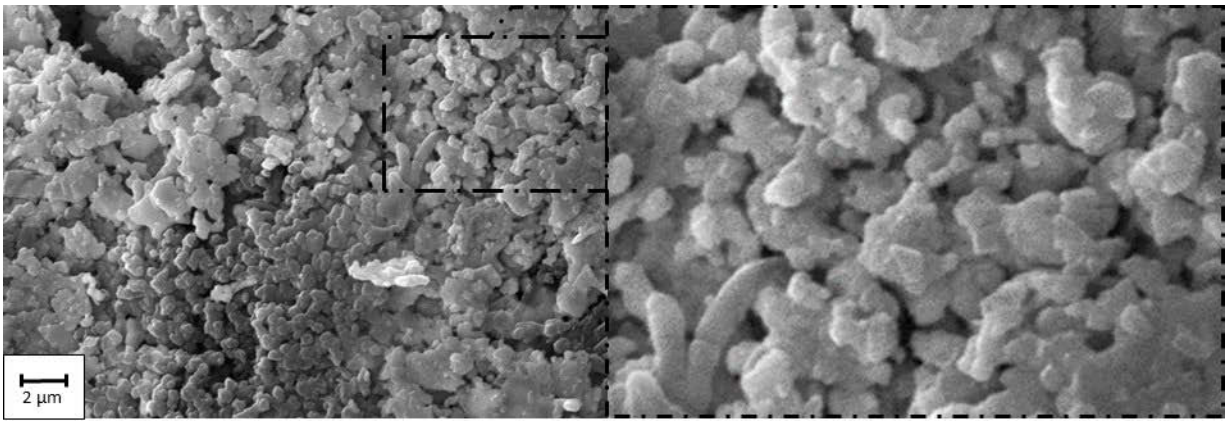

Figure 99: SEM micrograph of a compressed Ppy-silver electrode

The micrographs showing the Ppy and Ppy-RVC composite are quite similar in that they are flat in morphology. Given that the methodology involves compressing the powders under 8 tonnes of force, the flat morphology is expected. Both electrodes also appear to have pores, but neither is especially deep or wide. If one is to look carefully, the Ppy-RVC composite has slightly more pores which are deeper than the Ppy electrodes.

The Ppy-silver composite is quite different from the other two in that the image is clearer, indicating a more conductive material, and there is some semblance of chains of polymers. The pores are also deeper and there is a greater density of the pores. Interestingly, a micrograph of compressed CNTs by Zebda et al (Zebda et al. 2013; Zebda et al. 2011) shows similar porosity characteristics, typical of MWCNTs which are tubular and strand like in

nature. Their work showed power outputs in the milliwatt ranges, and the porous nature may play a part in this.

With the Ppy-silver composite electrodes being more porous, this may explain why they are able to provide a higher electrical output than all other electrodes tested in this study. Directly compressing the enzymes with the electrodes allows more enzymes to be embedded with the Ppy and a greater ability to simultaneously extract electrons. If the enzymes are only embedded on the surface, then there is a limit to the amount of enzymes able to extract electrons. By having more porous electrodes, we can then immobilise more enzymes throughout the inner parts of the electrode, allowing us to obtain the advantages of both methods, thus providing us with greater power output.

With the results such that we are now obtaining levels of power that are usable, it is appropriate to test whether this can happen. A GEBFC using Ppy-RVC composite electrodes with non-immobilised enzymes and a Texas Instruments BQ25504 energy harvesting step up converter was used in conjunction with a 470 μF capacitor to power an Omron 343F medical thermometer. The circuit schematic is shown in Figure 100 and a photo of the experimental setup and medical thermometer being powered in shown in Figure 101. To enable connection to the thermometer, the back cover and 1.5 V battery was first removed and wires were connected between the battery terminals and the breadboard but was not connected to the capacitor. The GEBFC was then connected to the input terminals of the step up converter and the battery charge terminals of the step up converter were connected to the 470 μF capacitor. After 8 minutes time, the capacitor was charged to 1.5 V and then was connected to the thermometer. The thermometer was able to take a reading within 10 seconds, and during this time, the voltage of the capacitor is decreasing to 1.11 V due to current draw to the thermometer. When the GEBFC was connected to the step up converter, due to the energy harvesters maximum power point tracking capabilities, the voltage of the GEBFC was 361

mV and dropped by approximately 30 mV to 330 mV and this would return upon disconnection. From Figure 93 and Figure 94, we know that this was not the maximum power point, but slightly less than the maximum, allowing the step up converter to obtain a higher voltage at its inputs. Multiple images illustrating this process are shown in Figure 102. This is a promising show of the use of GEBFCs powering an AIMD and again a novel use of the mechanical compression method and conductive polymers applied to GEBFCs.

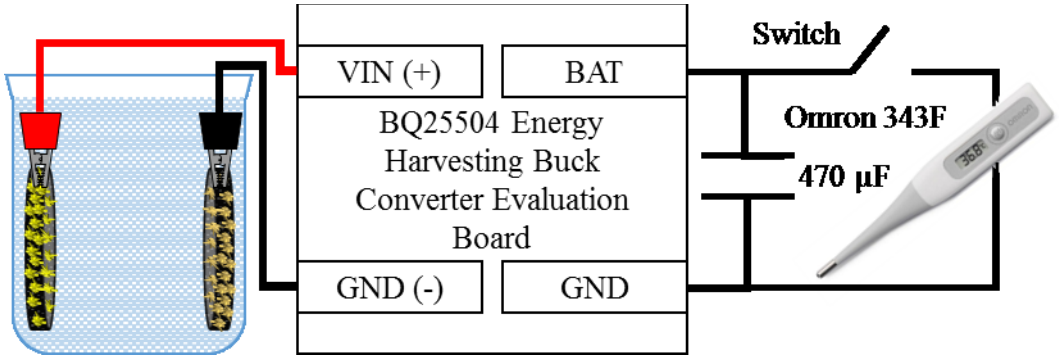

Figure 100: Schematic of Experiment for Powering a Medical Thermometer from a GEBFC

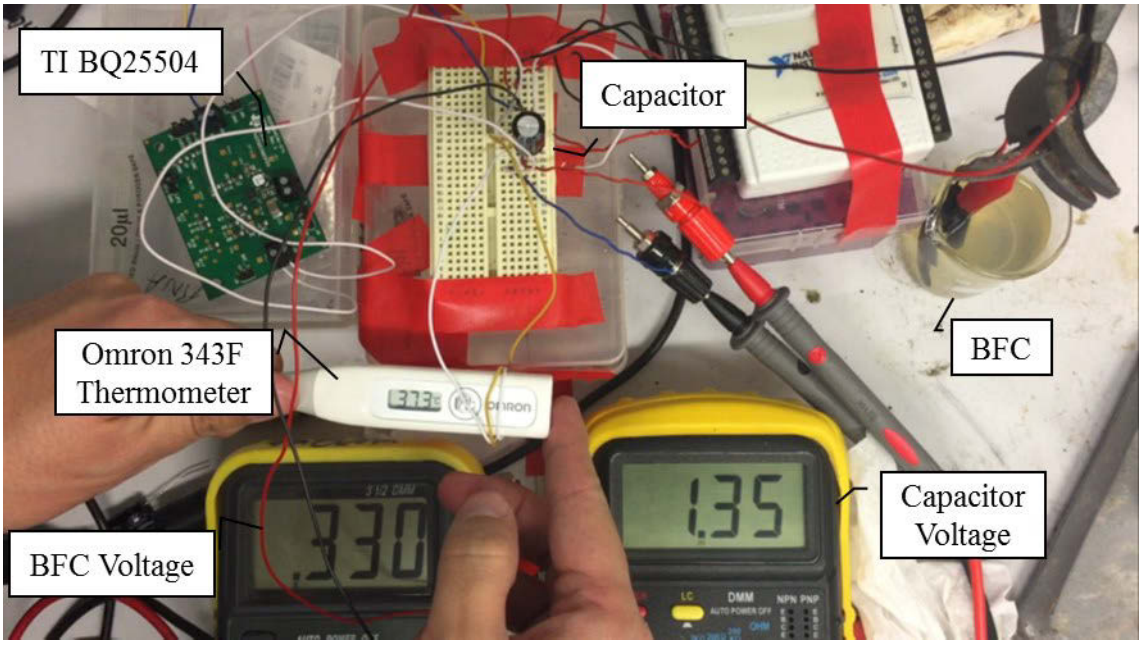

Figure 101: Photo of a body thermometer being powered by a BQ25504 and GEBFC

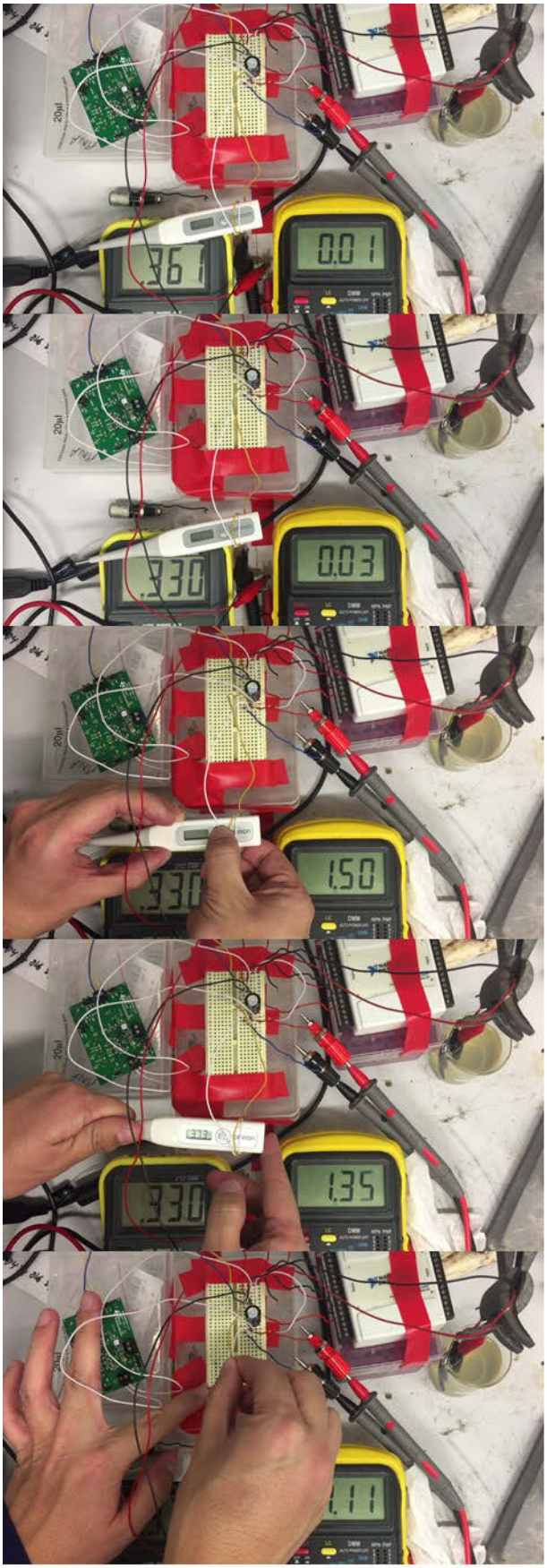

(a) Photo prior to any charging or connection showing the BFC voltage at 360 mV

(b) Photo after connection to the step up converter causing the voltage of the BFC to drop by 30 mV

(c) Photo after charging of the capacitor, after approximately 8 minutes, just before the thermometer is turned on

(d) Photo of the thermometer reading body temperature along with the capacitor voltage having decreased

(e) Turning off of the thermometer with the capacitor voltage having dropped by 0.39 V

Figure 102: Time Lapse of the Powering of a Medical Thermometer Experiment

CHAPTER 6 CONCLUSION & FUTURE DIRECTION

6. Conclusion and Future Direction

6.1. CONCLUSION

This thesis has presented contributions for improving the power output of MFCs and GEBFCs with regard to the powering of AIMDs. We began firstly by looking at how single chamber MFCs could be used if implanted, and how being implanted may affect their power output. In MFCs, orientation of the electrodes was tested, finding that power increases of up to 5.13 times can be achieved when a patient is standing as oppose to laying down asleep. This is a significant finding, since from an AIMD perspective, a patient is asleep ideally 8 hours per day, and awake and active for the rest. Design of electrodes implanted into the body can now take this into account. Further, active patients can increase device power by 119%, hence encouraging a patient to be active would not only be beneficial to the patient, but beneficial to their AIMD. These findings can allow future implantable MFCs to have their electrodes designed accordingly.

We then moved to DCMFCs where further significant results were obtained, including that an order of magnitude more power can be achieved as well as finding that nearly doubling the membrane size can nearly double the power output. Issues however around membrane cost and sustainability due to biofouling remain an issue. These experiments compared *S. oneidensis MR-1* with the mixed culture DCMFCs where the mixed culture DCMFCs achieved 2x more power than the single inoculate. Indeed, the mixed culture in the DCMFCs may have been from the human body, and their use in the body can not only double power output, but also may make it more biocompatible. Given that the DCMFCs are to be placed into the human body, and given that the human body has a plethora of different bacteria, further experimentation with these bacteria would be fascinating. Indeed, the upsizing of the membrane is an important optimisation to be made for implantable MFCs since this

depending on how it is done, could make the device larger, as does the use of a DCMFC over a SCMFC.

The stomach itself provides some inspiration for electrodes, given the stomach has a large surface area in a small space and high surface areas lead to higher power outputs. Some may say that this is an idea better left to academia and not for practical implementation, however at the same time, the field of biohacking has become incredibly popular in recent times (O'Neill 2017; Ockenden 2016; Ong 2016). Furthermore, the stomach could feed the bacteria, as it does already. In this regard, feeding the bacteria was also investigated, where LBB was able to achieve 8 times more power than the TSB DCMFCs. From these, 464.56 mV was measured and 9.68 μW extracted and with further optimisation, the technology could power an AIMD. Indeed, when 4 DCMFCs were combined, 1.619 V, 0.379 mA or 63.47 μW in series or parallel and parallel respectively was achieved, which is in the operating ranges for many electronics devices. These findings again have implications for the size and power density of the device, and thus design of future implantable MFCs.

All these achievements help to ascertain what a potential implanted biomedical DCMFC may look like. If one is to use a vitamin and mineral solution for helping feed the bacteria, one must find a way to get through the skin and to the device which must also prevent the bacteria from escaping and infecting the patient. One idea that was often proposed through the course of the project, was to use a self-sealing valve similar to how some car tires have the ability to heal themselves, allowing a driver to get to a mechanic for replacement. A person could inject through the skin into the device for a stock of several months, allowing the bacteria to live for such a time. Conversely, this may not be any better than needing to recharge a battery regularly and at least with recharging, currently patients can do it themselves at home.

Additionally, bacteria produce waste, which needs to be removed. It needs to be removed in a constant and timely manner since it can create a toxic environment, harmful to the bacteria. One good aspect of the DCMFC was that using PBS in the cathode chamber could help maintain pH in the anode as well. Membranes are useful in this regard for removing unwanted chemicals through concentration gradients. A design integrating such ideas would need an additional chamber with the membrane separating them and an ability to also refill this or at least for a large buffering capacity. Furthermore, bacteria are known to form biofilms on, not just the electrodes, but the membrane and this therefore provides the potential for further research avenues in material science. The difficulty here though which is also related to using multiple MFCs together to boost power, is that the design becomes increasingly difficult to implement with its design features and size, notwithstanding the fact that even with 4 DCMFCs it still has a low power density.

With these findings in hand, we proceeded to experiment with GEBFCs. Before beginning this work, there were already some advantages: (1) many of the biocompatibility issues would be alleviated by simply taking only the necessary parts of the bacteria, the enzymes, for the electron extraction, (2) no living bacteria means we can take more of a share of the energy in the system and (3) the methods and technology has developed such that it is simple to manufacturer the electrodes and it is possible to embed large amounts of enzymes, providing a path to high power density fuel cells.

To begin this work, a conductive material for the electrodes was first developed. A combination of two cutting edge methods, RAFT polymerisation and EP were used, which to the knowledge of the author, is the first combination of these two techniques. Not only this, but when applying RAFT polymerisation, the highest known conversion rate of 80.825% and a highly uniform polydispersity of 1.034 was achieved for this particular polymer.

Using EP required significant cost outside what could be provided for the project, so a Ppy synthesised through chemical oxidation was thus used and this led to the first ever studied GEBFC using compressed Ppy and enzymes electrodes. This was a major step forward and was a novel combination of this particular conductive polymer material, compression methodology and biofuel application. These electrodes were only 1.31 cm in diameter and 0.5 mm thick, making them good sizes for implantation. Additionally, 212.83 mV open circuit and 224.5 μA short circuit was achieved, which in particular for current was a significant step forward from both single and dual chamber MFCs.

In addition to the previously mentioned advantages of GEBFCs over MFCs, the GEBFCs were in fact providing more current for a smaller overall package. If through other methods we could not increase the voltage output, we could still connect several GEBFCs together and it would still be a smaller package than even one MFC. Additionally, it is easier to obtain a step up converter that works at lower voltages, but not one that operates at lower currents, thus eliminating MFCs. In deciding this, we begun to investigate what factors may be resulting in the lower power, especially when compared to the MWCNTs being using with the same compression method.

The experimental parameters included the material itself (which relates to conductivity, electrochemical behaviour and porosity), electrolyte, glucose concentration, amount of material used in each electrode, GOx and LAC mass, membrane use, compression force, use of water resistant glue for the wire connection and means of wire connection. Out of these, those that did not matter included the electrolyte (this was the same), glucose concentration and GOx and LAC masses (we use more, but this should help us). The rest of these factors we tested and searched for literature to find any differences that might give us a hint of what may be wrong.

When testing compression force, we measured how much difference there was in height of the electrode with a calliper for 4 Tonnes and 8 Tonnes and found there was no difference. Using less force than these resulted in a more brittle electrode. When testing MWCNTs, we found that it was overall more brittle regardless of how much force was used and once placed in the electrolyte, did occasionally fall apart.

We also found that when adding in the membrane, this helps to keep the MWCNTs together, as well as keep the enzymes in proximity to the conductive material, which also leached out especially quickly, perhaps due to MWCNTs being especially porous. The membrane acted as a form of mechanical strengthening and EI. Given these findings and that with Ppy we also had enzyme leaching, it seemed appropriate to devise a solution to this problem of enzyme leaching. Lastly, looking into the material properties, the electrodes were porous and that the electrochemical behaviour would not influence the power output heavily, however there was substantive differences in the conductivity, leading us to also work on this. In short, the author was able to determine that EI and conductivity were the key issues through a carefully achieved elimination process.

Between EI and IC, the bigger improvement came with the increasing of the conductivity of the electrodes. A distinct goal was to maintain the simplicity of the compression method (for manufacturing purposes) but also increase the conductivity. We thus decided to mix more conductive materials, silver and RVC with the Ppy and compress them together. With this, high voltages of between 400 and 450 mV, power increases 5 times to approximately 100 μW or more and current flows of over 1 mA were achieved from both the RVC and silver electrodes. These improved electrical output characteristics were a significant improvement on previous results for the project, and the first use of Ppy composites with the compression method for GEBFCs.

Our approach to EI involving the use of Glut as a crosslinker also obtained good and immediate results. Over the same two hour period as the non-immobilised Ppy electrodes, the voltage increases to over 200 mV rather than decreased to less than half this for the non-immobilised enzyme electrodes. There was also an improvement in current, giving approximately 2 times more as well as an improvement in the power, measuring approximately 5 times more than the original GEBFC. The more important achievement though was that enzyme leaching was not occurring and no membrane was used as with other studies. This is an important consideration in toxicology studies for implantation. The use of Glut is a potential issue, however once react, the highly reactive nature of Glut is no longer an issue, and excess Glut can and was washed away.

These EI results were then further improved on when combined with IC, where in the case of the Ppy-RVC electrodes, we were able to achieve over 500 mV. This increase however was not seen in the current and power, where approximately half the current of non-immobilised version was measured. Unusually however, the Ppy-Silver immobilised enzyme electrodes gave significantly more current than the non-immobilised version, giving a maximum of 1.469 mA and an improvement in power to 128.2 μW. This was an impressive result and again points to the good and novel application of conductive polymers, compression methodology and GEBFCs.

An important discovery regarding the compression method with Ppy is that it leads to the electrodes becoming especially dense and less porous as seen in the SEM images. This may explain why in the plain Ppy and Ppy-RVC electrodes, where immobilization is used and less current is measured, enzymes are mostly attached on the surface of the electrode. This is compared with the non-immobilised versions where more enzymes can be embedded throughout the electrode. This also explains why the Ppy-silver electrodes were able to provide more current and power through the two-fold effect. If the electrode is more porous,

enzymes can be immobilised not just superficially, but internally and there is easier access to those enzymes for the glucose and for gluconolactone to escape. These findings will be especially useful for further studies.

With this in mind, the challenge of immobilizing enzymes throughout the electrodes by immobilizing the enzymes on Ppy prior to or during compression was accepted. The biggest obstacle in this entire project was that Ppy is near impossible to dissolve, making any chemical method very difficult. Meta-cresol was the only solvent which gave a dispersion of Ppy that occasionally was workable. The first method attempted was to use a step by step process to crosslink Glut to Ppy and then the resultant molecules to enzymes, all in solution. Due to the indissolvability of Ppy, and perhaps its static interactions, whichever solvent was used would create clumps of Ppy which made this method inefficient, unusable and also ruled out dispersion chemistry since even with significant mixing and ultrasonification, the clumps could not be broken up. Meta-cresol was also not a suitable solvent for biological molecules such as enzymes. Additionally, without knowledge of the chain lengths for the Ppy, it was difficult to know how much Glut to use, therefore requiring us to use Glut always ‘in excess’.

The second method attempted involved using meta-cresol to create a dispersion, which was then deposited as a film on a Petrie dish and dried off on a hotplate in a hood. Glut was then deposited, washed and then a solution of enzymes deposited. Unfortunately with how sticky all three solutions and layers became, the method was time intensive and had a low yield. A alteration to this method involved additionally dissolving SDS in m-cresol, however when this was deposited and the m-cresol dried off, the SDS and Ppy could be washed away together since the SDS was heavier and settled at the bottom of the dish.

The last method attempted, involved a layer by layer approach, whereby the Ppy, RVC or silver and enzymes were mixed, then portions were added layer by layer. Between each

portion, Glut was added for crosslinking within and between each layer. The compression method however creates a high pressure and with Glut being in a 70% solution form, would leak out during the compression process, taking Ppy and enzymes with it.

Despite these challenges, with the Ppy-RVC non-immobilised enzyme electrodes, the significant achievement of powering a medical thermometer through an energy harvesting circuit was obtained, thus showing the high potential of compressed Ppy electrode GEBFCs. Given the Ppy-silver immobilised enzyme electrodes had greater power output, they would also be able to power the thermometer and may also provide more stability given the enzymes are immobilised. This was a significant step forward from the previous GEBFC and MFC results, which when attempts were made to use an energy harvester, failed. Additionally, as has been said, this was the first study of the combination of both Ppy and the compression method for GEBFCs, which is especially notable.

6.2. FUTURE DIRECTION

Whilst we may have increased our understanding of how an AIMD might be powered by either of the biological fuel cells, and indeed have actually been able to power an AIMD, there as always in research is still work to be done to answer further questions as a result of this work. This work concluded that GEBFCs had greater potential for powering AIMDs, however if particular breakthroughs were to occur with regard to microbiology and MFC research, MFCs could become a competitive option. Issues such as microbial population density, biocompatibility and electron transfer efficiency for bacteria are in theory controlled by the genetics of the bacteria. Genomics is allowing bacteria to do a vast array of different things, so perhaps one day it may be possible. If these were possible, then many of the design issues of the reactor could also be addressed.

This project was able to power a thermometer from the synthesised electrodes with an energy harvester much like those electrodes from Cinquin et al, however their electrodes were still generating significantly higher electrical output such that if two or three electrode sets were stacked, it would be possible to power the thermometer without an energy harvester at all. As was discussed in the previous section, there are several factors which may influence this, and the one that was not fully addressed was the connection of the wire to the electrode. This was found to be a major factor in the MFCs experiments, where if the wire was connected with silver conductive water resistant epoxy, the electricity output of the MFC was higher and more consistent. The difference however with the GEBFCs was that the enzymes degrade at the temperatures needed for the conductive epoxy to set properly. The immobilization of enzymes could have been a way around this since it was possible to perform the enzyme step after the heating process. However due to the plain Ppy and Ppy-RVC immobilised enzyme electrodes initially not providing as much current, this was not prioritised. Given that the Ppy-silver electrodes with immobilised enzyme did perform well, this possibility is something that should be explored.

Practicality was a major influence on the decision to use the commercial Ppy. If a conductive polymer were to be developed, characteristics such as higher conductivity and greater functionality and dissolvability could be worked on. Glut was a useful crosslinker for being able to keep the enzymes in close proximity to the Ppy. However, if it is possible to use a crosslinker that is even shorter on length, which is more conductive, or functionality is such that the enzyme can be more directly attached to the conductive material, this may provide further increases in power. Working directly on the conductive material could allow us the knowledge of knowing the chain lengths or concentrations of the molecules, which if combined with dissolvability, would allow us greater ease to work with it.

Crosslinking by itself is also a significant and considerable issue. Consider that enzymes are curly like structures composed of various amino acids, and factors such as pH and temperature may unravel and degrade them such that they lose their function. Multipoint immobilization crosslinks the enzyme on multiple points on the enzyme structure, giving the enzyme further rigidity and preventing it from unravelling. Further to this, because it is one particular part of the enzyme that interacts with the GOx or LAC, orientating the enzyme may also increase the chances of both interaction and increase reactivity. UV based immobilization techniques, which only create bonds on certain parts of the enzyme, may provide a way forward on this matter. If these methods and other conductive material factors allowed for better EI throughout the electrode rather than superficially, it could also help significantly. Layer by layer approaches may help with this with alterations to equipment, however other methods may exist which could provide better outcomes.

Whilst GEBFCs do not contain the same biocompatibility issues of MFCs with regard to bacteria, biocompatibility remains an issue for the materials and device design overall. Ppy is able to be functionalised, and one idea that has been proposed was to look at coating the surface of the electrode with glycopolymers which are sugar like molecules which could fool the body into not rejecting the electrode. Likewise, taking from ECG electrodes, the shape of the electrodes may need to be changed or equally other materials could be used as long as certain properties remain. Additionally, current methods for making medical devices biocompatible will destroy enzymes and new methods or stronger enzymes may need to be created.

A significant issue which has not been addressed thus far is fouling of the GEBFC electrodes. As the anode electrode in particular with GOx, reacts with glucose, gluconolactone is the by-product. With porosity as it is in these current electrodes, along with the way that gluconolactone did not seem to dissolve in PBS, it would build up on the electrodes. Our

experiments were not performed over a long enough time span, however it is expected that this would contribute to poor power output in the long term. This situation may be different when placed in the body, since gluconolactone may already be present and dissolved. Nonetheless, some possible solutions include, (1) make the pores larger to allow the gluconolactone a better ability to escape, (2) avoid pores altogether, since the objective is a large surface, as long as the surface area is sufficient, pores are not strictly necessary, (3) use a different enzyme which will result in a different by-product, (4) place the electrodes in a part of the body where greater flow occurs, allowing for by-products to be more easily washed away or (5) increase enzyme reaction efficiency and lower the amount of enzyme needed to less the amount of gluconolactone generated.

If biofouling, multipoint EI and biocompatibility were to be addressed, it follows that stability testing and toxicity tests, animal work and other biocompatibility tests should also be performed. This was not an express objective of this study, however it was kept in mind and was a frequent discussion point with the various stakeholders of the project. Additionally, the need for lower concentrations of D-glucose would be informative. The tricky part here is that with enzymes can react especially fast with the glucose such that it may not have been possible to collect the data over the time periods used. There are easily ways to get around this however with the right equipment. Along with this, further optimisations of the enzyme masses based on their relative reactivity may be appropriate. Indeed, if a scaffold like setup were used, it may even be possible to use the exact amount calculated.

CHAPTER 7
APPENDIX

Appendix

BASIC SCIENTIFIC METHODS

PREPARING GROWTH MEDIA

Tryptic Soy Broth, Luria Bertani Broth and Tryptic Soy Agar are received in dehydrated powder form. To prepare these culturing media at standard concentration, the following procedures are undertaken:

1. Weigh out the desired media at the respective concentration:
    - TSB: 30 g / 1 litre H_2O
    - TSA: 40 g / 1 litre H_2O
    - LBB: 25 g / 1 litre H_2O
2. Add to a Schott bottle, then add 18.2Ω milliQ DI to the desired concentration as per above.
3. Shake well.
4. Autoclave at 121°C for 15 minutes.
5. Store at room temperature with lid sealed and autoclave tape on or use as is.

PREPARATION OF TRYPIC SOY AGAR PLATES

To prepare TSA plates, the following procedures are undertaken:

1. Prepare a sterile workspace by either of the following:
    a. Wipe down a lab bench with ethanol and setup a Bunsen burner to blue flame.
    b. Wipe down a Class I (or above) laminar flow hood with ethanol and turn on air flow.
2. Layout Petrie dishes with lids down and dish facing upwards.
3. Ensure TSA is warm to hot – usually it is taken fresh from the autoclave, however it can be reheated via the microwave. Ensure it is well stirred to give uniform consistency.
4. Pour hot TSA into a dish to about half way or approximately 30 mL. Pour quickly and ensure it does not cool down and firm and that the consistency remains uniform.
5. If there are air bubbles, use a Bunsen burner to pop them.
6. Repeat as per the number of plates.

7. Allow to cool in sterile environment before replacing the lid to avoid moisture build up.
8. Store, upside down in a 4°C refrigerator.

PROPAGATION OF ATCC RECEIVED SHEWANELLA ONEIDENSIS MR-1

Shewanella oneidensis MR-1 was received from the ATCC in powder form and propagated as per the instructions reoutlined below (ATCC 2014):

1. Prepare an Erlenmeyer tube with 5.0 to 6.0 mL of Trypic Soy Broth.
2. Under sterile conditions, open the supplied vile with pellet and add 0.5 mL to 1.0 mL of Tryptic Soy Broth to rehydrate the pellet.
3. Once rehydrated, transfer to the Erlenmeyer tube and mix well.
4. Incubate tube for 24 hours at 30°C.

PREPARATION OF MICROBE GLYCEROL LABORATORY STOCKS

The following was performed to prepare the laboratory -80°C stock:

1. Add 250 µL of glycerol and 250 µL of milliQ water to a cryotube to create a 50% glycerol solution.
2. Add 500 µL of the overnight culture of *Shewanella oneidensis MR-1*.
3. Mix well with a benchtop shaker and label.
4. Freeze down to -80°C.

CYCLIC VOLTAMMETRY

An exact method for the how cyclic voltammetry (CV) experiments are conducted is given in section 4.4.3 Electrode Preparation and Characterization on page 133. The method is a common and powerful electrochemical tool used to elucidate reduction and oxidation (electron transfer) processes of materials. There are several components and parameters involved in the setup of a CV experiment. Experiments are usually run within an electrochemical cell like that shown in Figure 103, which is a glass vessel with cap, electrolyte solution and three electrodes including working, counter and reference electrodes.

Electrons flow between the working and counter electrodes, however the reference electrode is used to measure more accurately and control the applied voltage (Elgrishi et al. 2017).

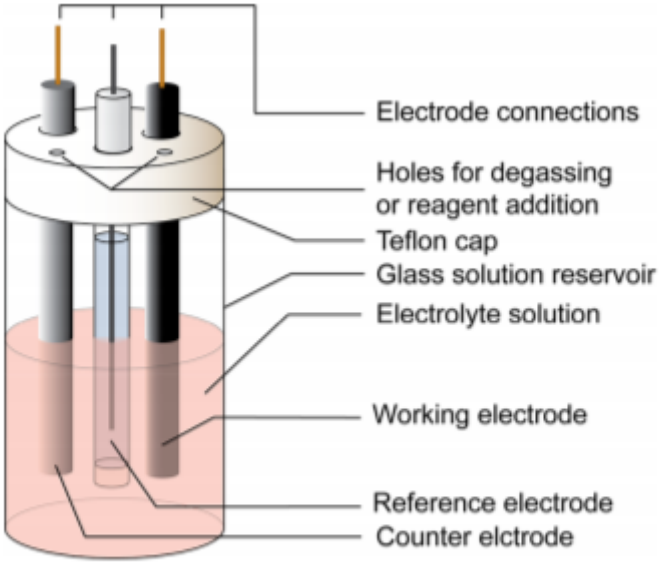

Figure 4. Schematic representation of an electrochemical cell for CV experiments.

Figure 103 Figure 4 from Elgrishi et al regarding a 'schematic representation of an electrochemical cell for CV experiments' (Elgrishi et al. 2017).

The electrolyte solution helps to maintain electrical neutrality by allowing for the migration of ions between electrodes in solution. It is usually a salt dissolved in a solvent and where necessary, the chemical under test. Other characteristics of the solvent include being liquid at experiment temperatures, within a potential range, it is stable for oxidation and reduction, no deleterious reactions occur and it is able to be purified. Regarding the electrolyte, it needs to be highly soluble in the solution, chemically and electrochemically stable within the conditions of the experiment and is able to be purified. Usually to minimise resistance in the electrolyte solution and to limit the migration of the material under test, large amounts of electrolyte are needed. The electrolyte solution is often sparged with nitrogen gas to alleviate any oxygen in solution which may interfere with the reactions (Elgrishi et al. 2017).

The working electrode is where the primary electrochemical event of interest takes place. A potentiostat is used to control the application of a voltage to this electrode in reference to the reference electrode. The electrode understandably needs to be redox active under the proposed experimental conditions and can be changed to suit the desired potential window (Elgrishi et al. 2017).

The reference electrode is a well-studied reaction producing a specific voltage. As such, these are often pre-made, off the shelf purchased electrodes of either saturated calomel electrode (SCE), standard hydrogen electrode (SHE) or AgCl/Ag electrode which have the electrode material sitting in a glass vessel with electrolyte and a porous glass frit separating these from the rest of the electrolyte solution. When showing CV data, it is common to quote the type of electrode used as it is easy to convert between them (Elgrishi et al. 2017).

When a voltage is applied to the working electrode, it is between the working and the counter electrode. Electrons will flow from the counter to the working and as such, the counter should be larger than the working so as not to inhibit the reaction at the working electrode (Elgrishi et al. 2017).

Once all the parts of the electrochemical cell are set up, the potentiostat must be setup with the relevant parameters. Once upon a time, these were circuits with power supplies, however modern potentiostats are large benchtop devices connected to PCs and capable of running several other electrochemical experiments. For CVs, parameters such as starting voltage, end voltage, scan rate, scan segments and current range are standard and may be presented in other terms depending on the manufacturer. Once the experiment is done, the software will usually display the data which can be exported to a spreadsheet (Elgrishi et al. 2017).

Figure 104 shows the typical voltage signal applied to the working electrode, where the scan rate is the gradient of the ramp. More than one cycle is not necessary, however for data

collection may be useful. Figure 105 shows a typical CV curve for a simple one electron transfer, reversible reaction. Between points A and F is where the reduction process occurs where the final potential at F is the end voltage, the scan is negative to give the reduction result and the cathodic current, designated as I_{pc}. Point D is the cathodic peak potential E_{pc} where all the substrate at the surface is reduced. From point F to point F, the scan is positive and results in the anodic current I_{pa}. E_{pa} at point J is the anodic peak potential and is the point at which the substrate has been completely oxidised at the surface of the electrode (Kissinger & Heineman 1983). A further complication to this is pseudocapacitance, which is when a capacitive effect occurs between different surfaces such as the electrolyte and electrode, causing a box shape in the data, masking the peaks (Bard & Faulkner 2000).

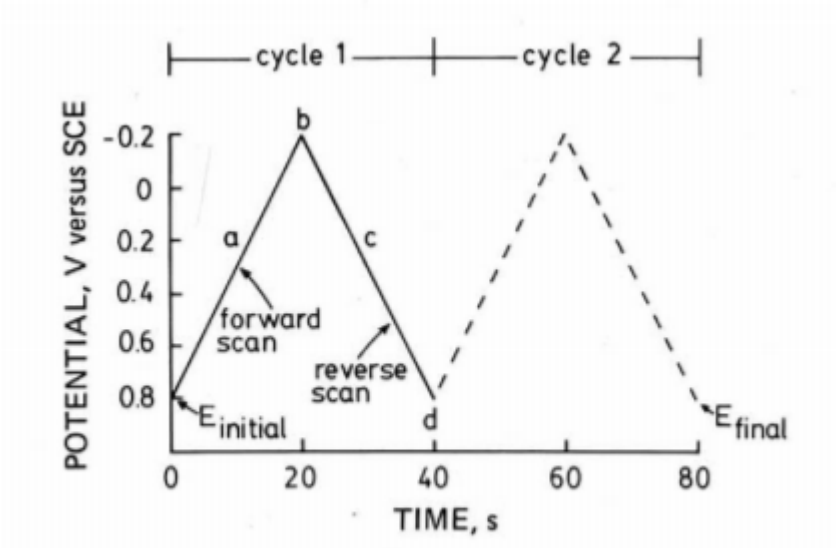

Figure 1. Typical excitation signal for cyclic voltammetry—a triangular potential waveform with switching potentials at 0.8 and −0.2 V versus SCE.

Figure 104 Figure 1 from Kissinger Heineman – 'Typical excitation signal for cyclic voltammetry—a triangular potential waveform with switching potentials at 0.8 and —0.2 V versus SCE' (Kissinger & Heineman 1983)

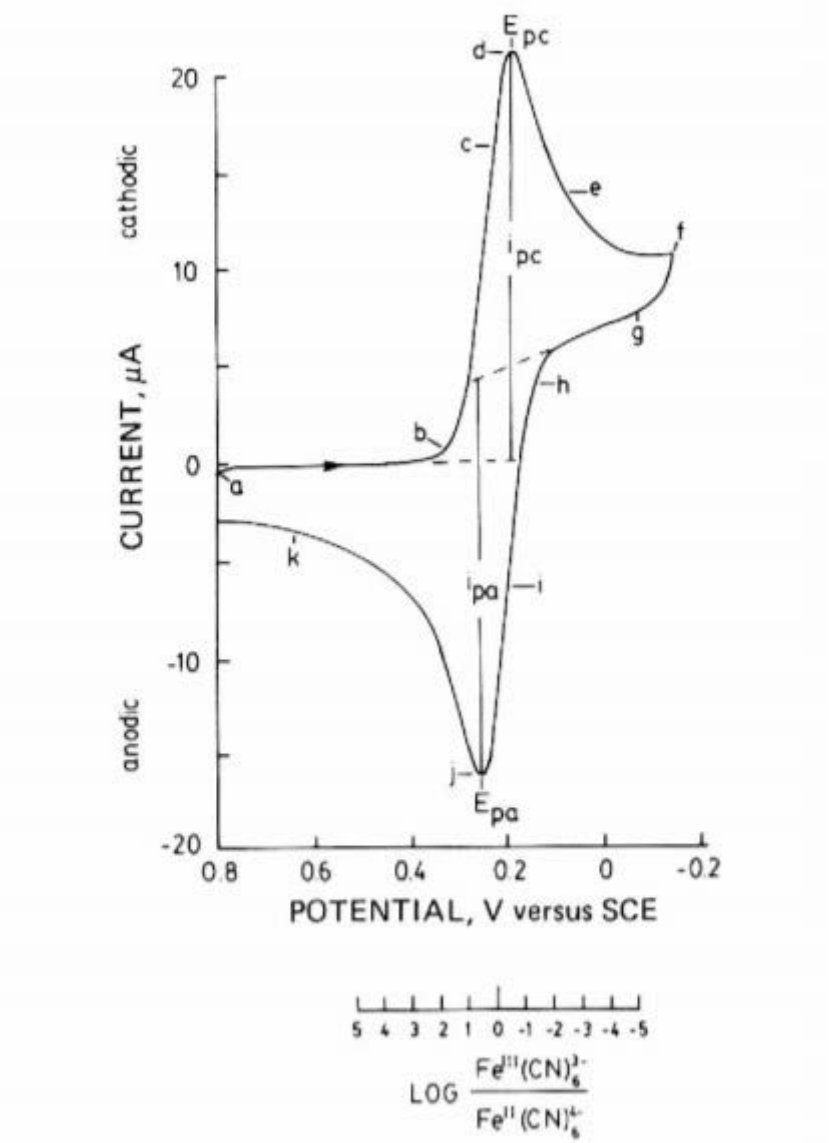

Figure 2. Cyclic voltammogram of 6 m*M* $K_3Fe(CN)_6$ in 1 *M* KNO_3. Scan initiated at 0.8 V versus SCE in negative direction at 50 mV/s. Platinum electrode, area = 2.54 mm^2.

Figure 105 Figure 2 from Kissinger and Heineman – 'Cyclic voltammogram of 6 mM $K_3Fe(CN)_6$ in 1 M KNO_3. Scan initiated at 0.8 V versus SCE in negative direction at 50 mV/s. Platinum electrode, area = 2.54 mm^2' (Kissinger & Heineman 1983).

STREAK PLATING

OBJECTIVE:

Need to have isolate colonies of the bacteria to be streak so that when the preparing a liquid culture of bacteria, the original bacteria are genetically similar.

GENERAL IDEA:

We take a small amount of bacteria from a glycerol stock of bacteria and essentially spread it along a TSA plate like butter. The spreading is important, since as you spread, the amount of bacteria left as you move along slowly goes down, such that at the end of the spread, you are left with what will grow into a single colony, rather than several colonies bunched together.

EQUIPMENT:

- Lab bench
- Bunsen burner with gas and lighter
- Streaking loop or sterile wooden sticks
- TSA plate
- Ethanol and wipes for cleaning
- Gloves
- Glycerol bacterial stock from -80°C
- 30°C incubator

METHOD:

1. Allow glycerol bacterial stock to thaw a little – ideally we do not want to leave this for too long.
2. Clean the bench with ethanol and allow to dry.
3. Turn on Bunsen burner flame to blue flame. Try to do all the below within 30 cm of the blue flame. The blue flame will create a sphere in which anything in the air floating in will likely burn from the heat, thus prevent any contamination and maintaining a sterile work space.
4. If using streaking loop, with one hand, burn the loop section with the blue flame. The loop should glow a bright orange / yellow / red showing it went extremely hot. This ensures all possible bacteria are no longer there.
5. Near the flame, with the other hand, open the thawed glycerol stock and dip the stick or loop into the mixture. Just the very tip is fine as you do not need much. Ensure the loop is not too hot still so as not to burn the bacteria. Close the glycerol stock.
6. Carefully streak the TSA plate as per Figure 106, ensuring the lid is kept upside down whilst doing this and then covering the plate and placing upside down again.

7. Label plate and place in incubator for 18 to 20 hours. Clean up with ethanol etc. Do not seal the plate with parafilm etc as air is required for microbial growth.

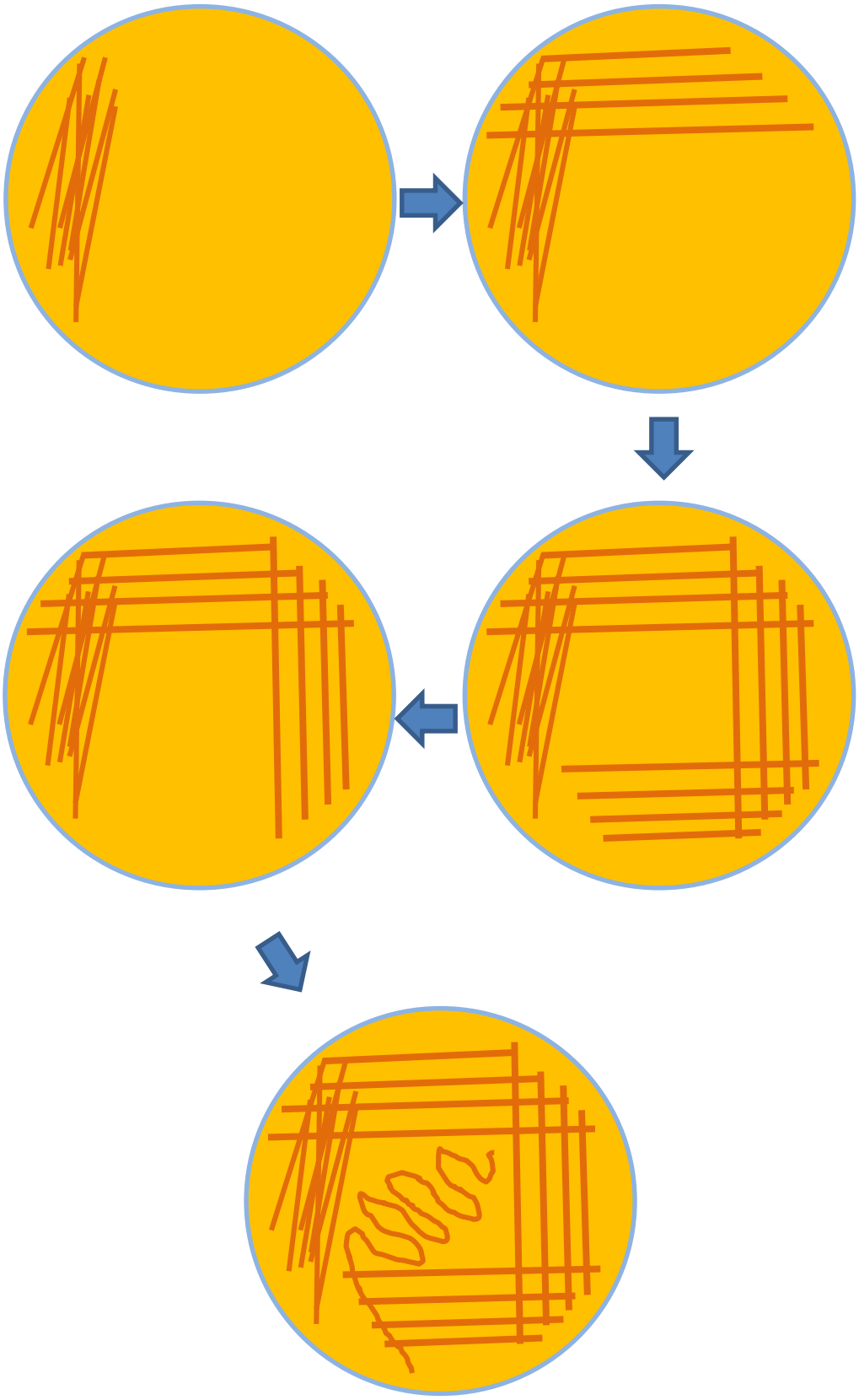

Figure 106 Illustration of how to streak a TSA plate with bacteria

DROP PLATING

OBJECTIVE:

We need to quantify the amounts of bacteria we are actually placing into the MFC during inoculation as well as relate the optical/ocular density to an actual amount of cells. This method will outline the drop plating method, and the optical density part will be added later.

GENERAL IDEA:

Taking an overnight grown culture, we dilute it out 10 fold in serial dilution with 8 steps on a 96 well plate with triplicate. We then use two Tryptic soy agar plates and drop small amounts onto the plate itself. The plates are incubated and we count the dots. Each dot, depending on dilution, will have come from a CFU (Colony Formation Unit). The amounts of CFU can be multiplied by the dilution, then by the mL amount and we then have an amount of cells contained within the overnight culture.

EQUIPMENT:

- Pipette (Multichannel is better, but single channel is okay)
- 20 µL – 200 µL pipette tips
- 100 mL Phosphate Buffer Saline
- 2 x Tryptic Soy Agar Plates
- 80% Ethanol and paper towel for cleaning
- 96-Well Plate
- 2 mL Overnight Grown Culture (S. oneidensis MR-1) in Tryptic Soy Broth
- Gloves

METHOD:

1. Dry the Tryptic Soy Agar (TSA) plates in the hood for an hour or until there is no moisture left. The moisture may help the cells outgrow the plate. Close them when taking them from the hood to the bench. Make sure the hood is wiped clean with ethanol, and properly used as per training.

2. Ethanol bench. Wait till dry, and then turn on the Bunsen burner. Ensure the next few steps are near the flame, particularly the segments to do with bacteria.
3. Label TSA plates. See diagram below as a recommendation.
4. Label the 96-well plate.
5. Using the 96-well plate, place PBS 180uL each into appropriate wells, as per table below.
6. Get new tips, and place 20 µL of cells into the first set of wells.
7. Serially dilute downwards for all 8 rows, and the 3 triplicates. Mix at each well by pipetting in and out. Take 20 µL from top, and insert 20 µL into the next row, following through to the bottom. New tips for each new transfer.
8. Get new tips, starting from the bottom row, take 20µL from each well and simply 'drop' them on the agar plate as per diagram below. Be sure not to break the surface of the agar as this may help mix the single colonies.
9. Leave to dry for approximately 10 minutes, or until you can no longer see the droplets on the surface of the agar. Can use the hood to help dry, but be sure not to mix the cells.
10. Clean benches.
11. Close the lids, turn of the Bunsen burner and move the plates into the incubation chamber at 30 °C overnight – or appropriate temperature for bacteria.
12. Clean benches again.
13. Once incubated, count the amounts of dots (representing a CFU) and calculate.
    a. Multiply the amount of dots by the dilution factor, and then multiply by the mL amount. This will give you a number of CFU/mL.
    b. Example calculation:
        i. Counted on average between 2 dots at the 6^{th} dilution 22.5 dots
        ii. Calculation is:
            1. $22.5 \times 50 \times 10^6$
            2. $= 1125 \times 10^6$ CFU / mL
            3. $= 1.125 \times 10^9$ CFU / mL
        iii. The 50 is a conversion to mL =>
            1. 1000 µL / 20 µL = 50

2. The 10^6 is the amount of dilution

NOTES:

	1	2	3	4	5	6	7	8	9	10	11	12
A	Triplicate 1 1/10 Dilution 180uL PBS, 20uL cells	Empty	Triplicate 2 1/10 Dilution 180uL PBS, 20uL cells	Empty	Triplicate 3 1/10 Dilution 180uL PBS, 20uL cells	Empty						
B	Triplicate 1 1/100 Dilution 180uL PBS, 20uL cells		Triplicate 2 1/100 Dilution 180uL PBS, 20uL cells		Triplicate 3 1/100 Dilution 180uL PBS, 20uL cells							
C	Triplicate 1 1/1000 Dilution 180uL PBS, 20uL cells		Triplicate 2 1/1000 Dilution 180uL PBS, 20uL cells		Triplicate 3 1/1000 Dilution 180uL PBS, 20uL cells							
D	Triplicate 1 1/10000 Dilution 180uL PBS, 20uL cells		Triplicate 2 1/10000 Dilution 180uL PBS, 20uL cells		Triplicate 3 1/10000 Dilution 180uL PBS, 20uL cells							
E	Triplicate 1 1/100000 Dilution 180uL PBS, 20uL cells		Triplicate 2 1/100000 Dilution 180uL PBS, 20uL cells		Triplicate 3 1/100000 Dilution 180uL PBS, 20uL cells							
F	Triplicate 1 1/1000000 Dilution 180uL PBS, 20uL cells		Triplicate 2 1/1000000 Dilution 180uL PBS, 20uL cells		Triplicate 3 1/100000 Dilution 180uL PBS, 20uL cells							
G	Triplicate 1 1/10000000 Dilution 180uL PBS, 20uL cells		Triplicate 2 1/10000000 Dilution 180uL PBS, 20uL cells		Triplicate 3 1/10000000 Dilution 180uL PBS, 20uL cells							
H	Triplicate 1 1/100000000 Dilution 180uL PBS, 20uL cells		Triplicate 2 1/100000000 Dilution 180uL PBS, 20uL cells		Triplicate 3 1/100000000 Dilution 180uL PBS, 20uL cells							

Well plate layout useful for when setting up for CFU counting. Note that these are arranged such that if one is to use the multi-channel pipette, you can use channels 1, 3 and 5. This is perfectly spaced for the droplets onto the TSA plate.

RESISTANCES USED

MFC EXPERIMENTS

3.9 MΩ	510 kΩ	110 kΩ	60 kΩ	29.5 kΩ	8.9 kΩ	5 kΩ	900 Ω
1.3 MΩ	330 kΩ	100 kΩ	56 kΩ	27 kΩ	8.2 kΩ	3.9 kΩ	820 Ω
1.2 MΩ	270 kΩ	90 kΩ	49 kΩ	20 kΩ	7.7 kΩ	2.7 kΩ	510 Ω
990 kΩ	219 kΩ	82 kΩ	39 kΩ	15 kΩ	6.35 kΩ	1.35 kΩ	300 Ω
820 kΩ	165 kΩ	78 kΩ	33 kΩ	10 kΩ	5.1 kΩ	1 kΩ	270 Ω
660 kΩ							

Table 23 Resistances used in MFC experiments for polarisation and power curves. Note that they were used in decending order.

GEBFC EXPERIMENTS

3.9 MΩ	100 kΩ	15 kΩ	1 kΩ	80 Ω
1.2 MΩ	82 kΩ	10 kΩ	820 Ω	40 Ω
820 kΩ	56 kΩ	8.2 kΩ	510 Ω	20 Ω
510 kΩ	33 kΩ	5.1 kΩ	270 Ω	
270 kΩ	27 kΩ	2.7 kΩ	160 Ω	

Table 24 Resistances used in GEBFC experiments for polarisation and power curves. Note that they were used in decending order.

LABVIEW PROGRAMS FOR MONITORING FUEL CELLS

Screenshots of the LabView programs used for monitoring the fuel cells are shown as follows:

- Figure 107: LabView GUI of MFC Data Logger
- Figure 108: LabView Backend of the MFC Data Logger
- Figure 109: LabView GUI of the GEBFC Data Logger
- Figure 110: LabView Back End of the GEBFC Data Logger

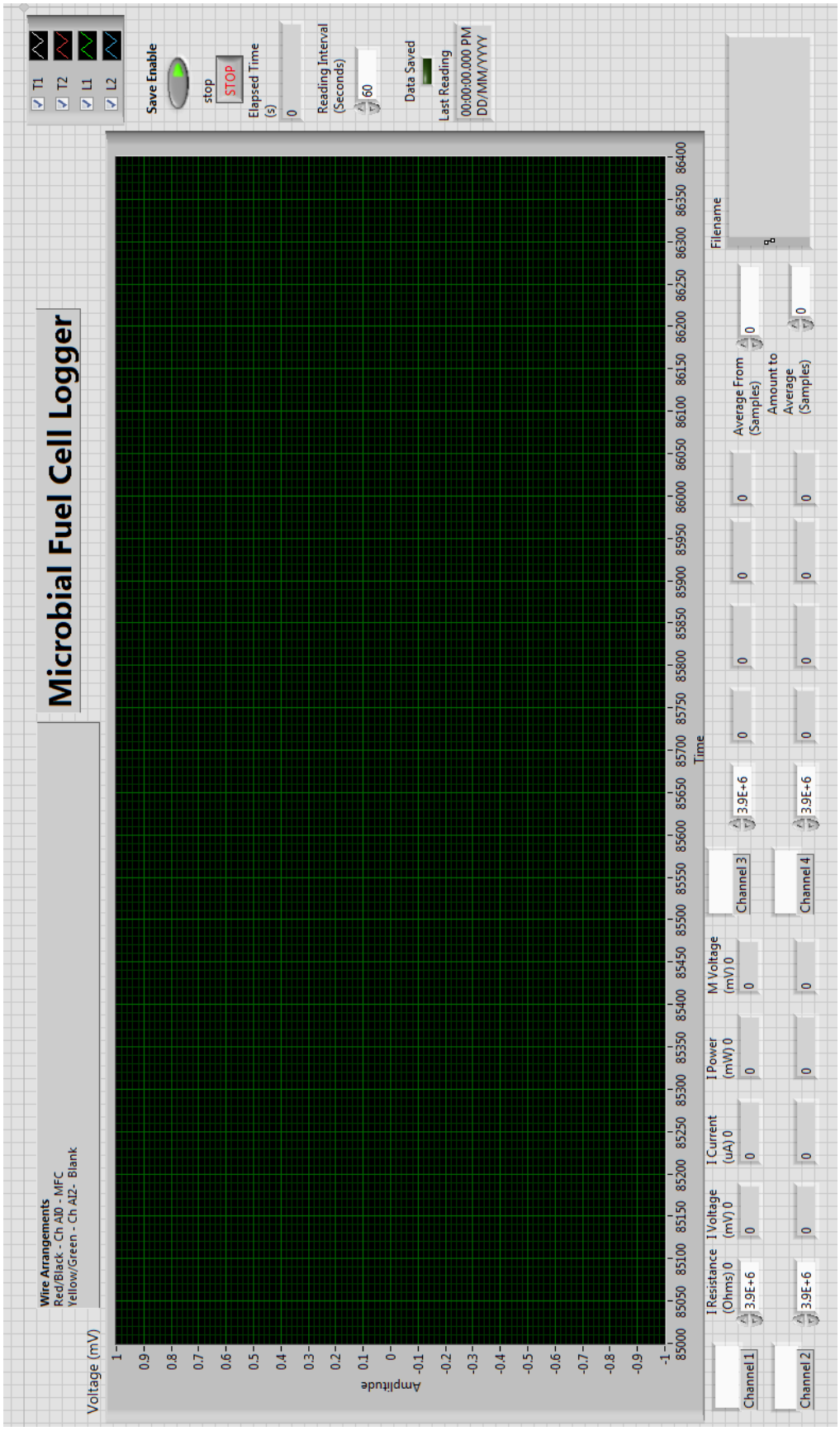

Figure 107: LabView GUI of MFC Data Logger

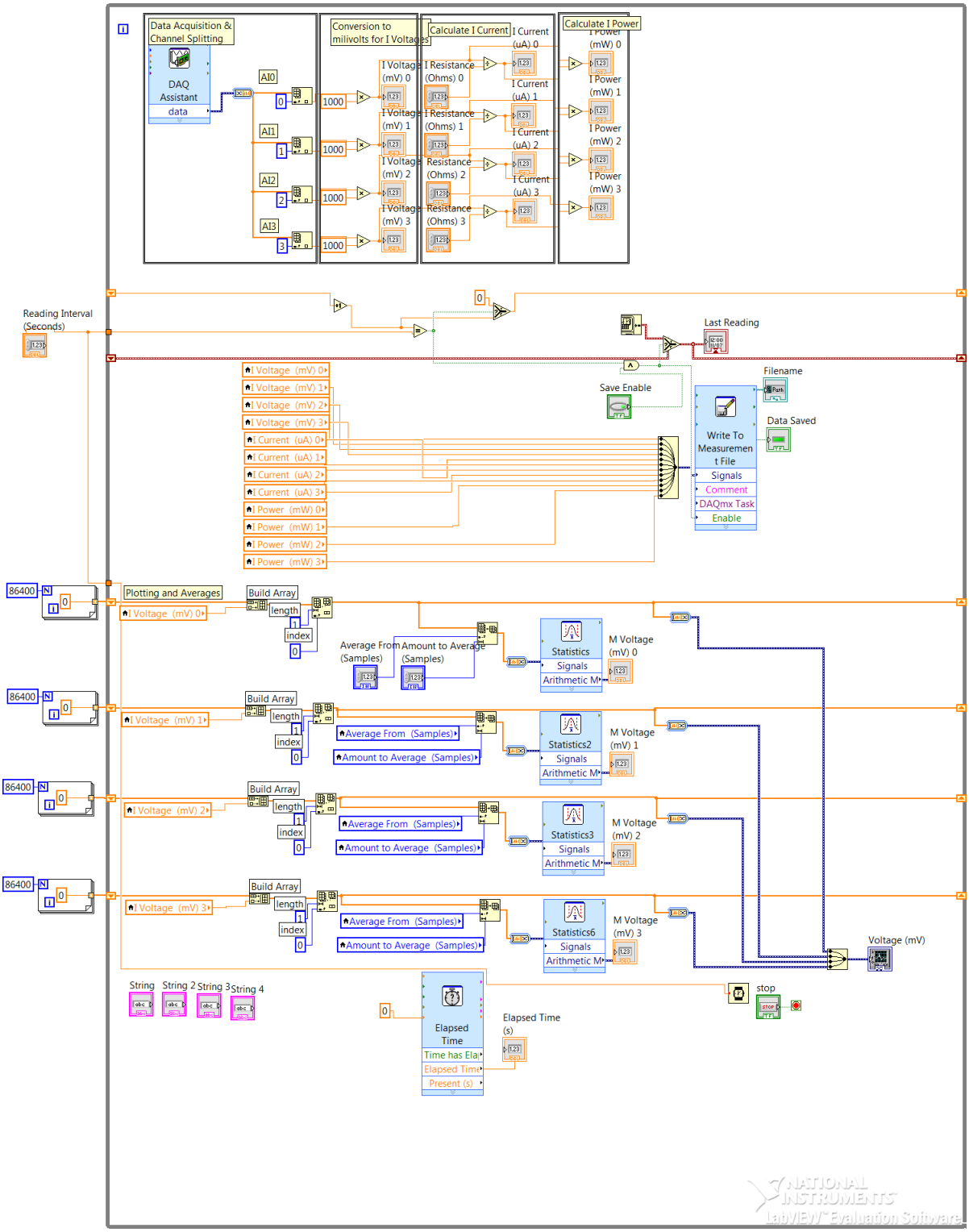

Figure 108: LabView Backend of the MFC Data Logger

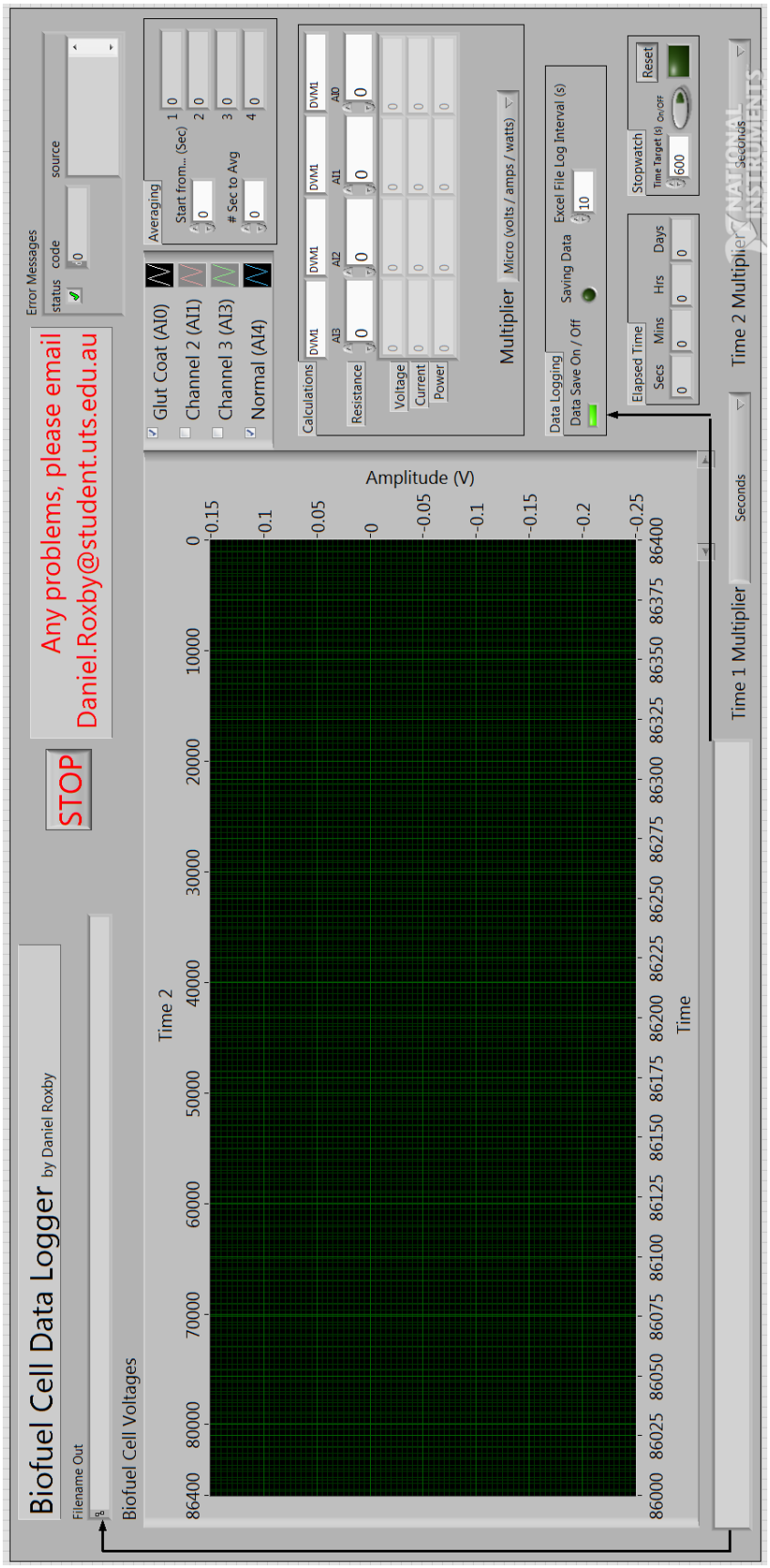

Figure 109: LabView GUI of the GEBFC Data Logger

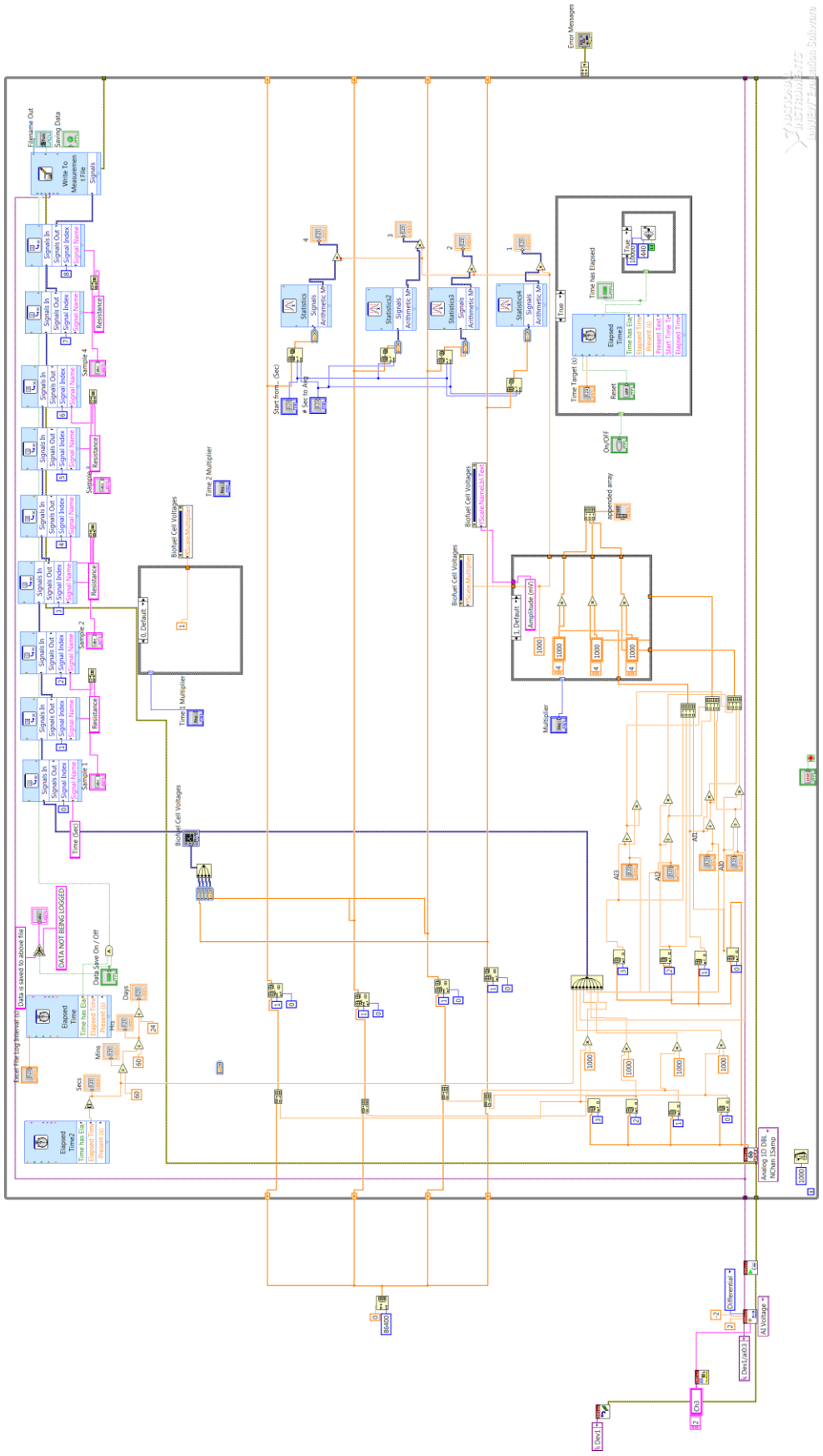

Figure 110: LabView Back End of the GEBFC Data Logger

ENZYME REACTION RATE CALCULATIONS

GLUCOSE OXIDASE

Conversion rate	= 100 000 units / gram
	= 100 000 micromole / min
Mass of enzyme added	= 100 mg
Total Units	= 10 000 micromole / min
Glucose Concentration Added	= 100 mM
	= 0.1 moles / L
Solution	= 50 mL
	= 0.05 L
Moles of Glucose	= 0.005 mol
	= 5000 μmol
Time taken	= 0.5 minutes

LACCASE

Parameters:

Conversion rate	= 500 units / gram
	= 500 micromole / min
Mass of enzyme added	= 100 mg
Total Units	= 50 micromole / min
Mol weight	= 16 grams / mol
Estimated Oxygen Concentration	= 2 mg/ L

Appendix

Solution	= 50 mL
	= 0.05 L
Mass of Oxygen	= 0.1 mg
Mole of Oxygen	= 0.00000625 mol
	= 6.25 μM
Time taken	= 0.125 minutes

HISTORY OF AIMDS

The most common AIMDs nowadays include the pacemaker, ICD, neuromodulators and cochlear implant and of course many newer devices continue to be developed today. Each of these devices has a long history leading up to what they are today. As can be seen in the histories below, pacemakers were the first to be developed, and with neuromodulators and cochlear implants being quite similar, they took inspiration from pacemakers and were concurrently developed.

PACEMAKERS

Summarised History of the Pacemaker	
1928	Australian anaesthesiologist Mark Lidwell used a needle inserted into a child's ventricle to inject alternating current, saving the child who been born into cardiac arrest. Whilst not much is known about the device, it was originally reported at the Third Congress of the Australian Medical Society in 1929
1932	Albert Hyman had also been working on the use of epinephrine to restart the heart and realised that the insertion of the needle as it punctured the cardiac wall seemed to actually be doing the trick. He eventually created a spring bound, hand cranked motor which he called an artificial pacemaker. At the time, the medical community and during WWII, the US Navy was not very receptive of the idea however.
1949	Wilfred Bigelow and John Callaghan, in 1949 conducted a similar experiment to Hyman, but on a dog, when he injected a needle on a stopped heart, only to find it restart and fully functioning. The Grass Manufacturing Co had also put together a stimulator for clinical and physiological lab applications during the 40s to 50s. Electrical engineer, John Hopps was perhaps the first person to build a purpose build cardiac pacemaker, achieving Atrial pacing with controlled heart rate comfortable.
1951	Paul Zoll famously builds a pacemaker after hearing of the work of Hopps, Bigelow and Callaghan. Its electrodes were placed on the skin over the heart and did prevent heart block despite it regularly shocking the patient. This was a tabletop device powered by mains electricity.
1957	On 30 January 1957, the surgeon Walton Lillehei successfully used the first semi-implantable pacemaker where myocardial wires were attached to a 3 year old girl's heart and used a Grass Manufacturing Co device as the stimulator. This had been developed since it was often children needing the technology but whom could not bear the electrical shocks of the Zoll device. The method became popular with several successful surgeries, however still ran off mains electricity supply. On 31 October of the same year, a baby who had been using of the devices tragically died due to power failure. Lillehei subsequently requested the help of Earl Bakken, the founder of the current largest biomedical engineering company in the world, Medtronic.

1958	Bakken develops first battery powered wearable pacemaker after reviewing a transistor metronome circuit from the April 1956 Popular Electronics magazine. After successful animal testing, he finds it already being used by Lillehei who said "The next day I returned to the hospital to work on another project when I happened to walk past a recovery room and spotted one of Lillehei's patients. I must have done a double take when I glanced through the door. The little girl was wearing the prototype I had delivered only the day before! I was stunned. I quickly tracked down Lillehei and asked him what was going on. In his typical calm, measured, no-nonsense fashion he explained that he'd been told by the lab the pacemaker worked and he didn't want to waste another minute without it. He said he wouldn't allow a child to die because we hadn't used the best technology available." October 8, cardiac surgeon Ake Senning and physician turned engineer Rune Elmqvist implant the first implantable pacemaker in Arne Larsson. They had originally developed the technology after noting the risk of infection from a wire running out through the skin. The device used a nickel-cadmium battery that was inductively recharged once a week for 12 hours and was encased in epoxy Araldite resin moulded from a shoe polish tin.
1958, 1959	Inductively charged cardiac pacemakers are used, allowing for survival rates of over 10 years.
1959	Elema-Ericsson lead was developed, allowing for at least 6 years of use.
1960	Electrical Engineer Wilson Greatbatch, Dr William Chardack and Dr Andrew Gage, known as the bow team, implant the first 'long term' pacemaker in a 77 year old patient, surviving two years without event before dying of natural causes. Later Greatbatch also developed the long-life lithium-iodine battery for the pacemaker.
Early 1960s	Implantation techniques improve and battery technologies change, allowing for long life as oppose to recharge. Emphasis was on improving therapy rather than just saving a life and electrotherapy became socially accepted and found uses in areas such as Parkinson's Disease, pain-control and drug delivery.
Mid 1960s	Implantation could occur without thoracotomy and without anaesthetic. "Demand" pacing was developed in which pacing is only provided when sensed to be necessary.
1970s	Batteries shifted to lithium-iodine batteries, improving the longevity of pacemakers. Titanium casing replaced the epoxy resins and silicone rubber previously used. Radio frequency telemetry links for programming the pacemaker to the changing clinical needs of the patient came into use. Dual chamber pacemakers developed.
1972	Radioisotope pacemaker implanted with an expected longevity of 20 years, however did not become widespread due to regulatory issues
1980s	Steroid eluting leads developed, helping to reduce inflammation. Mid 1980s saw the development of rate responsive pacemakers which used a sensor to detect patient activity.
1990s	Due to the use of microprocessors in pacemakers, several features became available including the detection and storage of events, changing the pacing needs to the patient automatically and an automatic adjustment of rate for patient activity level.
2000s	Biventricular pacing was introduced for heart failure, using an additional specially designed and implanted lead, leading to improved contraction, symptoms and survival. Data was also

	able to be uploaded wirelessly to the internet.

Table 25: Summarised History of Pacemakers – Adapted from Aquilina et al (Aquilina 2006)

DEEP BRAIN STIMULATORS AND OTHER NEUROMODULATORS

Summarised History of Deep Brain Stimulators	
1930s	Electrical stimulation is used at this time to explore different areas of the brain for ablative therapy, i.e. the destruction of parts of the brain that were thought to be malfunctioning.
1947	Apparatus built for the express purpose of exploring areas of the brain for ablative therapy
1950s and early 1960s	As electrical stimulation for ablative therapy becomes popular, to the point where it is considered one of the only means to treat certain disorders, a body of knowledge is built on the effects of stimulating different areas of the brain. In some cases, electrodes are left on the brain, sticking out of the scalp for weeks to identify the best ways to treat patients. Parkinson's Disease is one of the areas documented at this time.
1967	Neurosurgeon, Dr Norman Shealy, first adapts the pacemaker for use with chronic pain, using high frequency to modulate the perception of pain.
1968	Levodopa is developed and introduced to treat PD. Medtronic produces the first neurostimulator device.
1972	Avery Laboratories and Cordis, both pacemaker manufactures, produce neurostimulators following Medtronic.
1973	Hosobuchi produces results further indicating the effectiveness of deep brain stimulation as a means to treat pain, having seen that some of his patients had not responded to ablative therapies.
1970s	With the introduction of levodopa, along with a campaign against frontal lobotomy and ablative therapy, electrical stimulation and associated neurosurgeries effectively disappears. Neurostimulators had disseminated throughout the US and Europe through specialist centres who were using them for treatment of various motor disorders, cerebral palsy, epilepsy, schizophrenia and severe depression. Issues arose however such as lead and battery failure.
1980s	With developments in pacemakers taking place at the same time for leads and lithium battery technology, deep brain stimulators also benefited. More substantive clinical trials take place and the FDA begins to regulate neurostimulators.
1990s	After various clinical trials, other developments in Parkinson's Disease research and failed clinical trials of the use of DBS for pain, Medtronic team up with the Movement Disorder Society, to run clinical trials on neurostimulator use for tremor treatment as a result of Parkinson's. The Movement Disorder Society's Unified Parkinson's Disease Rating Scale is considered to be a major part of this move in defining the severity of PD.
1997	After being able to demonstrate the efficacy of DBS technology for tremor treatment resulting from Parkinson's disease, the FDA gives approval of the first implantable DBS, the Medtronic 3382 lead with ITREL stimulation system. There was still some concerns for

	safety and approval was only for severe tremor.
1998	Medtronic device is given regulatory approval in Europe.
2002	After successive sponsorship of clinical trials by Medtronic, the FDA gives approval of the Medtronic DBS for more general tremor treatment.
2003	Work continues to be performed, finding other areas of treatment for DBS technology. All the while, Medtronic receives approval for its use in treating dystonia, another movement disorder.
2000s to Present	Numerous clinical trials and companies for use of DBS to treat other conditions arise.

Table 26: Summarised History of Neuromodulators for DBS (Gardner 2013)

SPINAL CORD STIMULATORS

History of Spinal Cord Stimulators	
1965	Melzack and Wall publish research on gate theory, proposing that there existed a gate in the perception of pain that could be turned on or off with the activation of large or small neural fibres.
1967	Electrodes designed for cancer related pain by Shealy and Mortimer consisting of platinum plates placed in the spinal subarachnoid. System required external power supply provided through needles. Systems at this time were modified versions of pacemakers.
1968	Medtronic releases its first SCS for commercial use using radiofrequency and dorsal-column stimulators.
1970-1980	SCS architecture involving epidural placement with percutaneous leads is developed
1981	Medtronic releases the first rechargeable and fully implantable SCS system.
2000s	Multicontact leads and implantation of multilead array development augments the maximizing of paraesthesia coverage and the capture of dermatomal pain distributions.
2004	Boston Scientific releases a fully implantable, rechargeable SCS system.
2013	St Jude Medical releases Epiducer leads and Medtronic the S-Series paddle leads, enabling percutaneous placement of narrow paddle leads.
Present	Use of high frequency stimulation, eliminating paraesthesia feeling. Use of accelerometers have been used by Medtronic to detect patient position.

Table 27: History of Spinal Cord Stimulators (Gildenberg 2006; Thomson 2016)

COCHLEAR IMPLANTS

History of Cochlear Implants		
1800s	Common	Alessandro Volta, inventor of the battery, connects metal probes to the canals of his ears, switching on current, reporting that he felt a 'jolt to the head' and then sound of 'a kind of crackling, jerking or bubbling as if some dough or thick material was boiling'.
1855	Common	After stimulating his cochlea with alternating current rather than direct current, Duchenne de Boulogne hears sensations of buzzing, hissing and ringing.
1930	Common	Electrical potentials of the cochlear first recorded by Wever and Bray
1957	Common	First direct stimulation of the human auditory system is performed by André Djourno and Charles Eyriès. The patient could discriminate between some intensities, but not frequencies or between words. The device failed as did another patient's, leading to the project discontinued.
1961	Common	Having heard of the work of André Djourno and Charles Eyriès, Dr William House and Dr John Doyle continued the work and implant patients with direct current stimulation devices in LA. During this process, surgical techniques were further developed, and the patients were able to distinguish some basic frequency information and some words. Issues though arose with biocompatibility.
1966	Common	Simmons and his colleagues implant single wire electrodes into the auditory nerve, gathering fundamental results, including regarding perceived pitch and the use of wide band signals to single electrodes or single frequencies to different electrodes.
1970s	Common	Teams at the University of California, San Francisco including Robin Michelson and Michael Merzenich begin to implant single-electrode implants similar to those developed by House. They found limits regarding time-locked neural responses, leading them to focus on multi-electrode systems. By this time, several other researchers were beginning work, which would eventually lead to the numerous cochlear implant companies around today.
1973	Common	House, having been inspired by recent developments with pacemakers and ventriculoperitoneal shunts, enlists the help of Jack Urban, to create the first cochlear implant device able to be used outside the laboratory after collaboration with the 3M company.
1971	Cochlear	Graham Clarke at the University of Melbourne begins investigating the use of rate of electrical stimulation to code speech and other sounds, finding its limitations. His team's results suggested the cochlear location was most important.

1971	Sonova	Work leading to what is now known as Sonova, first began at University of California, San Francisco with Robin Michelson and Michael Merzenich. In 1971, Michelson presented her work on an implanted single-channel device in which the patient showed auditory sensations from stimulation but no word recognition. It was not well received at the time.
1973	Otticon	Henri Chouard and Mac Leod in collaboration with the Bertin Company, begin work on the French cochlear implant at INSERM. This was the first extra-cochlear single channel device called the Monomac.
1973	Cochlear	Clarke partners with electrical engineer David Dewhurst to develop the first 'Bionic Ear' prototype. Based on his observations curling grass and twigs up turban shells, he develops electrodes with graded stiffness for his surgical approach with a 20 electrode system.
1973	Sonova	Merzenich publishes work of the response of single units in response to sound stimulation from one ear and electrical stimulation from the other ear of unilaterally implanted cats in the cat's inferior colliculus.
1975	MED-EL	Work is begun by Kurt Burian and Ervin Hockmair, planning for a cochlear implant device based on the work of House previously. Their work involved features such as 8 Teflon insulated platinum-iridium wires moulded into a silicone carrier case, biocompatibility via gold/nickel paths along a glass substrate, multiple stimulation sights with multichannel processing.
1976	Otticon	Development at the University of Paris leads to an 8 channel device known as the Chorimac-8, first implanted in September of 1976.
1976	Cochlear	Clarke implants their first multi-channel implant with success. With further funding from the Australian government to make the device smaller, and a partnership with Nucleus to market the device, competition with 3M heats up.
1977	MED-EL	The first implant of the Hockmair Burian device is performed. Their testing involved several sound schemes in which some rudimentary speech understanding was possible and some support for lip reading. With this, they began to try further channels
1978	Common	The National Institute of Health releases the Bilger report to investigate cochlear implants. It finds that whilst expert opinion is not to hopeful and quite negative, results from patients showed increased patient outcomes in quality of life and that scores for lip-reading and speech production were on average better. This leads to increased investment in CIs by the NIH.
1978	MED-EL	The Vienna team develops a passive single channel broadband device made biocompatible by epoxy used for pacemakers. The device also had 2 or 4 channel possibilities. Again, some open speech understanding was found, and a major advantage of the device appeared to be its low power consumption.
1980	Sonova	Team focuses on developing a bipolar multichannel array for the scala tympani which is first implanted in the early 1980s and subsequently further improved for biocompatibility.

1981	MED-EL	Through an agreement with 3M, the Vienna implant was to be commercialised. The device at this point was completely redesigned and had not achieved the results it had originally obtained.
1985	Cochlear	Nucleus by this time has completed several clinical trials giving further insight into electrical stimulation of the auditory system and further competitive advantage. It hence presents this information to the FDA and gains approval.
1986	Otticon	Further improvements on the Chorimac-8 leads to a 12 channel device, the Chorimac-12. The surgical procedure involved 12 openings along the cochlea and lead to variability. Additionally, the testing itself was not standardised and the device itself was quite large. Nonetheless, Chouard states "vowels were well recognised, consonant voicing was well differentiated and different fricatives could be well distinguished'. This same year, MXM purchased Bertin's corporate patent.
1987	Sonova / Advanced Bionics	A partnership is formed with help of the NIH between the UCSF group, Storz Medical Instruments and the Research Triangle Institute. At this time, strategies for processing in single and multichannel devices are developed. A commercial partnership also begins to be developed with Alfred E. Mann, an owner of several medical device companies at the time. They formed the Advanced Bionics company.
1990	MED-EL	MED-EL is formed by the Hockmair group in collaboration with 3M and the university.
1991	Sonova / Advanced Bionics	Clinical Trials begin of the Advanced Bionics device at UCSF.
1992	Otticon	MXM releases its first cochlear implant, the DX-10.
1995	Cochlear	Cochlear is listed on the ASX, continues to develop its technologies.
1996	Sonova / Advanced Bionics	FDA approval is obtained for the Advanced Bionics device.
1997	Sonova / Advanced Bionics	Further features such as a unique headpiece, independent volume control and sensitivity controls are added and further approval is given for children.
2001	Sonova / Advanced Bionics	Launch of the CII Bionic eat with HiFocus electrode.
2002	Sonova / Advanced Bionics	Launch of the T-Mic microphone giving wireless connection to numerous consumer electronics devices including mobile phones and MP3 players. Some controversy of whether certain parts caused meningitis.
2003	Sonova /	HiRes 90K implant introduced

	Advanced Bionics	
2004	Sonova / Advanced Bionics	Boston Scientific acquires Advanced Bionics but legal issues mean it is sold off again.
2006	Sonova / Advanced Bionics	Harmony implant introduced
2009	Sonova / Advanced Bionics	Sonova purchases Advanced Bionics.
Present	Otticon	After several company manoeuvres, MXM's technology is now sold under the Otticon Medical company name.
Present	Cochlear	Cochlear is market leader
Present	MED-EL	Med-EL currently has FDA approval and also manufactures brain stem implants and electroacoustic stimulation devices.

Table 28: History of Cochlear Implants (Eshraghi et al. 2012)

BIBLIOGRAPHY

Bibliography

AAMI, A.f.t.A.o.M.I. 2010, *Aami tir42 evaluation of particulates associated with vascular medical devices*, IEEE.

Abbott Laboratories 2017a, 'Abbott announces U.S. approval for its assurity MRI pacemaker, the world's smallest, longest-lasting wireless mri-compatible pacemaker', https://www.prnewswire.com/news-releases/abbott-announces-us-approval-for-its-assurity-mri-pacemaker-the-worlds-smallest-longest-lasting-wireless-mri-compatible-pacemaker-300400307.html, <https://www.prnewswire.com/news-releases/abbott-announces-us-approval-for-its-assurity-mri-pacemaker-the-worlds-smallest-longest-lasting-wireless-mri-compatible-pacemaker-300400307.html>.

Abbott Laboratories 2017b, 'Abbott reports third-quarter 2017 results', PRNewswire, <https://www.prnewswire.com/news-releases/abbott-reports-third-quarter-2017-results-300538753.html>.

Abbott Laboratories 2017c, *Dorsal root ganglion therapy*, viewed 23 December 2017, <https://www.sjm.com/en/patients/chronic-pain/managing-chronic-pain/dorsal-root-ganglion-therapy>.

Abbott Laboratories 2017d, *Freestyle libre reader*, viewed 24 December 2017, <https://www.freestylelibre.com.au/freestyle-libre-reader>.

Abbott Laboratories 2017e, *Spinal cord stimulation (SCS)*, viewed 23 December 2017, <https://www.sjm.com/en/patients/chronic-pain/managing-chronic-pain/spinal-cord-stimulation>.

Acharya, T. 2012, *Oxidase test: principle procedure and oxidase positive organisms*, Microbe Online, https://microbeonline.com/oxidase-test-principle-procedure-and-oxidase-positive-organisms/, viewed 27 December 2017, <https://microbeonline.com/oxidase-test-principle-procedure-and-oxidase-positive-organisms/>.

Ahnood, A., Fox, K., Apollo, N., Lohrmann, A., Garrett, D.J., Nayagam, D.A., Karle, T., Stacey, A., Abberton, K. & Morrison, W. 2016, 'Diamond encapsulated photovoltaics for transdermal power delivery', *Biosensors and Bioelectronics*, vol. 77, pp. 589-97.

Al Idrus, A. 2017a, *Insulet unveils pediatric 'artificial pancreas' data*, FierceBiotech, viewed 24 December 2017, <https://www.fiercebiotech.com/medtech/insulet-unveils-pediatric-artificial-pancreas-data>.

Al Idrus, A. 2017b, *Medtronic's long-awaited 'artificial pancreas' makes U.S. debut*, FierceBiotech, viewed 24 December 2017, <https://www.fiercebiotech.com/medtech/medtronic-s-long-awaited-artificial-pancreas-makes-u-s-debut>.

Al Irus, A. 2017, *Axonics snags another $20M+ in oversubscribed series C*, viewed 23 December 2017, <https://www.fiercebiotech.com/medtech/axonics-snags-another-20m-oversubscribed-series-c>.

Amar, A.B., Kouki, A.B. & Cao, H. 2015, 'Power approaches for implantable medical devices', *Sensors*, vol. 15, no. 11, pp. 28889-914.

Anderson, R.R. & Parrish, J.A. 1981, 'The optics of human skin', *Journal of Investigative Dermatology*, vol. 77, no. 1, pp. 13-9.

Aquilina, O. 2006, 'A brief history of cardiac pacing', *Images in Paediatric Cardiology*, vol. 8, no. 2, p. 17.

Arnold, D.P., Herrault, F., Zana, I., Galle, P., Park, J.-W., Das, S., Lang, J.H. & Allen, M.G. 2006, 'Design optimization of an 8W, microscale, axial-flux, permanent-magnet generator', *Journal of Micromechanics and Microengineering*, vol. 16, no. 9, p. S290.

Artyushkova, K., Roizman, D., Santoro, C., Doyle, L.E., Fatima Mohidin, A., Atanassov, P. & Marsili, E. 2016, 'Anodic biofilms as the interphase for electroactive bacterial growth on carbon veil', *Biointerphases*, vol. 11, no. 3, p. 031013.

AS, A.S. 2015, *Implants for surgery - active implantable medical devices*.

ATCC, A.T.C.C. 2014, *Shewanella Oneidensis Venkateswaran et al. (ATCC® 700550™)*, ATCC, viewed 28 December 2017 2017, <https://www.atcc.org/products/all/700550.aspx>.

Autonomic Technologies 2015, *About the therapy*, viewed 23 December 2017, <http://www.ati-spg.com/us/en/ati-neurostimulation-system/about-the-therapy/>.

Axonics 2017, *First rechargeable & miniaturized system dedicated to sacral neuromodulation*, viewed 23 December 2017, <http://www.axonicsmodulation.com/product/>.

Baghayeri, M. 2015, 'Glucose sensing by a glassy carbon electrode modified with glucose oxidase and a magnetic polymeric nanocomposite', *RSC Advances*, vol. 5, no. 24, pp. 18267-74.

Baker, D.F. & Bragg, R.H. 1983, 'The electrical conductivity and Hall effect of glassy carbon', *Journal of Non-Crystalline Solids*, vol. 58, no. 1, pp. 57-69.

Bankar, S.B., Bule, M.V., Singhal, R.S. & Ananthanarayan, L. 2009, 'Glucose oxidase—an overview', *Biotechnology Advances*, vol. 27, no. 4, pp. 489-501.

Bard, A.J. & Faulkner, L.R. 2000, *Electrochemical methods: fundamentals and applications*, Wiley.

Barrière, F., Ferry, Y., Rochefort, D. & Leech, D. 2004, 'Targetting redox polymers as mediators for laccase oxygen reduction in a membrane-less biofuel cell', *Electrochemistry Communications*, vol. 6, no. 3, pp. 237-41.

Barrière, F., Kavanagh, P. & Leech, D. 2006, 'A laccase–glucose oxidase biofuel cell prototype operating in a physiological buffer', *Electrochimica Acta*, vol. 51, no. 24, pp. 5187-92.

Basaeri, H., Christensen, D., Roundy, S., Yu, Y., Nguyen, T., Tathireddy, P. & Young, D.J. 2016, 'Ultrasonically powered hydrogel-based wireless implantable glucose sensor', *Sensors*, IEEE, pp. 1-3.

Basaeri, H., Christensen, D.B. & Roundy, S. 2016, 'A review of acoustic power transfer for bio-medical implants', *Smart Materials and Structures*, vol. 25, no. 12, p. 123001.

Basaeri, H. & Roundy, S. 2017, 'A micromachined ultrasonic power receiver for biomedical implants', *SPIE Smart Structures and Materials + Nondestructive Evaluation and Health Monitoring*, International Society for Optics and Photonics, pp. 1016416--7.

Baudler, A., Langner, M., Rohr, C., Greiner, A. & Schröder, U. 2017, 'Metal–polymer hybrid architectures as novel anode platform for microbial electrochemical technologies', *ChemSusChem*, vol. 10, no. 1, pp. 253-7.

Baudler, A., Riedl, S. & Schröder, U. 2014, 'Long-term performance of primary and secondary electroactive biofilms using layered corrugated carbon electrodes', *Frontiers in Energy Research*, vol. 2, p. 30.

Baudler, A., Schmidt, I., Langner, M., Greiner, A. & Schröder, U. 2015, 'Does it have to be carbon? Metal anodes in microbial fuel cells and related bioelectrochemical systems', *Energy & Environmental Science*, vol. 8, no. 7, pp. 2048-55.

Beckman, C. 2018, *Light obscuration: optical method for particle detection*, Beckman Coulter, Indianapolis, viewed 21 May 2018, <https://www.beckman.com/resources/industry-standards/usp-787/light-obscuration-optical-method-for-particle-detection>.

Bedekar, V., Oliver, J. & Priya, S. 2009, 'Pen harvester for powering a pulse rate sensor', *Journal of Physics D: Applied Physics*, vol. 42, no. 10, p. 105105.

Biffinger, J.C., Byrd, J.N., Dudley, B.L. & Ringeisen, B.R. 2008, 'Oxygen exposure promotes fuel diversity for Shewanella oneidensis microbial fuel cells', *Biosensors and Bioelectronics*, vol. 23, no. 6, pp. 820-6.

Biffinger, J.C., Pietron, J., Ray, R., Little, B. & Ringeisen, B.R. 2007, 'A biofilm enhanced miniature microbial fuel cell using Shewanella oneidensis DSP10 and oxygen reduction cathodes', *Biosensors and Bioelectronics*, vol. 22, no. 8, pp. 1672-9.

Bigfoot Biomedical 2017, *Vision*, viewed 24 December 2017, <https://www.bigfootbiomedical.com/vision/>.

Bionic Vision Australia 2017a, *How does it work?*, viewed 23 December 2017, <http://bionicvision.org.au/eye/how_does_it_work>.

Bionic Vision Australia 2017b, *Who will it help?*, viewed 23 December 2017, <http://bionicvision.org.au/eye/who_will_it_help>.

Bionics Institute 2017, *FAQ bionic hearing*, viewed 23 December 2017, <http://www.bionicsinstitute.org/pages/contact/faq.aspx>.

Blanford, C.F., Foster, C.E., Heath, R.S. & Armstrong, F.A. 2009, 'Efficient electrocatalytic oxygen reduction by the 'blue' copper oxidase, laccase, directly attached to chemically modified carbons', *Faraday Discussions*, vol. 140, pp. 319-35.

Blanford, C.F., Heath, R.S. & Armstrong, F.A. 2007, 'A stable electrode for high-potential, electrocatalytic O2 reduction based on rational attachment of a blue copper oxidase to a graphite surface', *Chemical Communications*, no. 17, pp. 1710-2.

Boghani, H.C., Papaharalabos, G., Michie, I., Fradler, K.R., Dinsdale, R.M., Guwy, A.J., Ieropoulos, I., Greenman, J. & Premier, G.C. 2014, 'Controlling for peak power extraction from microbial fuel cells can increase stack voltage and avoid cell reversal', *Journal of Power Sources*, vol. 269, pp. 363-9.

Bond, D.R., Holmes, D.E., Tender, L.M. & Lovley, D.R. 2002, 'Electrode-reducing microorganisms that harvest energy from marine sediments', *Science*, vol. 295, no. 5554, pp. 483-5.

Bond, D.R. & Lovley, D.R. 2003, 'Electricity production by Geobacter sulfurreducens attached to electrodes', *Applied and Environmental Microbiology*, vol. 69, no. 3, pp. 1548-55.

Bond, D.R. & Lovley, D.R. 2005, 'Evidence for involvement of an electron shuttle in electricity generation by Geothrix fermentans', *Applied and Environmental Microbiology*, vol. 71, no. 4, pp. 2186-9.

Borole, A.P., O'Neill, H., Tsouris, C. & Cesar, S. 2008, 'A microbial fuel cell operating at low pH using the acidophile Acidiphilium cryptum', *Biotechnology Letters*, vol. 30, no. 8, pp. 1367-72.

Boston Scientific 2009, *Altrua 20 and altrua 40 system guide*, pamphlet, Boston Scientific, https://www.bostonscientific.com/content/dam/Manuals/us/current-rev-en/357894-003_EN_US_S.pdf.

Boston Scientific 2015, *Autogen EL ICD, Autogen Mini ICD, Dynagen EL ICD, Dynagen Mini ICD, Inogen EL ICD, Inogen Mini ICD, Origen EL ICD, Origen Mini ICD, Incepta ICD, Energen ICD, Punctua ICD, Punctua NE ICD, Teligen 100 ICD physician's technical manual*, pamphlet, Boston Scientific, http://www.bostonscientific.com/content/dam/Manuals/eu/current-rev-en/359404-001_Tachy_ICD_PTM_en-GBR_S.pdf.

Boston Scientific 2016a, *Accolate, Accolade MRI, Proponent, Proponent MRI, Essentio, Essentio MRI, Altrua 2, Formio, Formio MRI, Vitalio, Vitalio MRI, Ingenio, Ingenio MRI, Advantio, Advantio MRI physician's technical manual*, pamphlet, Boston Scientific, http://www.bostonscientific.com/content/dam/Manuals/au/current-rev-en/359251-002_Brady%20Pacer_PTM_en-AUS_S.pdf.

Boston Scientific 2016b, *Boston Scientific 2016 Annual Report Form 10-k*.

Boston Scientific 2017a, *Deep brain stimulation systems*, viewed 23 December 2017, <http://www.bostonscientific.com/en-US/products/deep-brain-stimulation-systems.html>.

Boston Scientific 2017b, *Precision Montage MRI*, viewed 22 December 2017, <http://www.bostonscientific.com/content/dam/bostonscientific/neuro/portfolio-group/Precision_Montage/Precision_Montage_IPG_940x940.png>.

Boston Scientific 2017c, *Spinal cord stimulator systems*, viewed 23 December 2017, <http://www.bostonscientific.com/en-US/products/spinal-cord-stimulator-systems.html>.

Boston Scientific 2017d, *Vercise Deep Brain Stimulation Physician Manual*, http://www.bostonscientific.com/content/dam/Manuals/us/current-rev-en/92093580-01_RevE_Vercise_DBS_Physician_Manual_DFU_en-US_S.pdf.

Bourourou, M., Elouarzaki, K., Lalaoui, N., Agnès, C., Le Goff, A., Holzinger, M., Maaref, A. & Cosnier, S. 2013, 'Supramolecular immobilization of laccase on carbon nanotube electrodes functionalized with (methylpyrenylaminomethyl) anthraquinone for direct electron reduction of oxygen', *Chemistry-A European Journal*, vol. 19, no. 28, pp. 9371-5.

Bretschger, O., Obraztsova, A., Sturm, C.A., Chang, I.S., Gorby, Y.A., Reed, S.B., Culley, D.E., Reardon, C.L., Barua, S. & Romine, M.F. 2007, 'Current production and metal oxide reduction by Shewanella oneidensis MR-1 wild type and mutants', *Applied and Environmental Microbiology*, vol. 73, no. 21, pp. 7003-12.

Brunel, L., Denele, J., Servat, K., Kokoh, K.B., Jolivalt, C., Innocent, C., Cretin, M., Rolland, M. & Tingry, S. 2007, 'Oxygen transport through laccase biocathodes for a membrane-less glucose/O_2 biofuel cell', *Electrochemistry Communications*, vol. 9, no. 2, pp. 331-6.

Calignano, F., Tommasi, T., Manfredi, D. & Chiolerio, A. 2015, 'Additive manufacturing of a microbial fuel cell—a detailed study', *Scientific Reports*, vol. 5, p. 17373.

Cao, H., Landge, V., Tata, U., Seo, Y.-S., Rao, S., Tang, S.-J., Tibbals, H., Spechler, S. & Chiao, J.-C. 2012, 'An implantable, batteryless, and wireless capsule with integrated impedance and pH sensors for gastroesophageal reflux monitoring', *IEEE Transactions on Biomedical Engineering*, vol. 59, no. 11, pp. 3131-9.

Carmo, J.P., Gonçalves, L.M. & Correia, J.H. 2010, 'Thermoelectric microconverter for energy harvesting systems', *IEEE Transactions on Industrial Electronics*, vol. 57, no. 3, pp. 861-7.

Centres for Disease Control and Prevention 2016, *Diabetes*, viewed 24 December 2017, <https://www.cdc.gov/chronicdisease/resources/publications/aag/diabetes.htm>.

Chae, K.J., Choi, M., Ajayi, F.F., Park, W., Chang, I.S. & Kim, I.S. 2007, 'Mass transport through a proton exchange membrane (Nafion) in microbial fuel cells', *Energy & Fuels*, vol. 22, no. 1, pp. 169-76.

Chang, T.C., Wang, M.L., Charthad, J., Weber, M.J. & Arbabian, A. 2017, '27.7 A 30.5 mm 3 fully packaged implantable device with duplex ultrasonic data and power links achieving 95kb/s with< 10− 4 BER at 8.5 cm depth', *Solid-State Circuits Conference (ISSCC) 2017*, IEEE, pp. 460-1.

Chang, T.C., Weber, M., Charthad, J., Nikoozadeh, A., Khuri-Yakub, P.T. & Arbabian, A. 2015, 'Design of high-efficiency miniaturized ultrasonic receivers for powering medical implants with reconfigurable power levels', *Ultrasonics Symposium (IUS)*, IEEE, pp. 1-4.

Charthad, J., Weber, M.J., Chang, T.C. & Arbabian, A. 2015, 'A mm-sized implantable medical device (IMD) with ultrasonic power transfer and a hybrid bi-directional data link', *IEEE Journal of Solid-State Circuits*, vol. 50, no. 8, pp. 1741-53.

Chaudhuri, S.K. & Lovley, D.R. 2003, 'Electricity generation by direct oxidation of glucose in mediatorless microbial fuel cells', *Nature Biotechnology*, vol. 21, no. 10, pp. 1229-32.

Chen, S., He, G., Carmona-Martinez, A.A., Agarwal, S., Greiner, A., Hou, H. & Schröder, U. 2011, 'Electrospun carbon fiber mat with layered architecture for anode in microbial fuel cells', *Electrochemistry Communications*, vol. 13, no. 10, pp. 1026-9.

Chen, S., He, G., Hu, X., Xie, M., Wang, S., Zeng, D., Hou, H. & Schröder, U. 2012, 'A three-dimensionally ordered macroporous carbon derived from a natural resource as anode for microbial bioelectrochemical systems', *ChemSusChem*, vol. 5, no. 6, pp. 1059-63.

Chen, S., Hou, H., Harnisch, F., Patil, S.A., Carmona-Martinez, A.A., Agarwal, S., Zhang, Y., Sinha-Ray, S., Yarin, A.L. & Greiner, A. 2011, 'Electrospun and solution blown three-dimensional carbon fiber nonwovens for application as electrodes in microbial fuel cells', *Energy & Environmental Science*, vol. 4, no. 4, pp. 1417-21.

Chiao, M. 2008, 'A microfabricated PDMS microbial fuel cell', *Journal of Microelectromechanical Systems*, vol. 17, no. 6, pp. 1329-41.

Chiao, M., Lin, L. & Lam, K.B. 2007, *US7160637B2 Implantable, miniaturized microbial fuel cell*.

Chiu, Y. & Tseng, V.F. 2008, 'A capacitive vibration-to-electricity energy converter with integrated mechanical switches', *Journal of Micromechanics and Microengineering*, vol. 18, no. 10, p. 104004.

Choi, D.-H., Han, C.-H., Kim, H.-D. & Yoon, J.-B. 2011, 'Liquid-based electrostatic energy harvester with high sensitivity to human physical motion', *Smart Materials and Structures*, vol. 20, no. 12, p. 125012.

Choi, S. & Chae, J. 2013, 'Optimal biofilm formation and power generation in a micro-sized microbial fuel cell (MFC)', *Sensors and Actuators A: Physical*, vol. 195, pp. 206-12.

Choi, S., Lee, H.-S., Yang, Y., Parameswaran, P., Torres, C.I., Rittmann, B.E. & Chae, J. 2011, 'A μL-scale micromachined microbial fuel cell having high power density', *Lab on a Chip*, vol. 11, no. 6, pp. 1110-7.

Christwardana, M. & Kwon, Y. 2015, 'Effects of multiple polyaniline layers immobilized on carbon nanotube and glutaraldehyde on performance and stability of biofuel cell', *Journal of Power Sources*, vol. 299, pp. 604-10.

Cima, M. 2007, *MEMS drug delivery devices*, viewed 24 December 2017, <http://web.mit.edu/cprl/www/research.shtml>.

Cinquin, P., Gondran, C., Giroud, F., Mazabrard, S., Pellissier, A., Boucher, F., Alcaraz, J.-P., Gorgy, K., Lenouvel, F. & Mathé, S. 2010, 'A glucose biofuel cell implanted in rats', *PloS one*, vol. 5, no. 5, p. e10476.

Çirpan, A., Alkan, S.y., Toppare, L., Hepuzer, Y.m. & Yağci, Y. 2002, 'Conducting graft copolymers of poly (3-methylthienyl methacrylate) with pyrrole and thiophene', *Journal of Polymer Science Part A: Polymer Chemistry*, vol. 40, no. 23, pp. 4131-40.

Clarke, T.A., Edwards, M.J., Gates, A.J., Hall, A., White, G.F., Bradley, J., Reardon, C.L., Shi, L., Beliaev, A.S. & Marshall, M.J. 2011, 'Structure of a bacterial cell surface decaheme electron conduit', *Proceedings of the National Academy of Sciences*, vol. 108, no. 23, pp. 9384-9.

Cochlear 2016, *2016 Cochlear annual report*.

Codman & Shurtleff 2017, *Products implantable pumps pump overview*, viewed 23 December 2017, <http://www.codmanpumps.com/Products_pumps_overview.asp>.

Conghaile, P.Ó., Kamireddy, S., MacAodha, D., Kavanagh, P. & Leech, D. 2013, 'Mediated glucose enzyme electrodes by cross-linking films of osmium redox complexes and glucose oxidase on electrodes', *Analytical and Bioanalytical Chemistry*, vol. 405, no. 11, pp. 3807-12.

Cosnier, S., Gross, A.J., Le Goff, A. & Holzinger, M. 2016, 'Recent advances on enzymatic glucose/oxygen and hydrogen/oxygen biofuel cells: achievements and limitations', *Journal of Power Sources*, vol. 325, pp. 252-63.

Cosnier, S., Le Goff, A. & Holzinger, M. 2014, 'Towards glucose biofuel cells implanted in human body for powering artificial organs', *Electrochemistry Communications*, vol. 38, pp. 19-23.

Cracknell, J.A., McNamara, T.P., Lowe, E.D. & Blanford, C.F. 2011, 'Bilirubin oxidase from Myrothecium verrucaria: X-ray determination of the complete crystal structure and a rational surface modification for enhanced electrocatalytic O_2 reduction', *Dalton Transactions*, vol. 40, no. 25, pp. 6668-75.

Crepaldi, L., Neto, S.A., Cardoso, F., Ciancaglini, P. & De Andrade, A. 2014, 'Ferrocene entrapped in polypyrrole film and PAMAM dendrimers as matrix for mediated glucose/O_2 biofuel cell', *Electrochimica Acta*, vol. 136, pp. 52-8.

Curlevski, N. 2017, '577030', personal communication, 14 March 2017, Castle Hill.

Cyberonics 2014, *About Cyberonics*, viewed 23 December 2017, <http://www.livanova.cyberonics.com/about>.

Delhi Pain Management Centre 2017, *Spinal cord stimulation*, <http://painhospital.in/en/wp-content/uploads/2016/07/intrathecal-pump-2.jpg>.

Deng, L., Li, F., Zhou, S., Huang, D. & Ni, J. 2010, 'A study of electron-shuttle mechanism in Klebsiella pneumoniae based-microbial fuel cells', *Chinese Science Bulletin*, vol. 55, no. 1, pp. 99-104.

Dewan, A., Beyenal, H. & Lewandowski, Z. 2008, 'Scaling up microbial fuel cells', *Environmental Science & Technology*, vol. 42, no. 20, pp. 7643-8.

Dexcom 2017, *Introducing the Dexcom G5® mobile CGM system*, viewed 24 December 2017, <https://www.dexcom.com/g5-mobile-cgm>.

Dietrich, L.E., Price-Whelan, A., Petersen, A., Whiteley, M. & Newman, D.K. 2006, 'The phenazine pyocyanin is a terminal signalling factor in the quorum sensing network of Pseudomonas aeruginosa', *Molecular Microbiology*, vol. 61, no. 5, pp. 1308-21.

Donelan, J.M., Li, Q., Naing, V., Hoffer, J., Weber, D. & Kuo, A.D. 2008, 'Biomechanical energy harvesting: generating electricity during walking with minimal user effort', *Science*, vol. 319, no. 5864, pp. 807-10.

Dong, K., Jia, B., Yu, C., Dong, W., Du, F. & Liu, H. 2013, 'Microbial fuel cell as power supply for implantable medical devices: A novel configuration design for simulating colonic environment', *Biosensors and Bioelectronics*, vol. 41, pp. 916-9.

Dos Santos, L., Climent, V., Blanford, C.F. & Armstrong, F.A. 2010, 'Mechanistic studies of the 'blue' Cu enzyme, bilirubin oxidase, as a highly efficient electrocatalyst for the oxygen reduction reaction', *Physical Chemistry Chemical Physics*, vol. 12, no. 42, pp. 13962-74.

Du Toit, H. & Di Lorenzo, M. 2015, 'Continuous power generation from glucose with two different miniature flow-through enzymatic biofuel cells', *Biosensors and Bioelectronics*, vol. 69, pp. 199-205.

Ecole Polytechnique Fédérale de Lausanne 2013, *Under the skin: a tiny laboratory*, viewed 24 December 2017, <http://sti.epfl.ch/page-92004-en.html>.

El Ichi, S., Zebda, A., Alcaraz, J.-P., Laaroussi, A., Boucher, F., Boutonnat, J., Reverdy-Bruas, N., Chaussy, D., Belgacem, M. & Cinquin, P. 2015, 'Bioelectrodes modified

with chitosan for long-term energy supply from the body', *Energy & Environmental Science*, vol. 8, no. 3, pp. 1017-26.

Elgrishi, N.m., Rountree, K.J., McCarthy, B.D., Rountree, E.S., Eisenhart, T.T. & Dempsey, J.L. 2017, 'A practical beginner's guide to cyclic voltammetry', *Journal of Chemical Education*.

EnteroMedics 2016, *Enteromedics Inc Form 10-K 2016*.

EnteroMedics 2017, *About EnteroMedics*, St Paul Minnoesota, viewed 23 December 2017.

Eshraghi, A.A., Nazarian, R., Telischi, F.F., Rajguru, S.M., Truy, E. & Gupta, C. 2012, 'The cochlear implant: historical aspects and future prospects', *The Anatomical Record*, vol. 295, no. 11, pp. 1967-80.

European Union 1990, 'Council Directive 90/385/EEC of 20 June 1990 on the approximation of the laws of the Member States relating to active implantable medical devices ', in E. Union (ed.), *31990L0385*, European Union, <http://eur-lex.europa.eu/LexUriServ/LexUriServ.do?uri=CELEX:31990L0385:en:HTML>.

Eversense 2017, *Eversense CGM system*, viewed 24 December 2017, <https://ous.eversensediabetes.com/products/>.

Falconer, S. 2016, *I was hooked up to Bigfoot's artificial pancreas*, viewed 24 December 2017, <http://insulinnation.com/research/i-was-hooked-up-to-bigfoots-artificial-pancreas/>.

Falk, M., Pankratov, D., Lindh, L., Arnebrant, T. & Shleev, S. 2014, 'Miniature direct electron transfer based enzymatic fuel cell operating in human sweat and saliva', *Fuel Cells*, vol. 14, no. 6, pp. 1050-6.

Faltys, M.A., Kuzma, J.A. & Gord, J.C. 2001, *US6272382B1 Fully implantable cochlear implant system*.

Fan, Y., Hu, H. & Liu, H. 2007, 'Enhanced coulombic efficiency and power density of air-cathode microbial fuel cells with an improved cell configuration', *Journal of Power Sources*, vol. 171, no. 2, pp. 348-54.

Federal Drug Administration 2017a, *Product classification*, viewed 26 December 2017, <https://www.accessdata.fda.gov/scripts/cdrh/cfdocs/cfPCD/classification.cfm?ID=NKE>.

Federal Drug Administration 2017b, *What is the pancreas? What is an artificial pancreas device system?*, viewed 24 December 2017, <https://www.fda.gov/MedicalDevices/ProductsandMedicalProcedures/HomeHealthandConsumer/ConsumerProducts/ArtificialPancreas/ucm259548.htm>.

Feng, Y., Lee, H., Wang, X., Liu, Y. & He, W. 2010, 'Continuous electricity generation by a graphite granule baffled air–cathode microbial fuel cell', *Bioresource Technology*, vol. 101, no. 2, pp. 632-8.

Feng, Y., Yang, Q., Wang, X. & Logan, B.E. 2010, 'Treatment of carbon fiber brush anodes for improving power generation in air–cathode microbial fuel cells', *Journal of Power Sources*, vol. 195, no. 7, pp. 1841-4.

Fiebus, M. 2017, *The first 'artificial pancreas' systems are coming to market*, viewed 24 December 2017, <https://www.usatoday.com/story/tech/columnist/2017/05/02/first-artificial-pancreas-systems-coming-market/100704988/>.

Flowonix Medical Inc 2017, *Prometra pump*, viewed 23 December 2017, <http://www.flowonix.com/healthcare-provider/products/prometra-pump>.

Forster, R.J., Walsh, D.A., Mano, N., Mao, F. & Heller, A. 2004, 'Modulating the redox properties of an osmium-containing metallopolymer through the supporting electrolyte and cross-linking', *Langmuir*, vol. 20, no. 3, pp. 862-8.

Fraunhoffer 2014, 'Hydrocephalus: sensors monitor cerebral pressure', viewed 23 December 2017, <https://www.fraunhofer.de/en/press/research-news/2014/january/hydrocephalus-sensors-monitor-cerebral-pressure.html>.

Fredrickson, J.K., Romine, M.F., Beliaev, A.S., Auchtung, J.M., Driscoll, M.E., Gardner, T.S., Nealson, K.H., Osterman, A.L., Pinchuk, G. & Reed, J.L. 2008, 'Towards environmental systems biology of Shewanella', *Nature Reviews Microbiology*, vol. 6, no. 8, pp. 592-603.

Freguia, S., Tsujimura, S. & Kano, K. 2010, 'Electron transfer pathways in microbial oxygen biocathodes', *Electrochimica Acta*, vol. 55, no. 3, pp. 813-8.

Gajda, I., Greenman, J., Melhuish, C., Santoro, C. & Ieropoulos, I. 2016, 'Microbial Fuel Cell-driven caustic potash production from wastewater for carbon sequestration', *Bioresource Technology*, vol. 215, pp. 285-9.

Gao, F., Viry, L., Maugey, M., Poulin, P. & Mano, N. 2010, 'Engineering hybrid nanotube wires for high-power biofuel cells', *Nature Communications*, vol. 1, p. 2.

Gardner, J. 2013, 'A history of deep brain stimulation: technological innovation and the role of clinical assessment tools', *Social Studies Of Science*, vol. 43, no. 5, pp. 707-28.

Ghasemi, M., Daud, W.R.W., Ismail, M., Rahimnejad, M., Ismail, A.F., Leong, J.X., Miskan, M. & Liew, K.B. 2013, 'Effect of pre-treatment and biofouling of proton exchange membrane on microbial fuel cell performance', *International Journal Of Hydrogen Energy*, vol. 38, no. 13, pp. 5480-4.

Ghassemi, H., McGrath, J.E. & Zawodzinski, T.A. 2006, 'Multiblock sulfonated–fluorinated poly(arylene ether)s for a proton exchange membrane fuel cell', *Polymer*, vol. 47, no. 11, pp. 4132-9.

Ghovanloo, M. & Najafi, K. 2007, 'A wireless implantable multichannel microstimulating system-on-a-chip with modular architecture', *IEEE Transactions on Neural Systems and Rehabilitation Engineering*, vol. 15, no. 3, pp. 449-57.

Gil, G.-C., Chang, I.-S., Kim, B.H., Kim, M., Jang, J.-K., Park, H.S. & Kim, H.J. 2003, 'Operational parameters affecting the performannce of a mediator-less microbial fuel cell', *Biosensors and Bioelectronics*, vol. 18, no. 4, pp. 327-34.

Gildenberg, P.L. 2006, 'History of electrical neuromodulation for chronic pain', *Pain Medicine*, vol. 7, no. Supplementary, pp. 7-13.

Giroud, F. & Minteer, S.D. 2013, 'Anthracene-modified pyrenes immobilized on carbon nanotubes for direct electroreduction of O_2 by laccase', *Electrochemistry Communications*, vol. 34, pp. 157-60.

Goldbeck, C.P., Jensen, H.M., TerAvest, M.A., Beedle, N., Appling, Y., Hepler, M., Cambray, G., Mutalik, V., Angenent, L.T. & Ajo-Franklin, C.M. 2013, 'Tuning promoter strengths for improved synthesis and function of electron conduits in Escherichia coli', *ACS Synthetic Biology*, vol. 2, no. 3, pp. 150-9.

Gorby, Y.A., Yanina, S., McLean, J.S., Rosso, K.M., Moyles, D., Dohnalkova, A., Beveridge, T.J., Chang, I.S., Kim, B.H. & Kim, K.S. 2006, 'Electrically conductive bacterial nanowires produced by Shewanella oneidensis strain MR-1 and other microorganisms', *Proceedings of the National Academy of Sciences*, vol. 103, no. 30, pp. 11358-63.

Goto, K., Nakagawa, T., Nakamura, O. & Kawata, S. 2001, 'An implantable power supply with an optically rechargeable lithium battery', *IEEE Transactions on Biomedical Engineering*, vol. 48, no. 7, pp. 830-3.

Granstrom, J., Feenstra, J., Sodano, H.A. & Farinholt, K. 2007, 'Energy harvesting from a backpack instrumented with piezoelectric shoulder straps', *Smart Materials and Structures*, vol. 16, no. 5, p. 1810.

Grattieri, M., Babanova, S., Santoro, C., Guerrini, E., Trasatti, S.P., Cristiani, P., Bestetti, M. & Atanassov, P. 2015, 'Enzymatic oxygen microsensor based on bilirubin oxidase applied to microbial fuel cells analysis', *Electroanalysis*, vol. 27, no. 2, pp. 327-35.

Guerrini, E., Cristiani, P., Grattieri, M., Santoro, C., Li, B. & Trasatti, S. 2014, 'Electrochemical behavior of stainless steel anodes in membraneless microbial fuel cells', *Journal of The Electrochemical Society*, vol. 161, no. 3, pp. H62-H7.

Guerrini, E., Grattieri, M., Trasatti, S.P., Bestetti, M. & Cristiani, P. 2014, 'Performance explorations of single chamber microbial fuel cells by using various microelectrodes applied to biocathodes', *International Journal of Hydrogen Energy*, vol. 39, no. 36, pp. 21837-46.

Guidant 2008, *System guide Ventak Prizm, Ventak Prizm HE, Ventak Prizm 2*, pamphlet, Guidant, https://www.bostonscientific.com/content/dam/Manuals/us/current-rev-en/355239-010_S.pdf.

Guo, K., Hidalgo, D., Tommasi, T. & Rabaey, K. 2016, 'Pyrolytic carbon-coated stainless steel felt as a high-performance anode for bioelectrochemical systems', *Bioresource Technology*, vol. 211, pp. 664-8.

Gwon, H., Hong, J., Kim, H., Seo, D.-H., Jeon, S. & Kang, K. 2014, 'Recent progress on flexible lithium rechargeable batteries', *Energy & Environmental Science*, vol. 7, no. 2, pp. 538-51.

H. Warner, B.W.R. 1967, 'Digest of the seventh international conference on medical and biological engineering', *Seventh International Conference on Medical and Biological Engineering*, Stockholm, Sweden, p. 520.

Haeberlin, A., Zurbuchen, A., Walpen, S., Schaerer, J., Niederhauser, T., Huber, C., Tanner, H., Servatius, H., Seiler, J. & Haeberlin, H. 2015, 'The first batteryless, solar-powered cardiac pacemaker', *Heart Rhythm*, vol. 12, no. 6, pp. 1317-23.

Haidar, A., Legault, L., Messier, V., Mitre, T.M., Leroux, C. & Rabasa-Lhoret, R. 2015, 'Comparison of dual-hormone artificial pancreas, single-hormone artificial pancreas, and conventional insulin pump therapy for glycaemic control in patients with type 1 diabetes: an open-label randomised controlled crossover trial', *The Lancet Diabetes & Endocrinology*, vol. 3, no. 1, pp. 17-26.

Hakami, H. 2016, *FDA approves Minimed 670G system – world's first hybrid closed loop system*, viewed 24 December 2017, <https://www.medtronicdiabetes.com/blog/fda-approves-minimed-670g-system-worlds-first-hybrid-closed-loop-system/>.

Halámková, L., Halámek, J., Bocharova, V., Szczupak, A., Alfonta, L. & Katz, E. 2012, 'Implanted biofuel cell operating in a living snail', *Journal of the American Chemical Society*, vol. 134, no. 11, pp. 5040-3.

Han, Y., Yu, C. & Liu, H. 2010, 'A microbial fuel cell as power supply for implantable medical devices', *Biosensors and Bioelectronics*, vol. 25, no. 9, pp. 2156-60.

Harnisch, F. & Schröder, U. 2009, 'Selectivity versus mobility: separation of anode and cathode in microbial bioelectrochemical systems', *ChemSusChem*, vol. 2, no. 10, pp. 921-6.

Harnisch, F., Schröder, U. & Scholz, F. 2008, 'The suitability of monopolar and bipolar ion exchange membranes as separators for biological fuel cells', *Environmental Science & Technology*, vol. 42, no. 5, pp. 1740-6.

Hartshorne, R.S., Jepson, B.N., Clarke, T.A., Field, S.J., Fredrickson, J., Zachara, J., Shi, L., Butt, J.N. & Richardson, D.J. 2007, 'Characterization of Shewanella oneidensis MtrC: a cell-surface decaheme cytochrome involved in respiratory electron transport to extracellular electron acceptors', *JBIC Journal of Biological Inorganic Chemistry*, vol. 12, no. 7, pp. 1083-94.

He, G., Gu, Y., He, S., Schröder, U., Chen, S. & Hou, H. 2011, 'Effect of fiber diameter on the behavior of biofilm and anodic performance of fiber electrodes in microbial fuel cells', *Bioresource Technology*, vol. 102, no. 22, pp. 10763-6.

He, Z., Minteer, S.D. & Angenent, L.T. 2005, 'Electricity generation from artificial wastewater using an upflow microbial fuel cell', *Environmental Science & Technology*, vol. 39, no. 14, pp. 5262-7.

Heidelberg, J.F., Paulsen, I.T., Nelson, K.E., Gaidos, E.J., Nelson, W.C., Read, T.D., Eisen, J.A., Seshadri, R., Ward, N. & Methe, B. 2002, 'Genome sequence of the dissimilatory metal ion–reducing bacterium Shewanella oneidensis', *Nature Biotechnology*, vol. 20, no. 11, pp. 1118-23.

Heller, A. 1992, 'Electrical connection of enzyme redox centers to electrodes', *The Journal of Physical Chemistry*, vol. 96, no. 9, pp. 3579-87.

Helmers, H., Wagner, L., Garza, C.E., Reichmuth, S.K., Oliva, E., Philipps, S.P., Lackner, D. & Bett, A.W. 2015, 'Photovoltaic cells with increased voltage output for optical power supply of sensor electronics', *Proceedings of the AMA Conferences*, vol. 2015, pp. 519-24.

Ho, J.S., Kim, S. & Poon, A.S. 2013, 'Midfield wireless powering for implantable systems', *Proceedings of the IEEE*, vol. 101, no. 6, pp. 1369-78.

Ho, J.S., Yeh, A.J., Neofytou, E., Kim, S., Tanabe, Y., Patlolla, B., Beygui, R.E. & Poon, A.S. 2014, 'Wireless power transfer to deep-tissue microimplants', *Proceedings of the National Academy of Sciences*, vol. 111, no. 22, pp. 7974-9.

Högberg, S., Mijatovic, N., Pedersen, J., Vuckovic, D., Jensen, B.B. & Holb, J. 2016, 'Axial permanent magnet generator for wearable energy harvesting', *2016 XXII International Conference on Electrical Machines (ICEM)*, IEEE, pp. 677-82.

Hollmer, M. 2014, *The pacemaker inside me: what I learned about the industry as a cardiac patient*, FierceBiotech, viewed 23 December 2017, <https://www.fiercebiotech.com/medical-devices/pacemaker-inside-me-what-i-learned-about-industry-as-a-cardiac-patient>.

Holmes, D.E., Bond, D.R. & Lovley, D.R. 2004, 'Electron transfer by Desulfobulbus propionicus to Fe (III) and graphite electrodes', *Applied and Environmental Microbiology*, vol. 70, no. 2, pp. 1234-7.

Holmes, D.E., Mester, T., O'Neil, R.A., Perpetua, L.A., Larrahondo, M.J., Glaven, R., Sharma, M.L., Ward, J.E., Nevin, K.P. & Lovley, D.R. 2008, 'Genes for two multicopper proteins required for Fe(III) oxide reduction in Geobacter sulfurreducens have different expression patterns both in the subsurface and on energy-harvesting electrodes', *Microbiology*, vol. 154, no. 5, pp. 1422-35.

Holmes, D.E., Nicoll, J.S., Bond, D.R. & Lovley, D.R. 2004, 'Potential role of a novel psychrotolerant member of the family Geobacteraceae, Geopsychrobacter electrodiphilus gen. nov., sp. nov., in electricity production by a marine sediment fuel cell', *Applied and Environmental Microbiology*, vol. 70, no. 10, pp. 6023-30.

Holt, H., Gahrn-Hansen, B. & Bruun, B. 2005, 'Shewanella algae and Shewanella putrefaciens: clinical and microbiological characteristics', *Clinical Microbiology and Infection*, vol. 11, no. 5, pp. 347-52.

Hoskins, M. 2017, *Implantable insulin pumps are near extinction, but still alive...* viewed 24 December 2017, <https://www.healthline.com/diabetesmine/implantable-insulin-pumps#1>.

Hou, J., Liu, Z., Yang, S. & Zhou, Y. 2014, 'Three-dimensional macroporous anodes based on stainless steel fiber felt for high-performance microbial fuel cells', *Journal of Power Sources*, vol. 258, pp. 204-9.

Hussein, L., Rubenwolf, S., Von Stetten, F., Urban, G., Zengerle, R., Krueger, M. & Kerzenmacher, S. 2011, 'A highly efficient buckypaper-based electrode material for mediatorless laccase-catalyzed dioxygen reduction', *Biosensors and Bioelectronics*, vol. 26, no. 10, pp. 4133-8.

Hussein, L., Urban, G. & Krüger, M. 2011, 'Fabrication and characterization of buckypaper-based nanostructured electrodes as a novel material for biofuel cell applications', *Physical Chemistry Chemical Physics*, vol. 13, no. 13, pp. 5831-9.

Ieropoulos, I., Greenman, J. & Melhuish, C. 2008, 'Microbial fuel cells based on carbon veil electrodes: stack configuration and scalability', *International Journal of Energy Research*, vol. 32, no. 13, pp. 1228-40.

Ieropoulos, I., Greenman, J. & Melhuish, C. 2010, 'Improved energy output levels from small-scale microbial fuel cells', *Bioelectrochemistry*, vol. 78, no. 1, pp. 44-50.

Ieropoulos, I.A., Greenman, J. & Melhuish, C. 2013, 'Miniature microbial fuel cells and stacks for urine utilisation', *International Journal of Hydrogen Energy*, vol. 38, no. 1, pp. 492-6.

Imthera 2017, *Sleep apnea implant therapy*, viewed 23 December 2017, <http://imtheramedical.com/sleep-apnea-implant/>.

Inoue, K., Leang, C., Franks, A.E., Woodard, T.L., Nevin, K.P. & Lovley, D.R. 2011, 'Specific localization of the c-type cytochrome OmcZ at the anode surface in current-producing biofilms of Geobacter sulfurreducens', *Environmental Microbiology Reports*, vol. 3, no. 2, pp. 211-7.

Inspire Medical Systems 2017, *Take comfort. Inspire therapy can help.*, <https://www.inspiresleep.com/what-is-inspire-therapy/how-inspire-therapy-works/>.

ISO, I.O.f.S. 2009, *ISO 10993 biological evaluation of medical devices*.

ISO, I.O.f.S. 2018, *How we develop standards*, viewed 24 May 2018.

Janda, J.M. 2014, 'Shewanella: a marine pathogen as an emerging cause of human disease', *Clinical Microbiology Newsletter*, vol. 36, no. 4, pp. 25-9.

Janda, J.M. & Abbott, S.L. 2014, 'The genus Shewanella: from the briny depths below to human pathogen', *Critical Reviews in Microbiology*, vol. 40, no. 4, pp. 293-312.

Jansen, D. 2002, *Day to day with my cochlear implant.*, Audiology Online, viewed 27 December 2017, <https://www.audiologyonline.com/articles/day-to-with-my-cochlear-1152>.

Japsen, B. 2016, *Medical technology sales to hit $500B within five years*, Forbes, viewed 27 December 2017 2017, <https://www.forbes.com/sites/brucejapsen/2016/10/17/medical-technology-sales-to-hit-500b-within-five-years/#3e2f8ca411be>.

Jayapriya, J. & Ramamurthy, V. 2012, 'Use of non-native phenazines to improve the performance of Pseudomonas aeruginosa MTCC 2474 catalysed fuel cells', *Bioresource Technology*, vol. 124, pp. 23-8.

Jiang, D., Curtis, M., Troop, E., Scheible, K., McGrath, J., Hu, B., Suib, S., Raymond, D. & Li, B. 2011, 'A pilot-scale study on utilizing multi-anode/cathode microbial fuel cells (MAC MFCs) to enhance the power production in wastewater treatment', *International Journal of Hydrogen Energy*, vol. 36, no. 1, pp. 876-84.

Jiang, D. & Li, B. 2009, 'Granular activated carbon single-chamber microbial fuel cells (GAC-SCMFCs): a design suitable for large-scale wastewater treatment processes', *Biochemical Engineering Journal*, vol. 47, no. 1, pp. 31-7.

Juárez, K., Kim, B.-C., Nevin, K., Olvera, L., Reguera, G., Lovley, D.R. & Methé, B.A. 2009, 'PilR, a transcriptional regulator for pilin and other genes required for Fe(III) reduction in Geobacter sulfurreducens', *Journal of molecular microbiology and biotechnology*, vol. 16, no. 3-4, pp. 146-58.

Jugović, B., Grgur, B., Antov, M., Knežević-Jugović, Z., Stevanović, J. & Gvozdenović, M. 2016, 'Polypyrrole-based enzyme electrode with immobilized glucose oxidase for electrochemical determination of glucose', *International Journal of Electrochemical Science*, vol. 11, pp. 1152-61.

Kang, C.S., Eaktasang, N., Kwon, D.-Y. & Kim, H.S. 2014, 'Enhanced current production by Desulfovibrio desulfuricans biofilm in a mediator-less microbial fuel cell', *Bioresource Technology*, vol. 165, pp. 27-30.

Karaśkiewicz, M., Nazaruk, E., Żelechowska, K., Biernat, J.F., Rogalski, J. & Bilewicz, R. 2012, 'Fully enzymatic mediatorless fuel cell with efficient naphthylated carbon nanotube–laccase composite cathodes', *Electrochemistry Communications*, vol. 20, pp. 124-7.

Karra, U., Manickam, S.S., McCutcheon, J.R., Patel, N. & Li, B. 2013, 'Power generation and organics removal from wastewater using activated carbon nanofiber (ACNF) microbial fuel cells (MFCs)', *International Journal of Hydrogen Energy*, vol. 38, no. 3, pp. 1588-97.

Katic, J., Rodriguez, S. & Rusu, A. 2016, 'A Dual-Output Thermoelectric Energy Harvesting Interface With 86.6% Peak Efficiency at 30μW and Total Control Power of 160 nW', *IEEE Journal of Solid-State Circuits*, vol. 51, no. 8, pp. 1928-37.

Katic, J., Rodriguez, S. & Rusu, A. 2017, 'A high-efficiency energy harvesting interface for implanted biofuel cell and thermal harvesters', *IEEE Transactions on Power Electronics*.

Katz, E. & MacVittie, K. 2013, 'Implanted biofuel cells operating in vivo–methods, applications and perspectives–feature article', *Energy & Environmental Science*, vol. 6, no. 10, pp. 2791-803.

Keller, K.L., Rapp-Giles, B.J., Semkiw, E.S., Porat, I., Brown, S.D. & Wall, J.D. 2014, 'New model for electron flow for sulfate reduction in Desulfovibrio alaskensis G20', *Applied and Environmental Microbiology*, vol. 80, no. 3, pp. 855-68.

Kelly, M.J., Fafilek, G., Besenhard, J.O., Kronberger, H. & Nauer, G.E. 2005, 'Contaminant absorption and conductivity in polymer electrolyte membranes', *Journal of Power Sources*, vol. 145, no. 2, pp. 249-52.

Kennedy, J., Ter Haar, G. & Cranston, D. 2003, 'High intensity focused ultrasound: surgery of the future?', *The British Journal of Radiology*, vol. 76, no. 909, pp. 590-9.

Kerzenmacher, S., Ducrée, J., Zengerle, R. & von Stetten, F. 2008, 'Energy harvesting by implantable abiotically catalyzed glucose fuel cells', *Journal of Power Sources*, vol. 182, no. 1, pp. 1-17.

Ketep, S.F., Bergel, A., Calmet, A. & Erable, B. 2014, 'Stainless steel foam increases the current produced by microbial bioanodes in bioelectrochemical systems', *Energy & Environmental Science*, vol. 7, no. 5, pp. 1633-7.

Khan, S., Dahiya, R.S. & Lorenzelli, L. 2014, 'Flexible thermoelectric generator based on transfer printed Si microwires', *2014 44th European Solid State Device Research Conference (ESSDERC)*, IEEE, pp. 86-9.

Kim, H., Lee, I., Kwon, Y., Kim, B.C., Ha, S., Lee, J.-h. & Kim, J. 2011, 'Immobilization of glucose oxidase into polyaniline nanofiber matrix for biofuel cell applications', *Biosensors and Bioelectronics*, vol. 26, no. 9, pp. 3908-13.

Kim, H.W., Batra, A., Priya, S., Uchino, K., Markley, D., Newnham, R.E. & Hofmann, H.F. 2004, 'Energy harvesting using a piezoelectric "cymbal" transducer in dynamic environment', *Japanese Journal of Applied Physics*, vol. 43, no. 9R, p. 6178.

Kim, J.-S., Lim, J.-H., Nam, H.-Y., Lim, H.-J., Shin, J.-S., Shin, J.-Y., Ryu, J.-H., Kim, K., Kwon, I.-C. & Jin, S.-M. 2012, 'In situ application of hydrogel-type fibrin–islet

composite optimized for rapid glycemic control by subcutaneous xenogeneic porcine islet transplantation', *Journal of Controlled Release*, vol. 162, no. 2, pp. 382-90.

Kim, J., Kim, S.I. & Yoo, K.-H. 2009, 'Polypyrrole nanowire-based enzymatic biofuel cells', *Biosensors and Bioelectronics*, vol. 25, no. 2, pp. 350-5.

Kim, J.R., Cheng, S., Oh, S.-E. & Logan, B.E. 2007, 'Power generation using different cation, anion, and ultrafiltration membranes in microbial fuel cells', *Environmental Science & Technology*, vol. 41, no. 3, pp. 1004-9.

Kim, R.E., Hong, S.-G., Ha, S. & Kim, J. 2014, 'Enzyme adsorption, precipitation and crosslinking of glucose oxidase and laccase on polyaniline nanofibers for highly stable enzymatic biofuel cells', *Enzyme and Microbial Technology*, vol. 66, pp. 35-41.

Kishi, M., Nemoto, H., Hamao, T., Yamamoto, M., Sudou, S., Mandai, M. & Yamamoto, S. 1999, 'Micro thermoelectric modules and their application to wristwatches as an energy source', *Eighteenth International Conference on Thermoelectrics 1999* IEEE, pp. 301-7.

Kissinger, P.T. & Heineman, W.R. 1983, 'Cyclic voltammetry', *Journal of Chemical Education*, vol. 60, no. 9, p. 702.

Kizling, M., Stolarczyk, K., Kiat, J.S.S., Tammela, P., Wang, Z., Nyholm, L. & Bilewicz, R. 2015, 'Pseudocapacitive polypyrrole–nanocellulose composite for sugar-air enzymatic fuel cells', *Electrochemistry Communications*, vol. 50, pp. 55-9.

Kizling, M., Stolarczyk, K., Tammela, P., Wang, Z., Nyholm, L., Golimowski, J. & Bilewicz, R. 2016, 'Bioelectrodes based on pseudocapacitive cellulose/polypyrrole composite improve performance of biofuel cell', *Bioelectrochemistry*, vol. 112, pp. 184-90.

Korenevsky, A.A., Vinogradov, E., Gorby, Y. & Beveridge, T.J. 2002, 'Characterization of the lipopolysaccharides and capsules of Shewanella spp', *Applied and Environmental Microbiology*, vol. 68, no. 9, pp. 4653-7.

Koulouridis, S., Bakogianni, S., Diet, A., Le Bihan, Y. & Pichon, L. 2016, 'Investigation of efficient wireless charging for deep implanted medical devices', *2016 IEEE International Symposium on Antennas and Propagation (APSURSI)*, IEEE, pp. 1045-6.

Kretzschmar, J., Riedl, S., Brown, R.K., Schröder, U. & Harnisch, F. 2017, 'eLatrine: lessons learned from the development of a low-tech MFC based on cardboard electrodes for the treatment of human feces', *Journal of The Electrochemical Society*, vol. 164, no. 3, pp. H3065-H72.

Kucklick, T.R. 2013, *The medical device R&D handbook*, CRC Press, Taylor & Francis Group.

Kumar, R. & Leech, D. 2014, 'Coupling of amine-containing osmium complexes and glucose oxidase with carboxylic acid polymer and carbon nanotube matrix to provide enzyme electrodes for glucose oxidation', *Journal of The Electrochemical Society*, vol. 161, no. 13, pp. H3005-H10.

Kwon, C.H., Lee, S.-H., Choi, Y.-B., Lee, J.A., Kim, S.H., Kim, H.-H., Spinks, G.M., Wallace, G.G., Lima, M.D. & Kozlov, M.E. 2014, 'High-power biofuel cell textiles from woven biscrolled carbon nanotube yarns', *Nature Communications*, vol. 5, p. 3928.

Lalaoui, N., De Poulpiquet, A., Haddad, R., Le Goff, A., Holzinger, M., Gounel, S., Mermoux, M., Infossi, P., Mano, N. & Lojou, E. 2015, 'A membraneless air-breathing hydrogen biofuel cell based on direct wiring of thermostable enzymes on carbon nanotube electrodes', *Chemical Communications*, vol. 51, no. 35, pp. 7447-50.

Lalaoui, N., Le Goff, A., Holzinger, M. & Cosnier, S. 2015, 'Fully oriented bilirubin oxidase on porphyrin-functionalized carbon nanotube electrodes for electrocatalytic oxygen reduction', *Chemistry-A European Journal*, vol. 21, no. 47, pp. 16868-73.

Lay-Ekuakille, A., Vendramin, G., Trotta, A. & Mazzotta, G. 2009, 'Thermoelectric generator design based on power from body heat for biomedical autonomous devices', *IEEE International Workshop on Medical Measurements and Applications (MeMeA) 2009*, IEEE, pp. 1-4.

Le Goff, A., Holzinger, M. & Cosnier, S. 2015, 'Recent progress in oxygen-reducing laccase biocathodes for enzymatic biofuel cells', *Cellular and Molecular Life Sciences*, vol. 72, no. 5, pp. 941-52.

Ledezma, P., Donose, B.C., Freguia, S. & Keller, J. 2015, 'Oxidised stainless steel: a very effective electrode material for microbial fuel cell bioanodes but at high risk of corrosion', *Electrochimica Acta*, vol. 158, pp. 356-60.

Leonov, V., Torfs, T., Van Hoof, C. & Vullers, R.J. 2009, 'Smart wireless sensors integrated in clothing: an electrocardiography system in a shirt powered using human body heat', *Sensors & Transducers*, vol. 107, no. 8, p. 165.

Lepage, G., Albernaz, F.O., Perrier, G. & Merlin, G. 2012, 'Characterization of a microbial fuel cell with reticulated carbon foam electrodes', *Bioresource Technology*, vol. 124, pp. 199-207.

Lepu, M. 2016, *Lepu Medical 2016 annual report*.

Leung, K.M., Wanger, G., El-Naggar, M.Y., Gorby, Y., Southam, G., Lau, W.M. & Yang, J. 2013, 'Shewanella oneidensis MR-1 bacterial nanowires exhibit p-type, tunable electronic behavior', *Nano Letters*, vol. 13, no. 6, pp. 2407-11.

Levy, S.B. 1998, 'The challenge of antibiotic resistance', *Scientific American*, vol. 278, no. 3, pp. 32-9.

Li, D., Wen, Y., He, H., Xu, J., Liu, M. & Yue, R. 2012, 'Polypyrrole–multiwalled carbon nanotubes composites as immobilizing matrices of ascorbate oxidase for the facile fabrication of an amperometric vitamin C biosensor', *Journal of Applied Polymer Science*, vol. 126, no. 3, pp. 882-93.

Li, X., Tsui, C.-Y. & Ki, W.-H. 2015, 'A 13.56 MHz wireless power transfer system with reconfigurable resonant regulating rectifier and wireless power control for implantable medical devices', *IEEE Journal of Solid-State Circuits*, vol. 50, no. 4, pp. 978-89.

Li, X., Zhong, G.-Z., Qiao, Y., Huang, J., Hu, W.H., Wang, X.-G. & Li, C.M. 2014, 'A high performance xylose microbial fuel cell enabled by Ochrobactrum sp. 575 cells', *RSC Advances*, vol. 4, no. 75, pp. 39839-43.

Liao, Q., Zhang, J., Li, J., Ye, D., Zhu, X. & Zhang, B. 2015, 'Increased performance of a tubular microbial fuel cell with a rotating carbon-brush anode', *Biosensors and Bioelectronics*, vol. 63, pp. 558-61.

Lima, M.D., Fang, S., Lepró, X., Lewis, C., Ovalle-Robles, R., Carretero-González, J., Castillo-Martínez, E., Kozlov, M.E., Oh, J. & Rawat, N. 2011, 'Biscrolling nanotube sheets and functional guests into yarns', *Science*, vol. 331, no. 6013, pp. 51-5.

Liu, H. & Logan, B.E. 2004, 'Electricity generation using an air-cathode single chamber microbial fuel cell in the presence and absence of a proton exchange membrane', *Environmental Science & Technology*, vol. 38, no. 14, pp. 4040-6.

Liu, H., Ramnarayanan, R. & Logan, B.E. 2004, 'Production of electricity during wastewater treatment using a single chamber microbial fuel cell', *Environmental Science & Technology*, vol. 38, no. 7, pp. 2281-5.

Liu, H., Wang, Y., Mei, D., Shi, Y. & Chen, Z. 2017, 'Design of a wearable thermoelectric generator for harvesting human body energy', *Wearable Sensors and Robots*, Springer, pp. 55-66.

Liu, H., Zhao, T., Jiang, W., Jia, R., Niu, D., Qiu, G., Fan, L., Li, X., Liu, W. & Chen, B. 2015, 'Flexible battery-less bioelectronic implants: wireless powering and

manipulation by near-infrared light', *Advanced Functional Materials*, vol. 25, no. 45, pp. 7071-9.
Liu, Y., Harnisch, F., Fricke, K., Schröder, U., Climent, V. & Feliu, J.M. 2010, 'The study of electrochemically active microbial biofilms on different carbon-based anode materials in microbial fuel cells', *Biosensors and Bioelectronics*, vol. 25, no. 9, pp. 2167-71.
LivaNova 2016, *LivaNova annual report 2016*.
Logan, B., Cheng, S., Watson, V. & Estadt, G. 2007, 'Graphite fiber brush anodes for increased power production in air-cathode microbial fuel cells', *Environmental Science & Technology*, vol. 41, no. 9, pp. 3341-6.
Logan, B.E., Hamelers, B., Rozendal, R., Schröder, U., Keller, J., Freguia, S., Aelterman, P., Verstraete, W. & Rabaey, K. 2006, 'Microbial fuel cells: methodology and technology', *Environmental Science & Technology*, vol. 40, no. 17, pp. 5181-92.
Logan, B.E., Wallack, M.J., Kim, K.-Y., He, W., Feng, Y. & Saikaly, P.E. 2015, 'Assessment of microbial fuel cell configurations and power densities', *Environmental Science & Technology Letters*, vol. 2, no. 8, pp. 206-14.
Lopez, R.J., Babanova, S., Ulyanova, Y., Singhal, S. & Atanassov, P. 2014, 'Improved interfacial electron transfer in modified bilirubin oxidase biocathodes', *ChemElectroChem*, vol. 1, no. 1, pp. 241-8.
Lord, P. 2017, *PhysioLogic Devices, Inc.*, viewed 24 December 2017, <http://physiologicdevices.com/>.
Lovley, D.R. 2006, 'Bug juice: harvesting electricity with microorganisms', *Nature Reviews Microbiology*, vol. 4, no. 7, pp. 497-508.
Lu, Z., Zhang, H., Mao, C. & Li, C.M. 2016, 'Silk fabric-based wearable thermoelectric generator for energy harvesting from the human body', *Applied Energy*, vol. 164, pp. 57-63.
Lv, Z., Xie, D., Yue, X., Feng, C. & Wei, C. 2012, 'Ruthenium oxide-coated carbon felt electrode: a highly active anode for microbial fuel cell applications', *Journal of Power Sources*, vol. 210, pp. 26-31.
MacVittie, K., Halámek, J., Halámková, L., Southcott, M., Jemison, W.D., Lobel, R. & Katz, E. 2013, 'From "cyborg" lobsters to a pacemaker powered by implantable biofuel cells', *Energy & Environmental Science*, vol. 6, no. 1, pp. 81-6.
Mano, N. & Edembe, L. 2013, 'Bilirubin oxidases in bioelectrochemistry: features and recent findings', *Biosensors and Bioelectronics*, vol. 50, pp. 478-85.
Mano, N., Mao, F. & Heller, A. 2002, 'A miniature biofuel cell operating in a physiological buffer', *Journal of the American Chemical Society*, vol. 124, no. 44, pp. 12962-3.
Mardanpour, M.M. & Yaghmaei, S. 2016, 'Characterization of a microfluidic microbial fuel cell as a power generator based on a nickel electrode', *Biosensors and Bioelectronics*, vol. 79, pp. 327-33.
Marshall, C.W. & May, H.D. 2009, 'Electrochemical evidence of direct electrode reduction by a thermophilic Gram-positive bacterium, Thermincola ferriacetica', *Energy & Environmental Science*, vol. 2, no. 6, pp. 699-705.
Mays, E., Barakat, S., Huynh, A. & Munro, J. 2016, 'Meta-analysis on optimised parameters for energy harvesting thermoelectric generators in the human body', *PAM Review: Energy Science & Technology*, vol. 3, pp. 49-63.
McArdle, W.D., Katch, F.I. & Katch, V.L. 2010, *Exercise physiology: nutrition, energy, and human performance*, Lippincott Williams & Wilkins.
Medical Expo 2017, *Medtronic Interstim II*, <http://img.medicalexpo.com/images_me/photo-m2/70691-3020285.jpg>.
MedTech Innovator 2017, *NeuroTronik Limited*, viewed 23 December 2017, <https://medtechinnovator.org/company/neurotronik/>.

Medtronic 2006, *RESTOREADVANCED 37713 implant manual*, pamphlet, Medtronic, http://manuals.medtronic.com/content/dam/emanuals/neuro/WCM_PROD042265.pdf.

Medtronic 2007, *RestoreULTRA™ 37712 multi-program rechargeable neurostimulator implant manual*, http://manuals.medtronic.com/content/dam/emanuals/neuro/WCM_PROD042256.pdf.

Medtronic 2010, *Activa® SC 37603 multi-program neurostimulator*, pamphlet, Medtronic, http://manuals.medtronic.com/content/dam/emanuals/neuro/CONTRIB_225372.pdf.

Medtronic 2012, *Recharger 37751 charging system user manual*, http://www.medtronic.com/content/dam/medtronic-com-m/mdt/neuro/documents/rechrg-sys-37751-patient.pdf.

Medtronic 2013, *ADVISA™ DR A4DR01 clinician manual*, pamphlet, Medtronic, http://manuals.medtronic.com/content/dam/emanuals/crdm/CONTRIB_171210.pdf.

Medtronic 2014a, *Activa® PC 37601 multi-program neurostimulator implant manual*, pamphlet, Medtronic.

Medtronic 2014b, *Activa® RC 37612 multi-program rechargeable neurostimulator implant manual*, pamphlet, Medtronic, http://manuals.medtronic.com/content/dam/emanuals/neuro/CONTRIB_208225.pdf.

Medtronic 2014c, *EVERA™ XT DR DDBB1D1 device manual*, pamphlet, Medtronic, http://manuals.medtronic.com/content/dam/emanuals/crdm/CONTRIB_170277.pdf.

Medtronic 2015a, *Visia AF MRI™ VR SureScan™ DVFB1D4 device manual*, pamphlet, Medtronic, http://manuals.medtronic.com/content/dam/emanuals/crdm/CONTRIB_235954.pdf.

Medtronic 2015b, *Visia AF™ VR DVAB1D1 digital single chamber implantable cardioverter defibrillator (vve-vvir)*, http://manuals.medtronic.com/content/dam/emanuals/crdm/CONTRIB_235956.pdf.

Medtronic 2016a, *ADAPTA® ADDR01/03/06, ADDRS1/L1*, pamphlet, Medtronic, http://manuals.medtronic.com/content/dam/emanuals/crdm/CONTRIB_244799.pdf.

Medtronic 2016b, *ADVISA DR MRI™ SURESCAN™ A2DR01, ADVISA SR MRI™ SURESCAN™ A3SR01 clinician manual*, http://manuals.medtronic.com/content/dam/emanuals/crdm/M961530A001C_view.pdf.

Medtronic 2016c, *Azure™ XT DR MRI SureScan™ W1DR01 device manual*, pamphlet, Medtronic, http://manuals.medtronic.com/content/dam/emanuals/crdm/CONTRIB_260109.pdf.

Medtronic 2016d, *FDA approves first automated insulin system for type 1 diabetes*, <https://s.aolcdn.com/hss/storage/midas/e04b8a1417c705ccc9bae769fafee37/204388475/medtronic-automated-insulin-delivery-system.jpg>.

Medtronic 2016e, *InterStim® therapy InterStim® II model 3058 neurostimulator InterStim® model 3023 neurostimulator*, pamphlet, Medtronic, http://manuals.medtronic.com/content/dam/emanuals/neuro/CONTRIB_255298.pdf.

Medtronic 2016f, *Medtronic annual report SEC 10-K filing for fiscal year 2016*, http://phx.corporate-ir.net/External.File?item=UGFyZW50SUQ9MzU1NDUwfENoaWxkSUQ9LTF8VHlwZT0z&t=1&cb=636126728213762010.

Medtronic 2016g, *Micra™ MC1VR01 clinician manual*, pamphlet, Medtronic, http://manuals.medtronic.com/content/dam/emanuals/crdm/CONTRIB_231758.pdf.

Medtronic 2016h, *PrimeAdvanced® SureScan® MRI 97702 neurostimulator implant manual*, pamphlet, Medtronic, http://manuals.medtronic.com/content/dam/emanuals/neuro/CONTRIB_255646.pdf.

Medtronic 2016i, *RestoreSensor™ 37714 multi-program rechargeable neurostimulator*, pamphlet, Medtronic, http://manuals.medtronic.com/content/dam/emanuals/neuro/CONTRIB_255645.pdf.

Medtronic 2016j, *RestoreUltra® SureScan® MRI 97712 rechargeable neurostimulator*, pamphlet, Medtronic, http://manuals.medtronic.com/content/dam/emanuals/neuro/CONTRIB_255647.pdf.

Medtronic 2017a, *DBS woman with recharger*, http://www.medtronicdbs.com/wcm/groups/mdtcom_sg/@mdt/@neuro/documents/images/dbs-woman-with-recharger.jpg.

Medtronic 2017b, *Drug infusion systems - SynchoMed II | Medtronic*, viewed 23 December 2017.

Medtronic 2017c, *How DBS may help*, viewed 22 December 2017, <https://www.medtronicdbs.com/parkinsons-deep-brain-stimulation/dbs-may-help/index.htm>.

Medtronic 2017d, *How to use your recharger if you have an Activa® RC neurostimulator, you must check the battery daily and charge the battery regularly.*, https://www.medtronicdbs.com/parkinsons-ongoing-therapy/battery-recharger-instructions/index.htm, viewed 27 December 2017, <https://www.medtronicdbs.com/parkinsons-ongoing-therapy/battery-recharger-instructions/index.htm>.

Medtronic 2017e, *Products information for healthcare professionals*, viewed 23 December 2017, <http://www.medtronic.com/us-en/healthcare-professionals/products.html>.

Medtronic 2017f, *Proven treatment option for bladder control and bowel control*, viewed 22 December 2017, <http://www.medtronic.com/us-en/healthcare-professionals/therapies-procedures/urology/sacral-neuromodulation/education-training/about-the-therapy.html>.

Medtronic 2017g, *What is continuous glucose monitoring?*, viewed 24 December 2017, <https://www.medtronic-diabetes.com.au/pump-therapy/continuous-glucose-monitoring>.

Mehta, T., Childers, S.E., Glaven, R., Lovley, D.R. & Mester, T. 2006, 'A putative multicopper protein secreted by an atypical type II secretion system involved in the reduction of insoluble electron acceptors in Geobacter sulfurreducens', *Microbiology*, vol. 152, no. 8, pp. 2257-64.

Meredith, M.T., Minson, M., Hickey, D., Artyushkova, K., Glatzhofer, D.T. & Minteer, S.D. 2011, 'Anthracene-modified multi-walled carbon nanotubes as direct electron transfer scaffolds for enzymatic oxygen reduction', *ACS Catalysis*, vol. 1, no. 12, pp. 1683-90.

Miller, B. 2014, *3-D printer creates transformative device for heart treatment*, viewed 24 December 2017, <https://source.wustl.edu/2014/02/3d-printer-creates-transformative-device-for-heart-treatment/>.

Milton, R.D., Hickey, D.P., Abdellaoui, S., Lim, K., Wu, F., Tan, B. & Minteer, S.D. 2015, 'Rational design of quinones for high power density biofuel cells', *Chemical Science*, vol. 6, no. 8, pp. 4867-75.

Min, B., Cheng, S. & Logan, B.E. 2005, 'Electricity generation using membrane and salt bridge microbial fuel cells', *Water Research*, vol. 39, no. 9, pp. 1675-86.

Mink, J.E., Rojas, J.P., Logan, B.E. & Hussain, M.M. 2012, 'Vertically grown multiwalled carbon nanotube anode and nickel silicide integrated high performance microsized (1.25 μL) microbial fuel cell', *Nano Letters*, vol. 12, no. 2, pp. 791-5.

Miyake, T., Haneda, K., Nagai, N., Yatagawa, Y., Onami, H., Yoshino, S., Abe, T. & Nishizawa, M. 2011, 'Enzymatic biofuel cells designed for direct power generation

from biofluids in living organisms', *Energy & Environmental Science*, vol. 4, no. 12, pp. 5008-12.

Mohan, S.V., Raghavulu, S.V. & Sarma, P. 2008, 'Biochemical evaluation of bioelectricity production process from anaerobic wastewater treatment in a single chambered microbial fuel cell (MFC) employing glass wool membrane', *Biosensors and Bioelectronics*, vol. 23, no. 9, pp. 1326-32.

Mond, H.G. & Proclemer, A. 2011, 'The 11th world survey of cardiac pacing and implantable cardioverter-defibrillators: calendar year 2009–a world society of arrhythmia's project', *Pacing and Clinical Electrophysiology*, vol. 34, no. 8, pp. 1013-27.

Monti, G., Arcuti, P. & Tarricone, L. 2015, 'Resonant inductive link for remote powering of pacemakers', *IEEE Transactions on Microwave Theory and Techniques*, vol. 63, no. 11, pp. 3814-22.

Moon, E., Blaauw, D. & Phillips, J.D. 2017, 'Infrared energy harvesting in millimeter-scale GaAs photovoltaics', *IEEE Transactions on Electron Devices*, vol. 64, no. 11, pp. 4554-60.

Moon, K.S., Ozturk, Y., Lee, S.Q., Youm, W., Hwang, G. & Park, H. 2017, 'Ultrasonic power transfer for medical implants'.

Mosenia, A. & Jha, N. 2017, 'Opsecure: a secure unidirectional optical channel for implantable medical devices', *IEEE Transactions on Multi-Scale Computing Systems*.

Murata, K., Kajiya, K., Nakamura, N. & Ohno, H. 2009, 'Direct electrochemistry of bilirubin oxidase on three-dimensional gold nanoparticle electrodes and its application in a biofuel cell', *Energy & Environmental Science*, vol. 2, no. 12, pp. 1280-5.

Nalwa, H.S. 1999, *Handbook of nanostructured materials and nanotechnology, five-volume set*, Academic Press.

Nandy, A., Kumar, V. & Kundu, P.P. 2013, 'Utilization of proteinaceous materials for power generation in a mediatorless microbial fuel cell by a new electrogenic bacteria Lysinibacillus sphaericus VA5', *Enzyme and Microbial Technology*, vol. 53, no. 5, pp. 339-44.

Nascimento, M.L.F. & Oliveira, H.d. 2015, 'Staphylococcus aureus biofilm formation on polypyrrole: an electrical overview', *Química Nova*, vol. 38, no. 8.

Nazaruk, E., Sadowska, K., Biernat, J., Rogalski, J., Ginalska, G. & Bilewicz, R. 2010, 'Enzymatic electrodes nanostructured with functionalized carbon nanotubes for biofuel cell applications', *Analytical and Bioanalytical Chemistry*, vol. 398, no. 4, pp. 1651-60.

Neuronetics 2017, *Transforming neurohealth with non-drug, non-invasive treatments*, viewed 23 December 2017, <https://neurostar.com/about-us/>.

Neuropace 2017, *Company overview*, viewed 23 December 2017, <http://www.neuropace.com/about-us-corporate/>.

NeuroStar, A.T. 2017, 'Neuronetics, Inc. Raises $15 Million in Series G Equity Financing, Led by Ascension Ventures', viewed 23 December 2017, <https://www.prnewswire.com/news-releases/neuronetics-inc-raises-15-million-in-series-g-equity-financing-led-by-ascension-ventures-300469405.html>.

Nevro Corp 2016, *Nevro Corp. form 10-K*, https://s21.q4cdn.com/478267292/files/doc_financials/Quarterly/2016/Q4/Form-10K-(2016)-FINAL.pdf.

Nevro Corp 2017, *We believe true innovation transforms more lives.*, viewed 23 December 2017 2017.

NIBIB 2013, *Wireless, implanted sensor broadens range of brain research*, viewed 24 December 2017, <https://www.nibib.nih.gov/news-events/newsroom/wireless-implanted-sensor-broadens-range-brain-research>.

Nico, V., Boco, E., Frizzell, R. & Punch, J. 2016, 'A high figure of merit vibrational energy harvester for low frequency applications', *Applied Physics Letters*, vol. 108, no. 1, p. 013902.

Niu, P., Chapman, P., Riemer, R. & Zhang, X. 2004, 'Evaluation of motions and actuation methods for biomechanical energy harvesting', *2004 IEEE 35th Annual Power Electronics Specialists Conference (PESC)*, vol. 3, IEEE, pp. 2100-6.

Nuvectra 2017a, *Nuvectra 2016 annual report*, http://www.annualreports.com/HostedData/AnnualReports/PDF/NASDAQ_NVTR_2016.pdf.

Nuvectra 2017b, *Powerful capabilities. Simplified designs.*, viewed 23 December 2017, <https://nuvectramedical.com/international/physician/about-algovita/>.

O'Neill, M. 2017, *Transhumanists, biohackers, grinders: who are they and can they really live forever?*, Australia.

Ockenden, W. 2016, *Living forever: biohackers focus on human longevity, say it is not as far away as you think*, Australia.

Oh, J.Y., Lee, J.H., Han, S.W., Chae, S.S., Bae, E.J., Kang, Y.H., Choi, W.J., Cho, S.Y., Lee, J.-O. & Baik, H.K. 2016, 'Chemically exfoliated transition metal dichalcogenide nanosheet-based wearable thermoelectric generators', *Energy & Environmental Science*, vol. 9, no. 5, pp. 1696-705.

Ohara, T.J., Rajagopalan, R. & Heller, A. 1993, 'Glucose electrodes based on cross-linked bis (2, 2'-bipyridine) chloroosmium (+/2+) complexed poly (1-vinylimidazole) films', *Analytical Chemistry*, vol. 65, no. 23, pp. 3512-7.

Okada, T., Møller-Holst, S., Gorseth, O. & Kjelstrup, S. 1998, 'Transport and equilibrium properties of Nafion® membranes with H+ and Na+ ions', *Journal of Electroanalytical Chemistry*, vol. 442, no. 1, pp. 137-45.

Okada, T., Nakamura, N., Yuasa, M. & Sekine, I. 1997, 'Ion and water transport characteristics in membranes for polymer electrolyte fuel cells containing H+ and Ca2+ cations', *Journal of the Electrochemical Society*, vol. 144, no. 8, pp. 2744-50.

Ong, T. 2016, *Biohacking: start-up sells technology allowing users to 'hack' their bodies*, Australia.

Ozeri, S. & Shmilovitz, D. 2014, 'Simultaneous backward data transmission and power harvesting in an ultrasonic transcutaneous energy transfer link employing acoustically dependent electric impedance modulation', *Ultrasonics*, vol. 54, no. 7, pp. 1929-37.

Paddock, C. 2014, *Artificial pancreas better than pump for managing type 1 diabetes*, viewed 24 December 2017, <https://www.medicalnewstoday.com/articles/286101.php>.

Pandit, S., Khilari, S., Roy, S., Pradhan, D. & Das, D. 2014, 'Improvement of power generation using Shewanella putrefaciens mediated bioanode in a single chambered microbial fuel cell: Effect of different anodic operating conditions', *Bioresource Technology*, vol. 166, pp. 451-7.

Pankratov, D., Falkman, P., Blum, Z. & Shleev, S. 2014, 'A hybrid electric power device for simultaneous generation and storage of electric energy', *Energy & Environmental Science*, vol. 7, no. 3, pp. 989-93.

Pant, D., Van Bogaert, G., De Smet, M., Diels, L. & Vanbroekhoven, K. 2010, 'Use of novel permeable membrane and air cathodes in acetate microbial fuel cells', *Electrochimica Acta*, vol. 55, no. 26, pp. 7710-6.

Park, H.S., Kim, B.H., Kim, H.S., Kim, H.J., Kim, G.T., Kim, M., Chang, I.S., Park, Y.K. & Chang, H.I. 2001, 'A novel electrochemically active and Fe (III)-reducing bacterium phylogenetically related to Clostridium butyricum isolated from a microbial fuel cell', *Anaerobe*, vol. 7, no. 6, pp. 297-306.

Parra, E. & Lin, L. 2009, 'Microbial fuel cell based on electrode-exoelectrogenic bacteria interface', *IEEE 22nd International Conference on Micro Electro Mechanical Systems (MEMS) 2009*, IEEE, pp. 31-4.

Patil, D.S., Pawar, S.A., Devan, R.S., Gang, M.G., Ma, Y.-R., Kim, J.H. & Patil, P.S. 2013, 'Electrochemical supercapacitor electrode material based on polyacrylic acid/polypyrrole/silver composite', *Electrochimica Acta*, vol. 105, pp. 569-77.

Patolsky, F., Weizmann, Y. & Willner, I. 2004, 'Long-range electrical contacting of redox enzymes by SWCNT connectors', *Angewandte Chemie International Edition*, vol. 43, no. 16, pp. 2113-7.

Patro, T.U. & Wagner, H.D. 2016, 'Influence of graphene oxide incorporation and chemical cross-linking on structure and mechanical properties of layer-by-layer assembled poly (Vinyl alcohol)-Laponite free-standing films', *Journal of Polymer Science Part B: Polymer Physics*, vol. 54, no. 22, pp. 2377-87.

Peighambardoust, S., Rowshanzamir, S. & Amjadi, M. 2010, 'Review of the proton exchange membranes for fuel cell applications', *International Journal of Hydrogen Energy*, vol. 35, no. 17, pp. 9349-84.

Peirs, J., Reynaerts, D. & Verplaetsen, F. 2003, 'Development of an axial microturbine for a portable gas turbine generator', *Journal of Micromechanics and Microengineering*, vol. 13, no. 4, p. S190.

Pham, C.A., Jung, S.J., Phung, N.T., Lee, J., Chang, I.S., Kim, B.H., Yi, H. & Chun, J. 2003, 'A novel electrochemically active and Fe(III)-reducing bacterium phylogenetically related to Aeromonas hydrophila, isolated from a microbial fuel cell', *FEMS Microbiology Letters*, vol. 223, no. 1, pp. 129-34.

Pillatsch, P., Yeatman, E. & Holmes, A. 2012, 'A scalable piezoelectric impulse-excited energy harvester for human body excitation', *Smart Materials and Structures*, vol. 21, no. 11, p. 115018.

Pires, D., de Kraker, M.E.A., Tartari, E., Abbas, M. & Pittet, D. 2017, '‘Fight antibiotic resistance—it’s in your hands’: call from the world health organization for 5th may 2017', *Clinical Infectious Diseases*, vol. 64, no. 12, pp. 1780-3.

Prasad, D., Arun, S., Murugesan, M., Padmanaban, S., Satyanarayanan, R., Berchmans, S. & Yegnaraman, V. 2007, 'Direct electron transfer with yeast cells and construction of a mediatorless microbial fuel cell', *Biosensors and Bioelectronics*, vol. 22, no. 11, pp. 2604-10.

Qian, F., Baum, M., Gu, Q. & Morse, D.E. 2009, 'A 1.5 μL microbial fuel cell for on-chip bioelectricity generation', *Lab on a Chip*, vol. 9, no. 21, pp. 3076-81.

Qiao, Y., Li, C.M., Bao, S.-J., Lu, Z. & Hong, Y. 2008, 'Direct electrochemistry and electrocatalytic mechanism of evolved Escherichia coli cells in microbial fuel cells', *Chemical Communications*, no. 11, pp. 1290-2.

Rabaey, K., Boon, N., Siciliano, S.D., Verhaege, M. & Verstraete, W. 2004, 'Biofuel cells select for microbial consortia that self-mediate electron transfer', *Applied and Environmental Microbiology*, vol. 70, no. 9, pp. 5373-82.

Rabaey, K., Clauwaert, P., Aelterman, P. & Verstraete, W. 2005, 'Tubular microbial fuel cells for efficient electricity generation', *Environmental Science & Technology*, vol. 39, no. 20, pp. 8077-82.

Raghavulu, S.V., Goud, R.K., Sarma, P. & Mohan, S.V. 2011, 'Saccharomyces cerevisiae as anodic biocatalyst for power generation in biofuel cell: influence of redox condition and substrate load', *Bioresource Technology*, vol. 102, no. 3, pp. 2751-7.

Rahimi-Eichi, H., Baronti, F. & Chow, M.-Y. 2014, 'Online adaptive parameter identification and state-of-charge coestimation for lithium-polymer battery cells', *IEEE Transactions on Industrial Electronics*, vol. 61, no. 4, pp. 2053-61.

Rahimnejad, M., Bakeri, G., Najafpour, G., Ghasemi, M. & Oh, S.-E. 2014, 'A review on the effect of proton exchange membranes in microbial fuel cells', *Biofuel Research Journal*, vol. 1, no. 1, pp. 7-15.

Rasmussen, M., Ritzmann, R.E., Lee, I., Pollack, A.J. & Scherson, D. 2012, 'An implantable biofuel cell for a live insect', *Journal of the American Chemical Society*, vol. 134, no. 3, pp. 1458-60.

Reeve, A., Simcox, E. & Turnbull, D. 2014, 'Ageing and parkinson's disease: why is advancing age the biggest risk factor?', *Ageing Research Reviews*, vol. 14, pp. 19-30.

Reguera, G., McCarthy, K.D., Mehta, T., Nicoll, J.S., Tuominen, M.T. & Lovley, D.R. 2005, 'Extracellular electron transfer via microbial nanowires', *Nature*, vol. 435, no. 7045, pp. 1098-101.

Rengaraj, S., Kavanagh, P. & Leech, D. 2011, 'A comparison of redox polymer and enzyme co-immobilization on carbon electrodes to provide membrane-less glucose/O_2 enzymatic fuel cells with improved power output and stability', *Biosensors and Bioelectronics*, vol. 30, no. 1, pp. 294-9.

Reuillard, B., Abreu, C., Lalaoui, N., Le Goff, A., Holzinger, M., Ondel, O., Buret, F. & Cosnier, S. 2015, 'One-year stability for a glucose/oxygen biofuel cell combined with pH reactivation of the laccase/carbon nanotube biocathode', *Bioelectrochemistry*, vol. 106, pp. 73-6.

Riemer, R. & Shapiro, A. 2011, 'Biomechanical energy harvesting from human motion: theory, state of the art, design guidelines, and future directions', *Journal of Neuroengineering and Rehabilitation*, vol. 8, no. 1, p. 22.

Riemer, S.M. & Alexander, J.A. 2016, 'Utilization of Implantable Devices for Pain: A Look at Intrathecal Pumps and Spinal Cord Stimulators', *Pain Management Nursing*, vol. 17, no. 2, p. 97.

Ringeisen, B.R., Henderson, E., Wu, P.K., Pietron, J., Ray, R., Little, B., Biffinger, J.C. & Jones-Meehan, J.M. 2006, 'High power density from a miniature microbial fuel cell using Shewanella oneidensis DSP10', *Environmental Science & Technology*, vol. 40, no. 8, pp. 2629-34.

Rodríguez-Rojas, A., Rodríguez-Beltrán, J., Couce, A. & Blázquez, J. 2013, 'Antibiotics and antibiotic resistance: a bitter fight against evolution', *International Journal of Medical Microbiology*, vol. 303, no. 6, pp. 293-7.

Rojas, J.P., Singh, D., Inayat, S.B., Sevilla, G.A.T., Fahad, H.M. & Hussain, M.M. 2017, 'Micro and nano-engineering enabled new generation of thermoelectric generator devices and applications', *ECS Journal of Solid State Science and Technology*, vol. 6, no. 3, pp. N3036-N44.

Rome, L.C., Flynn, L., Goldman, E.M. & Yoo, T.D. 2005, 'Generating electricity while walking with loads', *Science*, vol. 309, no. 5741, pp. 1725-8.

Roundy, S., Wright, P.K. & Pister, K.S. 2002, 'Micro-electrostatic vibration-to-electricity converters', *ASME International Mechanical Engineering Congress & Exposition*, ed. ASME, vol. 220, New Orleans, Louisiana, pp. 1-10.

Rowe, A. & Li, X. 2001, 'Mathematical modeling of proton exchange membrane fuel cells', *Journal of Power Sources*, vol. 102, no. 1, pp. 82-96.

Roy, J.N., Babanova, S., Garcia, K.E., Cornejo, J., Ista, L.K. & Atanassov, P. 2014, 'Catalytic biofilm formation by Shewanella oneidensis MR-1 and anode characterization by expanded uncertainty', *Electrochimica Acta*, vol. 126, pp. 3-10.

Rozendal, R.A., Hamelers, H.V. & Buisman, C.J. 2006, 'Effects of membrane cation transport on pH and microbial fuel cell performance', *Environmental Science & Technology*, vol. 40, no. 17, pp. 5206-11.

Ruhi, G. & Dhawan, S. 2014, 'Conducting polymer nano composite epoxy coatings for anticorrosive applications', *Modern Electrochemical Methods in Nano, Surface and Corrosion Science*, InTech.

Saha, A., Iqbal, S., Karmaker, M., Zinnat, S. & Ali, M. 2017, 'A wireless optical power system for medical implants using low power near-IR laser', *2017 39th Annual International Conference of the IEEE Engineering in Medicine and Biology Society (EMBC)*, IEEE, pp. 1978-81.

Saha, C., O'donnell, T., Wang, N. & McCloskey, P. 2008, 'Electromagnetic generator for harvesting energy from human motion', *Sensors and Actuators A: Physical*, vol. 147, no. 1, pp. 248-53.

Saluda Medical 2017a, *Introducing closed loop neuromodulation technology*, <http://www.saludamedical.com/technology/>.

Saluda Medical 2017b, 'Saluda Medical Secures AU$53 Million in Series D Financing', viewed 23 December 2017, <http://www.saludamedical.com/wp-content/uploads/2017/06/PR_Notice_25052017.pdf>.

Samad, F.A., Karim, M.F., Paulose, V. & Ong, L.C. 2016, 'A curved electromagnetic energy harvesting system for wearable electronics', *IEEE Sensors Journal*, vol. 16, no. 7, pp. 1969-74.

Santoro, C., Agrios, A., Pasaogullari, U. & Li, B. 2011, 'Effects of gas diffusion layer (GDL) and micro porous layer (MPL) on cathode performance in microbial fuel cells (MFCs)', *International Journal of Hydrogen Energy*, vol. 36, no. 20, pp. 13096-104.

Santoro, C., Arbizzani, C., Erable, B. & Ieropoulos, I. 2017, 'Microbial fuel cells: from fundamentals to applications. A review', *Journal of Power Sources*, vol. 356, pp. 225-44.

Santoro, C., Guilizzoni, M., Baena, J.C., Pasaogullari, U., Casalegno, A., Li, B., Babanova, S., Artyushkova, K. & Atanassov, P. 2014, 'The effects of carbon electrode surface properties on bacteria attachment and start up time of microbial fuel cells', *Carbon*, vol. 67, pp. 128-39.

Santoro, C., Ieropoulos, I., Greenman, J., Cristiani, P., Vadas, T., Mackay, A. & Li, B. 2013a, 'Current generation in membraneless single chamber microbial fuel cells (MFCs) treating urine', *Journal of Power Sources*, vol. 238, pp. 190-6.

Santoro, C., Ieropoulos, I., Greenman, J., Cristiani, P., Vadas, T., Mackay, A. & Li, B. 2013b, 'Power generation and contaminant removal in single chamber microbial fuel cells (SCMFCs) treating human urine', *International Journal of Hydrogen Energy*, vol. 38, no. 26, pp. 11543-51.

Santoro, C., Lei, Y., Li, B. & Cristiani, P. 2012, 'Power generation from wastewater using single chamber microbial fuel cells (MFCs) with platinum-free cathodes and pre-colonized anodes', *Biochemical Engineering Journal*, vol. 62, pp. 8-16.

Santoro, C., Li, B., Cristiani, P. & Squadrito, G. 2013, 'Power generation of microbial fuel cells (MFCs) with low cathodic platinum loading', *International Journal of Hydrogen Energy*, vol. 38, no. 1, pp. 692-700.

Schröder, U., Nießen, J. & Scholz, F. 2003, 'A generation of microbial fuel cells with current outputs boosted by more than one order of magnitude', *Angewandte Chemie International Edition*, vol. 42, no. 25, pp. 2880-3.

Schrott, G.D., Bonanni, P.S., Robuschi, L., Esteve-Nuñez, A. & Busalmen, J.P. 2011, 'Electrochemical insight into the mechanism of electron transport in biofilms of Geobacter sulfurreducens', *Electrochimica Acta*, vol. 56, no. 28, pp. 10791-5.

Schubart, I.W., Göbel, G. & Lisdat, F. 2012, 'A pyrroloquinolinequinone-dependent glucose dehydrogenase (PQQ-GDH)-electrode with direct electron transfer based on

polyaniline modified carbon nanotubes for biofuel cell application', *Electrochimica Acta*, vol. 82, pp. 224-32.

Serway, R.A. & Gordon, J.R. 1998, *Principles of physics*, Saunders College Pub.

Setpoint, M. 2017, *Bioelectronic medicine for inflammatory diseases*, viewed 23 December **2017**, <https://setpointmedical.com/technology/>.

Seviour, T., Doyle, L., Lauw, S., Hinks, J., Rice, S., Nesatyy, V., Webster, R., Kjelleberg, S. & Marsili, E. 2015, 'Voltammetric profiling of redox-active metabolites expressed by Pseudomonas aeruginosa for diagnostic purposes', *Chemical Communications*, vol. 51, no. 18, pp. 3789-92.

Shaquer, C.M. 2004, *US6810289B1 Transcutaneous power optimization circuit for cochlear implant*.

Shen, H.-B., Yong, X.-Y., Chen, Y.-L., Liao, Z.-H., Si, R.-W., Zhou, J., Wang, S.-Y., Yong, Y.-C., OuYang, P.-K. & Zheng, T. 2014, 'Enhanced bioelectricity generation by improving pyocyanin production and membrane permeability through sophorolipid addition in Pseudomonas aeruginosa-inoculated microbial fuel cells', *Bioresource Technology*, vol. 167, pp. 490-4.

Shephard, R. 2011, 'Compendium of physical activities: a second update of codes and met values', *Yearbook Of Sports Medicine*, vol. 2012, pp. 126-7.

Shi, L., Chen, B., Wang, Z., Elias, D.A., Mayer, M.U., Gorby, Y.A., Ni, S., Lower, B.H., Kennedy, D.W. & Wunschel, D.S. 2006, 'Isolation of a high-affinity functional protein complex between OmcA and MtrC: two outer membrane decaheme c-type cytochromes of Shewanella oneidensis MR-1', *Journal of Bacteriology*, vol. 188, no. 13, pp. 4705-14.

Shimatani, Y., Kato, H., Haraike, K. & Murata, T. 2013, 'A fully implantable subcutaneous emg sensor powered by transcutaneous near-infrared light irradiation', *Journal of the Japan Society of Applied Electromagnetics and Mechanics*, vol. 21, no. 1, pp. 66-71.

Shmilovitz, D., Ozeri, S., Wang, C.-C. & Spivak, B. 2014, 'Noninvasive control of the power transferred to an implanted device by an ultrasonic transcutaneous energy transfer link', *IEEE Transactions on Biomedical Engineering*, vol. 61, no. 4, pp. 995-1004.

Shree Pacetronix 2016, *Shree Pacetronix Ltd 28th annual report 2015 - 2016*, http://www.pacetronix.com/wp-content/uploads/2015/07/Annual-Report-2015-16.pdf.

Shreeram, D.D., Hassett, D.J. & Schaefer, D.W. 2016, 'Urine-powered microbial fuel cell using a hyperpiliated pilT mutant of Pseudomonas aeruginosa', *Journal of Industrial Microbiology & Biotechnology*, vol. 43, no. 1, pp. 103-7.

Siddique, A.R.M., Rabari, R., Mahmud, S. & Van Heyst, B. 2016, 'Thermal energy harvesting from the human body using flexible thermoelectric generator (FTEG) fabricated by a dispenser printing technique', *Energy*, vol. 115, pp. 1081-91.

Sigma Aldrich 2017, *577030 Aldrich polypyrrole*, Sigma Aldrich, Darmstadt, Germany, viewed 27 December 2017 2017, <https://www.sigmaaldrich.com/catalog/product/aldrich/577030?lang=en&region=AU>.

Smith, J.A., Tremblay, P.-L., Shrestha, P.M., Snoeyenbos-West, O.L., Franks, A.E., Nevin, K.P. & Lovley, D.R. 2014, 'Going wireless: Fe (III) oxide reduction without pili by Geobacter sulfurreducens strain JS-1', *Applied and Environmental Microbiology*, vol. 80, no. 14, pp. 4331-40.

So, K., Kawai, S., Hamano, Y., Kitazumi, Y., Shirai, O., Hibi, M., Ogawa, J. & Kano, K. 2014, 'Improvement of a direct electron transfer-type fructose/dioxygen biofuel cell with a substrate-modified biocathode', *Physical Chemistry Chemical Physics*, vol. 16, no. 10, pp. 4823-9.

Song, K., Han, J.H., Lim, T., Kim, N., Shin, S., Kim, J., Choo, H., Jeong, S., Kim, Y.C. & Wang, Z.L. 2016, 'Subdermal flexible solar cell arrays for powering medical electronic implants', *Advanced Healthcare Materials*, vol. 5, no. 13, pp. 1572-80.

Song, K., Han, J.H., Yang, H.C., Nam, K.I. & Lee, J. 2017, 'Generation of electrical power under human skin by subdermal solar cell arrays for implantable bioelectronic devices', *Biosensors and Bioelectronics*, vol. 92, pp. 364-71.

Sonova 2016, *Sonova annual report 2016 / 17*, https://www.sonova.com/en/system/files/01_sonova_annual_report_2016_17_full_en.pdf.

Sosna, M., Chrétien, J.-M., Kilburn, J.D. & Bartlett, P.N. 2010, 'Monolayer anthracene and anthraquinone modified electrodes as platforms for Trametes hirsuta laccase immobilisation', *Physical Chemistry Chemical Physics*, vol. 12, no. 34, pp. 10018-26.

Sosna, M., Stoica, L., Wright, E., Kilburn, J.D., Schuhmann, W. & Bartlett, P.N. 2012, 'Mass transport controlled oxygen reduction at anthraquinone modified 3D-CNT electrodes with immobilized Trametes hirsuta laccase', *Physical Chemistry Chemical Physics*, vol. 14, no. 34, pp. 11882-5.

Srikanth, S., Marsili, E., Flickinger, M.C. & Bond, D.R. 2008, 'Electrochemical characterization of Geobacter sulfurreducens cells immobilized on graphite paper electrodes', *Biotechnology and Bioengineering*, vol. 99, no. 5, pp. 1065-73.

St Jude Medical 2014, *St Jude Medical Ellipse VR*, <https://www.sjm.com/~/media/galaxy/product-catalog/e/6/e66101db-9ce3-4ae7-9a64-ed904fd21c2e.jpg>.

St Jude Medical 2015, *St. Jude Medical 2015 annual report 10-k*, http://www.annualreports.com/HostedData/AnnualReports/PDF/NYSE_STJ_2015.pdf.

St Jude Medical 2016, *Spinal cord stimulation fact sheet*, <http://media.sjm.com/newsroom/media-kits/fact-sheet-details/2014/Spinal-Cord-Stimulation-Fact-Sheet/default.aspx>.

Starner, T. 1996, 'Human-powered wearable computing', *IBM systems Journal*, vol. 35, no. 3.4, pp. 618-29.

Sterken, T., Fiorini, P., Baert, K., Puers, R. & Borghs, G. 2003, 'An electret-based electrostatic μ-generator', *12th International Conference on Transducers Solid-State Sensors Actuators and Microsystems 2003*, vol. 2, IEEE, pp. 1291-4.

Stimwave 2017, *Products*, viewed 23 December 2017, <http://stimwave.com/mobile/products/>.

Suarez, F., Nozariasbmarz, A., Vashaee, D. & Öztürk, M.C. 2016, 'Designing thermoelectric generators for self-powered wearable electronics', *Energy & Environmental Science*, vol. 9, no. 6, pp. 2099-113.

Suarez, F., Parekh, D.P., Ladd, C., Vashaee, D., Dickey, M.D. & Öztürk, M.C. 2017, 'Flexible thermoelectric generator using bulk legs and liquid metal interconnects for wearable electronics', *Applied Energy*, vol. 202, pp. 736-45.

Sukhu, T., Kennelly, M.J. & Kurpad, R. 2016, 'Sacral neuromodulation in overactive bladder: a review and current perspectives', *Research and Reports in Urology*, vol. 8, p. 193.

Sun, J., Hu, Y., Bi, Z. & Cao, Y. 2009, 'Improved performance of air-cathode single-chamber microbial fuel cell for wastewater treatment using microfiltration membranes and multiple sludge inoculation', *Journal of Power Sources*, vol. 187, no. 2, pp. 471-9.

Szczupak, A., Halámek, J., Halámková, L., Bocharova, V., Alfonta, L. & Katz, E. 2012, 'Living battery–biofuel cells operating in vivo in clams', *Energy & Environmental Science*, vol. 5, no. 10, pp. 8891-5.

Tal Medical 2016, *About: context*, viewed 23 December 2017, <http://www.talmedical.com/context/>.

Tashiro, R., Kabei, N., Katayama, K., Tsuboi, E. & Tsuchiya, K. 2002, 'Development of an electrostatic generator for a cardiac pacemaker that harnesses the ventricular wall motion', *Journal of Artificial Organs*, vol. 5, no. 4, pp. 0239-45.

Teater, B. 2017, *NeuroTronik raises $23.1 million to advance heart therapy*, viewed 23 December 2017, <https://www.ncbiotech.org/news/neurotronik-raises-231-million-advance-heart-therapy>.

ter Heijne, A., Hamelers, H.V., Saakes, M. & Buisman, C.J. 2008, 'Performance of non-porous graphite and titanium-based anodes in microbial fuel cells', *Electrochimica Acta*, vol. 53, no. 18, pp. 5697-703.

The Implantable Insulin Pump Foundation 2017, *Our story we live with type 1 diabetes and we have an implantable insulin pump*, viewed 24 December 2017, <http://theiipump.com/index.php/our-story/>.

Therapeutic Goods Administration (TGA) 2016, *Medtronic deep brain stimulation therapy DBS extension models 7483 and 37086*, Canberra, Australia, <https://www.tga.gov.au/sites/default/files/medtronic-deep-brain-stimulation-therapy-extension-models-7483-37086-01.jpg>.

Thomson, S. 2016, *Spinal cord stimulation's role in managing chronic disease symptoms*, International Neuromodulation Society, viewed 22 December 2017, <http://www.neuromodulation.com/spinal-cord-stimulation>.

Tominaga, M., Ohtani, M. & Taniguchi, I. 2008, 'Gold single-crystal electrode surface modified with self-assembled monolayers for electron tunneling with bilirubin oxidase', *Physical Chemistry Chemical Physics*, vol. 10, no. 46, pp. 6928-34.

Torfs, T., Leonov, V., Van Hoof, C. & Gyselinckx, B. 2006, 'Body-heat powered autonomous pulse oximeter', *5th IEEE Conference on Sensors*, IEEE, pp. 427-30.

Torfs, T., Leonov, V., Yazicioglu, R.F., Merken, P., Van Hoof, C., Vullers, R.J. & Gyselinckx, B. 2008, 'Wearable autonomous wireless electro-encephalography system fully powered by human body heat', *IEEE Sensors*, IEEE, pp. 1269-72.

Valdés-Ramírez, G., Li, Y.-C., Kim, J., Jia, W., Bandodkar, A.J., Nunez-Flores, R., Miller, P.R., Wu, S.-Y., Narayan, R. & Windmiller, J.R. 2014, 'Microneedle-based self-powered glucose sensor', *Electrochemistry Communications*, vol. 47, pp. 58-62.

Vigolo, B., Penicaud, A., Coulon, C., Sauder, C., Pailler, R., Journet, C., Bernier, P. & Poulin, P. 2000, 'Macroscopic fibers and ribbons of oriented carbon nanotubes', *Science*, vol. 290, no. 5495, pp. 1331-4.

Vihvelin, H., Leadbetter, J.R., Bance, M., Brown, J.A. & Adamson, R.B. 2016, 'Compensating for tissue changes in an ultrasonic power link for implanted medical devices', *IEEE Transactions on Biomedical Circuits and Systems*, vol. 10, no. 2, pp. 404-11.

Villarrubia, C.W.N., Lau, C., Ciniciato, G.P., Garcia, S.O., Sibbett, S.S., Petsev, D.N., Babanova, S., Gupta, G. & Atanassov, P. 2014, 'Practical electricity generation from a paper based biofuel cell powered by glucose in ubiquitous liquids', *Electrochemistry Communications*, vol. 45, pp. 44-7.

Von Canstein, H., Ogawa, J., Shimizu, S. & Lloyd, J.R. 2008, 'Secretion of flavins by Shewanella species and their role in extracellular electron transfer', *Applied and Environmental Microbiology*, vol. 74, no. 3, pp. 615-23.

Wan, C., Tian, R., Azizi, A.B., Huang, Y., Wei, Q., Sasai, R., Wasusate, S., Ishida, T. & Koumoto, K. 2016, 'Flexible thermoelectric foil for wearable energy harvesting', *Nano Energy*, vol. 30, pp. 840-5.

Wang, M.L., Chang, T.C., Teisberg, T., Weber, M.J., Charthad, J. & Arbabian, A. 2017, 'Closed-loop ultrasonic power and communication with multiple miniaturized active implantable medical devices', *IEEE International Ultrasonics Symposium (IUS)*, IEEE, pp. 1-4.

Wang, S., Lam, K.H., Sun, C.L., Kwok, K.W., Chan, H.L.W., Guo, M.S. & Zhao, X.-Z. 2007, 'Energy harvesting with piezoelectric drum transducer', *Applied Physics Letters*, vol. 90, no. 11, p. 113506.

Wang, T., Turhan, M. & Gunasekaran, S. 2004, 'Selected properties of pH-sensitive, biodegradable chitosan–poly (vinyl alcohol) hydrogel', *Polymer International*, vol. 53, no. 7, pp. 911-8.

Wang, X., Cheng, S., Feng, Y., Merrill, M.D., Saito, T. & Logan, B.E. 2009, 'Use of carbon mesh anodes and the effect of different pretreatment methods on power production in microbial fuel cells', *Environmental Science & Technology*, vol. 43, no. 17, pp. 6870-4.

Wang, Y.-C. 2014, 'Using red blood cells in microbial fuel cell catholyte solution to improve electricity generation', The Ohio State University.

Watkins, C., Shen, B. & Venkatasubramanian, R. 2005, 'Low-grade-heat energy harvesting using superlattice thermoelectrics for applications in implantable medical devices and sensors', *24th International Conference on Thermoelectrics (ICT) 2005*, IEEE, pp. 265-7.

We, J.H., Kim, S.J. & Cho, B.J. 2014, 'Hybrid composite of screen-printed inorganic thermoelectric film and organic conducting polymer for flexible thermoelectric power generator', *Energy*, vol. 73, pp. 506-12.

Webb, P. 1992, 'Temperatures of skin, subcutaneous tissue, muscle and core in resting men in cold, comfortable and hot conditions', *European Journal of Applied Physiology and Occupational Physiology*, vol. 64, no. 5, pp. 471-6.

Weber, J., Potje-Kamloth, K., Haase, F., Detemple, P., Völklein, F. & Doll, T. 2006, 'Coin-size coiled-up polymer foil thermoelectric power generator for wearable electronics', *Sensors and Actuators A: Physical*, vol. 132, no. 1, pp. 325-30.

Willey, J.M., Sherwood, L. & Woolverton, C.J. 2008, *Prescott, Harley, and Klein's microbiology*, McGraw-Hill Higher Education.

William Demant 2016, *Annual Report 2016*.

Wilson, R. & Turner, A. 1992, 'Glucose oxidase: an ideal enzyme', *Biosensors and Bioelectronics*, vol. 7, no. 3, pp. 165-85.

Winfield, J., Chambers, L.D., Rossiter, J., Greenman, J. & Ieropoulos, I. 2015, 'Urine-activated origami microbial fuel cells to signal proof of life', *Journal of Materials Chemistry A*, vol. 3, no. 13, pp. 7058-65.

Winfield, J., Chambers, L.D., Stinchcombe, A., Rossiter, J. & Ieropoulos, I. 2014, 'The power of glove: soft microbial fuel cell for low-power electronics', *Journal of Power Sources*, vol. 249, pp. 327-32.

Wolfson, S.K., Gofberg, S.L., Prusiner, P. & Nanis, L. 1968, 'The bioautofuel cell: a device for pacemaker power from direct energy conversion consuming autogenous fuel', *Transactions - American Society for Artificial Internal Organs*, vol. 14, no. 1, pp. 198-203.

World Bank 2017, *Life expectancy at birth, total (years)*, World Bank, viewed 27 December **2017**, <https://data.worldbank.org/indicator/SP.DYN.LE00.IN?cid=GPD_10>.

World Health Organization 2017, *Diabetes*, viewed 24 December 2017, <http://www.who.int/mediacentre/factsheets/fs312/en/>.

Wrighton, K., Thrash, J., Melnyk, R., Bigi, J., Byrne-Bailey, K., Remis, J., Schichnes, D., Auer, M., Chang, C. & Coates, J. 2011, 'Evidence for direct electron transfer by a

Gram-positive bacterium isolated from a microbial fuel cell', *Applied and Environmental Microbiology*, vol. 77, no. 21, pp. 7633-9.

Wu, S., He, W., Yang, W., Ye, Y., Huang, X. & Logan, B.E. 2017, 'Combined carbon mesh and small graphite fiber brush anodes to enhance and stabilize power generation in microbial fuel cells treating domestic wastewater', *Journal of Power Sources*, vol. 356, pp. 348-55.

Xiao, Y., Patolsky, F., Katz, E., Hainfeld, J.F. & Willner, I. 2003, '" Plugging into enzymes": nanowiring of redox enzymes by a gold nanoparticle', *Science*, vol. 299, no. 5614, pp. 1877-81.

Xing, D., Zuo, Y., Cheng, S., Regan, J.M. & Logan, B.E. 2008, 'Electricity generation by Rhodopseudomonas palustris DX-1', *Environmental Science & Technology*, vol. 42, no. 11, pp. 4146-51.

Xiong, Y., Shi, L., Chen, B., Mayer, M.U., Lower, B.H., Londer, Y., Bose, S., Hochella, M.F., Fredrickson, J.K. & Squier, T.C. 2006, 'High-affinity binding and direct electron transfer to solid metals by the Shewanella oneidensis MR-1 outer membrane c-type cytochrome OmcA', *Journal of the American Chemical Society*, vol. 128, no. 43, pp. 13978-9.

Xu, S. & Liu, H. 2011, 'New exoelectrogen Citrobacter sp. SX-1 isolated from a microbial fuel cell', *Journal of Applied Microbiology*, vol. 111, no. 5, pp. 1108-15.

Yang, Y., Harris, D.P., Luo, F., Xiong, W., Joachimiak, M., Wu, L., Dehal, P., Jacobsen, J., Yang, Z. & Palumbo, A.V. 2009, 'Snapshot of iron response in Shewanella oneidensis by gene network reconstruction', *BMC Genomics*, vol. 10, no. 1, p. 131.

Yang, Y., Xu, G.D. & Liu, J. 2014, 'A prototype of an implantable thermoelectric generator for permanent power supply to body inside a medical device', *Journal of Medical Devices*, vol. 8, no. 1, p. 014507.

Yasri, N.G. & Nakhla, G. 2017, 'The performance of 3-D graphite doped anodes in microbial electrolysis cells', *Journal of Power Sources*, vol. 342, pp. 579-88.

Yong, X.-Y., Shi, D.-Y., Chen, Y.-L., Jiao, F., Lin, X., Zhou, J., Wang, S.-Y., Yong, Y.-C., Sun, Y.-M. & OuYang, P.-K. 2014, 'Enhancement of bioelectricity generation by manipulation of the electron shuttles synthesis pathway in microbial fuel cells', *Bioresource Technology*, vol. 152, pp. 220-4.

You, J., Greenman, J., Melhuish, C. & Ieropoulos, I. 2016, 'Electricity generation and struvite recovery from human urine using microbial fuel cells', *Journal of Chemical Technology and Biotechnology*, vol. 91, no. 3, pp. 647-54.

Yousfi, K., Bekal, S., Usongo, V. & Touati, A. 2017, 'Current trends of human infections and antibiotic resistance of the genus Shewanella', *European Journal of Clinical Microbiology & Infectious Diseases*, pp. 1-10.

Yuming, F. & Hongyan, L. 2017, 'The effects of colonic inner environment on microbial fuel cell performance'.

Zafar, M.N., Tasca, F., Boland, S., Kujawa, M., Patel, I., Peterbauer, C.K., Leech, D. & Gorton, L. 2010, 'Wiring of pyranose dehydrogenase with osmium polymers of different redox potentials', *Bioelectrochemistry*, vol. 80, no. 1, pp. 38-42.

Zebda, A., Cosnier, S., Alcaraz, J.-P., Holzinger, M., Le Goff, A., Gondran, C., Boucher, F., Giroud, F., Gorgy, K. & Lamraoui, H. 2013, 'Single glucose biofuel cells implanted in rats power electronic devices', *Scientific Reports*, vol. 3.

Zebda, A., Gondran, C., Le Goff, A., Holzinger, M., Cinquin, P. & Cosnier, S. 2011, 'Mediatorless high-power glucose biofuel cells based on compressed carbon nanotube-enzyme electrodes', *Nature Communications*, vol. 2, p. 370.

Zeng, F.-G., Rebscher, S., Harrison, W., Sun, X. & Feng, H. 2008, 'Cochlear implants: system design, integration, and evaluation', *IEEE Reviews in Biomedical Engineering*, vol. 1, pp. 115-42.

Zhang, J.C.Y. 2017, *Single, Double, MultiWall Carbon Nanotube Properties & Applications*, Aldrich Materials Science, Sigma-Aldrich Co. LLC, viewed 27 December 2017, <https://www.sigmaaldrich.com/technical-documents/articles/materials-science/single-double-multi-walled-carbon-nanotubes.html>.

Zhang, L., Zhou, S., Zhuang, L., Li, W., Zhang, J., Lu, N. & Deng, L. 2008, 'Microbial fuel cell based on Klebsiella pneumoniae biofilm', *Electrochemistry Communications*, vol. 10, no. 10, pp. 1641-3.

Zhang, T., Cui, C., Chen, S., Ai, X., Yang, H., Shen, P. & Peng, Z. 2006, 'A novel mediatorless microbial fuel cell based on direct biocatalysis of Escherichia coli', *Chemical Communications*, no. 21, pp. 2257-9.

Zhang, X., Cheng, S., Wang, X., Huang, X. & Logan, B.E. 2009, 'Separator characteristics for increasing performance of microbial fuel cells', *Environmental Science & Technology*, vol. 43, no. 21, pp. 8456-61.

Zhang, Y., Zhang, F., Shakhsheer, Y., Silver, J.D., Klinefelter, A., Nagaraju, M., Boley, J., Pandey, J., Shrivastava, A. & Carlson, E.J. 2013, 'A batteryless 19μW MICS/ISM-band energy harvesting body sensor node SoC for ExG applications', *IEEE Journal of Solid-State Circuits*, vol. 48, no. 1, pp. 199-213.

Zhao, B., Kuo, N.-C. & Niknejad, A.M. 2017, 'A gain boosting array technique for weakly-coupled wireless power transfer', *IEEE Transactions on Power Electronics*, vol. 32, no. 9, pp. 7130-9.

Zhao, F., Rahunen, N., Varcoe, J.R., Chandra, A., Avignone-Rossa, C., Thumser, A.E. & Slade, R.C. 2008, 'Activated carbon cloth as anode for sulfate removal in a microbial fuel cell', *Environmental Science & Technology*, vol. 42, no. 13, pp. 4971-6.

Zhao, L., Li, J., Battaglia, F. & He, Z. 2016, 'Computational investigation of the flow field contribution to improve electricity generation in granular activated carbon-assisted microbial fuel cells', *Journal of Power Sources*, vol. 333, pp. 83-7.

Zheng, S., Yang, F., Chen, S., Liu, L., Xiong, Q., Yu, T., Zhao, F., Schröder, U. & Hou, H. 2015, 'Binder-free carbon black/stainless steel mesh composite electrode for high-performance anode in microbial fuel cells', *Journal of Power Sources*, vol. 284, pp. 252-7.

Zheng, W., Ma, J., Guo, F., Li, J., Zhou, H., Xu, X., Li, L. & Zheng, Y. 2014, 'A novel biofuel cell based on electrospun collagen-carbon nanotube nanofibres', *Bio-medical materials and engineering*, vol. 24, no. 1, pp. 229-35.

Zhou, M., Al-Furjan, M.S.H., Zou, J. & Liu, W. 2017, 'A review on heat and mechanical energy harvesting from human–Principles, prototypes and perspectives', *Renewable and Sustainable Energy Reviews*.

Zhou, X., Chen, X., Li, H., Xiong, J., Li, X. & Li, W. 2016, 'Surface oxygen-rich titanium as anode for high performance microbial fuel cell', *Electrochimica Acta*, vol. 209, pp. 582-90.

Zhu, N., Chen, X., Zhang, T., Wu, P., Li, P. & Wu, J. 2011, 'Improved performance of membrane free single-chamber air-cathode microbial fuel cells with nitric acid and ethylenediamine surface modified activated carbon fiber felt anodes', *Bioresource Technology*, vol. 102, no. 1, pp. 422-6.

Zhuang, L., Zheng, Y., Zhou, S., Yuan, Y., Yuan, H. & Chen, Y. 2012, 'Scalable microbial fuel cell (MFC) stack for continuous real wastewater treatment', *Bioresource Technology*, vol. 106, pp. 82-8.

Zhuang, L., Zhou, S., Wang, Y., Liu, C. & Geng, S. 2009, 'Membrane-less cloth cathode assembly (CCA) for scalable microbial fuel cells', *Biosensors and Bioelectronics*, vol. 24, no. 12, pp. 3652-6.

Zuo, Y., Cheng, S., Call, D. & Logan, B.E. 2007, 'Tubular membrane cathodes for scalable power generation in microbial fuel cells', *Environmental Science & Technology*, vol. 41, no. 9, pp. 3347-53.

Zuo, Y., Cheng, S. & Logan, B.E. 2008, 'Ion exchange membrane cathodes for scalable microbial fuel cells', *Environmental Science & Technology*, vol. 42, no. 18, pp. 6967-72.

Zuo, Y., Xing, D., Regan, J.M. & Logan, B.E. 2008, 'Isolation of the exoelectrogenic bacterium Ochrobactrum anthropi YZ-1 by using a U-tube microbial fuel cell', *Applied and Environmental Microbiology*, vol. 74, no. 10, pp. 3130-7.